

Technische Universität München

Fakultät für Maschinenwesen

Lehrstuhl für Fahrzeugtechnik

**Evaluation of Machine Learning Methods for
Diagnosing Automotive Damper Defects**

Thomas Zehelein, M.Sc.

Vollständiger Abdruck der von der Fakultät für Maschinenwesen der
Technischen Universität München zur Erlangung des akademischen Grades eines

Doktor-Ingenieurs

genehmigten Dissertation.

Vorsitzender:

Prof. Dr.-Ing. habil. Boris Lohmann

Prüfer der Dissertation:

1. Prof. Dr.-Ing. Markus Lienkamp

2. Prof. Dr.-Ing. Matthias Althoff

Die Dissertation wurde am 04. Dezember 2020 bei der Technischen Universität München eingereicht und durch die Fakultät für Maschinenwesen am 14. März 2021 angenommen.

Danksagung

Die vorliegende Arbeit entstand während meiner Tätigkeit am Lehrstuhl für Fahrzeugtechnik der Technischen Universität München vom Oktober 2014 bis April 2020.

Meinen ersten Dank möchte ich an meinen Doktorvater Prof. Dr.-Ing. Markus Lienkamp richten. Vielen Dank für die Freiheiten die ich in meiner Zeit am Lehrstuhl genießen durfte, Ihr Vertrauen in meine Arbeit sowie Ihre wegweisende Unterstützung. Weiterhin möchte ich Ihnen für die Vielfältigkeit der Erfahrungen danken, die ich am Lehrstuhl machen durfte.

Mein nächster Dank geht an Prof. Dr.-Ing. Matthias Althoff. Vielen Dank für die bereitwillige und unkomplizierte Übernahme der Zweitgutachterschaft.

Ein weiterer Dank geht an Prof. Dr.-Ing. Boris Lohmann für die Übernahme des Prüfungsvorsitzes.

Bei der Audi AG möchte ich mich für die Durchführung eines Kooperationsprojekts im Rahmen dieser Dissertation bedanken. Insbesondere bei Advait Valluri möchte ich mich für die unkomplizierte Zusammenarbeit bedanken.

Danken möchte ich ebenfalls allen Kollegen am Lehrstuhl und insbesondere der Forschungsgruppe Fahrdynamik. Neben den inhaltlichen Diskussionen möchte ich mich auch für die offene Atmosphäre in der Gruppe bedanken. Ein besonderer Dank geht an Matthias Förth und Matthias Brönnner für die inhaltlichen Diskussionen und Fokussierungsanstöße - nicht nur am Schreibtisch oder in der Kaffeeküche, sondern auch bei unzähligen Radtouren und Pendelfahrten. Ebenfalls möchte ich mich bei meinen weiteren Korrekturlesern Alexander Wischnewski, Maximilian Geißlinger, Sebastian Huber und Katharina Zehelein für Eure Verbesserungsvorschläge und Korrekturen bedanken.

Ich möchte mich bei allen Studenten bedanken, deren Arbeit ich in meiner Zeit am Lehrstuhl betreuen durfte. Durch Euer Engagement sind diese Dissertation sowie andere Projekte erst zu dem geworden, was sie sind.

Mein letzter und größter Dank geht an meine Eltern Lydia und Dieter Zehelein. Euer Vertrauen und Eure Unterstützung auf meinem kompletten Lebensweg haben mich zu meiner heutigen Person wachsen lassen. Danke für alle Freiheiten und Möglichkeiten, die ich in meinem Leben genießen durfte und darf.

München, im November 2020

Thomas Zehelein

Abstract

Changing conditions of automotive use-cases such as autonomous driving as well as an increasing availability of measurement data for data analysis are setting new challenges and opportunities for vehicle health state monitoring. Monitoring the health state of the chassis system is especially essential for autonomous vehicles. This thesis deals with automotive damper defect detection as a first step towards an online chassis system health monitoring system. The literature review of this thesis reveals that there are no existing damper diagnosis concepts that are suited for the ever-changing challenges and opportunities of the monitoring task. Machine learning approaches are applicable for these altered requirements. Therefore, this thesis evaluates machine learning methods for diagnosing automotive damper defects using driving data of Electronic Stability Control (ESC) sensors.

Using only ESC sensors results in an unknown road excitation for the monitoring algorithm. An analysis if it is theoretically possible to detect defective dampers with an unknown road excitation does not exist in literature. Therefore, the observability of a non-linear quarter vehicle model that includes an additional state of a varying damping coefficient is analyzed. Non-linear observability analysis as well as a stochastic observability analysis are performed for generating theoretical insights on beneficial driving conditions for the diagnosis task. The analysis shows that it is possible to detect defective dampers using only wheel speed signals with an unknown road excitation. A higher vehicle speed as well as a higher road excitation are beneficial for the damper defect detection task.

Machine learning concepts are discussed with regard to requirements for automotive diagnosis applications. The identified suitable concepts are supervised and unsupervised classification methods of shallow machine learning, representation learning and deep learning. Shallow machine learning is evaluated using two feature sets: one consists of statistical, mathematical and frequency-based features, the second feature set consists of Fast Fourier Transformation (FFT) data points. Representation learning is evaluated using one feature set that is generated using Autoencoders, and another feature set that is generated using Sparsefilter features. Feature-based classification is conducted using a Support Vector Machine (SVM) for supervised and an Local Outlier Factor (LOF) for unsupervised learning. Convolutional Neural Networks (CNNs) and Variational Autoencoder (VAE) are selected as representatives of supervised and unsupervised deep learning concepts. Post-processing of the classifier's output with regard to the temporal behavior of the health state is conducted using Hidden Markov Models (HMMs) and Linear Dynamical Systems (LDS).

An investigation of the importance for the classification of different features of the generated feature sets is performed. It is shown that representation learning methods for feature generation perform a frequency analysis similar to an FFT. The investigation of the kernels of the deep learning method CNN reveals that this method also performs a frequency analysis of the input signal. The overall diagnosis performances of the different methods are compared with regard to their robustness to changed conditions in driving data in terms of additional mass and winter instead of summer tires. Additionally, the importance of the different sensor signals is analyzed and the effect of a varying size of the training data is investigated. The theoretical insights of the observability analysis regarding the influence of the vehicle speed and the road roughness on the diagnosis performance are confirmed experimentally. A comparison of the performance of machine learning methods with a signal-based damper diagnosis approach shows the competitiveness of the machine learning approaches.

Abstrakt

Veränderte Nutzungsbedingungen von Fahrzeugen wie das autonome Fahren sowie die zunehmende Verfügbarkeit von Fahrdaten für die Datenanalyse stellen neue Herausforderungen und Möglichkeiten für die Überwachung des Fahrzeugzustands dar. Diese Dissertation befasst sich mit der Erkennung von defekten Fahrzeugdämpfern als erster Schritt hin zu einem Online-Zustandsüberwachungssystem für das Fahrwerk. Der Literaturüberblick zeigt, dass keine Konzepte zur Dämpferdiagnose existieren, die sich für die neuartigen Herausforderungen und Möglichkeiten der Überwachungsaufgabe eignen. Ansätze des Machine Learning sind hierfür jedoch prinzipiell geeignet. Daher werden in dieser Arbeit Methoden des Machine Learning zur Diagnose von Fahrzeugdämpferdefekten unter Verwendung von Fahrdaten von Sensoren der elektronischen Stabilitätskontrolle (ESP) evaluiert.

Die Verwendung von ESP-Sensoren führt zu einer unbekanntem Fahrbahnanregung für den Überwachungsalgorithmus. Eine theoretische Analyse der Erkennbarkeit defekter Dämpfer mit unbekannter Fahrbahnanregung existiert in der Literatur nicht. Daher wird die Beobachtbarkeit eines nichtlinearen Viertelfahrzeugmodells mit variablem Dämpfungskoeffizienten analysiert. Es werden eine nichtlineare und eine stochastische Beobachtbarkeitsanalyse durchgeführt, um theoretische Erkenntnisse über vorteilhafte Randbedingungen für die Diagnoseaufgabe zu gewinnen. Defekte Dämpfer können auf Basis von Raddrehzahlsignalen bei unbekannter Fahrbahnanregung erkannt werden. Sowohl eine höhere Fahrzeuggeschwindigkeit als auch eine höhere Fahrbahnanregung sind vorteilhaft für die Dämpferdefekterkennung.

Machine Learning-Konzepte werden im Hinblick auf Anforderungen aus automobilen Diagnoseanwendungen diskutiert. Geeignete Konzepte sind überwachte und unüberwachte Klassifikationsmethoden des Shallow Machine Learning, des Representation Learning und des Deep Learning. Das Shallow Machine Learning wird anhand von zwei Merkmalsätzen bewertet: Ein Merkmalsatz besteht aus statistischen, mathematischen und frequenzbasierten Merkmalen, der zweite Merkmalsatz besteht aus Datenpunkten der Fast Fourier Transformation (FFT). Representation Learning wird mit einem Autoencoder-basiertem Merkmalsatz, sowie einem Sparsefilter-basiertem Merkmalsatz evaluiert. Die merkmalsbasierte Klassifikation wird mit einer Support Vector Machine (SVM) für überwachtes und einem Local Outlier Factor (LOF) Algorithmus für unüberwachtes Lernen durchgeführt. Convolutional Neural Networks (CNNs) und Variational Autoencoder (VAE) werden als Vertreter von überwachtem und unüberwachtem Deep Learning ausgewählt. Die Nachbearbeitung des Klassifikationsergebnisses im Hinblick auf das zeitliche Verhalten des physikalischen Gesundheitszustands wird mit Hilfe von Hidden-Markov-Modellen (HMMs) und linearen dynamischen Systemen (LDS) durchgeführt.

Die Bedeutung der verschiedenen Merkmale der generierten Merkmalsätze für die Klassifikation wird untersucht. Es wird gezeigt, dass Representation Learning Methoden zur Merkmalgenerierung eine Frequenzanalyse ähnlich einer FFT durchführen. Die Kernel der Deep Learning Methode CNN führen ebenfalls eine Frequenzanalyse des Eingangssignals durch. Die Robustheit der Diagnoseleistungen der verschiedenen Methoden gegenüber veränderten Randbedingungen in den Fahrdaten werden mittels höherer Zuladung sowie der Nutzung von Winter- anstatt Sommerreifen verglichen. Zusätzlich wird die Wichtigkeit der verschiedenen Sensorsignale sowie die Auswirkung eines unterschiedlich großen Trainingsdatensatzes untersucht. Die Erkenntnisse der Beobachtbarkeitsanalyse bezüglich des Einflusses der Fahrzeuggeschwindigkeit und der Fahrbahnrauigkeit auf die Diagnoseleistung werden experimentell bestätigt. Ein Vergleich der Machine Learning Methoden mit einem signalbasierten Dämpferdiagnoseansatz zeigt die Konkurrenzfähigkeit der Ansätze des Machine Learning.

"We are drowning in information but starved for knowledge"

John Naisbitt

Contents

List of Abbreviations	V
Formula Symbols	VII
1 Introduction and Motivation	1
1.1 Motivation	1
1.2 Objective of the Thesis	3
1.3 Structure of the Thesis	3
2 State of the Art	5
2.1 Terminologies for Fault Detection and Predictive Maintenance	5
2.2 General Concepts of Diagnosis Methods	6
2.3 Chassis System Fault Diagnosis	7
2.3.1 Damper Fault Diagnosis	7
2.3.2 Fault Diagnosis of Other Chassis System Components	12
2.3.3 Summary of Chassis System Fault Diagnosis	14
2.4 Machine Learning	15
2.4.1 Evolution of Machine Learning for Fault Diagnosis	16
2.4.2 Machine Learning Methods for Fault Diagnosis	18
2.5 Commercial Diagnosis Systems for Automotive Applications	21
2.6 Criticism of the State of the Art	22
2.7 Derivation of the Research Objective	24
3 Analysis of Observability	25
3.1 Derivation of System Equations	26
3.2 Identification of Suitable Observability Analysis Methods	28
3.3 Analysis of Observability with Known Road Excitation	28
3.4 Analysis of Observability with Unknown Road Excitation	29
3.5 Stochastic Observability with Unknown Road Excitation	30
3.6 Analysis of Observability with Unknown Road Excitation and Unknown Road Class	35
3.7 Theoretical Insights	35

4	Machine Learning Methods for Damper Diagnosis	37
4.1	Identification of Suitable Methods	37
4.2	Data Acquisition and Observation Generation	41
4.3	Hand-crafted Feature Generation for Shallow Machine Learning	42
4.3.1	Manual Feature Generation	42
4.3.2	FFT Data Points as Features	43
4.4	Automated Feature Generation using Representation Learning	43
4.4.1	Automated Feature Generation using Autoencoders	43
4.4.2	Automated Feature Generation using Sparsefilters	46
4.5	Feature Reduction and Feature Importance Quantification	47
4.5.1	Recursive Feature Elimination	47
4.5.2	Fisher score	48
4.6	Shallow Classification Methods	48
4.6.1	Shallow Supervised Learning Methods for Classification	48
4.6.2	Shallow Unsupervised Learning Methods for Novelty Detection	50
4.7	Deep Learning Methods	51
4.7.1	Supervised Deep Learning Methods for Classification	51
4.7.2	Unsupervised Deep Learning Methods for Novelty Detection	53
4.8	Evaluation Metrics	56
4.8.1	Performance Metrics for Supervised Learning	57
4.8.2	Performance Metrics for Unsupervised Learning	57
4.8.3	Comparability of Performance Metrics	58
4.9	Post-Processing of Classifier Output	59
4.9.1	Hidden Markov Models for Post-Processing	60
4.9.2	Linear Dynamical Systems	62
5	Results	65
5.1	Description of the Dataset	65
5.2	Investigation of Feature Characteristics	66
5.2.1	Manual Features for Shallow Machine Learning	66
5.2.2	FFT Features for Shallow Machine Learning	67
5.2.3	Autoencoder Features for Representation Learning	70
5.2.4	Sparsefilter Features for Representation Learning	72
5.3	Analysis of the Classification Performance	73
5.3.1	Supervised Shallow Machine and Representation Learning	74

5.3.2	Unsupervised Shallow Machine and Representation Learning	74
5.3.3	Supervised Deep Learning	75
5.3.4	Unsupervised Deep Learning	77
5.4	Overall Comparison	78
5.4.1	Comparison of Results of Supervised Learning Approaches.....	78
5.4.2	Comparison of Results of Unsupervised Learning Approaches	79
5.4.3	Increasing Robustness of Unsupervised Learning Approaches	81
5.5	Performance Improvements by Post-Processing of the Apriori Classifier.....	82
5.5.1	Post-Processing of Supervised Learning using Hidden Markov Models	82
5.5.2	Post-Processing of Unsupervised Learning using Linear Dynamical Systems	85
5.6	Analysis of Sensor Signal Importance.....	86
5.7	Analysis of Training Data Size	88
5.8	Analysis of Influence of Vehicle Speed and Road Roughness	89
5.9	Comparison with Signal-Based Approach	91
6	Discussion	93
6.1	Overall Assessment of the Results	93
6.2	Implications for an Actual Implementation.....	96
6.3	Critical Assessment of the Overall Approach.....	96
6.4	Relevance of the Research Objective	98
7	Summary and Outlook	99
	List of Figures	i
	List of Tables	v
	Bibliography.....	vii
	List of Prior Publications	xxix
	Appendix	xxxv

List of Abbreviations

ABOD	Angular-Based Outlier Detection
ABS	Anti-lock Braking System
ANN	Artificial Neural Network
AR model	Auto-Regressive signal model
AUC	Area Under Curve
CM	Confusion Matrix
CNN	Convolutional Neural Network
DAE	Denosing Autoencoder
DBN	Deep Belief Network
DL	Deep Learning
DSKW	Damper Damage Value (for German Dämpferschadenskennwert)
ECU	Electronic Control Unit
ELBO	Evidence Lower Bound
ESC	Electronic Stability Control
FDI	Fault Detection and Isolation
FFT	Fast Fourier Transformation
FL	Front Left
FLOP	Floating Point Operation
FN	False Negatives
FP	False Positives
FPR	False Positive Rate
FR	Front Right
GAF	Gramian Angular Field
GAN	Generative Adversarial Network
HIL	Hardware-In-The-Loop
HMM	Hidden Markov Model
IF	Isolation Forest
IRI	International Roughness Index
KL	Kullback-Leibler
KNN	k -Nearest Neighbors
LDS	Linear Dynamical System
LOF	Local Outlier Factor
LOLIMOT	Local Linear Model Tree

LPV	Linear Parameter Varying
LSTM	Long Short-Term Memory
ML	Machine Learning
MLP	Multi-Layer Perceptron
NN	Neural Network
OBD-II	On-Board Diagnostics
OCNN	One-Class Neural Network
OCSVM	One-Class Support Vector Machine
OEM	Original Equipment Manufacturer
OSS	Output-To-State Stability
PCA	Principle Component Analysis
PDF	Probability Density Function
PP	Percentage Point
PSD	Power Spectral Density
PTI	Periodical Technical Inspection
ReLU	Rectified Linear Unit
RFE	Recursive Feature Elimination
RL	Representation Learning
RL	Rear Left
RNN	Recurrent Neural Network
ROC	Receiver Operating Characteristic
RP	Recurrence Plot
RR	Rear Right
RUL	Remaining Useful Life
SAE	Stacked Autoencoder
SDE	Stochastic Differential Equation
SML	Shallow Machine Learning
SMO	Sliding Mode Observer
STFT	Short-Time Fourier Transformation
SVDD	Support Vector Data Description
SVM	Support Vector Machine
TN	True Negatives
TP	True Positives
TPR	True Positive Rate
VAE	Variational Autoencoder
WT	Wavelet Transformation

Formula Symbols

Formula Symbols	Unit	Description
Latin Uppercase Letters		
A		Dynamic matrix of a linear system
A_{HMM}		State transition probability matrix of Hidden Markov Model
$\hat{A}(i j)$		Probability that a randomly chosen observation with true class j has a lower estimated probability of belonging to class i than a randomly chosen observation with true class i
$\hat{A}(i, j)$		Average of $\hat{A}(i, j) = \frac{\hat{A}(i j) + \hat{A}(j i)}{2}$ (intermediate variable of M -value calculation)
B		Input matrix of a linear system
B_{HMM}		Emission matrix of Hidden Markov Model
C		Output matrix of a linear system
C		Parameter of Support Vector Machine for trade-off between misclassification of the training data set and model complexity
D		Data set
F		General feature matrix
$F_{z,C}$	N	Vertical force in the contact patch of the tire
$F_{z,C,0}$	N	Vertical force in the contact patch of the tire at an operating point
$\Delta F_{z,C}$	N	Deviation of the vertical force in the contact patch of the tire from its operating point
\mathcal{I}		Interval
K		Number of consecutive observation sequences within a dataset
$\mathcal{L}_{\theta,\phi}(\mathbf{x})$		Evidence Lower Bound of Variational Autoencoder
$\tilde{\mathcal{L}}_{\theta,\phi}(\mathbf{x})$		Monte Carlo estimator for Evidence Lower Bound of Variational Autoencoder
L		Number of samples for latent variable z of Variational Autoencoder
M		M -value of supervised classification approach
N		Number of observations in a data set
O		Emission sequence of a Hidden Markov Model

Formula Symbols	Unit	Description
Q		State sequence of a Hidden Markov Model
\mathbb{R}		Set of real numbers
\mathbb{R}^n		Set of real numbers of dimensionality n
S_{HMM}		Set of hidden states of Hidden Markov Model
S_i		Sum of the ranks of the observations of true class i for the calculation of M -value
$S_{n,z,R}$		One-sided power spectral density of the stochastic white noise input of the road excitation model $n_{z,R}$
S_ω	$\left(\frac{\text{rad}}{\text{s}}\right)^2$ Hz	One-sided power spectral density of a wheel speed signal
T		Number of consecutive observations
V		Variance matrix of state variable of Linear Dynamical System
V_{HMM}		Set of emissions of Hidden Markov Model
W		General weight matrix
W_o		Observability Gramian matrix
W_o^ε		Empirical observability Gramian matrix
W_t		Brownian motion of a stochastic system
X		General input data matrix
X_t		General state vector of a stochastic system
Y_t		General output of a stochastic system

Latin Lowercase Letters

a_{LDS}		Transition parameter of Linear Dynamical System
$a_{X,\text{obs,max}}$	$\frac{\text{m}}{\text{s}^2}$	Threshold for maximum average longitudinal vehicle body acceleration of an observation
$a_{Y,\text{obs,max}}$	$\frac{\text{m}}{\text{s}^2}$	Threshold for maximum average lateral vehicle body acceleration of an observation
$a_{z,R}$	$\frac{1}{\text{m}}$	Parameter for low frequency cut-off behavior of the road excitation within the road excitation model
\mathbf{b}		General bias vector
$b_{z,R}$		Parameter for the general level of the road excitation within the road excitation model
$b_{z,R,0}$		Nominal general level of the road excitation within the road excitation model
c		Number of classes within a data set
c_{LDS}		Output parameter of Linear Dynamical System

Formula Symbols	Unit	Description
$c_{r,dyn,F,C}$	$\frac{N}{m}$	Stiffness of the dynamic tire radius with regard to the vertical force in the contact patch
$c_{z,Bo}$	$\frac{N}{m}$	Vehicle body spring stiffness projected into the wheel plane
$c_{z,T}$	$\frac{N}{m}$	Tire spring stiffness projected into the wheel plane
d		Depth of a Convolutional Neural Network in terms of the number of convolutional/pooling-layer-combinations
$d_{z,Bo}$	$\frac{Ns}{m}$	Vehicle body damping constant projected into the wheel plane
$d_{z,Bo,0}$	$\frac{Ns}{m}$	Nominal vehicle body damping constant projected into the wheel plane
e		Kernel size of a convolutional layer of a Convolutional Neural Network
$f_{E,i}$	Hz	i -th evaluation frequency of signal-based damper defect detection approach
$f_{R,i}$	Hz	i -th reference frequency of signal-based damper defect detection approach
\mathbf{h}		Vector of hidden layer of Autoencoder
k		Number of neighbors for nearest-neighbor algorithms
m_{Bo}	kg	Sprung mass of vehicle body
m_T	kg	Unsprung mass of tire and axle
n		Number of states of a general model
n_i		Number of observations of the true class i
$n_{z,R}$		Stochastic white noise input of the road excitation model
o_t		Emission within emission sequence of a Hidden Markov Model at time step t
p		Kernel size of a pooling layer of a Convolutional Neural Network
$p(i x_{k,j})$		Estimated probability of belonging to the class i for the k -th observation $x_{k,j}$ of the true class j
$p(s_j s_i)$		Probability within the state transition probability matrix A_{HMM} of a transition from the hidden state s_i to the hidden state s_j
$p(o_j s_i)$		Probability within the emission matrix of a Hidden Markov Model of an emission o_j given that being in the hidden state s_i
$p_\theta(\mathbf{x})$		Probability that is assigned to an observation \mathbf{x} by a model with the parameters θ
$p_\theta(\mathbf{z})$		Prior probability of the latent variable \mathbf{z}
$p_\theta(\mathbf{x}, \mathbf{z})$		Joint probability that is assigned by a model with the parameters θ for observing an observation \mathbf{x} and observing a latent variable \mathbf{z}

Formula Symbols	Unit	Description
$p_{\theta}(\mathbf{x} \mathbf{z})$		Conditional probability that is assigned by a model with the parameters θ for observing an observation \mathbf{x} given a latent variable \mathbf{z}
$p_{\theta}(\mathbf{z} \mathbf{x})$		Conditional probability that is assigned by a model with the parameters θ for observing a latent variable \mathbf{z} given an observation \mathbf{x}
$q_{\phi}(\mathbf{z} \mathbf{x})$		Approximate posterior of a Variational Autoencoder
q_t		State within state sequence of a Hidden Markov Model at time step t
r_{dyn}	m	Dynamic tire radius
$r_{\text{dyn},0}$	m	Dynamic tire radius at an operating point
$\Delta r_{\text{dyn},F,C}$	m	Deviation of the dynamic tire radius from its operating point due to a deviation of the vertical force in the tire contact patch
s_1		Hidden state within set of hidden states of Hidden Markov Model
t_{obs}	s	Duration of an observation
u		General one-dimensional input of a system
\mathbf{u}		General multi-dimensional input of a system
$\dot{\mathbf{u}}$		First time-derivative of a general multi-dimensional input of a system
$\mathbf{u}^{(n-1)}$		$(n-1)$ -th time-derivative of a general multi-dimensional input of a system
v	$\frac{\text{m}}{\text{s}}$	Vehicle speed
\mathbf{v}		Measurement noise of Linear Dynamical System
v_1		Emission within the set of emissions of a Hidden Markov Model
$v_{\text{obs,min}}$	$\frac{\text{m}}{\text{s}}$	threshold for minimum average vehicle speed of an observation
\mathbf{w}_n		Process noise of Linear Dynamical System
\mathbf{x}		General state vector of a system
\mathbf{x}_0		General state vector of a system at an operating point
y		General output of a system
z_{Bo}	m	Vertical displacement of sprung mass of vehicle body
\dot{z}_{Bo}	$\frac{\text{m}}{\text{s}}$	Vertical velocity of sprung mass of vehicle body
\ddot{z}_{Bo}	$\frac{\text{m}}{\text{s}^2}$	Vertical acceleration of sprung mass of vehicle body
z_{R}	m	Vertical displacement of the road excitation
z_{T}	m	Vertical displacement of unsprung mass of tire and axle
\dot{z}_{T}	$\frac{\text{m}}{\text{s}}$	Vertical velocity of unsprung mass of tire and axle
\ddot{z}_{T}	$\frac{\text{m}}{\text{s}^2}$	Vertical acceleration of unsprung mass of tire and axle

Formula Symbols	Unit	Description
\mathbf{z}		Vector of hidden layer of a Variational Autoencoder
$\mathbf{z}^{(l)}$		l -th sampled vector of hidden layer of a Variational Autoencoder
Greek Letters		
Γ		Variance matrix of process noise of Linear Dynamical System
Δ^ε		Error of the empirical observability Gramian due to finite selection of ε
ε		Perturbation variable of empirical observability
θ		General parameter vector of a model
$\kappa_{b,z,R}$		Relative deviation of the road parameter $b_{z,R}$ from its nominal value
$\kappa_{d,Bo}$		Relative deviation of the damping coefficient from its nominal value
$\underline{\lambda}(\cdot)$		Smallest eigenvalue of a matrix
μ		Mean value of Gaussian distribution
ξ		Slack variable for Support Vector Machine
π_{HMM}		Initial state vector of a Hidden Markov Model
π_i		Probability of the initial state matrix of a Hidden Markov Model of being in state s_i as start state
ρ		Desired average activation of neuron
$\hat{\rho}$		Average activation of neuron
Σ		Variance matrix of measurement noise of Linear Dynamical System
σ		Variance of Gaussian distribution
$\underline{\sigma}(\cdot)$		Smallest singular value of a matrix
$\overline{\sigma}(\cdot)$		Largest singular value of a matrix
τ		General variable for time representation
Φ^ε		Vector of output differences due to state perturbation ε
ϕ_T	$\frac{\text{rad}}{\text{s}}$	Free-rolling rotational speed of the tire

Functions and Operators

$\{\cdot\}$	Set
$\langle \cdot \rangle$	Sequence
$\ \cdot\ _1$	Operator for L1-norm
$\ \cdot\ _2$	Operator for Euclidean-norm (L_2 -norm)

Formula Symbols	Unit	Description
$[\cdot]^T$		Transposed of a matrix or vector
$D^k(\mathbf{p})$		Distance of an observation \mathbf{p} to its k -th nearest neighbor
$D_{\text{KL}}(\cdot \cdot)$		Kullback-Leibler divergence of two probability distributions
$d(\mathbf{p}, \mathbf{o})$		Distance between two observations \mathbf{p} and \mathbf{o}
$\text{dim}(\cdot)$		Dimension of input variable
$\mathbb{E}[\cdot]$		Expected value operator
$\text{Var}[\cdot]$		Variance operator
$\det \mathbf{Q}$		Determinant of matrix \mathbf{Q}
$\log(\cdot)$		Natural logarithm
$\mathbf{f}(\mathbf{x}, u)$		State derivative functions of a general nonlinear system
$\mathbf{f}(\mathbf{X}_t)$		Drift term of stochastic system
$\mathbf{g}(\mathbf{x}, u)$		Output function of a general nonlinear system
$\mathbf{g}(\mathbf{X}_t)$		Output term of stochastic system
$\frac{\partial}{\partial \mathbf{x}}$		Partial derivative with respect to each component of the vector \mathbf{x}
$h_1(\mathbf{x}, \mathbf{u}, \dot{\mathbf{u}})$		Lie-derivative
$k(\mathbf{x}_i, \mathbf{x})$		Kernel function of Support Vector Machine $k(\mathbf{x}_i, \mathbf{x}) = \phi(\mathbf{x}_i) \phi(\mathbf{x})$
$L_y(\mathbf{x}_0, \mathbf{e}_i)$		Fréchet derivative of a function y at \mathbf{x}_0 that is linear in the direction \mathbf{e}_i
$L_y^{(k)}(\cdot)$		k -th Fréchet derivative
$\text{LOF}_k(\mathbf{p})$		Local outlier factor of an observation \mathbf{p}
$\text{lrd}_k(\mathbf{p})$		Local reach-ability density of an observation \mathbf{p}
$\max_i(x_i)$		Maximum operator that selects maximal x_i across i
$\max(\cdot, \cdot)$		Maximum operator that selects the maximum of two inputs
$N_k(\mathbf{p})$		k -distance neighborhood of an observation \mathbf{p} that contains every observation vector whose distance to \mathbf{p} is less than or equal to the distance $D^k(\mathbf{p})$
$ N_k(\mathbf{p}) $		Number of elements in the k -distance neighborhood of \mathbf{p}
$\mathcal{N}(a; b, c)$		Gaussian distribution for variable a with mean b and variance c
$o(\cdot)$		Rest term
$\text{reach-dist}_k(\mathbf{p}, \mathbf{o})$		Reachability distance of an observation \mathbf{p} with respect to an observation \mathbf{o}
$\text{sup}(\cdot)$		Supremum operator
$\mathbf{v}(\cdot)$		Transformation function of random variable of Variational Autoencoder

Formula Symbols	Unit	Description
$\Gamma(t, \mathbf{x}_0)$		Intermediate calculation quantity of observability analysis
$\sigma(\mathbf{X}_t)$		Diffusion term of stochastic system
$\phi(\mathbf{x})$		Kernel transformation of vector \mathbf{x}
$\Psi(t_1, t_0)$		State-transition matrix from time t_1 to t_2
$\text{rank}(\cdot)$		Rank of a matrix
$\nabla_{\theta, \phi} \mathcal{L}_{\theta, \phi}(\mathbf{x})$		Gradient of Evidence Lower Bound of Variational Autoencoder $\mathcal{L}_{\theta, \phi}(\mathbf{x})$ with respect to the parameters θ and ϕ

1 Introduction and Motivation

1.1 Motivation

Driving safety and comfort are mainly influenced by the chassis system [1, p. 8]. Some main components of the chassis system are wheels, wheel carriers and bearings, brakes, springs, dampers, anti-roll bar and the steering system [1, p. 1]. An optimal setting of the chassis system results in a quick, predictable and precise reaction of the vehicle to the driver input [1, p. 8]. Therefore, the chassis system is an important factor for controlling the vehicle and avoiding critical driving situations [1, p. 8]. Especially dampers have a significant impact on driving safety and driving comfort [1, p. 69]. Guba et al. [2] analyze the impact of worn dampers on the vehicle stability. The characteristic curve of worn dampers of a Jeep Grand Cherokee with a mileage of 166 000 km was measured on a testbench and was implemented in a vehicle simulation. These worn dampers resulted in a 10 % increase of roll velocity for a J-turn maneuver at $64 \frac{\text{km}}{\text{h}}$ compared to new dampers. Defective dampers with 25 % of their initial damping force even resulted in a rollover. Bedük et al. [3] demonstrate similar effects of damper failures on the vehicle stability, even though ESC interventions prevent total instability. Dampers and springs are some of the most frequent deficient components, reported by TÜV Süd [4]. While only 0.2 % of vehicles with an age of up to 3 years have deficiencies of springs or dampers, the relative amount grows with increasing vehicle age: 0.6 % of vehicles up to 5 years, 1.9 % of vehicles up to 7 years, 3.7 % of vehicles up to 9 years and 5 % of vehicles up to 11 years. Therefore, assessing the health state of the chassis system is important. Up to now, this is performed by regular service and maintenance activities as well as Periodical Technical Inspection (PTI) that is conducted by a technical service association. In addition, the driver implicitly monitors the state of health of the vehicle while driving. These monitoring instances are in contrast to future trends in automobile usage.

Figure 1.1 shows a summary of trends and opportunities within the automotive industry that are influencing chassis system diagnosis. Future vehicles will be electric, autonomous, shared and connected [5, 6, 7]. Each of these trends already offers challenges and opportunities within its directly related technical domain. However, these trends also require changes and adjustments within other areas, such as the chassis system.

The trend of electric vehicles requires less service and maintenance because e.g. the powertrain does not require oil changes [8, p. 7]. If service activities of the vehicle are reduced, the number of inspections of other subsystems such as the chassis system is also likely to be reduced.

The trend of autonomous vehicles requires to monitor the vehicle's health state to ensure a safe operation. However, there is no human monitoring instance for the behavior of the vehicle. Increasing service activities or PTI increase costs, still imply periods of unmonitored driving between inspections and is in contrast with reduced service activities of electric vehicles. Therefore, the vehicle's health state needs to be monitored continuously by a technical system.

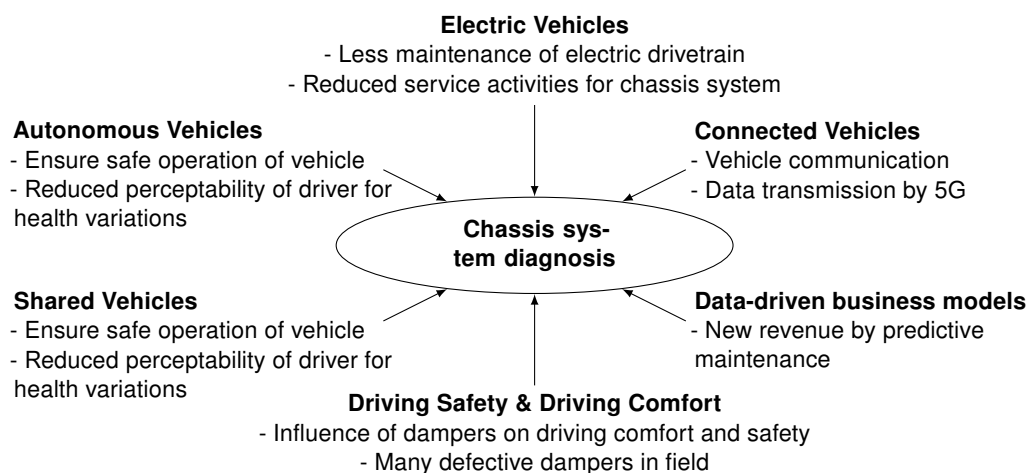


Figure 1.1: Automotive trends and opportunities with its impact on damper diagnosis

Shared vehicles have different users and an individual driver's perception for variations of the vehicle's health state is reduced. Therefore, ensuring driving comfort and driving safety of shared vehicles is facing identical issues as for autonomous vehicles.

Connected vehicles will communicate with other instances. This also implies network-based Vehicle-to-Network communication with servers [9, p. 4]. 5G cellular technology will enable faster and more reliable communication of the vehicle with other instances [9, p. 6]. Improved network communication enables cloud-based applications and services [9, p. 3].

Data-driven business models for connected vehicles are analyzed by Seiberth and Gruendinger [10]. Predictive maintenance is part of the connected-car services [10, p. 25] and is considered to be a key technology of the future [11]. Bertoncello et al. [12, p. 7 & p. 18] state that 73 % of automotive consumers globally are willing to pay for predictive maintenance. In combination with a high willingness of the customers to share technical vehicle data [12, p. 16], predictive maintenance is a use-case for supplying tailored advertisement e.g. for spare parts [12, p. 25]. A study of the changing automotive aftermarket was published by McKinsey in 2017 [13]. Predictive maintenance and remote on-board diagnostics are regarded as game changing opportunities for automotive suppliers to increase their revenue [13, p. 19]. Remote diagnostic is considered a high-margin opportunity within the trend of accessing car-generated data [13, p. 22].

Up to now, literature has focused on model- or signal-based diagnosis methods such as [14, 15, 16, 17]. However, there is no such system deployed in series production cars for monitoring the health state of the chassis system during driving. Model-based approaches are more accurate than machine learning-based approaches if a precise mathematical model is available [18, p. 7]. However, it is often difficult to find these models due to the system's complexity and uncertainty [18, p. 7]. In contrast to conventional approaches, machine learning-based approaches are better modifiable and its performance improves with increasing data [18, p. 8, 19, p. 1]. Increasing computing power, increasing data size and deep learning research made it possible for machine learning and especially deep learning methods to be applied to various machine health monitoring tasks in recent years [20]. Figure 1.2 shows the number of publications per year that are listed in the literature database Scopus [21] when searching for "Machine Learning", "Deep Learning" and "Model based" fault detection and diagnosis approaches in the field of engineering. While there is an almost linear trend concerning the number of publications dealing with model-based diagnosis, the number of publications using approaches of machine learning or deep learning has been growing exponentially in recent years.

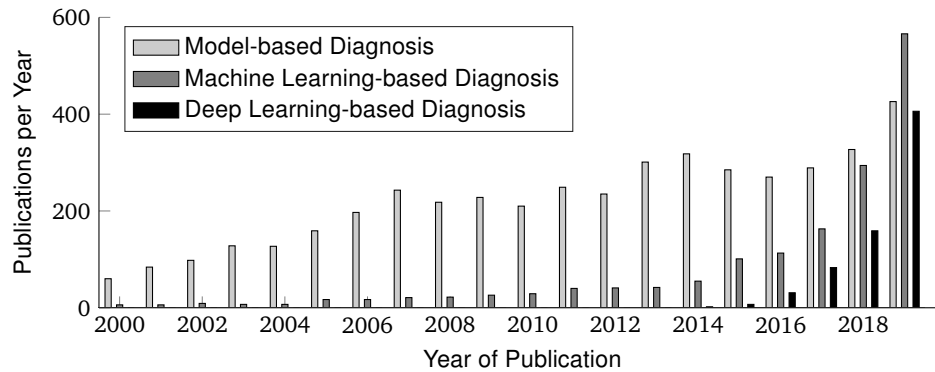


Figure 1.2: Number of Scopus [21] publications per year that deal with fault detection in the field of engineering¹

1.2 Objective of the Thesis

The objective of this thesis is the analysis of the suitability of Machine Learning (ML) methods for monitoring the health state of automotive dampers. While detecting defects is important for all chassis system components, this thesis analyzes the diagnosis of damper defects as a first step towards predictive maintenance of the chassis system.

1.3 Structure of the Thesis

Figure 1.3 visualizes the structure of the thesis, starting with automotive trends and opportunities outlined in Chapter 1. The changes of the vehicle usage and the automotive industry result in the necessity of new diagnosis approaches for chassis system components.

Chapter 2 gives a general introduction into fault detection and diagnosis as well as predictive maintenance. Existing damper diagnosis approaches are reviewed and categorized into model-based, signal-based and machine learning diagnosis approaches. Required sensor signals of these approaches are identified for assessing each method's applicability on series production vehicles. Reviewing existing diagnosis approaches of brakes, springs and sensors shows that these chassis system diagnosis approaches are mostly model-based. Machine learning concepts are introduced and their performance in other technical domains is presented. The criticism of the state of the art serves as basis for the derivation of this thesis' research topic.

Chapter 3 analyzes the observability of variations of the damping characteristic with an unknown road excitation. This observability analysis serves as justification of applying a diagnosis approach without measuring the road excitation. Theoretical insights are generated that can be used to improve the performance of damper defect detection algorithms.

Chapter 4 contains the overall analysis of this thesis. Advantages and disadvantages of various machine learning concepts are discussed and suitable concepts are identified. This is followed

¹exact search terms for Scopus are:

"TITLE-ABS-KEY("model based" AND (fault OR failure) AND (diagnosis OR detection)) AND (LIMIT-TO(SUBJAREA,"ENGI"))"

"TITLE-ABS-KEY("machine learning" AND (fault OR failure) AND (diagnosis OR detection)) AND (LIMIT-TO(SUBJAREA,"ENGI"))"

"TITLE-ABS-KEY("deep learning" AND (fault OR failure) AND (diagnosis OR detection)) AND (LIMIT-TO(SUBJAREA,"ENGI"))"

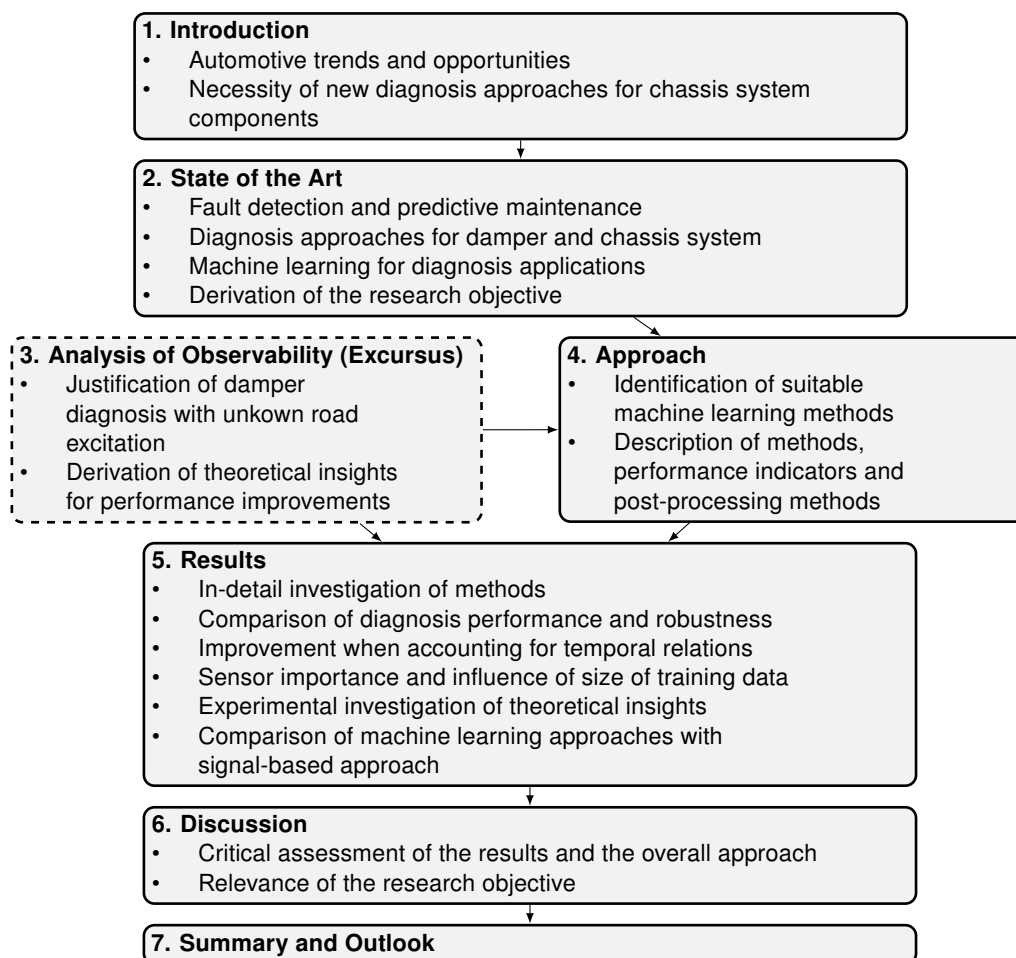


Figure 1.3: Structure of the thesis

by a detailed explanation of the applied machine learning methods. Appropriate performance evaluation metrics are identified that enable a quantitative comparison of supervised and unsupervised learning methods. Finally, post-processing methods that account for the temporal behavior of driving data are identified and explained.

Chapter 5 presents the results of this thesis. The implemented damper faults and the resulting dataset are explained. Characteristics of the generated features as well as performed data transformations of the machine learning concepts are investigated. The diagnosis performances of the applied methods are compared and an analysis of the robustness of the results is conducted. Performance improvements of temporal post-processing methods are investigated afterwards. The importance of the available sensor signals as well as the influence of the size of the training data is analyzed. That is followed by an experimental investigation of the generated theoretical insights of the observability analysis from Chapter 3. Finally, the performance of machine learning approaches is compared to an existing signal-based approach.

Chapter 6 evaluates the results by answering the research objective from Chapter 2. This is followed by a critical assessment of the overall approach as well as a discussion of the relevance of the research objective with regard to the scientific and the technical contribution, as well as the relevance for society. The thesis closes with a summary and outlook in Chapter 7.

2 State of the Art

This chapter reviews the state of the art with regard to existing approaches of damper defect detection. First, a general introduction into predictive maintenance as well as fault detection and diagnosis is given. This is followed by a review of existing damper diagnosis approaches. Reviewing diagnosis approaches of other chassis system components afterwards gives an overview of diagnosis methods within the same environmental circumstances. The next section gives a general introduction to machine learning and its evolution in the context of fault diagnosis. An overview of machine learning methods that are used for fault diagnosis with their strengths and limitations is provided. Reviewing commercial diagnosis systems for automotive applications shows discrepancy between research activities in academia and commercial implementations. Based on a criticism of the state of the art, the research objectives of this thesis are derived.

2.1 Terminologies for Fault Detection and Predictive Maintenance

Maintenance techniques can be divided into three types, known as reactive maintenance, preventive maintenance and predictive maintenance [22, p. 5]. These maintenance types are explained in [22, pp. 6-9] as follows: *Reactive maintenance* denotes that no maintenance is applied. Measures are only performed if a machine has failed completely. This concept is only used for non-critical machines. *Preventive maintenance* applies regular inspections or maintenance to a machine. Up until now, this is the typical process for vehicles. The chassis system is inspected on a regular basis and some components are replaced on a regular interval (such as engine oil). *Predictive maintenance* schedules maintenance actions according to the condition of a machine. Actions are taken when certain behaviors are detected that are known to result in failures in the future [23, p. 1]. Predictive maintenance is more economic and safer in the long run compared to preventive maintenance because maintenance actions can be scheduled according to available resources and downtime is reduced [22, p. 8].

Terminologies in the field of fault detection and diagnosis are given by Isermann and Ballé [24, p. 2] and are explained in [25, pp. 3-4]. A *fault* represents an “unpermitted deviation of at least one characteristic property or parameter of the system from the acceptable / usual / standard condition” [24, p. 2]. An *incipient fault* is initially almost unnoticed and develops slowly [25, p. 3]. A fault does not significantly affect the normal behavior of the system [25, p. 3]. Compared to a fault, a *failure* is a serious breakdown of a component and represents a permanent interruption of the system’s performance [24, p. 2, 25, p. 3]. To prevent a fault from leading to a serious failure, it is important to detect an existing fault as early as possible [25, p. 4]. The implementation of diagnosis methods that detect incipient faults early, provides enough time for maintenance or service activities [26, p. 2]. *Fault detection* determines whether a fault is present in a system [24, p. 2, 25, p. 4]. *Fault isolation* determines the location of the fault and *fault identification* estimates

the size of the fault [24, p. 2, 25, p. 4]. *Fault diagnosis* is a combination of fault isolation and fault identification [24, p. 2]. According to [25, p. 4] fault diagnosis is often named Fault Detection and Isolation (FDI). FDI is a must-have for all practical implementations of technical systems [27, p. 29]. Saufi et al. [28, p. 3] add Remaining Useful Life (RUL) prediction as fourth stage of fault diagnosis methods. These methods estimate the remaining lifetime of a component until its breakdown.

2.2 General Concepts of Diagnosis Methods

Figure 2.1 shows a categorization of quantitative diagnostic methods, based on [29, 30, 31, 32]. Venkatasubramanian et al. [30] categorize quantitative diagnostic methods into model-based and process history-based methods. Gao et al. [31] categorize diagnostic methods into model-based methods, signal-based methods, knowledge-based methods, hybrid methods and active fault diagnosis methods. Model-based approaches (Figure 2.2(a)) use a process or system model in the form of mathematical equations in combination with known input signals and measured output signals [26, p. 4]. Internal state estimates, parameter estimates or residuals are used as fault symptoms and are compared to their nominal fault-free values [26, p. 4]. Frequently used model-based approaches are observer-based methods, parity space-based residual generation methods, stochastic model-based fault diagnosis methods such as Kalman filters and parameter estimation methods [30, p. 8, 31]. Signal-based diagnosis methods (Figure 2.2(b)) monitor measured output signals without applying knowledge from input-output models of the system [31, p. 6]. These approaches generate symptoms using time-domain, frequency-domain or time-frequency-domain methods [31, p. 6]. Time-domain methods typically monitor signal features such as mean, standard deviation or slope [31, p. 6]. Frequency-domain methods monitor signal spectra that are generated using e.g. the FFT [31, p. 7]. Time-frequency-based methods are used for monitoring of dynamic signals. Typical methods are the Short-Time Fourier Transformation (STFT) or Wavelet Transformation (WT) [31, p. 7]. Process history-based methods, reviewed by Venkatasubramanian et al. in [29], and knowledge-based methods, reviewed by Gao et al. in [32], use identical assumptions of the availability of information about the diagnosed system: A large amount of historical process data needs to be available [29, p. 1, 32, p. 1]. Therefore, knowledge-based fault diagnosis is also known as data-driven fault diagnosis (Figure 2.2(c)) [32, p. 1]. Typical methods for quantitative data-driven fault diagnosis are statistical methods [29, p. 2] and machine learning techniques [32, p. 1]. Hybrid methods combine model-based, signal-based and data-driven approaches [32, p. 4]. Active fault diagnosis methods stimulate a system with an input signal that allows a good recognition of normal and fault conditions [32, p. 5]. Due to their increased complexity, hybrid and active fault diagnosis methods are not further reviewed in this thesis.

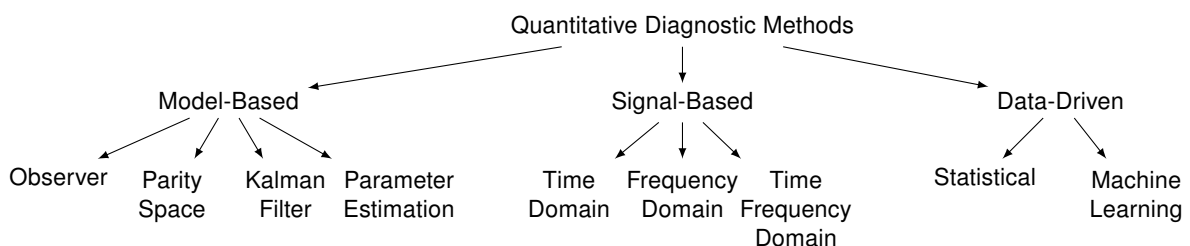


Figure 2.1: Categorization of quantitative diagnostic methods, based on [29, 30, 31, 32]

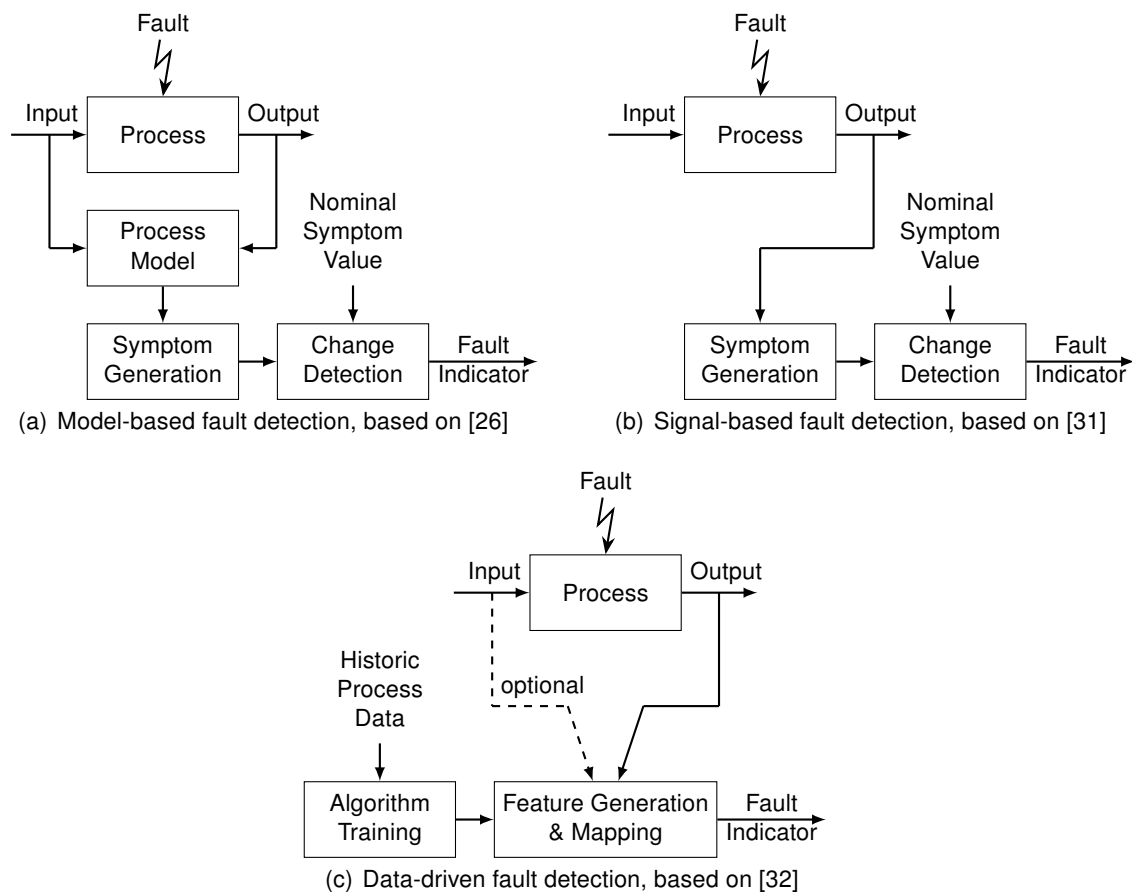


Figure 2.2: General schemes of fault detection methods

2.3 Chassis System Fault Diagnosis

This section provides an overview of existing approaches for the diagnosis of dampers and other chassis system components. The approaches to damper diagnosis are then summarized in terms of the applied diagnosis concept, the source of data that is used to prove their effectiveness and the required measurement signals. After considering further diagnosis approaches of other chassis system components, a time-based trend of the applied diagnosis methods is visualized.

2.3.1 Damper Fault Diagnosis

This section gives a chronological review of approaches for damper diagnosis. The distinction of publications that are relevant for diagnosis and those that are not is not always obvious for publications that deal with the estimation of the damping force. While the purpose of these approaches is not directly related to health monitoring of the dampers, the information could still be used for this purpose. Publications that rely on an internal damper model, such as [33, 34, 35, 36, 37, 38, 39, 40], are not further reviewed within this thesis because they rely on known model parameters for the damping forces estimation. Methods that are based on testing procedures that need to be performed by workshops such as [41, 42] are also not further investigated because these testing procedures cannot be performed during driving.

Already in 1992, Bußhardt et al. [43] present a method for the diagnosis of dampers resulting in a patent [44]. A model-based approach that uses a quarter-vehicle model is applied for the

estimation of the damping coefficient and other suspension system characteristics such as the vertical tire stiffness. The presented approach requires the measurement of the vertical dynamics such as the vertical body or tire acceleration. The effectiveness is proven both by simulation and by test bench measurements.

In 1993, Leonhardt et al. [45] propose a method for the classification of the state of a semi-active damper. Parameters of a simplified quarter-vehicle model are estimated using a recursive least squares algorithm, based on vertical dynamics sensors. The estimated parameters are then classified using a neural network. The effectiveness of the proposed approach is demonstrated using data from two vertical vehicle dynamics test benches.

In 1997, Weispfenning [46] proposes a parameter estimator for the detection of chassis system component faults. Based on a quarter-vehicle model, a model-based parameter estimation of the damping and stiffness coefficient as well as the coulomb friction of the suspension system is performed. The required measurements are vertical vehicle body acceleration as well as the suspension deflection. The effectiveness of the approach is demonstrated using driving data.

In 1998, Hardier [47] deploys a neural network to reconstruct the nonlinear behavior of the damper's force-velocity hysteresis. Measurements of the vehicle body's vertical acceleration as well as of the suspension deflection are used as input signals for a recurrent neural network. The performed estimation is able to distinguish worn and new damper conditions. The effectiveness of the approach is shown for a simulation model that consists of a quarter-vehicle model including a hysteresis model of a damper.

In 2002, Börner et al. [48] extend the parameter estimation approach of [46]. The estimated parameters are mapped to fault cases using a neural network. Required measurements are still the vertical vehicle body acceleration and suspension deflection. Driving data was used to show the effectiveness of the approach.

Also in 2002, Jautze [17] presents a signal-based algorithm for detecting damper defects based on wheel speed information. He shows that the wheel speed signal is influenced by the performance of the damper. An abstract index that indicates the damper health is generated by comparing the amplitude of the wheel speed signal at different frequencies. The monitored frequencies are the eigenfrequency of the vertical dynamics of the unsprung mass (around 10 Hz) as well as a given reference frequency (20 Hz or higher). A dependency of this index from the vehicle speed as well as road excitation remains. Even though this approach was invented in cooperation with an Original Equipment Manufacturer (OEM), this method is not applied in series production cars.

In 2007 and 2009, Azadi and Soltani [49, 50] analyze the vertical acceleration of the vehicle's body and tire when the vehicle is excited using a four-post rig. Two component defects are examined: a defective damper and a defective bushing. The authors show that the defects can be identified by investigating the wheel speed signal's frequency response using a Wavelet Transformation (WT). However, a specific diagnosis concept is not developed.

In 2008, Metallidis et al. [51] propose the estimation of parameters using an observer that is based on a finite-element model. A similar approach was already presented in 2003 by Metallidis et al. [52]. Damper defects are indicated by variations of the estimated parameters compared to the healthy condition. Even though the finite-element model is reduced in size, it still consists of 239 degrees of freedom. Required measurements are the four vertical accelerations at the upper strut mounts of the vehicle. The approach is tested in simulation.

Figure 2.3 visualizes the damper diagnosis publications from the years 2008 to 2019 chrono-

logically. Ventura et al. [53] and Ferreira et al. [54] criticized in 2008 and 2009 that until then there was no precise method for detecting damper defects that would work in normal vehicle operation. They suggest two different methodologies: An analysis of the quarter-vehicle model in the frequency domain results in a transmissibility index of the vertical acceleration of the tire that of the vehicle body. This index is dependent on the damping coefficient. The second method analyzes the transmissibility of the vertical body acceleration to the damper's internal pressure. Both methods are tested using real driving data. It is claimed that both generated indices are a good indicator for the damper health state. However, a specific defect detection metric that is based on the generated indices is not presented. The authors claim that measuring the required quantities of vertical accelerations and damper internal pressure is easy and cost-efficient. However, it seemed to be too complicated or too expensive in reality and the approach was not adopted in series production vehicles.

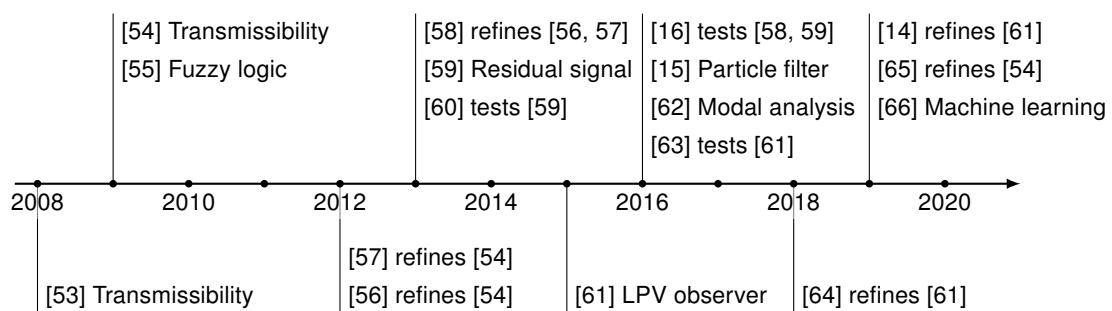


Figure 2.3: Damper diagnosis publications from the years 2008 to 2019 with their interconnections

Liu et al. [55] use fuzzy methods for fault detection in 2009. Details of the method are left open to the reader and the evaluation of the effectiveness of the proposed approach is lacking in-depth analysis. Real driving data is used. A required measurement signal is the vehicle body's vertical acceleration among others.

In 2012, Lozoya-Santos et al. [56, 57] improve the algorithm of [54] so that the requirement to measure the vertical acceleration is replaced with sensing suspension deflection travel and suspension deflection velocity. Their approach is compared with the approach using vertical acceleration measurement. The internal damper model is extended to account for variations of the electric current of magneto-rheologic dampers. The proposed algorithm is tested in simulation. The misclassification is around 26% when using acceleration measurements, and around 34% when using only suspension deflection sensors. In 2013, Hernandez-Alcantara et al. [58] further refine the approach. The transmissibility index is estimated at the vehicle body's vertical eigenfrequency which requires a selective band-pass filter. Even though the presented simulations are concluded as promising results by the authors, varying conditions of a real vehicle might be challenging for the parametrization of this approach.

From 2012 to 2015, the French national project INOVE ANR 2010 BLAN 0308 [67] dealt with fault-tolerant control and diagnosis of damper defects [59, 60]. Within the context of this project, a vehicle on a scale of 1:5 was developed for testing of fault detection approaches. This prototype is also used as testing facility in other publications.

In 2013, Tudon-Martinez et al. [59] generate a residual signal that is sensitive to damper faults but insensitive to exogenous inputs such as the road excitation. The required measurement signals are the vertical acceleration of the vehicle body and tire as well as the suspension deflection travel. The effectiveness of the approach is demonstrated in simulation. Hardware-In-The-Loop (HIL) tests of this approach are conducted in [60] but are still based on the simulation of a

quarter-vehicle model.

The approach in [59] is compared to the transmissibility index approach in [58] by Hernandez-Alcantara et al. [16] using the 1:5 scaled vehicle of the INOVE project [67] on a 4-post test rig in 2016. The road excitation is an ISO8608 [68] Type D road excitation. Defective dampers are simulated by varying the control input of the vehicle's semi-active dampers. The residual approach [59] results in a higher accuracy but has a higher implementation effort. The transmissibility approach [58] is more robust to road excitation.

In 2015, Tudón-Martínez and Morales-Menendez [61] deploy a Linear Parameter Varying (LPV) H_∞ -observer. The approach is based on a quarter-vehicle model with suspension deflection travel and suspension deflection velocity as measurement input. The algorithm is based on the methods presented in [69, 70]. The effectiveness of this method is shown using simulations with sinusoidal road excitation. A similar approach is compared with two other types of observers by Nguyen et al. [63] using a simulation with a sinusoidal road excitation. However, the comparison does not generate deeper insights into the investigated approaches.

In 2016, Alcantara et al. [15] use a particle filter that is based on a quarter-vehicle model. Measurement quantities are the vertical acceleration of the vehicle body and of the tire, suspension deflection travel and suspension deflection velocity as well as damper force and the non-linear component of the damper force. The effectiveness of the approach is analyzed in simulation using different road profiles. The accuracy depends on the parametrization of the particle filter and improves with using more particles. According to the authors, the computing time of this approach is challenging.

Also in 2016, Hamed [62] conducts modal analysis of vibration signals for damper defect detection using driving data. He states that online condition monitoring for an automotive suspension is possible using the proposed approach. However, the vertical acceleration is measured with a sampling rate of up to 7 kHz which is far from a series vehicle's sensor set.

In 2018, Morato et al. [64, 14] present a similar approach as Tudón-Martínez and Morales-Menendez [61]. An LPV observer-based method for the detection of defects in electro-rheological dampers based on a quarter-vehicle model is proposed. The required measurement quantities are vertical body acceleration as well as suspension deflection travel. The road excitation is estimated, which requires some model-based knowledge of the road excitation profile. The effectiveness of the approach is demonstrated in simulation in [64] as well as using a 4-post test bench with the 1:5 scaled vehicle of the INOVE project [67] in [14]. Even though the authors conclude that the approach is able to efficiently estimate a state of health of the damper, it should be mentioned that the chosen sinusoidal road excitation at the test bench is identical to the implemented sinusoidal road excitation model in the estimator algorithm. The effectiveness of the presented approach for the case of a real stochastic road excitation is not investigated.

In 2018 a patent [71] shows a similar approach as in [17] of detecting a defective damper by analyzing the wheel speed signal when driving over a significant road excitation such as a bump. The decaying behavior of the wheel speed shall be compared to a reference signal that was gathered with intact dampers. The reference signal may be either another tire from the same vehicle, historical data or measurements from other vehicles that have driven over the same bump. An actual implementation of this approach is not known to the author. Many implementation details are left open in this patent. It seems challenging due to the high variability in the usage of a vehicle.

In 2019, Savaresi et al. [65] propose an approach for the estimation of the reference current of

semi-active dampers based on the transmissibility of tire vertical acceleration and vehicle body acceleration. The approach is similar to [54], but the implementation in [65] enables an online damper diagnosis. The approach is tested using real driving data.

Also in 2019, Shahab and Moavenian [66] propose a Machine Learning (ML)-based Fault Detection and Isolation (FDI) approach for an active suspension system. Residuals of the measured signals compared to a simulated fault-free quarter-vehicle model are calculated. Afterwards, statistical and frequency-based properties of these residuals are fed into a classification algorithm that diagnoses the fault. The approach requires the measurement of the vehicle body displacement, the vehicle body acceleration, the suspension deflection travel, the force of the active suspension actuator and the road excitation. The investigated suspension faults are, among others, variations of the tire and body spring stiffness as well as of the body damping coefficient. The approach is tested using a quarter-vehicle model simulation and faults are induced by deviations of the corresponding linear parameters.

Figure 2.4 shows a categorization of the investigated existing approaches for detecting damper defects. 16 out of 26 approaches are model-based and only three publications use machine learning methods. Except for the approach of Jautze [17], all methods rely on the vertical dynamics of a quarter-vehicle model and require measurements of the vertical accelerations of the vehicle body, tires or both. Therefore they are not applicable if only ESC sensor signals are used. The damper health indicator that is generated by Jautze [17] is speed-dependent and was never applied in series production vehicles, even though, it was invented in cooperation with an OEM. Therefore, its real world suitability is questionable. 14 approaches are tested in simulation and four approaches are tested on a test bench with a synthetic road excitation profile. Only eight approaches are tested on the basis of real driving data with only Savaresi et al. [65] reporting a larger dataset that consists of 21 h of driving.

	ESC sensors	ESC + vertical dynamics sensors	ESC sensors	ESC + vertical dynamics sensors	ESC sensors	ESC + vertical dynamics sensors
Driving Data		[46] [48] [55] [62] [65]	[17]	[53] [54]		
Test Bench		[43] [14]		[16]		[45]
Simulation		[52] [51] [56] [57] [59] [60] [61] [15] [64]		[49] [50] [58]		[47] [66]
	Model-based		Signal-based		Machine Learning	

Figure 2.4: Categorization of existing approaches for damper diagnosis

2.3.2 Fault Diagnosis of Other Chassis System Components

This section investigates diagnosis methods of other chassis system components such as springs, brakes or sensors. Besides the damper diagnosis approach, Weispenning [46] and Börner et al. [48] demonstrate various further diagnosis approaches. Parity equations are applied for the detection of sensor faults. Hereby, a residual is calculated that is based on the transfer function of the vehicle body acceleration to the suspension deflection travel. Another diagnosis approach is the analysis of the spectrum of the vertical tire acceleration to detect tire pressure fluctuations. Lastly, a model-based diagnosis of Anti-lock Braking System (ABS) solenoid valves is presented. The stroke of the valve is reconstructed using a mathematical model of the magnetic flux based on the measured electric current and voltage. A defective valve is detected if the difference of the reconstructed stroke and its nominal trajectory exceeds a certain threshold. However, all approaches, except for the ABS diagnosis approach, require vertical acceleration sensors. Moreover, the approaches are only presented conceptually. A deeper investigation regarding robustness or an actual implementation are not demonstrated.

Spring Faults

Wang and Yin [72] propose a data-driven clustering-based fault detection approach for springs. Identical failure types with different failure strengths lie on one “fault line” in a hyper-dimensional feature space and each type of failure results in a specific fault line. These fault lines are generated based on the approach presented in [73]. The distance of the current health state from the “intact” cluster represents the failure strength. New fault types are detected based on the association of an observation to the existing fault lines. Vertical acceleration sensors are required at each corner of the vehicle body. The effectiveness is analyzed in simulation for reductions of the spring stiffness by 30 % to 80 % of the nominal value. A continued development of [72] is presented in [74]. The required measurements are changed to vertical accelerations of the wheels. It should be noted that the analyzed failures are far from a realistic failure scenario of an automotive chassis system [75, pp. 11-14].

Brake System Faults

Pisu et al. [76] present an FDI system based on multiple model-based residuals. These residuals are evaluated using a subsystem evaluation unit. The effectiveness of the approach is tested for a brake-by-wire system.

Jegadeeshwaran and Sugumaran [77] use a ML approach for the diagnosis of automotive brake system failures. Decision trees classify features that are calculated based on acceleration measurements. Nine different failure types are emulated using a rigid axle and an accuracy of above 97 % is reached. Continuation developments are presented in [78, 79, 80]. However, the proposed system does not run inside the vehicle. The axle is mounted on a test bench. The acceleration sensors are mounted on the rigid axle and are logged with 102.4 kHz, which is far from a series production automotive sensor sampling rate.

Sensor Faults

Schwall et al. [81] and Schwall and Gerdes [82] propose an approach to generate and analyze residuals for the diagnosis of vehicle and sensor faults. The residuals are generated using three different models: a bicycle model, a model of the yaw rate dependency on the wheel speeds, and

a longitudinal slip model. A Bayesian network analyzes the residuals. Required sensor signals are wheel speeds, yaw rate and steering angle. The analyzed failure types are malfunctions of the sensors as well as physical tire failures. A prototypical implementation is presented in [83].

Börner and Isermann [84] use residuals for the detection of sensor faults. A fuzzy logic is applied for fault classification.

Fischer et al. [85] present a diagnosis scheme for a semi-active suspension system. Parameters are estimated and residuals are calculated using the Local Linear Model Tree (LOLIMOT) method. Faults are classified using a simple table that connects symptoms and faults. In 2007, Fischer et al. [86] present a similar approach for lateral and vertical vehicle dynamics sensor faults. Residuals of various parity equations for yaw rate, lateral acceleration and steering wheel angle are calculated. A fuzzy logic is applied for the detection of sensor faults.

Unger and Isermann [87] propose a method for detecting faults of the lateral acceleration and yaw rate sensors. The measurement values are estimated using a model-based approach as well as the LOLIMOT approach. The reconstructed values are compared to the actual measured values and residuals are calculated.

González et al. [88] present an approach similar to [87] for the diagnosis of vehicle dynamics sensor faults. Residuals are generated by comparing the actual measurements of the vehicle dynamics sensors to a model-based reconstruction of the corresponding sensor readings. A fuzzy system is then applied for threshold monitoring of the residuals and a neural network is used for fault classification. Details of the neural network are not presented in the publication. Further development is presented in [89, 90, 91]. González et al. [90] use an auto-associative neural network (Autoencoder) to reconstruct the measurement signal. A residual is generated by comparing the original and the reconstructed signal. In [91], the fuzzy system classifier is replaced by a multiclass-SVM.

Zhang and Pisu [92] compare two FDI approaches for the detection of steering angle actuator faults as well as yaw rate sensor faults. One approach uses parity equations for the generation of a residual while the second approach uses a Sliding Mode Observer (SMO) for residual generation.

Haffner et al. [93] use model-based reconstructions of sensor signals for the generation of residuals. Fault detection is performed based on a simple logic table that connects these residuals with sensor failures of yaw rate, lateral acceleration and steering wheel angle.

Kim and Lee [94] propose a model-based approach for the detection of vertical body acceleration sensor faults. Multiple models are combined to calculate multiple residuals. The fault detection is based on decision rules.

In the context of the INOVE project [67], Varrier et al. [95] suggest to calculate residuals for the detection of yaw rate sensor faults using the parity-space method of [96]. A similar approach is presented by the same author in [97, 98] for lateral acceleration sensor faults. An H_∞ -observer for the detection of defective vertical acceleration sensors of the vehicle body and the wheels is presented in [69].

Jeong et al. [99] propose a residual based approach for the diagnosis of vehicle dynamics sensors and actuators for automated vehicles. A residual for the measured yaw rate is generated using a bicycle model. To account for parameter uncertainties, five differently parameterized models are used. The generated residuals are compared with adaptive thresholds for fault detection. Lin et al. [100] propose a similar approach as [99]. Various residuals are generated by comparing measured sensor signals with model-based reconstructions of the corresponding

sensor values. These residuals are compared to adaptive thresholds. A fault is detected using a simple table that connects residuals and sensor faults.

Na et al. [101] use a residual-based approach for sensor fault detection. Twelve residuals are calculated based on a bicycle model, a roll angle model and a quarter-vehicle model. The threshold values for the residuals consist of both static parts and dynamic parts based on the sensitivity of the residuals to other sensor measurements.

Jeong and Choi [102] propose a ML-based approach for the detection of vertical acceleration sensor faults. Model-based residuals of the sensor measurements are generated using an unknown input residual generator that is similar to an unknown input observer. These residuals as well as longitudinal and lateral acceleration are supplied to a SVM for fault detection. The effectiveness of the proposed approach is tested in simulation.

2.3.3 Summary of Chassis System Fault Diagnosis

The reviewed publications for chassis system diagnosis of dampers as well as other components and sensors are summarized in Figure 2.5. The used methods of each publication are categorized to show the main trends of applied diagnosis methods. Publications that use multiple methods are listed multiple times.

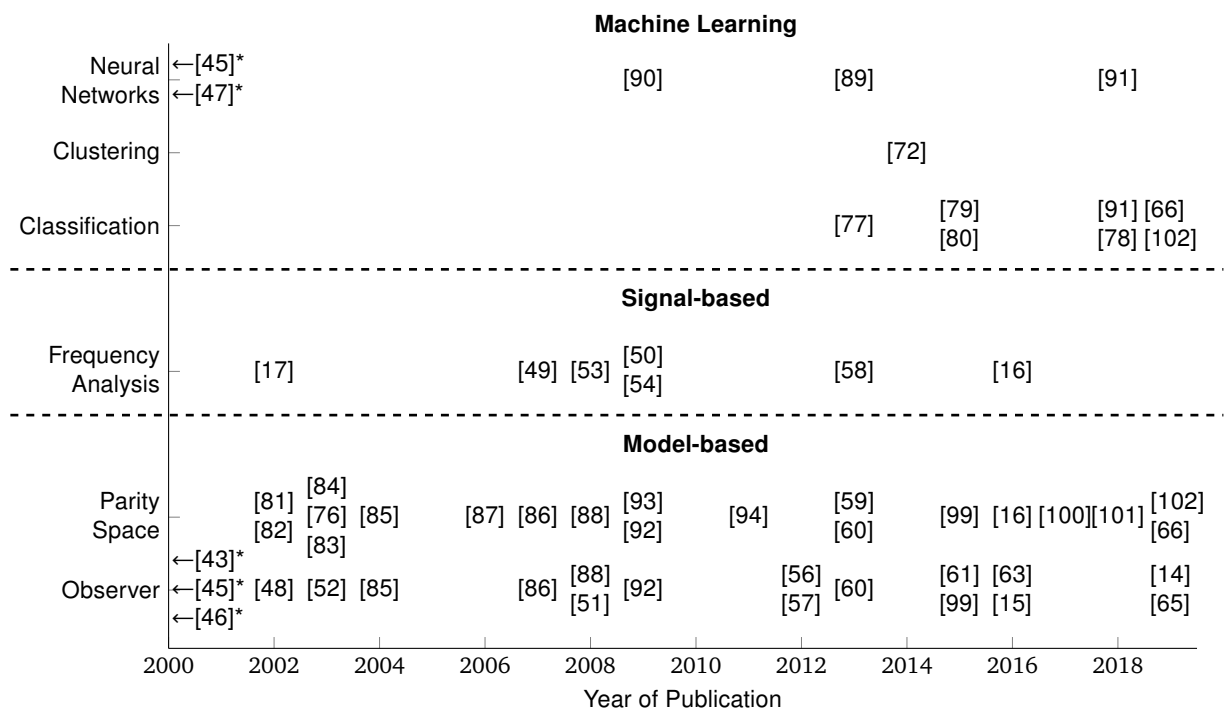


Figure 2.5: Chassis system diagnosis methods over publication time. Publications that use methods of more categories are listed multiple times.

* Publication of former years, that are shifted for visualization reasons
 [43] from 1992, [45] from 1993, [46] from 1997, [47] from 1998

Model-based approaches such as observers or parity space residual calculations are used by 39 of 59 reviewed publications. Both methods are consistently used over the last 20 years. There is no trend of a reduction of publications in these areas. The actual fault detection is often performed by applying a fuzzy logic for the classification of estimated parameters and residuals or threshold value monitoring.

Seven publications apply signal-based methods such as a frequency analysis of signals for the diagnosis of chassis system components or sensor faults. However, the number of publications that rely on frequency analyses reduced in the last ten years.

While there were three publications that used neural networks until 2012, machine learning approaches started to be used for chassis system diagnosis from 2013. So far, however, only 13 of 59 reviewed publications used machine learning methods.

2.4 Machine Learning

Subsection 2.3.3 showed that chassis system diagnosis is mainly performed using model-based approaches. Machine Learning (ML) approaches are only rarely applied for the diagnosis of chassis system components. Therefore, this section gives a general introduction to ML and its evolution in fault diagnosis. Typical methods that are applied for fault diagnosis are presented.

While there is no fixed definition of the term Machine Learning, Goodfellow et al. [103, pp. 1-2] define it as "the ability to acquire (...) knowledge, by extracting patterns from raw data". This definition includes a great variety of different types of results (knowledge) as well as a great variety of different processes for generating this knowledge. Therefore, there are several levels for a categorization of ML algorithms which are shown in the following.

Bishop divides ML based on the available training data into "supervised" and "unsupervised" learning algorithms [104, p. 3], with supervised learning being the most prevalent form [19, p. 1]. Supervised learning can be further divided into "regression" and "classification" algorithms. Unsupervised learning can be divided into "clustering", "density estimation" and "visualization" [104, p. 3]. Moya and Hush [105, p. 1] use the term "one-class classification" for algorithms that recognize new observations of the training class. Because one-class classification approaches only need observations of one class for training, they are also considered as unsupervised learning approaches.

Raw data is typically converted into features for further processing [104, p. 2]. The performance of a ML algorithm depends on the suitability of the selected features for data representation [106, p. 1, 103, p. 3]. Therefore, another categorization method is the feature generation process as presented in Figure 2.6. Shallow Machine Learning (SML) approaches use hand-crafted features. There is no defined term for machine learning methods that are not contained in Representation Learning (RL) or Deep Learning (DL). Publications such as [107, 108] use the term "Shallow Machine Learning". Herein, the mapping of the features to an output is the only step that is data-driven [103, p. 10]. However, engineering features that can extract information of a dataset is time-consuming [106, p. 1, 103, p. 1], requires domain expertise [19, p. 1] and, therefore, the right choice of features is difficult to find [103, p. 3]. Therefore, Representation Learning (RL) extends the data-driven steps to the feature generation process [103, pp. 4 & 10]. Thereby, features are generated automatically and human effort for feature engineering is not required [19, p. 1]. RL algorithms can be adapted to new tasks with minimal effort [103, p. 4]. However, the two steps of feature generation and mapping of the features to an output are still two separate steps of the data-driven training process. Therefore, Deep Learning (DL) was developed. DL approaches consist of several representation learning layers and are able to learn a more complex and high-level representation [19, 109, pp. 4-6]. Mapping of the features (mostly classification or regression) is part of the trained network. DL approaches require little manual engineering effort and can take advantage of an increasing amount of available training

data [19, p. 1]. Goodfellow et al. [103, p. 9] categorize algorithms into DL which is part of RL, which is in turn part of ML (Figure 2.6). Chollet [110, p. 4] uses a similar categorization.

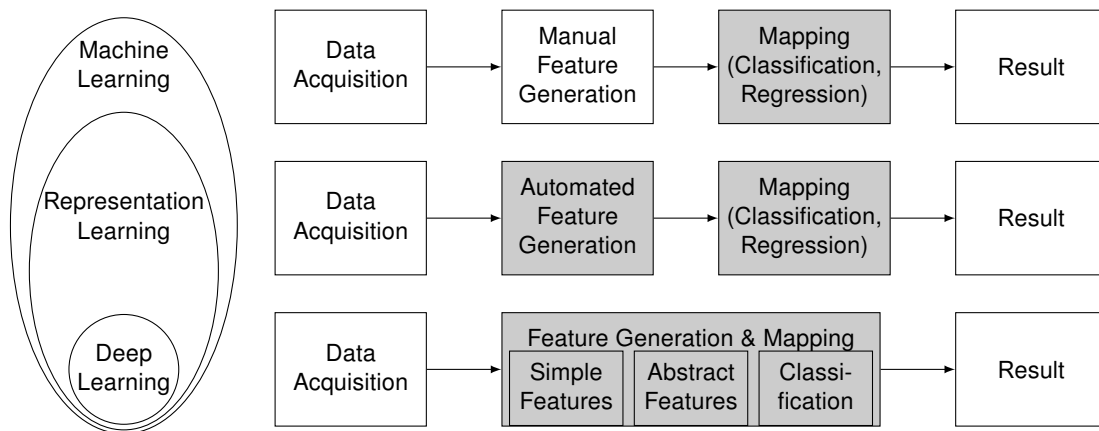


Figure 2.6: Categorization of Machine Learning, Representation Learning and Deep Learning with automated processes in gray, based on [103, pp. 8-10]

Darwish et al. [109, pp. 6-7] describe strengths and weaknesses of DL applications. DL approaches are stated to be a high-level feature extraction framework that works in a self-organizing manner. They shall provide the best solutions in fields of image recognition, speech recognition and natural language processing. It is stated that pattern recognition approaches can run in real time. Weaknesses, problems and challenges of DL methods are stated in [109, pp. 6 & 35-36]: DL methods require a great amount of training data [109, p. 6] and trained models are highly specialized to the trained application [109, p. 36]. The selection of a network architecture is not transparent and many hyper-parameters for the training process need to be selected or optimized [109, pp. 35-36]. Additionally there are high costs for an implementation in real life regarding training time and processing power [109, p. 36].

2.4.1 Evolution of Machine Learning for Fault Diagnosis

Section 2.3 showed that there is not yet a trend towards machine learning approaches in the area of automotive chassis system diagnosis. Therefore, other areas of machine health management are analyzed to further investigate the trend towards machine learning for diagnosis applications. Table 2.1 collects the main findings of eleven publications that review 892 Machine Learning (ML) methods for fault diagnosis. These findings are summarized in the following paragraphs.

ML methods are promising for dealing with industrial data [114, p. 11]. DL approaches are claimed to show good performance on fault diagnosis, degradation state detection as well as fault prognostics and it is suggested to expand the fields of application to other domains [112, p. 5]. The integration of multiple sensors may improve the fault detection performance of DL approaches [28, p. 11]. However, it is stated that the explainability of DL approaches is not well developed compared to SML approaches [117, p. 19]. It is criticized that complex component interactions are not investigated in many publications [113, p. 8]. The consideration of uncertainties within a neural network, the justification of a network selection and the integration of expert knowledge are open points for research [18, pp. 19-21]. Also appropriate benchmarks of different approaches are missing [18, p. 19]. The classification performance of SML methods is claimed to become stagnant with an increasing size of the training data [28, p. 3]. DL approaches are said to improve their performance with increasing training data [28, p. 3, 19, p. 1]. However, obtaining large datasets is challenging in industrial applications [28, p. 6]. Therefore, many

Table 2.1: Main findings of eleven publications that review ML methods for fault diagnosis

Publication	Review Basis	Findings
[111]	<ul style="list-style-type: none"> 14 ML publications of 86 in total for induction machine drives 	<ul style="list-style-type: none"> Combination of neural networks and expert knowledge may enhance the diagnosis performance
[29]	<ul style="list-style-type: none"> 31 neural network fault detection methods 	<ul style="list-style-type: none"> Neural network are robust to noise Computational complexity for online evaluation is minimal
[112]	<ul style="list-style-type: none"> Mechanical and electric equipment 29 DL approaches 	<ul style="list-style-type: none"> DL approaches show good performance on fault diagnosis, degradation state detection as well as fault prognostics Suggest to expand the fields of application to other domains
[113]	<ul style="list-style-type: none"> Bearing and gear health indication 45 ML approaches of 140 in total 	<ul style="list-style-type: none"> Only simple applications of gears and bearings are considered Complex interactions are not investigated in many publications Using signal-based health indicators as input for ML methods, instead of traditional statistical parameters improves accuracy DL methods shall be used for health monitoring
[18]	<ul style="list-style-type: none"> 63 DL approaches for system health management 	<ul style="list-style-type: none"> DL methods are successfully applied in several domains No consideration of uncertainties within a neural network, justification of a network selection and the integration of expert knowledge
[114]	<ul style="list-style-type: none"> 110 ML approaches for fault diagnosis of rotating machinery 	<ul style="list-style-type: none"> ML methods are promising for dealing with industrial data Hybrid systems that incorporate prior knowledge on failure mechanisms should be utilized to improve the diagnostic performance
[115]	<ul style="list-style-type: none"> Fault detection methods for gears, rotors and bearings 90 frequency-based methods and 27 ML methods 	<ul style="list-style-type: none"> Frequency-based methods require expert knowledge Information from multiple sensors should be merged to improve the diagnosis performance Computational complexity should be accounted for online application Robustness for real applications is unknown because many approaches are evaluated using test bench data
[20]	<ul style="list-style-type: none"> DL approaches for machine health monitoring 156 references 	<ul style="list-style-type: none"> Increasing computing power, increasing data size and research enabled to apply DL methods to machine health monitoring Performance of DL approaches depends on quality of dataset Incorporating prior domain knowledge can improve performance of DL approaches
[116]	<ul style="list-style-type: none"> 114 ML approaches for wind turbine condition monitoring 	<ul style="list-style-type: none"> Around 2/3 of the reviewed publications perform classification while the rest performs a regression Most used methods are neural networks, SVMs and decision trees Synthetically generated data may not generalize well to real-world data
[28]	<ul style="list-style-type: none"> DL methods for machinery fault detection 223 references 	<ul style="list-style-type: none"> SML requires carefully selected features Performance of SML becomes stagnant even with more training data DL improves performance with increasing training data Many publications are based on experimental data that is collected under controlled conditions with a less complex system and less environment disturbances and only few publications use real-life data Type of input data is important for the performance of DL approaches Integration of multiple sensors may improve the performance of DL approaches
[117]	<ul style="list-style-type: none"> 80 DL approaches for bearing fault diagnosis 	<ul style="list-style-type: none"> SML faces challenges regarding interference of additional vibration Sensitivity of SML for faults may differ for varying operating conditions Suggest to use SML for diagnosis environments with similar operating points and without much noise, or if sensors are mounted close to the monitored component Suggest to use DL methods if the diagnosis environment is noisy, consists of multiple operating points, or if more sensors are used Explainability of SML is better than that of DL approaches Future challenge of DL is the knowledge transfer from laboratories to real-world problems as well as the fusion of sensors of various domains

publications are based on experimental data that is collected under controlled conditions with a less complex system and less environment disturbances and only few publications use real-life data [28, p. 8, 115, p. 18]. However, using synthetically generated data may not generalize well to real-world data [116, p. 12]. Therefore, one major challenge for the future is the knowledge transfer from laboratories to real world problems because real-world data is said to be more noisy than experimental data [117, pp. 18-19].

Recommendations for the selection of SML and DL methods for diagnosis applications are given in [117, p. 18]: SML approaches may be sufficient for easy diagnosis environments with similar operating points and without much noise. If sensors are mounted close to the monitored component, SML methods might also be sufficient. The authors propose to use DL methods if the diagnosis environment is noisy or consists of multiple operating points. DL approaches might be more suitable if more sensors are used.

2.4.2 Machine Learning Methods for Fault Diagnosis

Numerous Machine Learning (ML) methods are applied for fault diagnosis as shown in Sub-section 2.4.1. Therefore, it is not intended to discuss all methods in detail in this section, but a general overview of possible basic ML methods is provided. Operating principles as well as strengths and weaknesses of these basic methods are presented in the following paragraphs. Khan and Yairi [18, pp. 10 & 13], Liu et al. [114, p. 11] and Zhang et al. [117, p. 15] present strengths and limitations of several typical ML algorithms for fault detection. These are summarized in Table 2.2 and Figure 2.7 visualizes these algorithms. Many cited statements in Table 2.2 for the different algorithms are rather general. This shows the difficulty of selecting an algorithm for a specific task. A detailed description of the algorithms that are used in this thesis can be found in the corresponding sections in Chapter 4 as well as in the corresponding publications [118, 119, 120, 121] of the author of this thesis.

A decision tree (Figure 2.7(a)) consists of test nodes and leaf nodes [145, p. 1]. Test nodes compute an outcome based on an attribute of a sample. Leaf nodes are labeled with a class. A sample is classified by starting at the top root node and computing the outcome of the first test node. This is repeated for the resulting sub-tree until a labeled leaf node is reached [145, p. 1].

Random forests (Figure 2.7(b)) are proposed by Breiman [146] in 2001. They are a combination of a large number of decision trees and each tree votes for a class [146, p. 6].

Support Vector Machines (SVMs) (Figure 2.7(c)) were first proposed by Cortes and Vapnik [147] in 1995. It is a binary classification algorithm that maps an input vector to a high-dimensional feature space using a non-linear kernel transformation. Separating different samples linearly in this high-dimensional feature space results in a non-linear separation in the original input space.

The nearest-neighbor rule was first formulated by Fix and Hodges [148] in 1951. The k -Nearest Neighbors (KNN) approach (Figure 2.7(d)) is a simple non-parametric decision procedure that assigns a sample to the class represented by most of its k nearest neighbors [149, pp. 1-2].

The terms Artificial Neural Network (ANN) and Multi-Layer Perceptron (MLP) are often used synonymously. A feed-forward neural network (Figure 2.7(e)) is used for the classification of an input vector [66, p. 6].

Convolutional Neural Networks (CNNs) (Figure 2.7(f)) evolved from image classification [19, p. 4]. Le Cun et al. [150] implemented the first CNN that is trained using backpropagation [19, p. 8]. CNNs consist of convolutional and pooling layers. Convolutional operations are

Table 2.2: Strengths and Limitations of Machine Learning methods for fault diagnosis applications based on [18, pp. 10 & 13, 114, p. 11, 117, p. 15]

Method	Strengths	Limitations	Applications
Decision Tree	<ul style="list-style-type: none"> • Easy to understand [18] • Non-parametric [18] • Good visualization [18] 	<ul style="list-style-type: none"> • May over-fit [18] • Can get stuck in local minima [18] • Heuristic [18] 	[77, 80, 122]
Random Forest	<ul style="list-style-type: none"> • Improved performance compared to Decision Tree [18] • Fast and scalable [18] • Trains faster than SVM [18] 	<ul style="list-style-type: none"> • Increase in bias [18] 	[122]
SVM	<ul style="list-style-type: none"> • High accuracy [18, 114] • Robust against noise [18] • Can deal with high-dimensional features [114] • Efficient for large datasets [18] 	<ul style="list-style-type: none"> • Fundamentally a binary classifier [18] • Memory intensive [18] • Low efficiency for big data [114] 	[66, 79, 91, 102, 122, 123, 124, 125]
KNN	<ul style="list-style-type: none"> • Mature theory and easy to implement [114] • Can be used for classification and regression [114] 	<ul style="list-style-type: none"> • Large computation [114] • Memory intensive [114] • Selection of k has high influence [114] 	[66, 122, 126]
MLP / ANN	<ul style="list-style-type: none"> • High classification accuracy [114] • Good approximation of complex nonlinear function [114] 	<ul style="list-style-type: none"> • Many parameters [114] • Prone to overfitting [18, 114] 	[66]
CNN	<ul style="list-style-type: none"> • Exhibits good denoising capability [117] • Good for multi-dimensional data [18] • Good performance in local feature extraction [18] 	<ul style="list-style-type: none"> • May require many layers to find an entire hierarchy [117] • Requires large training data [114, 117] • May require more training time [18] 	[127, 128, 129, 130, 131, 132, 133, 134]
RNN / LSTM	<ul style="list-style-type: none"> • Memorizes sequential events [117] • Models time dependencies [117] • Capable of receiving inputs of variable length [117] 	<ul style="list-style-type: none"> • Frequent learning issues due to gradient vanishing [117] • DL requires large training dataset [114] 	[135, 136, 137]
GAN	<ul style="list-style-type: none"> • Requires almost no modifications when transferring to new applications [117] • Requires no Monte Carlo approximations to train [117] • Does not introduce deterministic bias [117] 	<ul style="list-style-type: none"> • Training is unstable as it requires finding the Nash equilibrium of a game [117] • Hard to learn to generate discrete data such as text [117] • DL requires large training dataset [114] 	[114, 138, 139]
(Deep) Autoencoder	<ul style="list-style-type: none"> • Does not require labeled data [117] • Autoencoder variants may improve noise resilience and robustness [117] 	<ul style="list-style-type: none"> • Captures as much information as possible rather than as much relevant information [18] • Training may suffer from vanishing errors [117] • May require large training dataset [18] 	[91, 140, 141, 142, 143]

performed by sliding a kernel across the input data. Thereby, features are generated as the weighted sum of the layer's input data across the kernel. Pooling layers reduce the data size and introduce local invariance of the generated features by taking the mean or maximum of the layer's input data across the kernel of the layer. The generated abstract features are classified using fully-connected layers of neurons [19, p. 4].

Recurrent Neural Networks (RNNs) (Figure 2.7(g)) incorporate a temporal representation and save information within a hidden state [19, p. 6]. Training of RNNs is problematic because of vanishing or exploding gradients [19, p. 6]. In 1997, Hochreiter and Schmidhuber [151] proposed a special recurrent network architecture, called Long Short-Term Memory (LSTM) network. It is

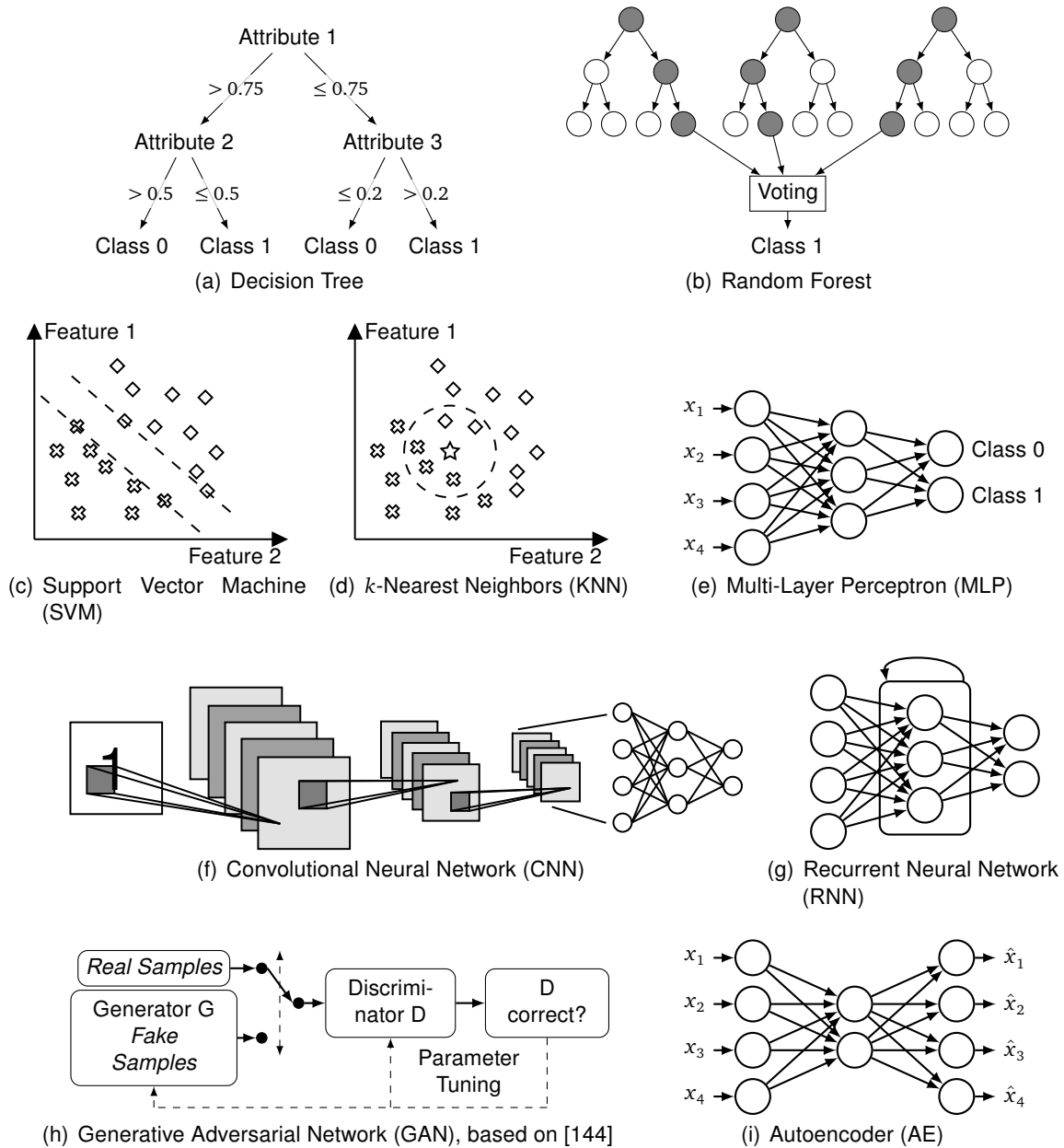


Figure 2.7: Illustration of machine learning methods

proven that LSTM networks are more efficient than conventional RNNs [19, p. 7].

Generative Adversarial Networks (GANs) (Figure 2.7(h)) were first proposed by Goodfellow et al. [152]. GANs consist of a generative and a discriminative model. The generative model captures the data distribution and generates new samples. The discriminative model estimates the probability that a generated sample comes from the training data. The training goal is to maximize the probability that generated samples are mistakenly classified as consisting to the training data. GANs are used for data augmentation of unbalanced datasets [138, 139]. However, network architectures for fault diagnosis that incorporate GANs are also proposed [153].

An Autoencoder (Figure 2.7(i)) is a neural network whose input and output layers have an equal size. Multiple hidden layers are typically configured in a bottleneck architecture with a symmetrical encoder and decoder [106, p. 13]. The training goal of the Autoencoder is the reconstruction of the input data [106, p. 13, 154, p. 45].

2.5 Commercial Diagnosis Systems for Automotive Applications

The reviewed publications in the sections above originate from research in academia. However, according to [117, p. 20], transferring the fault detection systems from laboratories to actual real-world applications is a difficult but important step to generate a benefit from the research publications. Therefore, this section reviews commercial implementations of FDI systems for automotive applications. Due to the fact that information about commercial systems are not publicized in research articles, the information in this section relies mostly on alternative information sources such as press releases and websites.

The company “We Predict” [155] was founded in 2009 [156]. “We Predict” analyzes repair order information of different brands and multiple model years of OEM dealers and independent service facilities. Based on this data, current failure rates are calculated and future component performance is predicted [157]. “We Predict” deals with data analytics. However, no information about in-vehicle diagnosis is published.

“Carly” [158] is a startup in Munich that was founded in 2014. “Carly” offers an On-Board Diagnostics (OBD-II) adapter that pairs with a mobile phone app. The app gives a car health indicator that is based on the number of faults that were detected [159]. However, no specific information on the generation of this car health indicator can be found. Further research on the company’s homepage indicates that the functionality is mainly based on OBD-II fault codes.

“Compredict” [160] is a German startup that was founded in 2016 [161]. “Compredict” deals with the design of virtual sensors and component wear prediction within the automotive area [160]. Virtual sensors are designed for estimating physical quantities based on existing sensors [162]. Conducted methods for the development of these virtual sensors are based on system identification, optimization algorithms and ML [162]. Rainflow-counting is applied for wear prediction [163]. Further details regarding the performed analytics or which components are analyzed in particular are not available.

In 2013, a presentation of BMW [164] shows a predictive analytics framework called “FACTS” for discovering failure patterns in vehicles. The diagnostic processes are provided to workshops as a set of apps. The system does not deal with on-board diagnosis based on driving data.

In 2017, BMW launched “CarData” [165]. Vehicle data is transmitted to servers and third-party companies may use this data to provide additional services. The data consists of condition data like mileage, usage-based data such as fuel consumption and event data such as an automated service call [166, p. 6]. Relevant time-signals for predictive maintenance are not part of the transmitted data. Possible service providers are garages, insurance companies and fleet managers [165]. Additional information regarding predictive maintenance is not found.

Since 2019, vehicle data of BMW and Mini is available at the platform of the startup “High Mobility” [167], shortly after the announcement of the availability of Mercedes-Benz data on this platform [168]. “High Mobility” was founded in 2013 [169]. The type of the available data for BMW and Mercedes-Benz is similar to BMW “CarData” [170, 171]. Time signals that are relevant for predictive maintenance are not included in the available data.

In 2019, a message in the cockpit of a Tesla was reported that indicated that an unexpected condition of the power conversion system was detected by the car [172]. Tesla mentions on its homepage that they could remotely diagnose 90% of the vehicle’s issues [173]. More information on the detection concept or the monitored subsystems is not published.

2.6 Criticism of the State of the Art

This section derives requirements for diagnosis concepts based on the aspects of the motivation in Section 1.1. The state of the art is critically reviewed with regard to these requirements.

Predictive maintenance and remote on-board diagnostics will be highly important for the future automotive aftermarket [13, p. 19]. Car-generated data will be available and usable to improve the performance of future diagnosis approaches. Therefore, diagnosis approaches are required to improve their performance by making use of a high amount of available data.

⇒ R1: Potential performance improvement with more data

The growth of car data-based diagnostics and services may result in changes of the market shares of the automotive aftermarket and an increasing aftermarket activity of OEMs is expected [13, p. 17]. Therefore, diagnosis approaches need to be quickly transferable from one component to another with low manual engineering effort.

⇒ R2: Potential transferability to other components

Lastly, it shall be possible to implement a diagnosis approach in a variety of vehicles. Therefore, it is necessary to limit the required sensors to a standard ESC system sensor set because vertical dynamics sensors of semi-active suspension systems are only available in upper class vehicles [174]. However, if more relevant sensors are available, it shall be possible to use these additional sensors for the diagnosis system.

⇒ R3: Potential applicability using only ESC sensors

⇒ R4: Potential modularity for using additional sensors

The following paragraphs discuss the fulfillment of the requirements for different diagnosis concepts.

Model-based Approaches

Figure 2.4 in Subsection 2.3.1 shows that many approaches for damper diagnosis are model-based e.g. they employ observers or rely on parity-space-based residuals. Ding et al. [175, p. 6] state that model-based Fault Detection and Isolation (FDI) is often unrealistic due to missing models, sophisticated modeling procedure and the need of theoretical system knowledge. Even though the quarter-vehicle model is a well known simple model of the vertical dynamics, these model-based approaches are still lacking series implementations for damper diagnosis.

The parameters of model-based approaches need to be fine-tuned. Even though this process is time-consuming, the number of parameters is still low. Therefore, the performance of model-based approaches does not improve if more data is available for the design of the diagnosis system. Furthermore, model-based approaches are designed for one specific diagnostic purpose due to the incorporated model. Conducting fault diagnosis for another component requires another model. Designing this new model requires yet more domain knowledge and expertise again. Therefore, it is not possible to transfer model-based fault diagnosis approaches to other components.

All reviewed model-based damper diagnosis approaches in Subsection 2.3.1 require vertical dynamics sensor measurements such as the vertical acceleration of the vehicle body or the tire. Hence, existing model-based damper diagnosis approaches cannot be employed using only ESC sensor signals. Incorporating additional measurement signals is only possible for sensor signals that are related to the used model.

Signal-based Approaches

Signal-based approaches monitor time-domain, frequency-domain or time-frequency-domain characteristics. These methods can be applied to ESC sensor signals as shown by Jautze [17]. It is possible to incorporate additional sensor signals. The transferability of signal-based approaches to other components is practicable. However, manual engineering effort for finding relations of signal characteristics to component faults is required. Due to the fact that signal-based approaches only monitor signal characteristics for certain thresholds, the number of tuneable parameters is relatively low. Therefore, the performance of signal-based approaches does not significantly improve if more data is available for the design of the diagnosis system.

Figure 2.4 in Subsection 2.3.1 shows that one signal-based damper diagnosis approach exists that uses only ESC sensors. Even though the approach presented by Jautze [17] was conducted in cooperation with an OEM and patents were claimed [176, 177], this approach is not employed in series production vehicles. This raises doubts on the reliability of the approach when used on a greater database of driving data with additional environmental influences such as temperature, road excitation, vehicle mass etc. The sensitivity to the road excitation and vehicle speed is explicitly mentioned in [17, p. 112]. However, this approach serves as a basis for a comparison of the performance of the investigated diagnosis approaches within this thesis.

Machine Learning Approaches

Machine learning and especially deep learning approaches' performance improves if more data is available [19, p. 1]. Hereby, the robustness of these methods can be refined. Diagnosis concepts for one component are transferable to other components. While re-training is necessary, the manual effort for transferring a diagnosis concept is low. So far, there is no diagnosis concept based on machine learning that uses only ESC sensor values. However, monitoring frequency-based features similar to the signal-based approach of Jautze [17] gives reasons to expect at least a competitive performance of machine learning approaches. Adding more sensors is always possible.

Summary

Table 2.3 summarizes the fulfillment of the requirements of the different diagnosis concepts. Model-based and signal-based diagnosis concepts are not appropriate for future automotive component fault detection. Therefore, no existing approach from Subsection 2.3.1 is suited for the diagnosis of damper faults. Machine learning approaches show promising diagnosis performance in other domains (Subsection 2.4.1). However, up until now, no suited machine learning diagnosis systems for chassis system components exist.

Table 2.3: Fulfillment of derived requirements for different diagnosis approaches. Fulfillment is visualized using "+" for fulfilled, "-" for not fulfilled and "○" for fulfillment depending on the specific method.

	Model-based	Signal-based	Machine Learning
R1: Potential performance improvement with more data	-	-	+
R2: Potential transferability to other components	-	○	+
R3: Potential applicability using only ESC sensors	-	+	+
R4: Potential modularity for using additional sensors	○	+	+

The review of commercial activities in Section 2.5 depicts that there are no suitable commercial implementations of automotive diagnosis concepts that are published transparently. Only Tesla

and Compredict show activities of diagnosis based on actual driving data. However, according to available information, Compredict conducts only load-counting instead of fault detection. Information about Tesla's approach for fault detection is not available.

The last point of criticism addresses all reviewed publications for damper diagnosis: The road excitation is not measured in any reviewed approach, but there is no theoretical analysis whether it is possible to detect defective dampers with unknown road excitation. Jautze [17] only showed that the frequency spectra of the wheel speed signals are different for varying damper configurations.

2.7 Derivation of the Research Objective

The criticism of the state of the art in Section 2.6 depicts that machine learning concepts may be used for damper diagnosis. However, there are no such approaches in current research. Therefore, the research topic of this thesis is the analysis of the suitability of machine learning methods for automotive damper diagnosis.

The research topic is refined into the following research questions:

- I. Which requirements need to be fulfilled for the detection of defective dampers?
 - a. Is it possible to detect defective dampers using only wheel speed measurements with unknown road excitation?
 - b. Which circumstances limit or benefit the detection of defective dampers?
- II. Which machine learning concepts are suited for the diagnosis of defective automotive dampers?
- III. What is the detection performance of specific approaches of the identified machine learning concepts?
 - a. How accurate are the results?
 - b. How robust are the results?
 - c. What is the influence of a varying size of training data on the detection performance?
 - d. Which sensor signals are most relevant?
 - e. How is the performance of machine learning approaches compared to the signal-based diagnosis approach of Jautze [17]?
- IV. Is it possible to derive physical findings from the investigation of the mathematical transformations that are performed within machine learning methods?

3 Analysis of Observability

A theoretical analysis of the damper defect detection problem investigates if defective dampers can theoretically be detected using a limited amount of sensor signals. Furthermore, it provides insights regarding circumstances of the driving situation that may improve or deteriorate the performance of a health monitoring system. In the scope of the reviewed publications in Subsection 2.3.1, there is no theoretical analysis whether the detection of defective dampers is possible with unknown road excitation. Even though Jautze [17] detects damper defects based on the wheel speed signal with unknown road excitation, the damper defect detection is not theoretically evaluated. The road excitation is also not measured within this thesis because such a sensor is not part of an ESC sensor setup. Therefore, the damper defect detection problem with unknown road excitation is theoretically analyzed in this chapter.

A defective damper is a variation of the damping coefficient parameter of a vehicle. If this parameter is interpreted as additional state of a mathematical vehicle model, the system must be observable. A brief illustration of the observability is, whether the state vector x (for readability, the time-dependence of variables (e.g. $x(t)$) is not shown in this chapter) can be reconstructed based on the system's output signal y and its $(n - 1)$ time-derivatives (with the number of states n) [178, p. 507]. This means, if the mathematical vehicle model is observable, the damping coefficient could theoretically be calculated using the sensor signals and their time derivatives. Therefore, for an observable system a mapping [178, p. 507]

$$x = q^{-1} \left([y \quad \dot{y} \quad \ddot{y} \quad \dots \quad y^{(n-1)}]^T \right). \quad (3.1)$$

exists. Finding a mapping q^{-1} can be difficult especially for nonlinear systems [178, p. 507]. However, easier criteria can be used that investigate only whether the mapping q^{-1} exists [178, p. 508]. These criteria are evaluated within this chapter.

The specific observation problem in this thesis is the analysis of the observability of a vehicle model that includes the variation of the damping coefficient with an unknown road excitation and wheel speed as output signal. An observability analysis is especially important because the road profile excites the vehicle but it is unknown to the defect detection algorithm. This means, the defect detection algorithm could misinterpret the vehicle behavior while driving over a rough road with the presence a defective damper because the algorithm is not aware of the high road excitation. Furthermore, the observability of a nonlinear system, can be dependent on the system's excitation [178, p. 512].

The following section derives the system's model equations. Suitable control theory methods for the analysis of the observability are discussed afterwards on the basis of the form of the model equations. The analysis is performed iteratively for increasingly complex circumstances from a known deterministic road excitation to an unknown stochastic road excitation.

3.1 Derivation of System Equations

The observability analysis is conducted using the wheel speed signal as measurement quantity. Measurements of the yaw rate as well as lateral or longitudinal acceleration of the vehicle body are not considered to be able to use the quarter-vehicle as basic model. If observability is given without these vehicle body measurements, it is also given with them.

A general introduction to the quarter-vehicle model can be found in [1, p. 75, 179]. It is visualized in Figure 3.1. The model consists of a vehicle body mass m_{Bo} that is connected with a linear spring $c_{z,Bo}$ and damper $d_{z,Bo}$ to the tire mass m_T . The tire mass is connected via the tire spring $c_{z,T}$ to the vertical road profile. The derivation of the linear system equations is stated in Appendix A.1 based on [17, pp. 28-29].

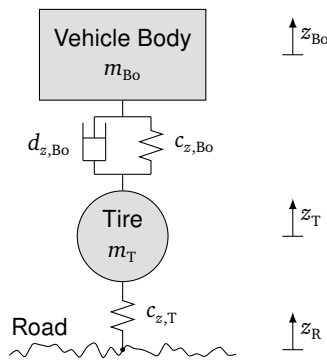


Figure 3.1: Quarter-vehicle model

Using the road excitation z_R as input of the system and the deviation of the vertical tire force in the contact patch from its stationary value as output of the system, the system equations of the linear quarter-vehicle model are given by

$$\begin{bmatrix} \dot{z}_T \\ \ddot{z}_T \\ \dot{z}_{Bo} \\ \ddot{z}_{Bo} \end{bmatrix} = \begin{bmatrix} 0 & 1 & 0 & 0 \\ -\frac{c_{z,Bo}+c_{z,T}}{m_T} & -\frac{d_{z,Bo}}{m_T} & \frac{c_{z,Bo}}{m_T} & \frac{d_{z,Bo}}{m_T} \\ 0 & 0 & 0 & 1 \\ \frac{c_{z,Bo}}{m_{Bo}} & \frac{d_{z,Bo}}{m_{Bo}} & -\frac{c_{z,Bo}}{m_{Bo}} & -\frac{d_{z,Bo}}{m_{Bo}} \end{bmatrix} \begin{bmatrix} z_T \\ \dot{z}_T \\ z_{Bo} \\ \dot{z}_{Bo} \end{bmatrix} + \begin{bmatrix} 0 \\ \frac{c_{z,T}}{m_T} \\ 0 \\ 0 \end{bmatrix} z_R \quad (3.2)$$

$$\Delta F_{z,C} = c_{z,T} (z_R - z_T) \quad (3.3)$$

with the vertical displacement of the mass of the unsprung tire and axle z_T and its velocity \dot{z}_T as well as the vertical displacement of the mass of the sprung vehicle body z_{Bo} and its velocity \dot{z}_{Bo} .

To analyze the observability of a defective damper within this thesis, the damping coefficient $d_{z,Bo}$ of the linear quarter-vehicle model is modified by incorporating a relative deviation of the damping coefficient from a nominal value $d_{z,Bo} = (1 + \kappa_{d,Bo}) d_{z,Bo,0}$. The variation of the damping coefficient is modeled in a multiplicative manner (compared to an additive manner) because the magnitude of changes of the system behavior depend on the magnitude of the fault and the system's states. The relative deviation of the damping coefficient $\kappa_{d,Bo}$ is introduced as additional state to the states of the quarter-vehicle model. This results in the state vector

$$\mathbf{x} = [x_1 \ x_2 \ x_3 \ x_4 \ x_5]^T = [z_T \ \dot{z}_T \ z_{Bo} \ \dot{z}_{Bo} \ \kappa_{d,Bo}]^T. \quad (3.4)$$

The vertical tire stiffness $c_{z,T}$ connects the vertical force in the tire contact patch $F_{z,C}$ with the static radius of tire r_{stat} as visualized in Figure 3.2. The dynamic tire radius r_{dyn} is slightly different

from the static tire radius and is therefore not directly correlated to the vertical tire force by the vertical tire stiffness $c_{z,T}$. Therefore, the dynamic tire radius is split into $r_{\text{dyn},0}$ at an operating point and $\Delta r_{\text{dyn},F,C}$ as the deviation from this operating point that is caused by a deviation of the vertical force in the tire-road contact patch [17, pp. 37-41]. The vertical force in the tire contact patch is also split into $F_{z,C,0}$ at an operating point and a deviation from this operating point $\Delta F_{z,C}$. A linear approximation of $\Delta r_{\text{dyn},F,C}$ is then given by [17, p. 39]

$$\Delta r_{\text{dyn},F,C} = \Delta F_{z,C} \frac{1}{c_{r,\text{dyn},F,C}} \quad (3.5)$$

with the stiffness of the dynamic tire radius with regard to the vertical force in the tire contact patch $c_{r,\text{dyn},F,C}$.

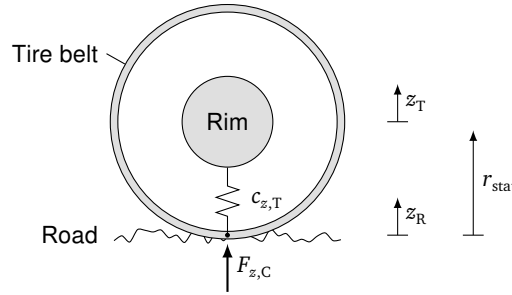


Figure 3.2: Dependency of tire radius from vertical force

The free-rolling rotational speed of the tire is [17, p. 39]

$$\dot{\varphi}_T = \frac{v}{2\pi (r_{\text{dyn},0} + \Delta r_{\text{dyn},F,C})}. \quad (3.6)$$

Combining Equations (3.5) and (3.6) and linearizing it by a Taylor series expansion for $\Delta F_{z,C} = 0$ results in [17, pp. 39-41]

$$\dot{\varphi}_T = \frac{v}{2\pi r_{\text{dyn},0}} - \frac{v}{2\pi r_{\text{dyn},0}^2 c_{r,\text{dyn},F,C}} \Delta F_{z,C}. \quad (3.7)$$

Using the wheel speed from Equations (3.7) as output of the quarter-vehicle model $y = \dot{\varphi}_T$ and the road excitation as system input $u = z_R$, the system for the analysis of the observability can be written in the form

$$\dot{\mathbf{x}} = \mathbf{f}(\mathbf{x}, u) \quad (3.8)$$

$$y = g(\mathbf{x}, u) \quad (3.9)$$

with

$$\dot{\mathbf{x}} = \begin{bmatrix} -\frac{c_{z,T} + c_{z,\text{Bo}}}{m_T} x_1 - \frac{d_{z,\text{Bo},0}}{m_T} x_2 + \frac{c_{z,\text{Bo}}}{m_T} x_3 + \frac{d_{z,\text{Bo},0}}{m_T} x_4 - \frac{d_{z,\text{Bo},0}}{m_T} x_2 x_5 + \frac{d_{z,\text{Bo},0}}{m_T} x_4 x_5 + \frac{c_{z,T}}{m_T} u \\ \frac{c_{z,\text{Bo}}}{m_{\text{Bo}}} x_1 + \frac{d_{z,\text{Bo},0}}{m_{\text{Bo}}} x_2 - \frac{c_{z,\text{Bo}}}{m_{\text{Bo}}} x_3 - \frac{d_{z,\text{Bo},0}}{m_{\text{Bo}}} x_4 + \frac{d_{z,\text{Bo},0}}{m_{\text{Bo}}} x_2 x_5 - \frac{d_{z,\text{Bo},0}}{m_{\text{Bo}}} x_4 x_5 \\ 0 \end{bmatrix} \quad (3.10)$$

$$y = \frac{v}{2\pi r_{\text{dyn},0}} - \frac{c_{z,T} v}{2\pi r_{\text{dyn},0}^2 c_{r,\text{dyn},F,C}} (u - x_1). \quad (3.11)$$

3.2 Identification of Suitable Observability Analysis Methods

Due to the incorporation of the variation of the damping coefficient as additional parameter, the system's dynamics in Equations (3.10) became nonlinear. Therefore, methods are required that deal with the observability of nonlinear systems.

Nonlinear observability is considered by Hermann and Krener [180]. The observability criterion is based on analyzing the invertibility of the original mapping q of Equations (3.1) using a rank condition. This rank condition leads to a statement of the local observability at an operating point. Another approach is a set-valued framework as presented by Kassara [181]. This set-valued framework leads to a global observability statement. However, local statements regarding the observability use widely known mathematics and are sufficient within the scope of this thesis, because the observability statement is only considered to prove that a damper defect detection is possible in general.

At first, the observability analysis is conducted using the local nonlinear methods of [180]. To generate comprehensible theoretical insights, the system is firstly considered with a known road excitation, even though this is not possible in real life. Afterwards, the complexity of the observability analysis is increased step-wise to prove the observability with an unknown road excitation. Hereby, it is possible to also analyze the dependability of the observability from the road excitation profile.

3.3 Analysis of Observability with Known Road Excitation

A criterion for the existence of the mapping q^{-1} from Equations (3.1) is based on the implicit function theorem. According to this theorem the mapping q^{-1} exists for a single operation point, if its Jacobi-matrix has rank n at this operation point [178, p. 508]. This can be tested by evaluating the determinant of the Jacobian matrix Q [178, p. 512]. Therefore, a nonlinear system of the form of Equations (3.8) and (3.9) is locally weakly observable if [178, p. 512, 180]

$$\det Q(\mathbf{x}, \mathbf{u}, \dot{\mathbf{u}}, \ddot{\mathbf{u}}, \dots, \mathbf{u}^{(n-1)}) = \det \frac{\partial \mathbf{q}(\mathbf{x}, \mathbf{u}, \dot{\mathbf{u}}, \ddot{\mathbf{u}}, \dots, \mathbf{u}^{(n-1)})}{\partial \mathbf{x}} \neq 0 \quad (3.12)$$

with the number of states n , and the vector q that consists of the output y with its time-derivatives

$$\mathbf{q}(\mathbf{x}, \mathbf{u}, \dot{\mathbf{u}}, \ddot{\mathbf{u}}, \dots, \mathbf{u}^{(n-1)}) = \begin{bmatrix} y \\ \dot{y} \\ \ddot{y} \\ \dots \\ y^{(n-1)} \end{bmatrix} = \begin{bmatrix} g(\mathbf{x}, \mathbf{u}) \\ h_1(\mathbf{x}, \mathbf{u}, \dot{\mathbf{u}}) \\ h_2(\mathbf{x}, \mathbf{u}, \dot{\mathbf{u}}, \ddot{\mathbf{u}}) \\ \dots \\ h_{n-1}(\mathbf{x}, \mathbf{u}, \dot{\mathbf{u}}, \dots, \mathbf{u}^{(n-1)}) \end{bmatrix} \quad (3.13)$$

that are calculated by Lie-derivating the output

$$y^{(n-1)} = h_{n-1}(\mathbf{x}, \mathbf{u}, \dot{\mathbf{u}}, \dots, \mathbf{u}^{(n-1)}) = \frac{\partial h_{n-2}}{\partial \mathbf{x}} f(\mathbf{x}, \mathbf{u}) + \sum_{i=1}^{n-1} \frac{\partial h_{n-2}}{\partial \mathbf{u}^{(i-1)}} \mathbf{u}^{(i)}. \quad (3.14)$$

Evaluating Equations (3.12) for the nonlinear quarter-car model given by Equations (3.10) and (3.11) leads to a condition for locally weak observability. See Appendix A.2 for intermediate results. Evaluating this condition for the operation point $\mathbf{x}_0 = [0 \ 0 \ 0 \ 0 \ 0]^T$ results in a condition for locally weak observability at \mathbf{x}_0 [180, p. 6] that is

$$\det \mathbf{Q}(\mathbf{x}, \mathbf{u}, \dot{\mathbf{u}}, \ddot{\mathbf{u}}, \dots, \mathbf{u}^{(n-1)}) \Big|_{\mathbf{x}_0} = \frac{c_{z,Bo}^2 c_{z,T}^6 v^5 (d_{z,Bo,0} (m_T + m_{Bo}) u - m_T m_{Bo} \dot{u})}{32 c_{r,dyn,F,C}^5 m_T^5 m_{Bo} r_{dyn,0}^{10} \pi^5} \neq 0. \quad (3.15)$$

With the road excitation as input $u = z_R$, the observability is dependent on the road excitation. Equations (3.15) is 0 for all $t \geq 0$ for $u(t) = \dot{u}(t) \equiv 0$. This corresponds to an ideally flat road profile, which is highly unlikely in reality. Equations (3.15) is also 0 for

$$u(t) = C_1 \exp\left(\frac{d_{z,Bo,0} t (m_T + m_{Bo})}{m_T m_{Bo}}\right) \quad (3.16)$$

with an arbitrary constant C_1 . This corresponds to a vertical road profile with an exponential increase over time (and the traveled distance). This road profile is also highly unlikely in reality. Therefore, the system is locally weakly observable at \mathbf{x}_0 under the assumption of a known road excitation $z_R(t)$.

3.4 Analysis of Observability with Unknown Road Excitation

The road excitation is not measured in this research. Various observability concepts such as Output-To-State Stability (OSS) and detectability for nonlinear systems [182] or nonlinear norm-observability [183] are based on the system norm of inputs and outputs instead of the specific time behavior of these signals. However, these observability concepts rely on finding functions with specific properties (e.g. Lyapunov function) which is not straightforward.

Therefore, a road excitation model is incorporated into the initial quarter-vehicle model and the local weak observability condition from Equations (3.12) is evaluated again. The road excitation can be modeled as colored noise that is generated by filtering white noise [184, 185, 186, 187, p. 18]. Löhle et al. [186] present a road model for the vertical and roll excitation. The roll excitation is not relevant for this analysis. Therefore, only the vertical road excitation model

$$\dot{z}_R(t) = -v a_{z,R} z_R(t) + v b_{z,R} n_{z,R}(t) \quad (3.17)$$

is applied with the stochastic white noise input $n_{z,R}(t)$, the vehicle velocity v , and the road parameters $a_{z,R}$ and $b_{z,R}$. Choosing $u = n_{z,R}$, incorporating Equations (3.17) into Equations (3.10) with $\mathbf{x}_6 = z_R$ and performing the analysis for the local weak observability at $\mathbf{x}_0 = [0 \ 0 \ 0 \ 0 \ 0 \ 0]^T$ results in

$$\det \mathbf{Q}(\mathbf{x}, \mathbf{u}, \dot{\mathbf{u}}, \ddot{\mathbf{u}}, \dots, \mathbf{u}^{(n-1)}) \Big|_{\mathbf{x}_0} = \frac{a_{z,R}^2 b_{z,R} c_{z,Bo}^2 c_{z,T}^7 v^9 (d_{z,Bo,0} (m_T + m_{Bo}) u - m_T m_{Bo} \dot{u})}{64 c_{r,dyn,F,C}^6 m_T^6 m_{Bo}^2 r_{dyn,0}^{12} \pi^6} * \quad (3.18)$$

$$\left((m_T + m_{Bo}) (c_{z,Bo} - a_{z,R} d_{z,Bo,0} v) + a_{z,R}^2 m_T m_{Bo} v^2 \right) \neq 0.$$

Equations (3.18) is similar to the form of Equations (3.15). However, the system's input is the unknown stochastic input $u(t) = n_{z,R}(t)$. Therefore, setting conditions on $u(t)$ for observability

does not make sense. But it is still possible to derive requirements on the road excitation model.

Equations (3.18) is 0 for $a_{z,R} = 0$ or $b_{z,R} = 0$. Löhe et al. [186, p. 4] choose $a_{z,R} = 0$. This results in an unbound Power Spectral Density (PSD) for low frequencies as shown in [68, p. 17] and the road excitation model can generate a large vertical excitation with a large spatial extension (e.g. mountains). Choosing $a_{z,R} \neq 0$ results in a low-pass filter characteristic of the generated road excitation. Setting $a_{z,R} \neq 0$ prevents the generation of these mountains but has no effect on the relevant road excitation characteristic within this thesis.

Equations (3.18) is 0 for $b_{z,R} = 0$. This is obvious because in this case, there would be no road excitation and the system would remain at its initial state x_0 . However, this is also an indicator that the observability is better conditioned with an increasing road excitation of a rougher road. This might improve the performance of a damper fault monitoring system.

The last bracket in Equations (3.18) is a second order polynomial in $a_{z,R}$. It sets the condition

$$a_{z,R} \neq \frac{d_{z,Bo,0} (m_T + m_{Bo}) \pm \sqrt{(m_T + m_{Bo}) (d_{z,Bo,0}^2 (m_T + m_{Bo}) - 4c_{z,Bo} m_T m_{Bo})}}{2 m_T m_{Bo} v}. \quad (3.19)$$

for an observable system. Equations (3.19) connects vehicle parameters to road excitation parameters. Therefore, it can be regarded as vehicle design requirement and is of no major restriction for the observability.

3.5 Stochastic Observability with Unknown Road Excitation

With the incorporation of the road excitation model of Equations (3.17), the system can also be described as a stochastic nonlinear system of the form [188, p. 52, 189, p. 135]

$$\begin{aligned} d\mathbf{X}_t &= \mathbf{f}(\mathbf{X}_t) dt + \sigma(\mathbf{X}_t) dW_t \\ Y_t &= g(\mathbf{X}_t) \end{aligned} \quad (3.20)$$

with the stochastic state variable \mathbf{X}_t , the drift term $\mathbf{f}(\mathbf{X}_t)$, the diffusion term $\sigma(\mathbf{X}_t)$ and the Brownian motion W_t . The Stochastic Differential Equation (SDE) of the quarter-vehicle with

Equations (3.10) and (3.11) and the road excitation model of Equations (3.17) are

$$\begin{aligned}
 d\mathbf{X}_t = & \begin{bmatrix} -\frac{c_{z,T}+c_{z,Bo}}{m_T} x_1 - \frac{d_{z,Bo,0}}{m_T} x_2 + \frac{c_{z,Bo}}{m_T} x_3 + \frac{d_{z,Bo,0}}{m_T} x_4 - \frac{d_{z,Bo,0}}{m_T} x_2 x_5 + \frac{d_{z,Bo,0}}{m_T} x_4 x_5 + \frac{c_{z,T}}{m_T} x_6 \\ \frac{c_{z,Bo}}{m_{Bo}} x_1 + \frac{d_{z,Bo,0}}{m_{Bo}} x_2 - \frac{c_{z,Bo}}{m_{Bo}} x_3 - \frac{d_{z,Bo,0}}{m_{Bo}} x_4 + \frac{d_{z,Bo,0}}{m_{Bo}} x_2 x_5 - \frac{d_{z,Bo,0}}{m_{Bo}} x_4 x_5 \\ 0 \\ -v a_{z,R} x_6 \end{bmatrix} dt \\
 & + \begin{bmatrix} 0 \\ 0 \\ 0 \\ 0 \\ 0 \\ v b_{z,R} \end{bmatrix} dW_t \\
 Y_t = & \frac{v}{2\pi r_{dyn,0}} - \frac{c_{z,T} v}{2\pi r_{dyn,0}^2 c_{r,dyn,F,C}} (x_6 - x_1).
 \end{aligned} \tag{3.21}$$

A concept for stochastic observability is presented by Powel [188] using the Gramian observability. This observability concept is recapitulated in the following. For a linear system

$$\begin{aligned}
 \dot{\mathbf{x}} &= \mathbf{A} \mathbf{x} + \mathbf{B} u \\
 \mathbf{y} &= \mathbf{C} \mathbf{x}
 \end{aligned} \tag{3.22}$$

with $\mathbf{x} \in \mathbb{R}^n$, the observability Gramian is [190, p. 12, 191, pp. 140-141]

$$\mathbf{W}_o(\tau) = \int_0^\tau \boldsymbol{\Psi}(t,0)^T \mathbf{C}^T \mathbf{C} \boldsymbol{\Psi}(t,0) dt \tag{3.23}$$

with $\boldsymbol{\Psi}(t_1, t_0)$ being the state-transition matrix $\mathbf{x}(t_1) = \boldsymbol{\Psi}(t_1, t_0) \mathbf{x}(t_0)$ of the solution of $\mathbf{x}(t)$. \mathbf{W}_o is the solution of the Lyapunov equation [191, p. 139]

$$\mathbf{A}^T \mathbf{W}_o + \mathbf{W}_o \mathbf{A} = -\mathbf{C}^T \mathbf{C}. \tag{3.24}$$

If the observability Gramian has full rank [188, p. 14]

$$\text{rank}(\mathbf{W}_o) = n, \tag{3.25}$$

the system is observable. Additionally, the eigenvalues of the observability Gramian are a quantitative measure for the observability of the system [191, pp. 142-143].

For a nonlinear system

$$\begin{aligned}
 \dot{\mathbf{x}} &= \mathbf{f}(\mathbf{x}, u) \\
 \mathbf{y} &= \mathbf{g}(\mathbf{x})
 \end{aligned} \tag{3.26}$$

an empirical observability Gramian can be expressed by [188, p. 20, 192, p. 2]

$$\mathbf{W}_o^\varepsilon(\tau, \mathbf{x}_0, u) = \frac{1}{4\varepsilon^2} \int_0^\tau \boldsymbol{\Phi}^\varepsilon(t, \mathbf{x}_0, u) \boldsymbol{\Phi}^\varepsilon(t, \mathbf{x}_0, u)^T dt \tag{3.27}$$

with

$$\Phi^\varepsilon(t, \mathbf{x}_0, u) = \begin{bmatrix} y^{+1} - y^{-1} \\ y^{+2} - y^{-2} \\ \dots \\ y^{+n} - y^{-n} \end{bmatrix} = \begin{bmatrix} y^{+1}(t, \mathbf{x}_0, u) - y^{-1}(t, \mathbf{x}_0, u) \\ y^{+2}(t, \mathbf{x}_0, u) - y^{-2}(t, \mathbf{x}_0, u) \\ \dots \\ y^{+n}(t, \mathbf{x}_0, u) - y^{-n}(t, \mathbf{x}_0, u) \end{bmatrix} \quad (3.28)$$

$$y^{+i}(t, \mathbf{x}_0, u) = y^{+i} = y(t, \mathbf{x}_0 + \varepsilon \mathbf{e}_i, u) \quad (3.29)$$

$$y^{-i}(t, \mathbf{x}_0, u) = y^{-i} = y(t, \mathbf{x}_0 - \varepsilon \mathbf{e}_i, u) \quad (3.30)$$

with \mathbf{e}_i as the i -th unity vector and ε being a perturbation variable of the initial state $\mathbf{x}_0 = \mathbf{x}(0)$.

For $\varepsilon \rightarrow 0$, the nonlinear system in Equations (3.26) is weakly observable at \mathbf{x}_0 for $\tau > 0$ if

$$\text{rank} \left(\lim_{\varepsilon \rightarrow 0} \mathbf{W}_o^\varepsilon(\tau, \mathbf{x}_0, u) \right) = n. \quad (3.31)$$

Equations (3.27) can be written element-wise for the i -th row and the j -th column as [188, p. 21]

$$(\mathbf{W}_o^\varepsilon)_{ij} = \frac{1}{4\varepsilon^2} \int_0^\tau (y^{+i} - y^{-i})(y^{+j} - y^{-j}) dt. \quad (3.32)$$

For the stochastic nonlinear system in Equations (3.20) the expected value of the observability Gramian is [188, p. 57]

$$\mathbb{E}[\mathbf{W}_o^\varepsilon(\tau, \mathbf{x}_0, u)] = \bar{\mathbf{W}}_o^\varepsilon(\tau, \mathbf{x}_0, u) + \hat{\mathbf{W}}_o^\varepsilon(\tau, \mathbf{x}_0, u) \quad (3.33)$$

with the elements in the i -th row and the j -th column

$$(\bar{\mathbf{W}}_o^\varepsilon)_{ij} = \frac{1}{4\varepsilon^2} \int_0^\tau (\mathbb{E}[y^{+i}] - \mathbb{E}[y^{-i}])(\mathbb{E}[y^{+j}] - \mathbb{E}[y^{-j}]) dt \quad (3.34)$$

$$(\hat{\mathbf{W}}_o^\varepsilon)_{ii} = \frac{1}{4\varepsilon^2} \int_0^\tau (\text{Var}[y^{+i} + y^{-i}]) dt. \quad (3.35)$$

For an arbitrary nonlinear system, the analytic calculation cannot go any further than this [188, p. 58]. However, the variance of the output signal $\text{Var}[y^{+i}] = \text{Var}[y^{+i}(t, \mathbf{x}_0 + \varepsilon \mathbf{e}_i, u)]$ and the expected value $\mathbb{E}[y^{+i}] = \mathbb{E}[y^{+i}(t, \mathbf{x}_0 + \varepsilon \mathbf{e}_i, u)]$ can be generated by simulating the system. This requires the selection of a finite ε and the observability rank condition in Equations (3.31) is not valid anymore. The selection of a finite ε results in an error of the empirical observability Gramian of [188, p. 26]

$$\Delta^\varepsilon(\tau, \mathbf{x}_0, u) = \mathbf{W}_o^\varepsilon(\tau, \mathbf{x}_0, u) - \lim_{\varepsilon \rightarrow 0} \mathbf{W}_o^\varepsilon(\tau, \mathbf{x}_0, u). \quad (3.36)$$

This error is bounded from above by [188, p. 27]

$$\|\Delta^\varepsilon(\tau, \mathbf{x}_0, u)\|_2 \leq \sup_{t \in [0, \tau]} \left(\frac{\sqrt{n} \varepsilon^2 \tau}{3} \left\| \frac{\partial y(t, \mathbf{x}_0)}{\partial \mathbf{x}_0} \right\|_2 \Gamma(t, \mathbf{x}_0) + \frac{n \varepsilon^4 \tau}{36} \Gamma(t, \mathbf{x}_0)^2 \right) \quad (3.37)$$

with [188, p. 28]

$$\Gamma(t, \mathbf{x}_0) = \max_i \left(\sup_{\boldsymbol{\eta} \in \mathcal{I}_i^\varepsilon} \left\| L_y^{(3)}(\boldsymbol{\eta}, \mathbf{e}_i, \mathbf{e}_i, \mathbf{e}_i) \right\|_1 \right) \quad (3.38)$$

with the maximum across all states $i = 1, 2, \dots, n$ and the supremum of the third Fréchet derivative $L_y^{(3)}(\boldsymbol{\eta}, \mathbf{e}_i, \mathbf{e}_i, \mathbf{e}_i)$ across the interval $\mathcal{I}_i^\varepsilon = [\mathbf{x}_0 - \varepsilon \mathbf{e}_i, \mathbf{x}_0 + \varepsilon \mathbf{e}_i]$.

An explanation of the calculation of Fréchet derivatives can be found in Appendix A.3. The k -th Fréchet derivative can be calculated as a mixed partial derivative [193, p. 3]

$$L_y^{(k)}(\mathbf{x}_0, \mathbf{e}_1, \dots, \mathbf{e}_k) = \frac{\partial}{\partial v_1} \dots \frac{\partial}{\partial v_k} \Big|_{(v_1, \dots, v_k)=0} y(\mathbf{x}_0 + v_1 \mathbf{e}_1 + \dots + v_k \mathbf{e}_k). \quad (3.39)$$

Therefore, Equations (3.38) reduces to

$$\Gamma(t, \mathbf{x}_0) = \max_i \left(\sup_{\boldsymbol{\eta} \in \mathcal{I}_i^\varepsilon} \left\| L_y^{(3)}(\boldsymbol{\eta}, \mathbf{e}_i, \mathbf{e}_i, \mathbf{e}_i) \right\|_1 \right) = \max_i \left(\sup_{\boldsymbol{\eta} \in \mathcal{I}_i^\varepsilon} \left\| \frac{\partial^3}{\partial v^3} \Big|_{v=0} y(\boldsymbol{\eta} + v \mathbf{e}_i) \right\|_1 \right). \quad (3.40)$$

Applying Krener and Ide's [192] concept of the "Local Unobservability Index" as the inverse of the smallest eigenvalue $\underline{\lambda}(\mathbb{E}[\mathbf{W}_o^\varepsilon])$ (respectively the smallest singular value $\underline{\sigma}(\mathbb{E}[\mathbf{W}_o^\varepsilon])$) of the expected observability Gramian, the system is weakly observable at \mathbf{x}_0 if [188, p. 30]

$$\frac{1}{\underline{\lambda}(\mathbb{E}[\mathbf{W}_o^\varepsilon])} = \frac{1}{\underline{\sigma}(\mathbb{E}[\mathbf{W}_o^\varepsilon])} < \frac{1}{\sup_{t \in [0, \tau]} \left(\frac{\sqrt{n} \varepsilon^2 \tau}{3} \left\| \frac{\partial y(t, \mathbf{x}_0)}{\partial \mathbf{x}_0} \right\|_2 \Gamma(t, \mathbf{x}_0) + \frac{n \varepsilon^4 \tau}{36} \Gamma(t, \mathbf{x}_0)^2 \right)} \quad (3.41)$$

The left side of inequality 3.41 is the "Local Unobservability Index" and the right side of this inequality is called the "Upper Bound for Local Unobservability Index".

Krener and Ide [192] also introduced the "Local Estimation Condition Number" as a measure for the unobservability. This is the ratio of the largest singular value to the smallest singular value of the expected Gramian observability

$$\text{Estimation Condition Number} = \frac{\overline{\sigma}(\mathbb{E}[\mathbf{W}_o^\varepsilon])}{\underline{\sigma}(\mathbb{E}[\mathbf{W}_o^\varepsilon])}. \quad (3.42)$$

If the estimation condition number is large, then the impact on the measurement value of a small change of the initial state in one direction might be obscured by a change of the initial state in another direction. The estimation problem is then ill-defined [192, p. 2].

Calculating a closed solution for the requirement for weak local observability in Equations (3.41) is close to impossible for a nonlinear stochastic system of the form of Equations (3.20). Therefore, Equations (3.41) is analyzed numerically. The Stochastic Differential Equation (SDE) in Equations (3.21) is implemented using white noise as input signal of the road excitation model with a one-sided Power Spectral Density (PSD) $S_{n,z,R}(f) = \frac{2\pi}{v}$ as Brownian motion W_t . The Fréchet derivative in Equations (3.40) and the gradient $\frac{\partial y(t, \mathbf{x}_0)}{\partial \mathbf{x}_0}$, which is the first Fréchet derivative, is approximated numerically using the finite difference method of [194]. The perturbation variable is chosen as $\varepsilon = 0.03$ and the interval $\mathcal{I}_i^\varepsilon = [\mathbf{x}_0 - \varepsilon \mathbf{e}_i, \mathbf{x}_0 + \varepsilon \mathbf{e}_i]$ is divided into six sub-intervals for the numerical derivation of the supremum in Equations (3.40). The vehicle parameters are selected from [17, p. 124]. The parameters of the road excitation model are selected as class C road from [186, p. 4] which resembles a country road [195, p. 343]. The parameters are listed in Appendix A.4 in Table A.1. Figure 3.3 shows the unobservability index, the upper bound of the unobservability index as well as the local estimation condition index for an observation time of up to 5 s. Since the unobservability index is below the upper bound from Equations (3.41), the system is locally weakly observable at the evaluated operating point $\mathbf{x}_0 = [0 \ 0 \ 0 \ 0 \ 0 \ 0]^T$.

The estimation problem is ill-defined for very short observation times ($t < 0.1$ s) because the local estimation condition index is high. However, the local estimation condition index is in a good range for larger observation times.

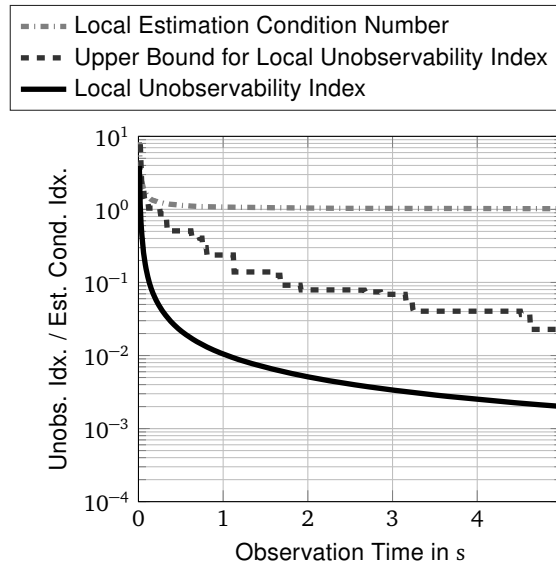
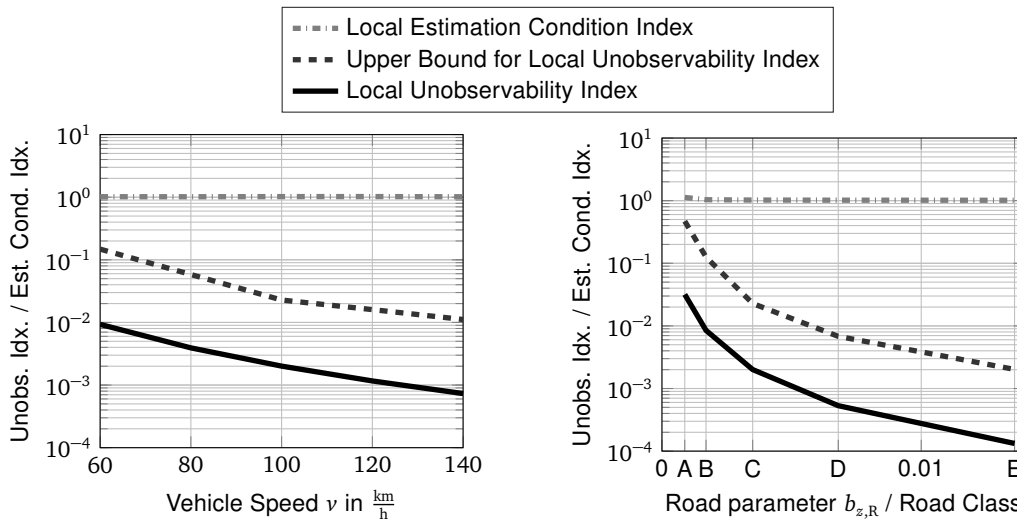


Figure 3.3: Local estimation condition number, local unobservability index and its upper bound of the stochastic system with an unknown road excitation of a street class C ($b_{z,R} = 0.0035$) and a vehicle speed $v = 100 \frac{\text{km}}{\text{h}}$ for an observation time of up to 5 s

An analysis of the influence of the vehicle speed and the road class on the observability is performed. Figure 3.4(a) shows the local estimation condition index, the local unobservability index and its upper bound for an observation time of $t = 5$ s for a parameter variation of the vehicle speed v . Figure 3.4(b) shows the same quantities for a parameter variation of the road class parameter $b_{z,R}$.



(a) Varying vehicle speed v and fixed road class of category C with $b_{z,R} = 0.0035$

(b) Varying road class $b_{z,R}$ and fixed vehicle speed $v = 100 \frac{\text{km}}{\text{h}}$

Figure 3.4: Local estimation condition index, local unobservability index and maximum upper bound of the local unobservability index for varying vehicle speed and varying known road class for an observation time of $t = 5$ s

The unobservability index is below the upper bound for all examined parameters of vehicle speed and road class. Therefore, local weak observability at x_0 is given independently of the vehicle

speed and road class. An increasing vehicle speed as well as an increasing roughness of the road (higher $b_{z,R}$) improve the observability. The estimation condition number decreases slightly with higher speeds and rougher road.

3.6 Analysis of Observability with Unknown Road Excitation and Unknown Road Class

Section 3.5 analyzes the observability of the system with an unknown road excitation. However, a known road class of [68] was implicitly assumed because the road excitation parameter $b_{z,R}$, that represents a specific road class [186, p. 4], was regarded as a fixed parameter. In reality, the road class might also be unknown. Therefore, an additional state $x_7 = \kappa_{b,z,R}$ is introduced that represents the relative deviation of the road class parameter from a base value $b_{z,R,0}$ with $b_{z,R} = (1 + \kappa_{b,z,R}) b_{z,R,0}$. The dynamic behavior of this state is

$$\dot{x}_7 = 0. \quad (3.43)$$

The analytic analysis of Section 3.4 for the extended system at $\mathbf{x}_0 = [0 \ 0 \ 0 \ 0 \ 0 \ 0 \ 0]^T$ leads to

$$\det \mathbf{Q}(\mathbf{x}, \mathbf{u}, \dot{\mathbf{u}}, \ddot{\mathbf{u}}, \dots, \mathbf{u}^{(n-1)}) \Big|_{\mathbf{x}_0} = \frac{a_{z,R}^2 b_{z,R,0}^2 c_{z,Bo}^2 c_{z,T}^8 d_{z,Bo,0} v^{11}}{128 c_{r,dyn,F,C}^7 m_T^8 m_{Bo}^4 r_{dyn,0}^{14} \pi^7} * \quad (3.44)$$

$$\left((c_{z,Bo} - a_{z,R} d_{z,Bo,0} v) (m_T + m_{Bo}) + a_{z,R}^2 m_T m_{Bo} v^2 \right) f(\mathbf{u}, \dot{\mathbf{u}}, \ddot{\mathbf{u}}, \dots, \mathbf{u}^{(n-1)}) \neq 0.$$

The form of Equations (3.44) is similar to Equations (3.18) with an additional term $f(\mathbf{u}, \dot{\mathbf{u}}, \ddot{\mathbf{u}}, \dots, \mathbf{u}^{(n-1)})$. The term is not shown for readability reasons. The full equation is shown in Appendix A.5. This term prevents the analytic analysis of Equations (3.44). However, it shows that some principles for the observability of the system remain with changing to an unknown road class. Obviously, the base road class parameter $b_{z,R,0}$ is still required to be different from 0. The behavior of the numerical unobservability index and its upper bound is similar to Figure 3.3 and Figure 3.4 and is therefore not visualized here but can be found in Appendix A.5 in Figure A.1 and Figure A.2.

3.7 Theoretical Insights

Before theoretical insights of the observability are summarized, remarks regarding the conducted analyses are recapitulated. Local observability analysis methods were applied. Therefore, the conducted analyses allow only for assured statements of the observability at the analyzed operation point. The selected operation point \mathbf{x}_0 corresponds to the system being in a steady state. Selecting an operation point that is not a steady state should improve the observability due to the nature of the damping coefficient variation. However, this was not analyzed in this section. Conclusions of the observability analysis in analytic form in Section 3.3 and 3.4 assume a known road excitation or a known stochastic input signal. The stochastic observability analysis might vary in its exact numbers because of the numerical approximation of the gradients of the stochastic system. However, the characteristic of the performed stochastic observability analysis

is conservative [188, pp. 91-92]. Therefore, the validity of the stochastic analysis is given. In conclusion, the combination of the results of the analytic analysis and the stochastic analysis is sufficient for drawing conclusions for engineering applications which is the purpose of this thesis.

The property of observability is connected to the selected mathematical vehicle model as well as the selected model inputs and measurement outputs. This chapter analyzed the observability on the basis of a wheel-individual quarter-vehicle model. Using combinations of sensor signals as measurement signals (e.g. the comparison of the wheel speed of the front and rear axle) requires a new observability analysis with a more complex model (e.g. a half-vehicle model) and additional simplifying assumptions to reduce the model complexity (e.g. assuming an identical road excitation for different wheels). However, simplifying assumptions will not necessarily hold in reality and therefore, statements regarding the observability for combinations of sensor signals would not necessarily hold in reality. Therefore, an investigation of the observability by means of a simple, small and isolated model is most useful.

It is possible to detect deviations of the damping coefficient by measuring only the wheel speed signal without explicitly measuring the road excitation. Increasing the observation time improves the observability. It is sufficient to select a couple of seconds as observation time (e.g. five seconds).

Observability is given regardless of the vehicle speed and road roughness. However, a higher velocity and a greater road excitation (rougher road) improve the observability and should therefore enhance the performance of a damper health monitoring system. This knowledge can be used as activation condition for a damper defect detection system.

4 Machine Learning Methods for Damper Diagnosis

This chapter shows the overall approach for the evaluation of Machine Learning (ML) methods for the detection of defective automotive dampers. First, Section 4.1 discusses different ML concepts with regard to a real-world implementation and identifies the most suitable concepts. The structure of the remaining chapter is then explained at the end of Section 4.1 in alignment with the identified suitable methods and the general machine learning workflow. The developed software for damper defect detection is publicly available in [196].

4.1 Identification of Suitable Methods

Section 2.4 demonstrates that a great variety of ML algorithms exists and that it is not possible to analyze all methods for their suitability for the diagnosis of damper defects. Therefore, it is necessary to identify the most promising concepts with regard to a real-world implementation.

Comparison of a Continuous and a Discrete Health Indicator

Health monitoring systems may indicate different levels of information about the monitored system's health [197, p. 5]. They might only detect the presence or absence of a fault, classify the nature of a fault, estimate a continuous health indicator, or even estimate the Remaining Useful Life (RUL).

A continuous value of a system's health (e.g. a health indicator in percent or RUL) would be the most interesting because this supplies more information compared to a discrete health indicator (e.g. "defect" or "intact" classification). However, this places increased demands on the availability of training data with varying degrees of fault severity. The realization of a continuously aging damper for data acquisition proved to be difficult in [198, p. 5]. Even if the generation of driving data with different fault severities would be possible in the context of a research project, it cannot be assumed that this effort will be spent by an OEM during series development for a real-life implementation of the damper health state monitoring for each vehicle type. The classification to an "intact" or "defect" health state leads to the least requirements for data availability. A dataset that consists of only two health states of each damper is required. Therefore, this thesis focuses on methods for the estimation of a discrete health state.

Comparison of Supervised and Unsupervised Learning

The main difference of supervised and unsupervised learning method is the requirement of labeled training data. Supervised learning methods are expected to lead to a better performance

for the health state monitoring compared to unsupervised learning approaches due to the additional information that is available in the labeled training data. However, these labels are not available for driving data of fleets or of former development vehicles at an OEM. Therefore, driving data with a labeled chassis system health state has to be generated for supervised learning approaches. While this data generation is possible on a small scale within the scope of this thesis, it might be a major challenge for OEMs on a large scale due to various different vehicle models. It also generates additional costs during the vehicle development phase.

Unsupervised learning methods are expected to lead to a lower diagnosis performance compared to supervised learning methods. However, labeled training data is not necessary and unlabeled driving data of fleets or of former development vehicles at an OEM can be used for the training of unsupervised methods. If existing data is used, no additional costs are generated.

In summary, the decision of using supervised or unsupervised learning has to be made upon the required performance of the health monitoring system and the costs for data generation. This trade-off cannot be answered at this point of the thesis. Therefore, both concepts are investigated for health monitoring. Due to the discussed requirement of generating a discrete health indicator, supervised classification as well as unsupervised one-class classification approaches are evaluated in this thesis.

Comparison of Shallow Machine Learning, Representation Learning and Deep Learning

The advantages and disadvantages of Shallow Machine Learning (SML), Representation Learning (RL) or Deep Learning (DL) with regard to a real-world application are discussed based on the following aspects:

- **Traceability of the method** so that it is possible to derive human understandable causalities from input to output and understand what happens within the trained ML method.
- **Incorporation of prior knowledge** so that it is possible to add existing knowledge from technical experts or from existing model-based systems to the ML approach, e.g. incorporating model-based estimated parameters.
- **Expected performance** that results from applying a ML method to a given dataset based on information of the state of the art.
- **Expected required size of the training data** because requiring more training data leads to higher costs for generating this data.
- **Transferability to other defects or applications** so that it is possible to apply a process of health monitoring to other defects or applications with low additional manual effort
- **Data size for transmission** because it may be necessary to run a health monitoring system on a remote server instead of running it on an Electronic Control Unit (ECU). Therefore, the size of the data for transmission should be as low as possible.

Computational and memory requirements are not considered within this thesis because they are not only dependent on the method itself but also on its actual implementation. The characteristics of each concept are summarized in Figure 4.1 and are explained in the following paragraphs.

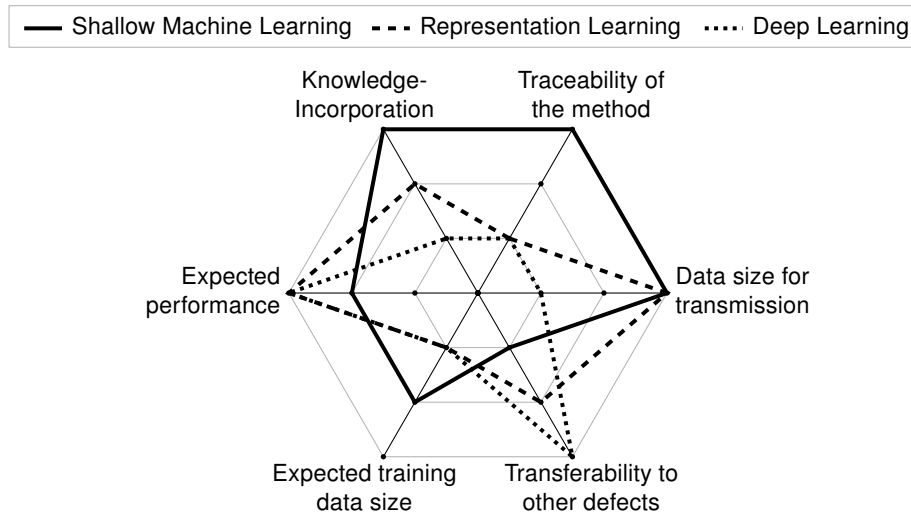


Figure 4.1: Assessment of suitable machine learning concepts for damper health state monitoring. The outer line represents a positive, the middle line a neutral and the inner line a negative fulfillment of the discussed characteristic. The expected training data size and the data size for transmission are “positive” if a low amount of data is required for training or needs to be transmitted.

Shallow Machine Learning (SML) operates on hand-crafted features and the performance is dependent on engineering discriminative features. This is a drawback in case that no good features are found. However, the inclusion of expert knowledge by adding self-developed features (e.g. model-based estimated component parameters) is easily possible. Furthermore, the calculation of features compresses the size of the required data. If the health monitoring application runs on a server, the features can be calculated on the ECU within the vehicle and the amount of data that needs to be transferred via mobile network is reduced.

Representation Learning (RL) generates features automatically and classifies them in a second step. Compared to SML approaches, the transferability to other defects is increased due to the automatic feature generation [103, p. 4]. However the traceability of the system’s behavior is reduced because the generated features do not have a physical interpretation anymore. The expected required size of the training data is higher than for SML approaches because not only the classifier’s parameters need to be trained but also the parameters for the feature generation method. This increases the number of trainable parameters and the complexity of the overall approach. Therefore it is expected that the required training data is increased [199, p. 1]. The expected accuracy of RL approaches is higher compared to SML approaches [103, p. 4].

Deep Learning (DL) leads to a better performance compared to other SML approaches in many fields of science and engineering [19, p. 1]. Therefore, the expected accuracy is high. The traceability of the system behavior is low and the incorporation of existing knowledge is difficult because DL is able to learn abstract and complicated features [19, p. 3]. These abstract features lead to a good transferability to other defects on the one hand, but to the expectation of a large amount of required training data on the other hand. A DL system of a high complexity might need to be executed on a remote server. This requires the transmission of the data via a mobile network from an ECU to the server. The data transmission for DL methods is extended compared to SML approaches, because many DL systems for machine health monitoring are designed as end-to-end structure that process raw sensor data or use data pre-processings that do not reduce the data size significantly (e.g. FFT).

The assessment showed that each ML concept has its advantages and disadvantages. This

corresponds to existing statements in literature claiming that there is no concept that is superior to the other concepts [114, p. 11, 18, p. 19]. Therefore, it is not possible to select one specific concept, but methods of SML, RL and DL are evaluated within this thesis. Selecting supervised and unsupervised methods of these three concepts leads to a matrix of investigated methods as shown in Figure 4.2. The feature generation methods for SML and RL are described in Section 4.3 and 4.4. Classification of the SML and RL feature sets is performed using the same methods whereas the supervised learning approach is described in Subsection 4.6.1 and the unsupervised learning approach is described in Subsection 4.6.2. Supervised and unsupervised DL methods are presented in Subsection 4.7.1 and 4.7.2. The remaining structure of this chapter is aligned with the general machine learning workflow as visualized in Figure 4.3. A brief overview of data acquisition and the observation generation is provided in Section 4.2. Feature reduction techniques are described in Section 4.5. Evaluation metrics for the comparison of the different ML concepts are introduced in Section 4.8. Finally, post-processing methods that account for temporal relations of the health monitoring are presented in Section 4.9. Accounting for temporal relations after the actual classification step avoids the necessity of recurrent methods (e.g. LSTMs) and therefore leads to comparable ML architectures across SML, RL and DL. Recurrent networks would also imply more strict requirements on the temporal relations in the training data that can not be granted within this thesis.

	Supervised Learning <i>Subsection 4.6.1</i>	Unsupervised Learning <i>Subsection 4.6.2</i>
Shallow Machine Learning <i>Section 4.3</i>	<i>Section 4.3</i> <i>Subsection 4.6.1</i>	<i>Section 4.3</i> <i>Subsection 4.6.2</i>
Representation Learning <i>Section 4.4</i>	<i>Section 4.4</i> <i>Subsection 4.6.1</i>	<i>Section 4.4</i> <i>Subsection 4.6.2</i>
Deep Learning <i>Section 4.7</i>	<i>Subsection 4.7.1</i>	<i>Subsection 4.7.2</i>

Figure 4.2: Matrix of investigated machine learning concepts and structure within this thesis

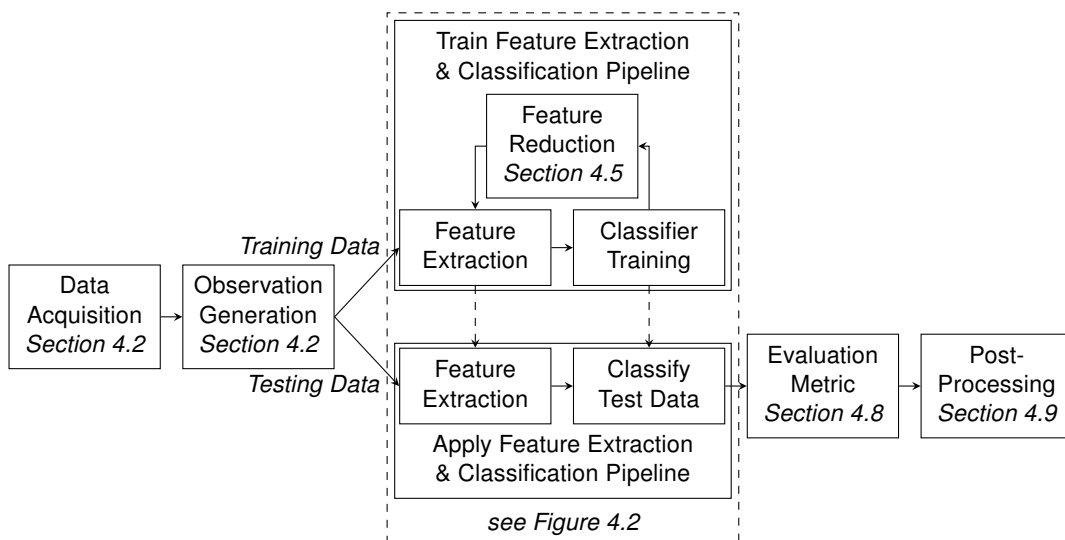


Figure 4.3: Overall machine learning workflow and structure within this thesis

4.2 Data Acquisition and Observation Generation

The evaluation of the suitability of machine learning approaches for the health monitoring of automotive dampers requires a dataset that consists of driving data of different damper health states. There are various root causes for damper defects in reality [200, p. 338]. A common fault is leakage of the damper [200, p. 338, 201]. Hernández-Alcántara et al. [16] and Guba et al. [2] conduct test bench measurements using different oil levels of a damper. The damper characteristic shows a reduced damper force at given damper speeds. Jautze [17, p. 7] simulates defective dampers by changing the stationary force of the damper by switching semi-active dampers from the vehicle's "Sport" to "Comfort" configuration.

This thesis conducts measurements of driving data using an upper class sedan vehicle of a Bavarian manufacturer. The vehicle is equipped with semi-active dampers, similar to the system presented in [202]. It enables the variation of the stationary damper force by varying the electric current of electro-hydraulic damper valves. Figure 4.4 shows the characteristic curves of the selected damper configurations for a front and a rear axle damper. An "intact" curve represents a damper configuration that complies to a vehicle with conventional passive dampers. A defective damper is simulated by a characteristic curve that generates significantly less damping force than the intact configuration. The following four different vehicle health configurations are generated:

- all dampers intact - representing an intact vehicle,
- all dampers defect - representing wear on all dampers,
- a single defect of the Front Left (FL) damper with the other dampers being intact and
- a single defect of the Rear Right (RR) damper with the other dampers being intact.

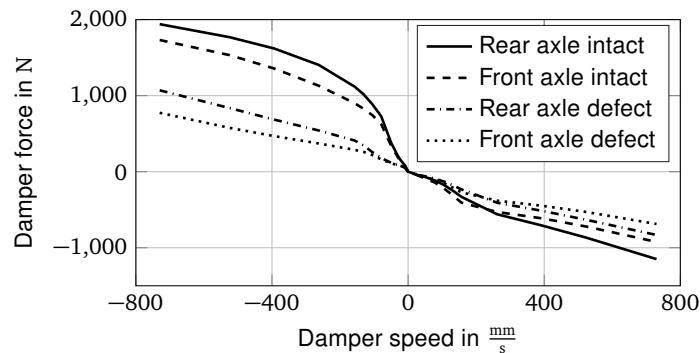


Figure 4.4: Characteristic curve of a single damper [121, p. 5]

It shall be possible to apply the approaches of this thesis to a great number of vehicles. Therefore, only standard ESC system sensor readings are used, even though the upper class vehicle supplies additional sensors such as the vertical acceleration of the wheels. The values are logged from the vehicle's internal bus system with a sampling frequency of 100 Hz. Seven sensor signals are used in total: four wheel speed signals, longitudinal acceleration, lateral acceleration and yaw rate.

The observation generation is based on Merk [203, pp. 34-35]. The common procedure of cutting continuous log data into observations is applied [28, p. 4]. Based on the theoretical insights from Section 3.7 an observation time of 5.12 s is selected. Hereby, no padding is required for the calculation of an FFT. An observation is generated if the average speed within the selected observation time is above the threshold $v_{\text{obs,min}}$ and the average longitudinal and average lateral acceleration are below the thresholds $a_{X,\text{obs,max}}$ and $a_{Y,\text{obs,max}}$. The resulting

amount of observations is then split into 80 % training and 20 % testing data by random selection of individual observations. The selected thresholds $v_{\text{obs,min}}$, $a_{X,\text{obs,max}}$ and $a_{Y,\text{obs,max}}$ can be used as parameters to limit the datasets to certain circumstances.

The only pre-processing of the dataset is removing the moving average (detrending) of the sensor signals. This allows for a focus on relevant oscillations of higher frequencies. Also due to this focus, delaying the front wheel speed signals using the wheelbase and the vehicle speed to match the rear wheel speed signals is not performed. A vehicle speed of $100 \frac{\text{km}}{\text{h}}$ with a sampling frequency of 100 Hz results in a traveled distance of 27.8 cm per sample point. Therefore, both signals could not be matched exactly for higher frequencies.

The training data is used to train the pipeline of feature extraction and classification as visualized in Figure 4.3. The feature extraction process transforms the time-based sensor data of each observation to a feature vector. These feature vectors are then classified. The trained pipeline is applied to the testing data for assessing unknown data. Temporal relations of consecutive observations of one measurement file can be accounted by post-processing of the apriori classification result.

4.3 Hand-crafted Feature Generation for Shallow Machine Learning

This thesis uses two approaches for the generation of hand-crafted features for SML concepts. One feature set consists of features of several domains (e.g. time domain or frequency domain). Within this thesis, this feature set is called “manual features” and is described in Subsection 4.3.1. The second feature set consists of FFT data points that are interpreted as features. Details on the FFT feature set are explained in Subsection 4.3.2.

4.3.1 Manual Feature Generation

The approach of the manual feature generation is based on Merk [203] and Bykanov [204]. The overall approach is presented by Zehelein et al. [120]. This section gives a brief introduction to the calculated features. A summary is presented in Appendix B in Table B.1.

Every mathematical transformation of a vector or a matrix to a number can be interpreted as a feature generation method [205, p. 90]. Therefore, there is a great number of methods for manual feature generation in literature [205, p. 90]. Simple time domain-based features are calculated for each signal such as the minimal or maximal value of a time signal. Statistic properties such as the variance, skewness and kurtosis of each sensor signal are evaluated and accounted as features. Frequency-domain characteristics such as the amplitudes and locations of eigenfrequencies, or the signal energy within given frequency ranges or in the vicinity of eigenfrequencies are also considered as features. But also more complex features are calculated. An Auto-Regressive signal model (AR model) is a method for modeling and predicting stochastic signals using linear combinations of former values of the corresponding signal [206, p. 1]. An AR model is fitted to each sensor signal for each observation. The resulting AR model coefficients capture the characteristics of the original signal and are interpreted as features. The selected order of the AR model determines the resulting number of features and is selected as ten in this thesis. An information theory-based feature is the signal entropy, which is a measure of the average information content. There are different entropies such as the sample

entropy, the log-energy entropy, the shannon entropy or the approximate entropy that are used as features. Singular values of a matrix are also selected as features. A matrix that consists of the time signal values of each sensor as columns is created for each observation. Calculating the singular values of this matrix results in a number of features that is equal to the amount of sensor signals. The manual feature set consists of 378 features.

4.3.2 FFT Data Points as Features

The manual feature set contains many frequency-based features. However, the generation of these features requires expert knowledge e.g. in terms of selecting proper ranges for bandwidth energies. Therefore, the question arises if it is sufficient to use the data points of the FFT of each sensor signal as feature set. Even though this does not require any manual feature engineering, it is not categorized as Representation Learning (RL) because the FFT is only a transformation of data without any training phase.

Averaging of features was found to be beneficial for classification in [207, p. 5] and was confirmed for FFT input data for the damper diagnosis by Werk [208, p.58] and Trumpp [209, p.42]. Therefore, each observation is divided into smaller segments. The FFT is then applied to each segment and the resulting FFT data points are averaged across the segments of one observation. This suppresses random feature values caused by noise in the logged data and also reduces the amount of features. Both effects are especially important for the FFT feature set because the fourier transformation generates a large number of features. This will result in noisy features. The length of each segment as well as the overlap of the segments can be used as tuneable parameters. A segment length of 128 time signal data points with 50% overlap is selected. Hereby, the FFT feature set for seven sensor signals with an FFT length of $128/2 = 64$ datapoints for each signal consists of $7 \times 64 = 448$ features.

4.4 Automated Feature Generation using Representation Learning

Representation Learning (RL) reduces the manual effort for finding discriminative features. The most common RL algorithm are Autoencoders [103, p. 4]. Therefore, this is one selected method for automated feature generation that is evaluated in this thesis.

While the performance of Autoencoders is dependent on many hyperparameters, the feature learning method Sparsefilter requires only one hyperparameter which is the number of features. Due to this simplicity, Sparsefilters are the second automated feature learning method.

The presented approach is based on Werk [208] and Bykanov [204] and is presented by Zehelein et al. [118]. The following two subsections summarize the presented methods starting with an explanation of the theory followed by a description of the parameterization of the algorithm at the end of each subsection.

4.4.1 Automated Feature Generation using Autoencoders

An Autoencoder, as shown in Figure 4.5, is a feed-forward neural network that is trained in an unsupervised manner to reconstruct its input data at the output. Therefore the number of input and output neurons is identical. The hidden layers of a typical under-complete Autoencoder

generate a bottleneck to force an information compression.

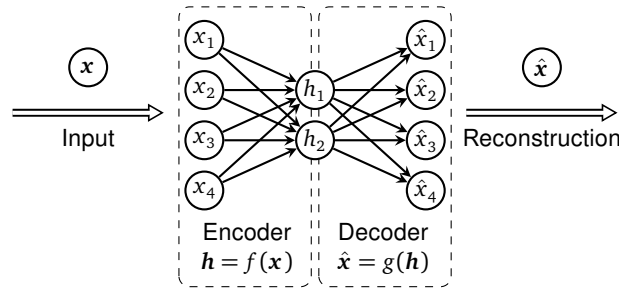


Figure 4.5: Visualization of an Autoencoder

An Autoencoder is a nonlinear generalization of the Principle Component Analysis (PCA) and can be used for the reduction of data dimensionality [210, p. 1]. Using one hidden layer in combination with a linear activation function of the hidden neurons and the mean squared error L_{MSE} as loss function results in learning the same subspace as a PCA [211, 212]. Adding a nonlinear activation function to the output layer or adding additional components to the loss function results in Autoencoder features that are different from the subspace of a PCA.

Vincent et al. [213] propose a layer-wise pre-training of an Autoencoder architecture that consists of multiple hidden layers. The encoder part of the pre-trained network is then combined with a classification stage. The resulting network is fine-tuned using a supervised learning criterion. However, since this procedure combines feature extraction and classification in one combined training phase, it is regarded as DL in this thesis.

The Autoencoder-based feature generation method in this thesis is based on the presented approach of Zehelein et al. [118]. The Autoencoder is used for pure feature extraction and is trained using an unsupervised input reconstruction criterion without supervised fine-tuning. The Autoencoder feature set, consists of the generated values at the middle hidden layer of the trained Autoencoders.

The following paragraphs summarize the mathematical background of the Autoencoder based on [118] for one hidden layer. A more detailed description can be found in [103, chapter 14].

The hidden layer's activation \mathbf{h} is based on the input vector \mathbf{x} by

$$\mathbf{h} = f(\mathbf{x}) = f'(\mathbf{W}^{(1)}\mathbf{x} + \mathbf{b}^{(1)}) \quad (4.1)$$

with the activation function $f'(\cdot)$, the encoder weight matrix $\mathbf{W}^{(1)}$ and the encoder bias vector $\mathbf{b}^{(1)}$. Similarly, the reconstruction $\hat{\mathbf{x}}$ of the input vector is calculated by

$$\hat{\mathbf{x}} = g(\mathbf{h}) = g'(\mathbf{W}^{(2)}\mathbf{h} + \mathbf{b}^{(2)}) \quad (4.2)$$

using the decoder activation function $g'(\cdot)$, the decoder weight matrix $\mathbf{W}^{(2)}$ and the decoder bias vector $\mathbf{b}^{(2)}$. The loss function of the training data matrix $\mathbf{X} = [\mathbf{x}_1, \mathbf{x}_2, \dots, \mathbf{x}_N]$ of N training observations and its reconstruction $\hat{\mathbf{X}}$ is calculated by

$$L(\mathbf{X}, \hat{\mathbf{X}}) = L_{\text{MSE}} + \lambda L_{L_2} + \beta L_{\text{Sparse}} \quad (4.3)$$

and consists of the mean squared reconstruction error L_{MSE} , an L_2 -weight regularization error L_{L_2} as well as a sparsity regularization term L_{Sparse} . The weighting is adjustable using the L_2 -weight regularization coefficient λ and the sparsity regularization coefficient β . The mean squared reconstruction error for the training data matrix \mathbf{X} with an observation dimension $\mathbf{x} \in \mathbb{R}^K$ is

calculated by

$$L_{\text{MSE}}(\mathbf{X}, \hat{\mathbf{X}}) = \frac{1}{N} \sum_{n=1}^N \sum_{k=1}^K (x_{k,n} - \hat{x}_{k,n})^2 \quad (4.4)$$

with the element $x_{k,n}$ in the k -th row and n -th column of \mathbf{X} . The L_2 -weight regularization prevents overfitting caused by an excessive growth of the internal weights of the Autoencoder. The corresponding loss term is calculated by

$$L_{L_2} = \frac{1}{2} \sum_{d=1}^D \sum_{k=1}^K w_{d,k}^2 \quad (4.5)$$

with the number of neurons D in the hidden layer and the element $w_{d,k}$ in the d -th row and k -th column of the weight matrix \mathbf{W} . Sparsity improves the performance of an Autoencoder [214, p. 2]. The sparsity regularization term enforces a specific activation of each neuron across all observations. Therefore, the average activation $\hat{\rho}_d$ of the d -th neuron is calculated by

$$\hat{\rho}_d = \frac{1}{N} \sum_{n=1}^N f'(\mathbf{w}_d^T \mathbf{x}_n + b_d). \quad (4.6)$$

The average neuron activation is interpreted as Bernoulli random variable with mean $\hat{\rho}_d$. The sparsity regularization term is the Kullback-Leibler (KL) divergence of $\hat{\rho}_d$ to a Bernoulli random variable with the mean of the desired neuron activation ρ [215, p. 15] and is calculated by

$$L_{\text{Sparse}} = \sum_{d=1}^D D_{\text{KL}}(\rho \parallel \hat{\rho}_d) \quad (4.7)$$

$$= \sum_{d=1}^D \rho \log\left(\frac{\rho}{\hat{\rho}_d}\right) + (1 - \rho) \log\left(\frac{1 - \rho}{1 - \hat{\rho}_d}\right). \quad (4.8)$$

The focus of Zehelein et al. [118] is the analysis of the suitability of Autoencoder features for diagnosing damper defects. Therefore, the parameters of the overall approach regarding different variants of the sensor signal fusion, pre-processing of input data as well as the Autoencoder network configuration itself are analyzed. The performance indicator is the classification accuracy on the testing dataset using a linear SVM.

Raw time signal sensor data as well as FFT data are used as input data for the Autoencoders in [118]. Using FFT input data outperforms raw time signals. Therefore, this thesis uses FFT data as input data for the Autoencoders. The segmentation parametrization of the FFT generation is identical to the generation of FFT features in Subsection 4.3.2.

Four different variants for sensor fusion of the seven sensor signals are evaluated in [118]. Training one single Autoencoder for all sensor signals increases the amount of training data for the Autoencoder and leads to the best performance in [118]. Within this thesis, one individual Autoencoder is trained for each sensor signal because this enables the analysis of the importance of the sensor signals at a later point in this thesis. The performance of this sensor fusion method is in a similar range compared to training one single Autoencoder for all sensor signals in [118].

The Autoencoder network configuration analysis in [118] shows that adding more hidden layers does not increase the overall classification performance. All network configurations result in a comparable accuracy on the test dataset when using FFT input data. Therefore, each

Autoencoder is set up to have one hidden layer with 50 neurons that generates 50 features per sensor signal. This results in 350 features. The hyperparameters regarding sparsity and L_2 -weight regularization are optimized using a Bayesian optimization with 100 iterations.

4.4.2 Automated Feature Generation using Sparsefilters

Sparsefilters were invented by Ngiam et al. [216] based on their critique that many feature learning algorithms consist of a high number of hyperparameters. Therefore, Sparsefilters consist of only one parameter: the amount of generated features.

Sparsefilters transform input data into a feature representation using a simple matrix multiplication $F = WX$. The weight matrix W is selected so that the feature matrix F shows population sparsity while enforcing high dispersal [216, p. 3]. The mathematical description of these properties is explained in the following paragraphs based on [216] and the summary presented by Zehelein et al. [118]. A detailed analysis of Sparsefilters can be found in [217].

High dispersal requires each feature to be equally active across all observations. This property can be implemented into a mathematical optimization by a L_2 -normalization of the j -th feature (row) vector $f^{(j)}$ across all observations with

$$\tilde{f}^{(j)} = \frac{f^{(j)}}{\|f^{(j)}\|_2}. \quad (4.9)$$

Population sparsity requires that each observation (column) vector x_i is represented only by few active elements in its corresponding feature vector f_i . Therefore, the resulting features from Equations (4.9) are L_2 -normalized per observation

$$\hat{f}_i = \frac{\tilde{f}_i}{\|\tilde{f}_i\|_2}. \quad (4.10)$$

Finally, the weight matrix W is selected to minimize the sum across all N observations of the L_1 -norm of these normalized features with

$$\min_W \sum_{i=1}^N \|\hat{f}_i\|_1 = \min_W \sum_{i=1}^N \left\| \frac{\tilde{f}_i}{\|\tilde{f}_i\|_2} \right\|_1. \quad (4.11)$$

The suitability of Sparsefilter features for damper defect detection is analyzed by Zehelein et al. in [118], identically to the Autoencoder analysis in Subsection 4.4.1. Using detrended time signal input data outperforms FFT input data. The best sensor fusion method is one single Sparsefilter for all signals. However, due to the named aspects in Subsection 4.4.1, an individual Sparsefilter is trained for each sensor signal in this thesis. Segmentation of the time signal input data improves the classification accuracy. Hereby, the input data of one observation is split into multiple segments. The Sparsefilter is then applied to each segment individually and the resulting features are averaged across all segments of one observation. The number of generated features is set to 50 per sensor signal. This results in a feature set of 350 features.

4.5 Feature Reduction and Feature Importance Quantification

Feature reduction addresses the problem that using many features is not necessarily beneficial for a classifier's performance. This behavior is also called the curse of dimensionality [104, pp. 33-38, 218]. There is a large variety of methods to find the best discriminative features as shown in the survey papers [219, 220, 221, 222]. Feature selection methods can be categorized based on their search strategy into filter, embedded and wrapper methods [222, p. 10]. Filter methods generate an index for the discriminative power of each feature that is often based on statistics or mutual information criteria. The result is independent from the type of the used classifier and the process of filtering is fast. However, dependencies and correlations of features are not considered. Embedded methods use built-in characteristics of classifiers to quantify the discriminative power of features (e.g., the path length of a decision tree or the corresponding weight within a linear SVM). Only some specific classifiers generate an internal ranking of the features, and the results depend on the employed classifier. Wrapper methods use a performance score for quantifying the discriminative power of the employed feature subset. Varying the employed feature subset allows an importance ranking of features. Wrapper methods tend to use excessive computation power [222, pp. 10-11] but are said to lead to a better performance than filter methods [220, p. 2].

The classification performance is analyzed using wrapper methods because of their ability to find better feature subsets compared to filter methods and their ability to be used with all types of classifiers. While wrapper methods are inappropriate for large datasets, applying these methods is computationally possible for the dataset within this thesis. The quantification of the discriminative power of features is conducted using the Fisher score. Both methods are explained in the following sections.

4.5.1 Recursive Feature Elimination

The Recursive Feature Elimination (RFE) algorithm is a wrapper method that is proposed in [223, pp. 6-7]. The following algorithm is implemented for a backwards features elimination:

1. Train the classifier based on the initial feature subset and compute the misclassification rate of the trained classifier on a validation dataset
2. Remove one feature from the initial feature set
3. Train the classifier on the reduced feature subset and compute the misclassification rate
4. Repeat step 2 and 3 until each feature has been deactivated once
5. Remove the feature that results in the lowest performance score. This is the least important feature of the current feature subset in step 1
6. Repeat the whole process beginning from step 1

Instead of removing one feature, it is also possible to remove multiple features at a time (e.g. all features of a specific feature extraction method from Table B.1). Hereby it is possible to rank the importance of feature extraction methods as well as the importance of different sensor signals.

4.5.2 Fisher score

The Fisher score is a widely used feature selection criterion for supervised learning approaches [224, p. 1]. It quantifies the ratio of between-class and within-class distance of the feature space and is calculated for the j -th feature to [224, p. 2]

$$f^j = \frac{\sum_{k=1}^c n_k (\mu_k^j - \mu^j)^2}{\sum_{k=1}^c n_k (\sigma_k^j)^2} \quad (4.12)$$

with the number of classes c , the amount of observations n_k for the class k , the mean feature value μ_k^j and the variance σ_k^j of the j -th feature for observations of class k as well as the mean feature value μ^j of the j -th feature of the complete dataset. The Fisher score is high for features with a high discriminative power (e.g. a high mean distance of data points between classes and a small variance of data points within one class).

This simple version of the Fisher score does not account for correlations of features or synergy effects by combination of features. Therefore, the Fisher score is only employed to quantify the importance of single features within this thesis.

4.6 Shallow Classification Methods

The final step for assessing the damper health state is the actual classification. This section briefly describes the employed supervised and unsupervised learning approaches for Shallow Machine Learning (SML) and Representation Learning (RL) feature sets.

4.6.1 Shallow Supervised Learning Methods for Classification

While there exist various supervised learning algorithms in literature [225, p. 2, 114, p. 2], the choice of an algorithm is often less important than parameter tuning [226, p. 68]. Since the focus of this thesis is the analysis of the suitability of the overall machine learning approaches for damper diagnosis, a single shallow supervised learning algorithm is selected for comparison of the SML and RL feature sets. Neural Networks (NNs), decision trees, KNN and SVM [147] are common representatives for supervised classification [226, p. 58]. NNs are said to produce more compact classifiers than SVMs [104, p. 226]. However, the training of a SVM is a convex optimization and is therefore faster than the nonconvex training of a NN [104, p. 226]. Since this thesis is not about the actual implementation of a classifier and deep NNs will be investigated in Subsection 4.7.1, NNs are not considered for classifying SML and RL features. Various configurations of decision trees, KNN and SVMs were tested for the damper diagnosis approach by Merk [203, p. 57]. A SVM using a linear kernel showed the best performance. Therefore, a SVM using a linear kernel is employed as supervised learning classifier for the comparison of the suitability of SML and RL features.

The overall process of classifying the generated feature sets is based on Merk [203] and Werk [208] and is presented by Zehelein et al. [120] for the manual feature set from Subsection 4.3.1 and in [118] for the FFT feature set (Subsection 4.3.2) as well as for the RL feature sets using Autoencoder (Subsection 4.4.1) and Sparsefilters (Subsection 4.4.2).

The following paragraphs present a summary of the mathematics of a SVM. A detailed description can be found in [147] and [104, chapter 7].

The basic SVM classification problem for a feature vector \mathbf{x} is formulated as linear model. Because the dataset might not be linearly separable, the feature input vector \mathbf{x} is transformed into a higher feature space using a transformation $\phi(\mathbf{x})$. The classification problem is then formulated as [147, p. 10, 104, p. 326]

$$f(\mathbf{x}) = \mathbf{w}^T \phi(\mathbf{x}) + b \quad (4.13)$$

with the weight vector \mathbf{w}^T and the bias b . The training process of the SVM aims to find a hyperplane $\mathbf{w}_0^T \phi(\mathbf{x}) + b_0 = 0$ that separates the training observations with maximal distance of the nearest observation of the training data to the optimal hyperplane [147, p. 6]. The training dataset consists of N observations. A certain amount of misclassifications of the training observations \mathbf{x}_i with the corresponding true class label $y_i \in \{-1, 1\}$ is possible due to introducing a slack variable $\xi_i \geq 0$ [147, p. 8, 104, p. 331]. The optimization is then subjected to [147, p. 8, 104, p. 332]

$$(\mathbf{w}^T \phi(\mathbf{x}_i) + b) y_i \geq 1 - \xi_i. \quad (4.14)$$

The distance of the nearest observation to the optimal hyperplane is maximized by minimizing $\|\mathbf{w}\|_2$. Incorporating a trade-off of misclassifications leads to [147, p. 9, 104, p. 332]

$$\min_{\mathbf{w}} \left(C \sum_{i=1}^N \xi_i + \frac{1}{2} \|\mathbf{w}\|_2 \right) \quad (4.15)$$

with the parameter C as a trade-off between misclassifications of the training dataset and model complexity [104, p. 332, 227, p. 11]. Expressing the weight vector as linear combination of the training data observations [147, p. 10, 104, p. 328]

$$\mathbf{w} = \sum_{i=1}^N a_i y_i \phi(\mathbf{x}_i) \quad (4.16)$$

with the weights a_i , and introducing the kernel function $k(\mathbf{x}_i, \mathbf{x}) = \phi(\mathbf{x}_i)^T \phi(\mathbf{x})$ changes the initial classification problem in Equations (4.13) to [104, p. 329]

$$f(\mathbf{x}) = \sum_{i=1}^N a_i y_i k(\mathbf{x}_i, \mathbf{x}) + b. \quad (4.17)$$

The Lagrangian form of the optimization problem in Equations (4.15) can then be formulated as the maximization problem [104, p. 333]

$$\max_{\mathbf{a}} \left(\sum_{i=1}^N a_i - \frac{1}{2} \sum_{i=1}^N \sum_{m=1}^N a_i a_m y_i y_m k(\mathbf{x}_i, \mathbf{x}_m) \right) \quad (4.18)$$

with respect to $\mathbf{a} = (a_1, \dots, a_N)^T$, subjected to the constraints

$$0 \leq a_i \leq C \quad (4.19)$$

$$\sum_{i=1}^N a_i y_i = 0. \quad (4.20)$$

Due to the classification task in this thesis being a multiclass-classification, several SVMs are trained in a one-vs-all fashion.

4.6.2 Shallow Unsupervised Learning Methods for Novelty Detection

The terms novelty detection, anomaly detection and outlier detection are often used interchangeably [228, p. 3]. However, Géron states that, in contrast to anomaly detection, novelty detection algorithms are trained on a clean dataset without outliers [229, p. 267]. Novelty detection methods are often similar or identical to anomaly detection methods [230, p. 3]. According to Chandola et al., “anomaly detection refers to the problem of finding patterns in data that do not conform to expected behavior” [230, p. 1], while novelty detection “aims at detecting previously unobserved (emergent, novel) patterns in the data” [230, p. 3]. Markou and Singh describe novelty detection as the ability “to differentiate between known and unknown object information during testing” [231, p. 1] and Pimentel et al. define novelty detection “as the task of recognising that test data differ in some respect from the data that are available during training” [228, p. 2]. Within this thesis, damper defects shall be detected during the testing of a ML system without any information on these defects within the training data. Therefore, this thesis will use the phrase “novelty detection”.

The lack of information about damper defects within the training necessitates the use of unsupervised learning methods. Shallow unsupervised learning approaches are often similar to supervised learning methods because unsupervised learning can be conducted as one-class classification [232, 228, p. 2].

Several review papers exist for novelty, anomaly and outlier detection [228, 230, 231, 233, 234, 235]. 14 different algorithms are tested on 15 different datasets in [234] with regard to the classification performance and implementation details such as training time and memory usage. The authors state that overall an Isolation Forest (IF) is the best algorithm. However, investigating the classification performance more closely reveals that there is no algorithm that outperforms the other algorithms.

The approach in this thesis is based on Schuck [236] and the results are presented by Zehelein et al. in [119]. Four common unsupervised learning algorithms are evaluated in [119] for damper diagnosis. The algorithms Angular-Based Outlier Detection (ABOD), k -Nearest Neighbors (KNN), Local Outlier Factor (LOF) and One-Class Support Vector Machine (OCSVM) are tested on the SML and RL feature sets as described in Section 4.3 and 4.4. The influence of different scaling methods is also evaluated in [119]. The following paragraphs summarize the results of [119] and describe the unsupervised learning method that is employed in this thesis.

FFT, Autoencoder or Sparsefilter feature sets in combination with the nearest neighbor algorithms LOF, KNN or ABOD lead to a robust performance with regard to the selected feature scaling method. Using the manual feature set leads to a larger performance variation for each classification algorithm across the different scaling methods. Using a scaling algorithm that transforms the distribution of each feature across the dataset to a Gaussian distribution shows competitive results for each combination of feature set and classification method.

The OCSVM leads to the most unrobust performance regarding different feature sets. The nearest neighbor algorithm’s performance (ABOD, KNN and LOF) is similar for different feature sets. The LOF shows the most competitive performance across the four feature sets. Therefore, this thesis uses the LOF algorithm as unsupervised learning method for SML and RL approaches.

The LOF algorithm was first presented by Breunig et al. [237]. Its novelty score is calculated as the ratio of the datapoint-density in the area of the newly considered observation relative to the point-densities of its k neighbors within the hyper-dimensional feature space. The algorithm’s mathematical background is summarized in the following paragraphs as presented in [119].

$N_k(\mathbf{p})$ is the k -distance neighborhood of an observation \mathbf{p} and contains every observation vector whose distance to \mathbf{p} is less than or equal to $D^k(\mathbf{p})$. $D^k(\mathbf{p})$ is the distance of \mathbf{p} to its k -th nearest neighbor. The reachability distance of an observation \mathbf{p} with respect to an observation \mathbf{o} is defined as

$$\text{reach-dist}_k(\mathbf{p}, \mathbf{o}) = \max(D^k(\mathbf{p}), d(\mathbf{p}, \mathbf{o})) \quad (4.21)$$

with the vector distance $d(\mathbf{p}, \mathbf{o})$ between two observations \mathbf{p} and \mathbf{o} . This distance is selected as Euclidean distance within this thesis. The local reachability density of an observation \mathbf{p} is defined as

$$\text{lrd}_k(\mathbf{p}) = \left(\frac{\sum_{\mathbf{o} \in N_k(\mathbf{p})} \text{reach-dist}_k(\mathbf{p}, \mathbf{o})}{|N_k(\mathbf{p})|} \right)^{-1} \quad (4.22)$$

with the number of elements $|N_k(\mathbf{p})|$ in the k -distance neighborhood of \mathbf{p} . The local outlier factor of an observation \mathbf{p} is then defined as

$$\text{LOF}_k(\mathbf{p}) = \frac{\sum_{\mathbf{o} \in N_k(\mathbf{p})} \frac{\text{lrd}_k(\mathbf{o})}{\text{lrd}_k(\mathbf{p})}}{|N_k(\mathbf{p})|}. \quad (4.23)$$

Due to the results in [119], the number of neighbors is selected as $k = 2$.

4.7 Deep Learning Methods

One of the main arguments for deep architectures can be derived from logical circuits: A function can be more compact when it is sufficiently deep compared to an architecture that is insufficiently deep [154, p. 16]. Various Deep Learning (DL) methods exist for time series classification. Fawaz et al. [238, p. 12] categorize methods into discriminative and generative methods. Discriminative methods are further divided into models that are based on hand engineered features and end-to-end learning methods [238, p. 13]. Because the first category would only be a substitute for a shallow classifier from Subsection 4.6.1, only end-to-end learning methods are considered as DL methods in this thesis. Generative methods are said to learn a representation of the time series in an unsupervised manner first [238, p. 12]. Autoencoders are typical representatives of this class and are evaluated in Subsection 4.7.2.

4.7.1 Supervised Deep Learning Methods for Classification

Some of the most frequently used DL architectures for supervised learning are Convolutional Neural Networks (CNNs), Deep Belief Networks (DBNs) and Recurrent Neural Networks (RNNs) [117]. CNNs are the most frequently-used representatives for supervised end-to-end time series classification [238, p. 14]. CNNs are also the prevailing DL model for prognostics and health management using vibration data [239, p. 6]. CNNs leverage the concepts of sparse interactions and shared parameters. Both ideas reduce the amount of parameters of a network [103, pp. 330-331]. Sparse interactions additionally reduce the number of mathematical operations within a network [103, pp. 330-331].

Research in the area of CNNs is progressing rapidly [103, p. 327]. However, there are no applications of CNNs in the area of health monitoring for an automotive chassis system yet.

Therefore, they are applied in this thesis for damper diagnosis.

Figure 4.6 shows a simple CNN architecture. A convolutional layer generates new feature maps by sliding its kernel of the size $e \times e \times n_{\text{Input}}$ across the input data. The third dimension of the convolutional kernel is the size of the third dimension of the input of the convolutional kernel and is therefore not considered as tuning parameter in this thesis. The value of a feature map at the corresponding location is the result of a convolutional operation of the windowed input data and the kernel weights. The convolutional layer is followed by a pooling layer. The two-dimensional pooling kernel of size $p \times p$ is moved across each input feature map and a statistical quantity (typically the mean or the maximum value) of the pooling kernel's input is the resulting value of the pooling layer at the corresponding position. This operation adds local invariance of the features and reduces the size of the feature maps [240, p. 7]. Local invariance is desirable because in many cases the pure existence of patterns in the input data is more important than its exact location within the input data [103, p. 336].

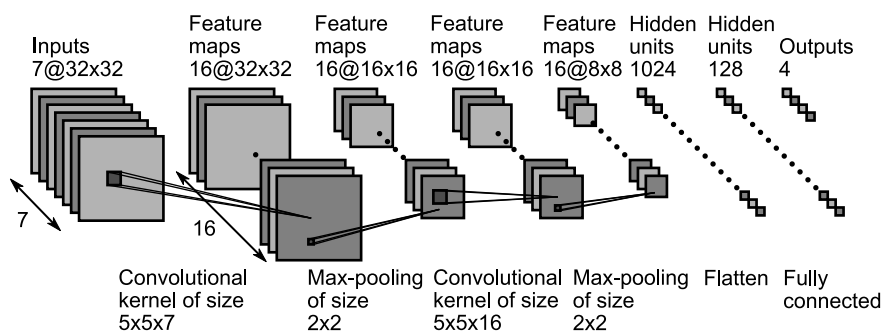


Figure 4.6: Visualization of a Convolutional Neural Network (CNN), based on [240, p. 6], created with [241]

Because CNNs emerged from image classification [154, p. 44], time series data is often transformed to a two-dimensional image and is then classified. Therefore, there are various pre-processing methods for time series data into a two-dimensional representation to be used as input data for a CNN. This includes transforming time series data to a simple gray-scale image [131, 242, 243], using time-frequency analyses such as STFT [244] or WT [127, 128, 245], as well as transformations such as Recurrence Plots (RPs) [246] or Gramian Angular Fields (GAFs) [247, 248]. But also one-dimensional time series data representations are used as input data for CNNs such as using raw signal data [249, 250, 251] or FFT frequency analysis [133]. Therefore, several pre-processing methods for the input data of a CNN are analyzed regarding their suitability for damper diagnosis by Hemmert-Pottmann [252] and are presented by Zehelein et al. [121]. The corresponding software as presented in [121] is publicly available in [253]. The approach is summarized in the following paragraphs.

Input data that results from the following pre-processing methods is analyzed in [121]:

- raw sensor data (one-dimensional)
- detrended sensor data (one-dimensional)
- detrended sensor data with additional scaling (one-dimensional)
- detrended sensor data that is transformed using a FFT (one-dimensional)
- detrended sensor data that is transformed to a grayscale image (two-dimensional)
- detrended sensor data that is transformed using a STFT (two-dimensional)
- detrended sensor data that is transformed using GAFs (two-dimensional)
- detrended sensor data that is transformed using RPs (two-dimensional)
- detrended sensor data that is transformed using a WT (two-dimensional)

Using FFT or STFT pre-processed input data results in the best performance with about 90 % classification accuracy in [121]. Therefore, these methods were selected for further investigation of the architecture of the CNN as well as an analysis of the learned kernel weights. Using detrended time series input data results in about 80 % classification accuracy. To gain further insights on the performed analyses of a CNN, detrended time series input data was also selected for further analysis.

A parameter variation of the network architecture for the three different types of input data was performed as next step in [121]. The network depth as number of consecutive combinations of Convolution/Pooling-layers d , the kernel size of the convolutional layer e and the size of the pooling layer's kernel p were varied. The impact of these variations on the classification accuracy was studied and relations to physical aspects of the input data are stated. These statements regarding physical aspects are further substantiated on the basis of an investigation of the kernel weights. The results of the investigation of the kernel weights and the accuracy of the CNN using this thesis' dataset are presented in Subsection 5.3.3.

4.7.2 Unsupervised Deep Learning Methods for Novelty Detection

The following paragraph discusses existing concepts of unsupervised deep learning methods for novelty detection. One suitable approach is selected, different versions of this approach are introduced and one specific method is identified for the evaluation in this thesis.

Chalapathy and Chawla [254] present a survey of deep learning anomaly detection methods. They categorize existing techniques into semi-supervised, unsupervised and hybrid methods as well as One-Class Neural Networks (OCNNs) [254, p. 6]. Hybrid methods are combinations of feature extractors (e.g. an Autoencoder) and a shallow classifier (e.g. an OCSVM) as performed in [255]. Within this thesis, such an approach is categorized as RL and therefore not considered as DL. Unsupervised deep architectures rely on detecting intrinsic properties of the available data. Autoencoders are said to be the core of unsupervised deep learning techniques [254, p. 6]. Semi-supervised methods are trained on only one class under the assumption of no outliers or novelties within the training dataset. Common semi-supervised methods are also Autoencoders. Unsupervised and semi-supervised methods are conceptually identical for novelty detection with the assumption of the availability of one class as training data. OCNNs combine the feature extraction of deep architectures with the one-class classification approach (e.g. of an OCSVM). Chalapathy et al. [256] present an OCNN and Ruff et al. [257] present a deep Support Vector Data Description (SVDD) method. Both concepts are a consequent realization of a deep architecture for anomaly detection because they directly incorporate an anomaly training objective for finding a hyperplane that separates the training observations from the origin in space. However, investigating the performance in [256, p. 11] shows that an Autoencoder performs better than the OCNN and the deep SVDD. Due to the mentioned circumstances regarding labels and the current state-of-the-art in the area of OCNN and deep SVDD, Autoencoders are chosen as representative for the unsupervised deep learning methods for novelty detection.

As presented in Subsection 4.4.1, an Autoencoder is trained to reconstruct the input data. The coding in the middle layer was used as features for SML in Subsection 4.4.1. In this section, the Autoencoder is used in its intended manner and the input data is reconstructed based on the coding in the middle layer. The reconstruction error can then be used as a measure of novelty of the processed observation. However, various versions of the specific network architecture and training goals of an Autoencoder exist. Common versions are briefly presented in the following

paragraphs and one specific Autoencoder version is selected for the analysis in this thesis.

To ensure the learning of efficient representations, under-complete bottleneck architectures are typically chosen [258, p. 7]. Hereby, a data compression of the coding in the middle layer of the Autoencoder is ensured. Increasing the number of hidden layers leads to a Stacked Autoencoder (SAE).

In contrast to an under-complete Autoencoder, an over-complete Autoencoder consists of more neurons in the middle layer compared to the input layer. Learning of an identity transformation from input to output would be mathematically possible [258, p. 7]. Adding noise to the input data and reconstructing the original noise-free input data prevents learning of an identity transformation and leads to a Denoising Autoencoder (DAE).

An and Cho [259] propose using a Variational Autoencoder (VAE) for anomaly detection that was first introduced by Kingma and Welling [260]. In contrast to a traditional Autoencoder, a VAE is based on a probabilistic model and provides a reconstruction probability rather than a reconstruction error [259, p. 2]. VAEs are stated to be an ideal method for anomaly detection in noisy environments [18, p. 20].

Under-complete SAE, over-complete DAE and VAE are evaluated for damper fault detection by Trumpp [209]. VAE lead to the best diagnosis performance and are therefore selected as unsupervised deep learning architecture in this thesis.

Figure 4.7 visualizes the general structure of a VAE. The encoder models the parameters of the distribution of a probabilistic latent variable z based on the input data x . The decoder models the probabilistic generation of the reconstructed input data based on a sampled instance of the latent variable z . A good mathematical introduction to VAEs is provided in [261, chapter 2] and is summarized in the following paragraphs.

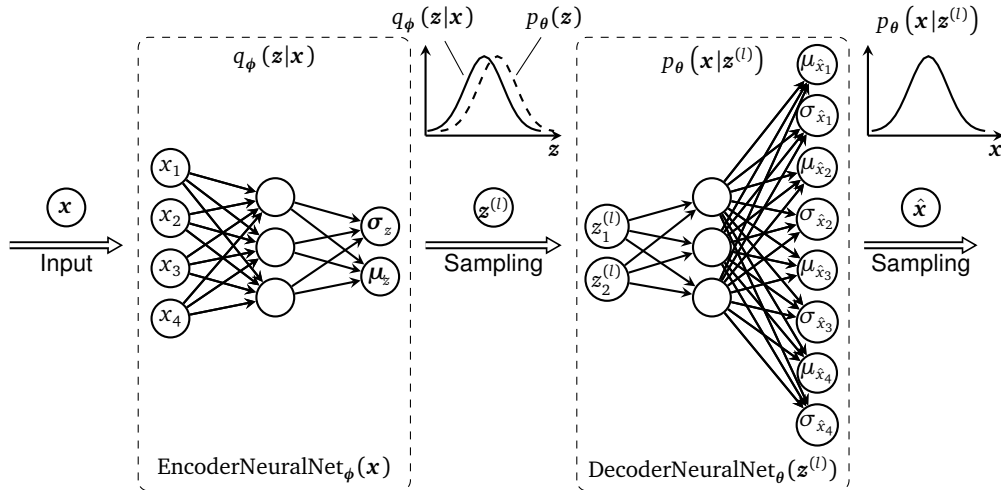


Figure 4.7: Visualization of the network architecture of a Variational Autoencoder (VAE), based on [209, p. 35]

The log-probability that is assigned by a model to the dataset \mathcal{D} , under the assumption of independently and identically distributed observations x , is given by [261, p. 10]

$$\log p_{\theta}(\mathcal{D}) = \sum_{x \in \mathcal{D}} \log p_{\theta}(x) \quad (4.24)$$

with the parameters θ . The marginal probability of one observation can be expressed based on

the latent variable \mathbf{z} by [261, p. 12]

$$p_{\theta}(\mathbf{x}) = \int p_{\theta}(\mathbf{x}, \mathbf{z}) d\mathbf{z} = \int p_{\theta}(\mathbf{z}) p_{\theta}(\mathbf{x}|\mathbf{z}) d\mathbf{z} \quad (4.25)$$

with the so called prior probability distribution $p_{\theta}(\mathbf{z})$ and the conditional probability distribution $p_{\theta}(\mathbf{x}|\mathbf{z})$. The VAE encoder models the so-called approximate posterior $q_{\phi}(\mathbf{z}|\mathbf{x})$. Therefore, the encoder's parameters ϕ are optimized so that the approximate posterior $q_{\phi}(\mathbf{z}|\mathbf{x})$ matches the true (but intractable) posterior $p_{\theta}(\mathbf{z}|\mathbf{x})$ [261, p. 15]. For any choice of distribution for $q_{\phi}(\mathbf{z}|\mathbf{x})$, the log-probability of a single observation can be expressed as [261, p. 18]

$$\log p_{\theta}(\mathbf{x}) = \underbrace{\mathbb{E}_{q_{\phi}(\mathbf{z}|\mathbf{x})} \left[\log \left[\frac{p_{\theta}(\mathbf{x}, \mathbf{z})}{q_{\phi}(\mathbf{z}|\mathbf{x})} \right] \right]}_{\mathcal{L}_{\theta, \phi}(\mathbf{x})} + \underbrace{\mathbb{E}_{q_{\phi}(\mathbf{z}|\mathbf{x})} \left[\log \left[\frac{q_{\phi}(\mathbf{z}|\mathbf{x})}{p_{\theta}(\mathbf{z}|\mathbf{x})} \right] \right]}_{D_{\text{KL}}(q_{\phi}(\mathbf{z}|\mathbf{x})||p_{\theta}(\mathbf{z}|\mathbf{x}))} \quad (4.26)$$

with the so-called Evidence Lower Bound (ELBO) $\mathcal{L}_{\theta, \phi}(\mathbf{x})$ and the Kullback-Leibler (KL) divergence $D_{\text{KL}}(q_{\phi}(\mathbf{z}|\mathbf{x})||p_{\theta}(\mathbf{z}|\mathbf{x}))$ between $q_{\phi}(\mathbf{z}|\mathbf{x})$ and $p_{\theta}(\mathbf{z}|\mathbf{x})$. The KL divergence is a measure of how different one probability distribution is from a second probability distribution [262, p. 1]. Because the KL divergence is always non-negative, the ELBO is a lower bound of the log-likelihood of a single observation in Equations (4.26) [261, p. 18, 263, p. 18]. Therefore, maximizing the ELBO $\mathcal{L}_{\theta, \phi}(\mathbf{x})$ with respect to its parameters θ and ϕ optimizes two things [261, p. 19]: On the one hand, it maximizes the marginal likelihood $p_{\theta}(\mathbf{x})$ and hereby improves the model. On the other hand, it minimizes the KL divergence between the approximate posterior $q_{\phi}(\mathbf{z}|\mathbf{x})$ and the true posterior $p_{\theta}(\mathbf{z}|\mathbf{x})$ and hereby improves the encoder model.

The ELBO can further be expressed as [260, p. 3]

$$\mathcal{L}_{\theta, \phi}(\mathbf{x}) = \mathbb{E}_{q_{\phi}(\mathbf{z}|\mathbf{x})} \left[\log \left[\frac{p_{\theta}(\mathbf{x}, \mathbf{z})}{q_{\phi}(\mathbf{z}|\mathbf{x})} \right] \right] \quad (4.27)$$

$$= \mathbb{E}_{q_{\phi}(\mathbf{z}|\mathbf{x})} [\log p_{\theta}(\mathbf{x}, \mathbf{z}) - \log q_{\phi}(\mathbf{z}|\mathbf{x})] \quad (4.28)$$

$$= \mathbb{E}_{q_{\phi}(\mathbf{z}|\mathbf{x})} [\log p_{\theta}(\mathbf{z}) + \log p_{\theta}(\mathbf{x}|\mathbf{z}) - \log q_{\phi}(\mathbf{z}|\mathbf{x})] \quad (4.29)$$

$$= \mathbb{E}_{q_{\phi}(\mathbf{z}|\mathbf{x})} [\log p_{\theta}(\mathbf{x}|\mathbf{z})] - D_{\text{KL}}(q_{\phi}(\mathbf{z}|\mathbf{x})||p_{\theta}(\mathbf{z})) \quad (4.30)$$

For the optimization of the ELBO it is necessary to calculate the gradient $\nabla_{\theta, \phi} \mathcal{L}_{\theta, \phi}(\mathbf{x})$ with respect to the parameters θ and ϕ . A Monte Carlo estimator could be calculated for the gradient $\nabla_{\theta} \mathcal{L}_{\theta, \phi}(\mathbf{x})$ with respect to θ [261, p. 20]. However, this is not possible for the gradient $\nabla_{\phi} \mathcal{L}_{\theta, \phi}(\mathbf{x})$ with respect to ϕ because the expected value in Equations (4.30) is taken with respect to the approximate posterior $q_{\phi}(\mathbf{z}|\mathbf{x})$, that is dependent on ϕ [261, p. 20]. Therefore, a reparametrization trick of the latent variable is conducted. The latent variable \mathbf{z} is expressed as a transformation $\mathbf{v}(\cdot)$ of another random variable ϵ by [261, p. 20]

$$\mathbf{z} = \mathbf{v}(\epsilon, \theta, \mathbf{x}). \quad (4.31)$$

Hereby, the expected value from Equations (4.30) changes to being taken with respect to the probability distribution $p(\epsilon)$ and the ELBO from Equations (4.30) can be expressed as [264, p. 11, 261, p. 34]

$$\mathcal{L}_{\theta, \phi}(\mathbf{x}) = \mathbb{E}_{p(\epsilon)} [\log p_{\theta}(\mathbf{x}|\mathbf{z})] - D_{\text{KL}}(q_{\phi}(\mathbf{z}|\mathbf{x})||p_{\theta}(\mathbf{z})). \quad (4.32)$$

A Monte Carlo estimator $\tilde{\mathcal{L}}_{\theta, \phi}(\mathbf{x})$ for Equations (4.32) using a sampled $\boldsymbol{\varepsilon}^{(l)}$ is given by [260, p. 4]

$$\boldsymbol{\varepsilon}^{(l)} \sim p(\boldsymbol{\varepsilon}) \quad (4.33)$$

$$\mathbf{z}^{(l)} = \mathbf{v}(\boldsymbol{\varepsilon}^{(l)}, \boldsymbol{\theta}, \mathbf{x}) \quad (4.34)$$

$$\tilde{\mathcal{L}}_{\theta, \phi}(\mathbf{x}) = \underbrace{-D_{\text{KL}}(q_{\phi}(\mathbf{z}|\mathbf{x})||p_{\theta}(\mathbf{z}))}_{\text{Regularization term}} + \underbrace{\frac{1}{L} \sum_{l=1}^L \log p_{\theta}(\mathbf{x}|\mathbf{z}^{(l)})}_{\text{Negative reconstruction error}} \quad (4.35)$$

with the number of drawn samples L . The optimization objective of a VAE is the maximization of the ELBO in Equations (4.35) [261, p. 16]. Therefore, both terms need to be expressed further. The first term, the KL divergence $D_{\text{KL}}(q_{\phi}(\mathbf{z}|\mathbf{x})||p_{\theta}(\mathbf{z}))$, acts as a regularization term and can be calculated analytically for some specific probability distributions. The approximate posterior $q_{\phi}(\mathbf{z}|\mathbf{x})$ can be chosen arbitrarily and is parameterized by the output of the encoder neural network. It can for example be chosen as an isotropic Gaussian distribution $q_{\phi}(\mathbf{z}|\mathbf{x}) = \mathcal{N}(\mathbf{z}; \boldsymbol{\mu}_{\mathbf{z}}, \text{diag}(\boldsymbol{\sigma}_{\mathbf{z}}^2))$. This leads to the following interpretation of the encoder output variables [261, p. 16]

$$(\boldsymbol{\mu}_{\mathbf{z}}, \log \boldsymbol{\sigma}_{\mathbf{z}}) = \text{EncoderNeuralNet}_{\phi}(\mathbf{x}). \quad (4.36)$$

Selecting the prior distribution as an isotropic Gaussian distribution with zero mean and identity variance $p_{\theta}(\mathbf{z}) = \mathcal{N}(\mathbf{z}; 0, \mathbf{I})$ leads to a KL divergence $D_{\text{KL}}(q_{\phi}(\mathbf{z}|\mathbf{x})||p_{\theta}(\mathbf{z}))$ that can be calculated analytically by [260, p. 10, 264, p. 9]

$$D_{\text{KL}}(q_{\phi}(\mathbf{z}|\mathbf{x})||p_{\theta}(\mathbf{z})) = -\frac{1}{2} \sum_{i=1}^{\dim(\mathbf{z})} \left(1 + \log(\sigma_{z,i}^2) - \mu_{z,i}^2 - \sigma_{z,i}^2 \right). \quad (4.37)$$

The second term of Equations (4.35) is the conditional log-probability of the input data \mathbf{x} under the condition of a sampled $\mathbf{z}^{(l)}$ and acts as a negative reconstruction error. Selecting $L = 1$ is sufficient according to [260, p. 4]. The probability distribution $p_{\theta}(\mathbf{x}|\mathbf{z}^{(l)})$ should be selected in accordance to the form of the input data [260, p. 5]. For continuous input data, selecting a Gaussian probability distribution $p_{\theta}(\mathbf{x}|\mathbf{z}^{(l)}) = \mathcal{N}(\mathbf{x}; \boldsymbol{\mu}_{\hat{\mathbf{x}}}, \text{diag}(\boldsymbol{\sigma}_{\hat{\mathbf{x}}}^2))$ is suggested with

$$(\boldsymbol{\mu}_{\hat{\mathbf{x}}}, \log \boldsymbol{\sigma}_{\hat{\mathbf{x}}}) = \text{DecoderNeuralNet}_{\theta}(\mathbf{z}^{(l)}). \quad (4.38)$$

This results in the log-probability [265, p. 110]

$$\log p_{\theta}(\mathbf{x}|\mathbf{z}^{(l)}) = \sum_{i=1}^{\dim(\mathbf{x})} \log \left(\frac{1}{\sqrt{2\pi\sigma_{\hat{x},i}^2}} \exp \left[-\frac{(x_i - \mu_{\hat{x},i})^2}{2\sigma_{\hat{x},i}^2} \right] \right) \quad (4.39)$$

In accordance with [259], the log-reconstruction probability $p_{\theta}(\mathbf{x}|\mathbf{z}^{(l)})$ from Equation 4.39 is used as novelty score in this thesis.

4.8 Evaluation Metrics

This section describes evaluation metrics for supervised and unsupervised learning concepts in Subsection 4.8.1 and 4.8.2. The investigation of this thesis shall enable a quantitative

comparison of both concepts. Therefore, a common metric for both is required. It shall account for the additional information regarding the type of failure that is available by supervised learning methods. A suited common evaluation metric is presented in Subsection 4.8.3.

4.8.1 Performance Metrics for Supervised Learning

Various performance metrics exist for classification tasks [266]. Many essential metrics can be derived from the Confusion Matrix (CM) that is indicated for a binary classification task in Table 4.1.

Table 4.1: Confusion Matrix

		Predicted Class	
		Negative	Positive
True Class	Negative (N)	True Negatives (TN)	False Positives (FP)
	Positive (P)	False Negatives (FN)	True Positives (TP)

The most frequently used metric is the accuracy that is calculated by

$$\text{Accuracy} = \frac{\text{TP} + \text{TN}}{\text{TP} + \text{TN} + \text{FP} + \text{FN}}. \quad (4.40)$$

Besides from accuracy, commonly used metrics are Precision = $\frac{\text{TP}}{\text{TP} + \text{FP}}$, Recall = $\frac{\text{TP}}{\text{TP} + \text{FN}}$ and F-Score = $\frac{\text{Precision} \cdot \text{Recall}}{\text{Precision} + \text{Recall}}$ [267, p. 1]. Precision is a measure of the correctness of a specific predicted class. Recall measures the ability to detect a specific class and F-Score is the harmonic mean of these quantities. For multi-class classification, these measures can be calculated by macro- or micro-averaging [266, p. 4]. Macro-averaging calculates the metric for each class and averages the class-specific measures across all classes. Micro-averaging accumulates the counts (TP, TN, FP, FN) and calculates the measure out of these cumulative counts. Accuracy is identical for micro- and macro-averaging. Sokolova and Lapalme [266] analyze invariance properties of 24 metrics regarding changes in the CM. Each invariance property can be beneficial or disadvantageous, depending on the context of the classification task. Accuracy is a robust measure for the overall performance of an algorithm [266, p. 8]. Therefore, the accuracy is the performance measure for supervised learning classification within this thesis. A balanced dataset with an equal number of observations for each class is generated.

4.8.2 Performance Metrics for Unsupervised Learning

Most unsupervised learning methods result in a continuous novelty score instead of a binary label of consisting to a specific class [268, p. 1]. Comparing the novelty scores of the observations of a dataset with a given threshold would result in a CM and the accuracy could be calculated. However, the resulting CM as well as the accuracy would change with altering the threshold, even though the classifier's performance remains unchanged. Therefore, a metric is required that is independent from this threshold [268, p. 2].

The most popular performance measure of outlier detection methods is the Receiver Operating Characteristic (ROC) and its Area Under Curve (AUC) [269, p. 3, 270, p. 1] as visualized in Figure 4.8. The ROC is a plot with the TruePositiveRate(TPR) = Recall = $\frac{\text{TP}}{\text{Positive}(P)}$ on the y -axis and the FalsePositiveRate(FPR) = $\frac{\text{FP}}{\text{Positive}(P)}$ on the x -axis [271]. Selecting one specific threshold for the comparison of the novelty score results in a single point in the ROC plot. Plotting the

resulting points for all possible selections of the threshold leads to a characteristic curve of the investigated classifier. A perfect classifier results in a curve that reaches the top left corner of the ROC plot with an AUC of 1. A classification by chance results in a curve from the lower left to the top right corner in the ROC with an AUC of 0.5. The probabilistic interpretation of the AUC is the probability that a randomly chosen observation of the (unknown) outlier class has a higher novelty score than a randomly chosen observation of the (known) normal class [272, p. 2]. The AUC is the preferred performance measure for unsupervised learning classification within this thesis because it describes the classifier's performance in a single quantity.

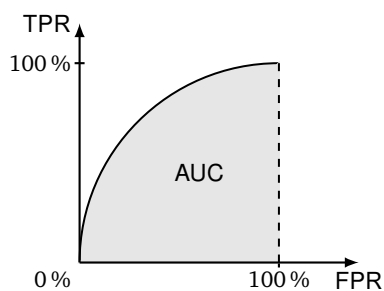


Figure 4.8: ROC curve and AUC

4.8.3 Comparability of Performance Metrics

As shown in Subsection 4.8.1 and 4.8.2, the preferred performance metrics are different for supervised and unsupervised learning. However, the scope of this thesis is the quantitative comparison of supervised and unsupervised learning methods and therefore a common performance metric is required.

Transforming the AUC to an accuracy by selecting a specific threshold for the novelty scores limits the significance of the insights regarding the performance of unsupervised learning concepts. Huang and Ling [273, p. 11] state that AUC is a better measure than accuracy. Therefore, an extension of the AUC for multi-class classification approaches is used as performance metric for the quantitative comparison of supervised and unsupervised learning methods. A great variety of extensions of the AUC to the multi-class case exists but there is no performance indicator that is superior in its behavior [274].

Hand and Till [270] present an extension of the AUC to multi-class classification problems. The basis of their approach is the pairwise comparison of the assigned probability (or score) for each observation of belonging to a class i compared to belonging to class j . Hereby, the classifier's ability to distinguish classes is taken into account even if the overall correct classification rate may be small [270, p. 6]. Sampat et al. [274] compare the approach of Hand and Till with other multi-class performance indicators. The major drawback of Hand and Till's approach is that no deeper insight regarding the discrimination of certain classes is provided [274, p. 12]. However, other performance indicators generate multiple performance measures and therefore do not allow for an easy comparison based on a single quantity. Despite the shown drawbacks in [274], Hand and Till's extension is stated as the most noteworthy extension of an ROC to multi-class problems in [275, p. 131]. Fawcett [271, p. 12] states that the extension of Hand and Till is well justified and is insensitive to unbalanced datasets. For the binary classification case, it reduces to the standard form of the AUC [270, p. 15]. Therefore, Hand and Till's so-called M -value is selected as performance indicator for the quantitative comparison of supervised and unsupervised learning approaches. However, because the accuracy measure is more intuitive, it

is still used to compare the performance of different supervised learning approaches.

For the calculation of the M -value, a ranking of the class affiliation probabilities that are generated by the classifier for each observation is required. Let $f_k = p(i|x_{k,i})$ be the estimated probability of belonging to the class i for the k -th observation $x_{k,i}$ of the true class i with $k = 1, \dots, n_i$. Similarly, let $g_k = p(i|x_{k,j})$ be the estimated probability of belonging to the class i of the k -th observation $x_{k,j}$ of the true class j with $k = 1, \dots, n_j$. Rank the set $[g_1, \dots, g_{n_j}, f_1, \dots, f_{n_i}]$ of the estimated probabilities of belonging to class i of the observations of the true class i and j in increasing order. Let r_k be the rank of the k -th observation with true class i (lowest probability is rank 1, highest probability is rank $n_i + n_j$). The probability that a randomly chosen observation with true class j has a lower estimated probability of belonging to class i than a randomly chosen observation with true class i is [270, p. 4]

$$\hat{A}(i|j) = \frac{1}{n_i n_j} \left(\sum_{k=1}^{n_i} r_k - \frac{n_i(n_i + 1)}{2} \right) = \frac{S_i - n_i(n_i + 1)/2}{n_i n_j}. \quad (4.41)$$

with S_i being the sum of the ranks of the observations of true class i . As in general $\hat{A}(i|j) \neq \hat{A}(j|i)$, the multi-class AUC value M is calculated using the average $\hat{A}(i, j) = \frac{\hat{A}(i|j) + \hat{A}(j|i)}{2}$ to [270, p. 7]

$$M = \frac{2}{c(c-1)} \sum_{i=1}^c \sum_{j=1}^i \hat{A}(i, j) = \frac{2}{c(c-1)} \sum_{i=1}^c \sum_{j=1}^i \left(\frac{\hat{A}(i|j) + \hat{A}(j|i)}{2} \right) \quad (4.42)$$

with the number of classes c .

4.9 Post-Processing of Classifier Output

The presented machine learning approaches do not consider temporal relations of observation. It is therefore possible that in a series of consecutive observations, some observations may be assigned to a different class than the rest of the observations. However, switching several times between health states is physically not possible for the component's true health state. Therefore, methods that consider temporal relations of consecutive observations are employed as post-processing of the classifier output (which is the observation's class affiliation probability or novelty score).

The most intuitive and obvious approach of post-processing the classifier's output is calculating the mean a priori classifier output for consecutive observations. This can be extended to calculating the moving mean or a weighted mean of the classifier output. Even though this might increase the accuracy and AUC, there is no probabilistic justification of these approaches. Taking the mean of the estimated probabilities of consecutive observations does not account for possible real varying health states [104, p. 635] and extending it to a weighted average is hardly optimal [104, p. 636]. Therefore, these approaches are not considered as post-processing of the classifier's output.

Lenser and Veloso [276] present a state-based prediction algorithm for time series data. The approach is an extension of a simple Hidden Markov Model (HMM) [276, p. 1]. Implementing their approach showed an improvement of accuracy and AUC. However, there is no further continuation or discussion of this approach in literature. Therefore, this approach is not considered as post-processing of the classifier output.

Bishop [104, chapter 13] proposes to use HMMs for the post-processing of state-based classification methods and Linear Dynamical System (LDS) for continuous outputs of novelty detection algorithms. These basic algorithms are evaluated for the post-processing of the apriori classifier's estimation result.

4.9.1 Hidden Markov Models for Post-Processing

This section gives a general introduction into HMM, followed by a description of the implementation within this thesis.

A HMM is a tool for representing two combined stochastic processes [277, p. 2, 278, p. 2]. One stochastic process is the discrete transition of hidden states. The second stochastic process issues emissions depending on the current state. A HMM consists of [279, p. 2]

- a set of hidden states $S_{\text{HMM}} = \{s_1, s_2, \dots, s_n\}$ with the number of hidden states n ,
- a set of emissions $V_{\text{HMM}} = \{v_1, v_2, \dots, v_m\}$ with the number of possible discrete emissions m ,
- the state transition probability matrix A_{HMM} with the probability $a_{i,j} = p(s_j | s_i)$ of a transition from the hidden state s_i to the hidden state s_j ,
- the emission matrix B_{HMM} with the probability $b_{i,j} = p(v_j | s_i)$ of an emission v_j given that being in the hidden state s_i and
- the initial state vector π_{HMM} with the probability π_i of being in state s_i as start state.

The application of a HMM consists of three problems [277, p. 5]. The learning problem is the process of finding parameters for $(A_{\text{HMM}}, B_{\text{HMM}}, \pi_{\text{HMM}})$ that maximize the probability of an emission sequence $O = \langle o_1, o_2, \dots, o_T \rangle$ for T discrete time-steps. The Baum-Welch algorithm is an iterative procedure to solve this problem [277, p. 8]. The evaluation problem is the process of computing the probability $p(O | (A_{\text{HMM}}, B_{\text{HMM}}, \pi_{\text{HMM}}))$ of the emission sequence O for a given HMM with the parameters $(A_{\text{HMM}}, B_{\text{HMM}}, \pi_{\text{HMM}})$. Even though the direct calculation of this probability is mathematically possible, it is computationally infeasible. The forward-backward procedure is an efficient procedure for solving this task [277, p. 6]. The third problem is the estimation problem. A state sequence $Q = \langle q_1, q_2, \dots, q_T \rangle$ needs to be found that is most-likely to produce the emission sequence O given the HMM with parameters $(A_{\text{HMM}}, B_{\text{HMM}}, \pi_{\text{HMM}})$. The Viterbi algorithm is an algorithm for finding the single best state sequence [277, pp. 7-8].

Esmael et al. [279] improve the classification accuracy of an apriori classifier by applying a HMM as second classification stage. They use the sequence of the apriori classifier's estimated classes as emission sequence for the HMM and increase the classification accuracy by 14 Percentage Points (PPs). Hereby, each hidden state s_i represents a class i of the apriori classifier and the number of states n is the number of classes c . Even though they improve the classification performance, it is still possible to further improve the post-processing because [279] neglects the information of the apriori estimated class affiliation probabilities.

Therefore, this thesis uses the apriori estimated damper health class affiliation probabilities as emission sequence of the HMM. Hereby, the discrete set of emissions V_{HMM} changes to a vector that contains continuous values and the discrete emission probability matrix B_{HMM} changes to a Probability Density Function (PDF). An introduction to HMM using continuous emissions is given in [280, p. 11]. According to [280, p. 11], the PDF is typically based on Gaussian distributions and can consist of multiple Gaussian models for each state i . Within this thesis, the apriori estimated

class affiliation probabilities for observations that belong to the same true class are represented with one multi-dimensional Gaussian model. Therefore, the probability of an emission vector \mathbf{v} for the i -th state is represented by

$$b_i(\mathbf{v}) = \mathcal{N}(\mathbf{v}; \boldsymbol{\mu}_i, \boldsymbol{\sigma}_i^2) \quad (4.43)$$

with the vector $\boldsymbol{\mu}_i$ as the mean vector and $\boldsymbol{\sigma}_i^2$ as the variance matrix of the apriori estimated class affiliation probabilities for observations that belong to the true class i .

Esmael et al. [279] calculate the transition matrix based on the training dataset. Within this thesis, a different approach is suggested: A transition from one hidden state to another represents a transition of the physical health state of a component. Therefore, the transition matrix is used to parameterize the physically possible dynamic behavior of a component's health state. It is expected that damper defects develop only gradually over a long period of time in reality. Therefore, the transition from a health state i to another health state j is quite unlikely and the elements of the transition matrix \mathbf{A}_{HMM} with

$$a_{i,j} = \begin{cases} 0.95 & i = j \\ \frac{0.05}{c-1} & i \neq j \end{cases} \quad (4.44)$$

are set to a high probability of remaining at the current health state with the number of health classes c . The parameters of the transition matrix \mathbf{A}_{HMM} can be used as tuning parameters of the HMM post-processing.

In [279], the initial state probability $\boldsymbol{\pi}_{\text{HMM}}$ is set identically for each state to $\pi_i = \frac{1}{c}$. This approach is reasonable for an online execution of the HMM. Assuming an offline computation leads to the availability of consecutive observations. Therefore, the initial state probability is set to the average of the apriori estimated class affiliation probability of the apriori classifier with $\pi_i = 1/T \sum_{t=1}^T o_{t,i}$ with the number of consecutive observations T .

Due to several definitions of optimality, there exist several ways of finding a hidden state sequence Q that is associated with a given emission sequence [280, p. 7]. The Viterbi algorithm finds the single best state sequence by maximizing the conditional probability $p(Q|O, (\mathbf{A}_{\text{HMM}}, \mathbf{B}_{\text{HMM}}, \boldsymbol{\pi}_{\text{HMM}}))$ of a state sequence Q given an emission sequence O and the parameters of the HMM $(\mathbf{A}_{\text{HMM}}, \mathbf{B}_{\text{HMM}}, \boldsymbol{\pi}_{\text{HMM}})$ [280, p. 8]. However, to be able to further process the posterior classification performance (e.g. using Hand and Till's M -value), posterior estimated class affiliation probabilities are required. The estimated probabilities of the Viterbi algorithm do not consider the complete measurement but are calculated recursively with time. Therefore, the forward-backward procedure is applied to find a sequence of the individually most likely hidden states [280, p. 6].

The forward-backward procedure is briefly described in the following based on [280, pp. 6-7]. The forward path calculates the probability of being in state s_i at time step t and the partial observation sequence $\langle \mathbf{o}_1, \mathbf{o}_2, \dots, \mathbf{o}_t \rangle$ given the HMM $(\mathbf{A}_{\text{HMM}}, \mathbf{B}_{\text{HMM}}, \boldsymbol{\pi}_{\text{HMM}})$ by

$$\alpha_t(i) = p(\mathbf{o}_1, \mathbf{o}_2, \dots, \mathbf{o}_t, q_t = s_i | (\mathbf{A}_{\text{HMM}}, \mathbf{B}_{\text{HMM}}, \boldsymbol{\pi}_{\text{HMM}})). \quad (4.45)$$

This can be calculated recursively by

$$\alpha_1(i) = \pi_i b_i(\mathbf{o}_1) \quad (4.46)$$

$$\alpha_{t+1}(j) = \left[\sum_{i=1}^c \alpha_t(i) a_{i,j} \right] b_j(\mathbf{o}_{t+1}) \quad (4.47)$$

with $1 \leq i \leq c$, $1 \leq t \leq T-1$ and $1 \leq j \leq c$ and the number of classes c . Similarly, the backward variable

$$\beta_t(i) = p(\mathbf{o}_{t+1}, \mathbf{o}_{t+2}, \dots, \mathbf{o}_T | q_t = s_i, (\mathbf{A}_{\text{HMM}}, \mathbf{B}_{\text{HMM}}, \boldsymbol{\pi}_{\text{HMM}})) \quad (4.48)$$

is the probability of the partial emission sequence from $t+1$ to T , under the condition of being in state s_i at time t . This can be calculated recursively by

$$\beta_T(i) = 1 \quad (4.49)$$

$$\beta_t(i) = \sum_{j=1}^c a_{i,j} b_j(\mathbf{o}_{t+1}) \beta_{t+1}(j) \quad (4.50)$$

with $1 \leq i \leq c$ and $t = T-1, T-2, \dots, 1$. The probability $\gamma_t(i) = p(q_t = s_i | O, (\mathbf{A}_{\text{HMM}}, \mathbf{B}_{\text{HMM}}, \boldsymbol{\pi}_{\text{HMM}}))$ of being in state $q_t = s_i$ at time t given the full emission sequence $O = \langle \mathbf{o}_1, \mathbf{o}_2, \dots, \mathbf{o}_T \rangle$ is calculated by

$$\gamma_t(i) = \frac{\alpha_t(i) \beta_t(i)}{\sum_{i=1}^c \alpha_t(i) \beta_t(i)} \quad (4.51)$$

and the individually most-likely state q_t at time t is

$$q_t = \arg \max_{1 \leq i \leq c} \gamma_t(i). \quad (4.52)$$

Theoretically, the forward-backward procedure might find state sequences that are not valid in case that some state transitions are prohibited by choosing some $a_{i,j} = 0$ [280, p. 8]. This needs to be considered for the selection of the transition probability matrix \mathbf{A}_{HMM} but is no further problem as a transition from one health state to another is always possible in reality with a small probability.

4.9.2 Linear Dynamical Systems

Novelty scores cannot be post-processed by HMMs because there is no discrete hidden state involved. It would still be possible to calculate the mean, moving mean or weighted mean of the novelty score of consecutive observations. However, this is not further evaluated due to the reasons mentioned in Subsection 4.9.1. Bishop [104, chapter 13.3] suggests to model the dynamic behavior of a continuous latent variable by Linear Dynamical System (LDS). This latent variable represents the posteriori estimated novelty score.

Using a linear-Gaussian state-space model results in the Kalman Filter equation of [281] for the forward recursion of the hidden latent variable \mathbf{z} [104, p. 637]. The Kalman smoother equations (or Rauch-Tung-Striebel equations) [282] can be used for a forward-backward recursion if the algorithm is calculated offline and the complete sequence of apriori estimated novelty scores of consecutive observations is available [104, p. 637]. The derivation of the final equations for the post-processing of the apriori novelty scores can be found in [104, pp. 637-641]. The

following paragraphs summarize the approach for a general multi-dimensional posterior latent state variable \mathbf{z} .

The model

$$\mathbf{z}_t = \mathbf{A} \mathbf{z}_{t-1} + \mathbf{w}_t \quad (4.53)$$

$$\mathbf{x}_t = \mathbf{C} \mathbf{z}_t + \mathbf{v}_t \quad (4.54)$$

$$\mathbf{z}_1 = \boldsymbol{\mu}_0 + \mathbf{u} \quad (4.55)$$

represents the dynamic behavior of the hidden latent variable \mathbf{z} of the posteriori estimated novelty score based on the apriori estimated novelty score \mathbf{x} . $\boldsymbol{\mu}_0$ is the initial guess for the hidden latent variable. While index t represents the discrete time step for time-based dynamic systems, it represents the index of the current observation in the context of the classifier post-processing. Hereby, it represents the time indirectly. The process and measurement noise terms \mathbf{w}_t and \mathbf{v}_t as well as the uncertainty of the initial value are sampled from the Gaussian distributions

$$\mathbf{w} \sim \mathcal{N}(\mathbf{w} | 0, \boldsymbol{\Gamma}) \quad (4.56)$$

$$\mathbf{v} \sim \mathcal{N}(\mathbf{v} | 0, \boldsymbol{\Sigma}) \quad (4.57)$$

$$\mathbf{u} \sim \mathcal{N}(\mathbf{u} | 0, \mathbf{V}_0) \quad (4.58)$$

with zero mean and covariance $\boldsymbol{\Gamma}$, $\boldsymbol{\Sigma}$ and \mathbf{V}_0 . A Gaussian distribution $\mathcal{N}(\mathbf{z}_t | \boldsymbol{\mu}_t, \mathbf{V}_t)$ is then defined for the posterior estimated novelty score. If the Kalman Filter is calculated online, the distribution's parameters are calculated by forward recursion of

$$\boldsymbol{\mu}_t = \mathbf{A} \boldsymbol{\mu}_{t-1} + \mathbf{K}_t (\mathbf{x}_t - \mathbf{C} \mathbf{A} \boldsymbol{\mu}_{t-1}) \quad (4.59)$$

$$\mathbf{P}_{t-1} = \mathbf{A} \mathbf{V}_{t-1} \mathbf{A}^T + \boldsymbol{\Gamma} \quad (4.60)$$

$$\mathbf{V}_t = (\mathbf{I} - \mathbf{K}_t \mathbf{C}) \mathbf{P}_{t-1} \quad (4.61)$$

$$\mathbf{K}_t = \mathbf{P}_{t-1} \mathbf{C}^T (\mathbf{C} \mathbf{P}_{t-1} \mathbf{C}^T + \boldsymbol{\Sigma})^{-1}. \quad (4.62)$$

If the post-processing is performed offline and the apriori estimated novelty scores of all consecutive observations are available, the posteriori estimation is improved by backwards recursion with $t = T - 1, T - 2, \dots, 1$ of

$$\hat{\boldsymbol{\mu}}_t = \boldsymbol{\mu}_t + \mathbf{J}_t (\hat{\boldsymbol{\mu}}_{t+1} - \mathbf{A} \boldsymbol{\mu}_{t+1}) \quad (4.63)$$

$$\hat{\mathbf{V}}_t = \mathbf{V}_t + \mathbf{J}_t (\hat{\mathbf{V}}_{t+1} - \mathbf{P}_t) \mathbf{J}_t^T \quad (4.64)$$

$$\mathbf{J}_t = \mathbf{V}_t \mathbf{A}^T (\mathbf{P}_t)^{-1} \quad (4.65)$$

$$\hat{\boldsymbol{\mu}}_T = \boldsymbol{\mu}_T \quad (4.66)$$

$$\hat{\mathbf{V}}_T = \mathbf{V}_T. \quad (4.67)$$

The parameters of the Kalman Filter could be determined using an expectation maximization approach [104, p. 637]. However, within this thesis, they are selected to incorporate a physically possible dynamical behavior of the component's health state.

The component's health state is expected to have no self-reinforcing tendencies. Hereby, the internal dynamic of the LDS reduces to a low-pass filter. Therefore, the transition parameter of the latent hidden novelty score \mathbf{z} is selected as $\mathbf{A} = a_{\text{LDS}} = 1$ (for a one-dimensional novelty score, matrix parameters reduce to singular values that are written in small letters). The output matrix is selected as $\mathbf{C} = c_{\text{LDS}} = 1$ because the apriori estimated novelty score x_t is a direct measure of the

latent hidden novelty score z_t . The variance of the apriori estimated novelty scores of consecutive observations is considered as the measurement noise v_t . The corresponding variance of the noise v_t is therefore selected as the average of the variance of the apriori estimated novelty scores of all consecutive observations within a validation dataset. It is calculated by

$$\Sigma = \Sigma = \frac{1}{K} \sum_{k=1}^K \left(\frac{1}{T_k - 1} \sum_{t=1}^{T_k} (x_{k,t} - \mu_k)^2 \right) \quad (4.68)$$

with the number of consecutive observation sequences K in the validation dataset (e.g. the number of individual measurements), the corresponding number of consecutive observations T_k in the k -th consecutive observation sequence, the corresponding apriori estimated novelty score $x_{k,t}$ of the t -th observation of the k -th consecutive observation sequence and the corresponding mean μ_k of the apriori estimated novelty scores for the k -th sequence of consecutive observations.

The process noise of the Kalman Filter w_t represents the uncertainty of the modeled physically possible dynamic behavior of the component's health state and the latent hidden novelty score. The parameterization of the Kalman Filter shall comply to the modeled dynamics in the HMM in Subsection 4.9.1. However, a direct translation of the parameters is not possible because the HMM is a discrete and the Kalman Filter is a continuous model. The parameterization of a 95 % probability of remaining in the same discrete hidden state in the HMM is translated to a process noise variance of $\Gamma = \Gamma = 0.05 \Sigma$.

The mean of the apriori estimated novelty scores of T consecutive observations is selected as initial guess for the latent hidden novelty score

$$\mu_0 = \mu_0 = \frac{1}{T} \sum_{t=1}^T x_t \quad (4.69)$$

and the corresponding variance

$$V_0 = \frac{1}{T - 1} \sum_{t=1}^T (x_t - \mu_0)^2. \quad (4.70)$$

5 Results

This chapter presents the results of this thesis. First, the underlying dataset is explained. This is followed by an investigation of the characteristics of the generated feature sets for Shallow Machine Learning (SML) and Representation Learning (RL) approaches. An investigation of the learned transformations of Machine Learning (ML) methods reveals possible connections to physical characteristics of the damper defects. Afterwards, the classification performance of each method is analyzed and compared across all applied methods. The performance improvements by conducting post-processing are shown and the importance of individual sensor signals and the size of the training data is analyzed. The theoretical insights of the observability analysis regarding vehicle speed and road excitation are investigated on the experimental data. Finally, the performance of the ML approaches is compared to a signal-based diagnosis approach.

5.1 Description of the Dataset

Observations are generated according to Section 4.2. The observation length is set to $t_{\text{obs}} = 5.12\text{s}$ to ensure that the number of samples per observation is a power of two for performing frequency analyses. The maximal average longitudinal and average lateral acceleration of an observation need to be below $a_{X,\text{obs,max}} = a_{Y,\text{obs,max}} = 1 \frac{\text{m}}{\text{s}^2}$ and the average vehicle speed of an observation is required to be above $30 \frac{\text{km}}{\text{h}}$.

The dataset consists of about 18 h of driving with a covered distance of 1650 km on German Autobahn, national and country roads as well as on bad roads. This results in 12 624 observations that are evenly distributed among the four classes mentioned in Section 4.2 (all dampers intact, all dampers defect, FL damper defect with the other dampers being intact, RR damper defect with the other dampers being intact). The dataset is divided into 80 % training data and 20 % testing data. Training is performed using a 5-fold cross validation.

For the analysis of the robustness of the investigated approaches, two additional test datasets are used. One dataset consists of 1270 observations from 180 km of driving with an additional mass of 200 kg in the trunk. Due to the package of the vehicle, this additional mass mainly influences the rear axle. The second robustness dataset consists of 2049 observations from 270 km of driving with winter tires instead of summer tires. These measurements were conducted on partly equal and partly different roads compared to the training and testing dataset. The driven road categories are German Autobahn as well as national and country roads. See Appendix C.1 for further description of the datasets.

5.2 Investigation of Feature Characteristics

This section provides a deeper understanding of the characteristics of the generated features for SML and RL by investigating their importance for classification. Rankings of feature importance are generated using the Recursive Feature Elimination (RFE) and the discriminative power of the features is investigated using the Fisher score of Section 4.5.

5.2.1 Manual Features for Shallow Machine Learning

The analysis of the manual feature set of Subsection 4.3.1 is based on the computation of a feature importance ranking applying the RFE algorithm of Subsection 4.5.1 using the removal of complete blocks of features. Hereby, the suitability of the feature generation methods in Table B.1 is analyzed. The selection of specific feature generation methods reduces the computational effort for feature generation in a later real-life implementation of the classification process. The RFE is conducted using the training data of Section 5.1. The training data is further split into 20 % hold-out validation data and 80 % actual training data for the RFE. Linear SVMs are trained in a 5-fold cross-validation approach. Feature generation methods are eliminated based on the mean of the classification accuracy on the hold-out validation data across all folds. A hyper-parameter optimization of the SVM is not performed due to the computational effort for an optimization of a SVM for each feature subset and cross-validation fold. Table 5.1 shows the ten most important feature generation methods. The ranking shows that more complex features (e.g. ARfit, Autocorr or two entropies) tend to have a high importance. But there are also simple feature generation methods (e.g. Skewness, Kurtosis or TimeSeriesDiff) among the most important features.

Table 5.1: Ranking of the ten most important manual feature generation methods

Rank	Name	Description	Number of features
1.	ARfit	Parameters of an auto-regressive signal model of 10th order that is fitted on a sensor signal for each observation and each sensor signal [120, p. 11]	10 (per signal)
2.	Autocorr	Auto-correlation coefficient for 1 to 8 lags of sample points [120, pp. 11-12]	8 (per signal)
3.	EigNorm	Ratio of signal amplitudes at vertical tire and vehicle body eigenfrequency	1 (per signal)
4.	TimeSeriesDiff	Square root of cumulative sum of time series differences $\sqrt{\sum_{n=3}^N (x_n - x_{n-2})}$	1 (per signal)
5.	CorCoeff	Correlation coefficient of two different sensor signals	21 (in total)
6.	Skewness	Skewness of the time signal data points of each sensor signal	1 (per signal)
7.	LogEnEntr	Log-energy entropy of a signal $E(s) = \sum_{n=1}^N \log(s_n^2)$ with the convention $\log(0) = 0$ for a signal s with its data points s_n [283, p. 2]	1 (per signal)
8.	SampEntr	Sample entropy as measure of the complexity of a time signal	1 (per signal)
9.	Kurtosis	Kurtosis of the time signal data points of each sensor signal	1 (per signal)
10.	Bandpower	Energy of a sensor signal in the frequency ranges 1 Hz to 5 Hz, 5 Hz to 10 Hz, 10 Hz to 15 Hz, 15 Hz to 20 Hz, 20 Hz to 25 Hz	5 (per signal)

The ranking of the feature blocks does not enable a quantitative comparison of the suitability of different feature generation methods. Therefore, the discriminative power of the individual

features is analyzed by calculating the Fisher scores of the resulting 224 individual features of the ten most important feature generation methods from Table 5.1.

Figure 5.1(a) shows the Fisher scores of the individual features in descending order. There is only a small number of individual features with a high Fisher score. This indicates that a further reduction of the feature set to consist of only the most discriminative features is further beneficial for the classification performance.

Figure 5.1(b) shows a bar plot of the corresponding Fisher scores grouped by the corresponding feature generation methods (because a feature generation method that generates one feature per signal results in seven features). The central mark indicates the median, the box indicates the 25-th and 75-th percentile. Whiskers extend to the most extreme data points not considering outliers, while outliers are plotted individually [284]. The order of the feature generation methods corresponds to the ranking in Table 5.1.

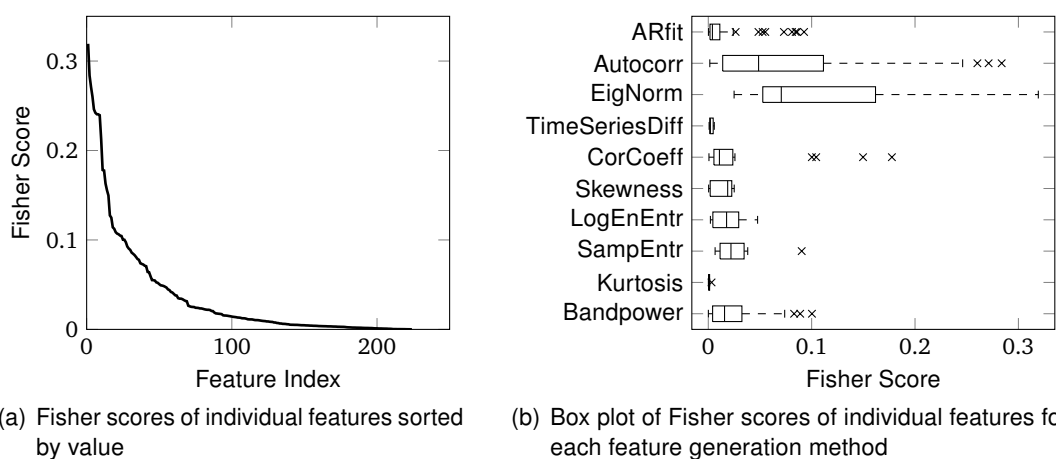


Figure 5.1: Fisher score of individual features of the most important manual feature generation methods from Table 5.1

The most important feature generation method “ARfit” consists only of some features that have a high Fisher score. Most ARfit features have a small Fisher score. Therefore, using only these individual discriminative features would further improve the classification performance. The second most important feature block “Autocorr” consists of many individual features with a high Fisher score. Therefore, this feature generation method is of high discriminative power. The feature generation method “EigNorm” consists of many individual features with a high Fisher score. It is therefore a competitive feature generation method. The concept of this feature is similar to the signal-based approach of Jautze [17]. The feature generation methods “TimeSeriesDiff” and “Kurtosis” consist only of features with a low Fisher score. Even though the RFE ranked them as important, these features are probably not beneficial for the classification.

The above analysis of the feature generation methods shows a process of further feature reduction that would improve the classification performance. An additional possibility for the improvement of the classification performance is the tuning of each feature generation method. This was conducted partly by Merk [203].

5.2.2 FFT Features for Shallow Machine Learning

This section investigates the FFT feature set from Subsection 4.3.2. The discriminative power of the fourier-transformed sensor signals is analyzed using the Fisher score. This is followed by an

investigation of the importance of frequency shares for a supervised classification based on a RFE, because the discriminative power that is indicated by the Fisher score is no direct measure for the importance of a feature for classification.

Figure 5.2 shows the Fisher score of each FFT data point as well as the mean FFT across all observations for each damper health state. Investigating the FFT of the wheel speed signals in Figure 5.2(a) - 5.2(d) reveals that these signals deviate significantly from the characteristic of the intact state if a damper defect is located at the corresponding damper. However, there is no such deviation of the FFT signal if there is no defect at the related damper. The FFT of the vehicle body sensor signals, lateral and longitudinal accelerations as well as yaw rate, deviate from their intact characteristics with all defective states. However, the relative deviation is smaller compared to the deviation of the wheel speed signals.

The most important frequency range of all sensor signals is from 10 Hz to 15 Hz. A typical vertical tire eigenfrequency is at 10 Hz to 11 Hz [285, p. 4]. Therefore, the peaks in the FFT of the sensor signals as well as the corresponding Fisher score peak are related to the vertical tire eigenfrequency. Frequencies above 20 Hz are unimportant for all sensor signals because there are no deviations of the FFT for different health states and the Fisher score is small. However, a high sampling frequency is still important because the availability of more datapoints improves the quality of the FFT also for small frequencies.

The wheel speed signal FL reaches the highest Fisher score at 15 Hz. This is due to the large deviation of its FFT of two of the four health states. An additional peak of the Fisher score is at 4.75 Hz. This frequency range is related to vehicle body movements. The wheel speed signals Front Right (FR) and Rear Left (RL) both contain a peak at the tire vertical eigenfrequency. However, only one health state (“all defect”) can be identified based on these wheel speed signals because the dataset does not contain single defects of the FR or RL damper. Both sensors also have a Fisher score peak at a possible vehicle body eigenfrequency at 1.6 Hz. The wheel speed signal RR consists of smaller Fisher scores compared to the other wheel speed signals, even though this sensor signal enables the detection of the “RR defect” case. Vehicle body sensor signals contain also Fisher score peaks in the area of the tire vertical eigenfrequency. Especially the yaw rate signal contains two high peaks of the Fisher score. One peak is located at the tire vertical eigenfrequency and another peak at 5.6 Hz. The high Fisher score peaks indicate a high ability to detect defective dampers based on the yaw rate signal’s FFT features because the FFT of the yaw rate is different for each class of the dataset.

A feature importance score is generated for evaluating the importance of the FFT features for the classification process. A RFE is conducted to rank the importance of the individual FFT features. The generated importance score of a FFT frequency f_i (that is equivalent to the i -th feature feature_i) is the inverse of the RFE feature ranking $\text{rank}_{\text{RFE}}(f_i)$ relative to the number of features n_{features} . It is calculated by

$$\text{importance}_{\text{FFT}}(f_i) = \frac{n_{\text{features}} - (\text{rank}_{\text{RFE}}(\text{feature}_i) - 1)}{n_{\text{features}}}. \quad (5.1)$$

Figure 5.3 visualizes a smoothed curve of the feature importance score with respect to the frequency location of the features. The highest possible importance score is 1. Due to the moving average filter with a span of ± 4.76 Hz, importance scores for frequencies below this threshold as well as above 45.24 Hz are prone to noise and can therefore be neglected for investigation. Very small importance values do not exist due to the smoothing process.

Wheel speed signals are again more important than vehicle body signals. The high Fisher score

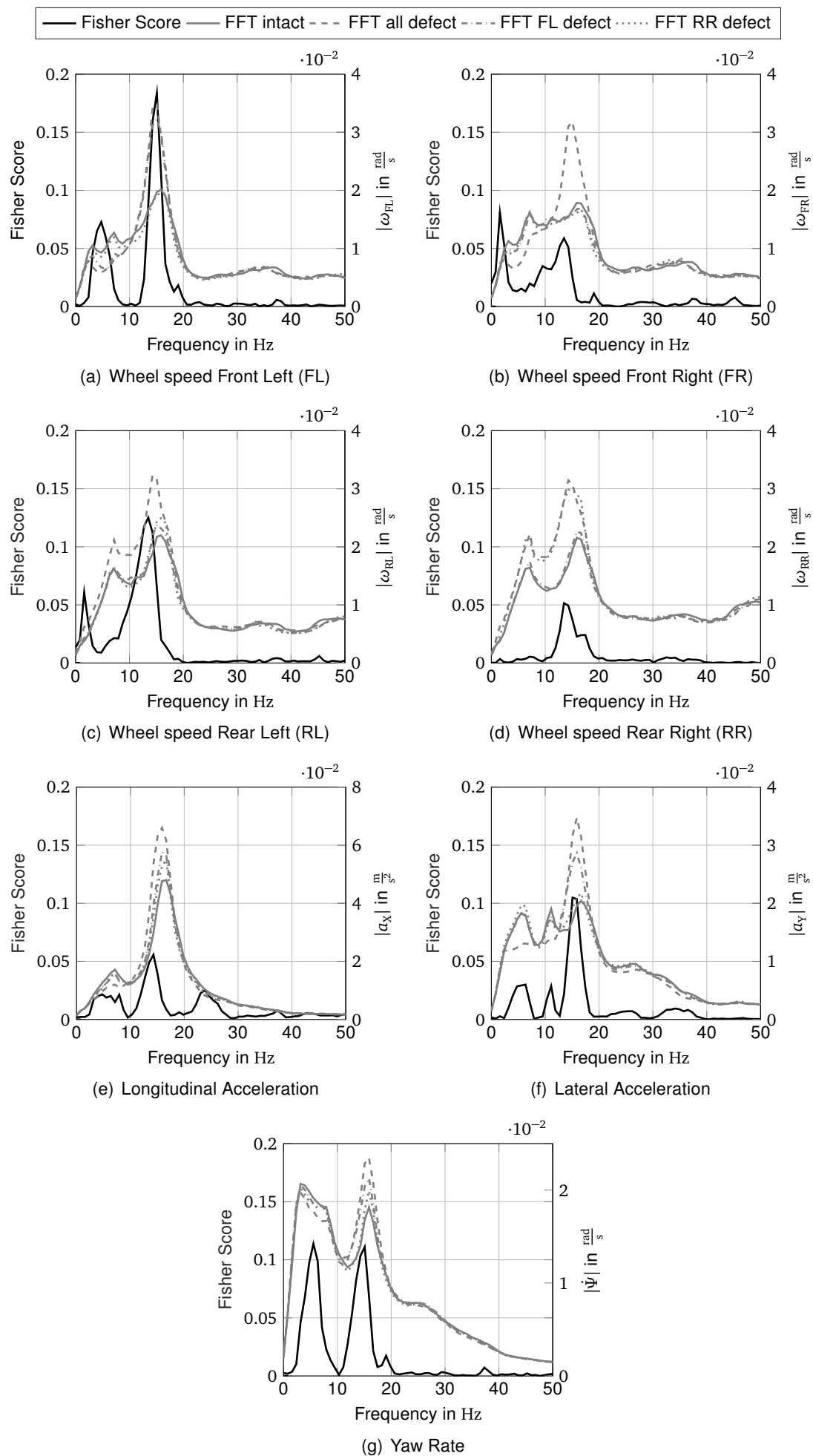


Figure 5.2: Fisher score and mean FFT of sensor signals for each damper health state

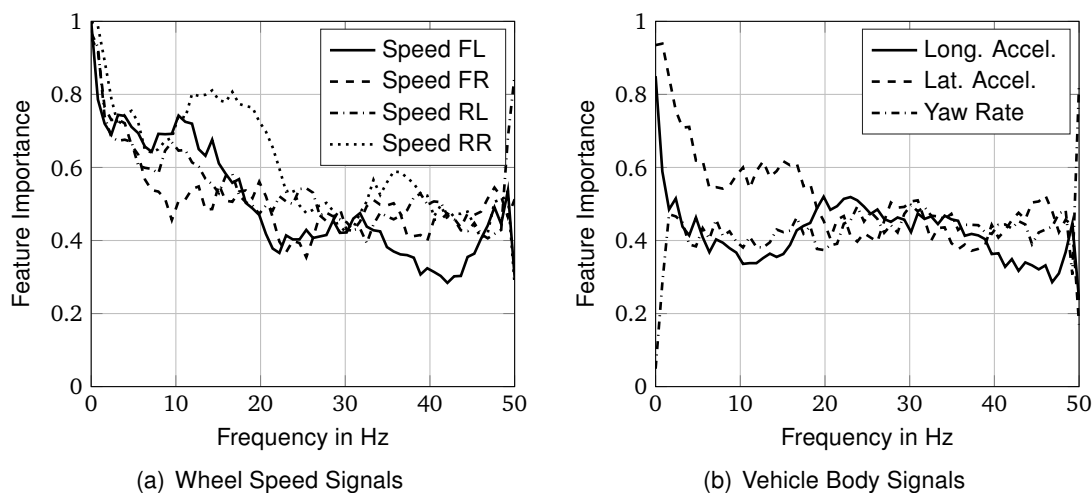


Figure 5.3: FFT feature importance for classification as mean inverse rank of RFE feature ranking

of the wheel speed FL at 15 Hz is less important for classification than the range of 10 Hz to 20 Hz of the wheel speed RR. A frequency range of around 35 Hz of the wheel speed RR is considered as important for classification. This was not revealed by investigating the Fisher score. The lateral acceleration in a frequency range of below 15 Hz is ranked as important for classification. This finding is equivalent to the lateral acceleration's Fisher score in this frequency range.

The investigation of the Fourier-transformed sensor signals and the corresponding Fisher scores showed that many discriminative features are located in the area of known eigenfrequencies of the vehicle body and tires. However, there are also features that provide information for classification that are not obviously based on the vehicle's or tire's eigenfrequencies or the Fisher score.

5.2.3 Autoencoder Features for Representation Learning

The analysis of the Autoencoder feature set from Subsection 4.4.1 is conducted by analyzing the Autoencoder weights. Hereby, insights regarding the transformations that are performed by an Autoencoder are provided. The importance of the signal's frequency shares are analyzed by generating an importance score similar to the importance score in Subsection 5.2.2.

Figure 5.4 visualizes the weights of one kernel of the trained Autoencoder for the wheel speed signal FL. The mean FFT of each health state is also visualized as reference. With the Autoencoder's input data being FFT data, the Autoencoder compares FFT amplitudes at different frequencies. The absolute value of an Autoencoder weight at a specific frequency quantifies the importance of the signal amplitude at the respective frequency for a comparison with the amplitude at other frequency shares. The sign of a weight value is only a matter of subtraction or addition of the amplitude at the corresponding frequency.

An importance score is generated for the Autoencoder kernel weights to further aggregate the importance of the different frequency shares of the input data. This paragraph describes the mathematical background of the generated score. For each generated Autoencoder feature, the corresponding absolute values of the Autoencoder weights are multiplied with the respective RFE feature importance. Taking the absolute value of this product accounts for the importance, independent of the sign of the Autoencoder weight. An independence of the importance score

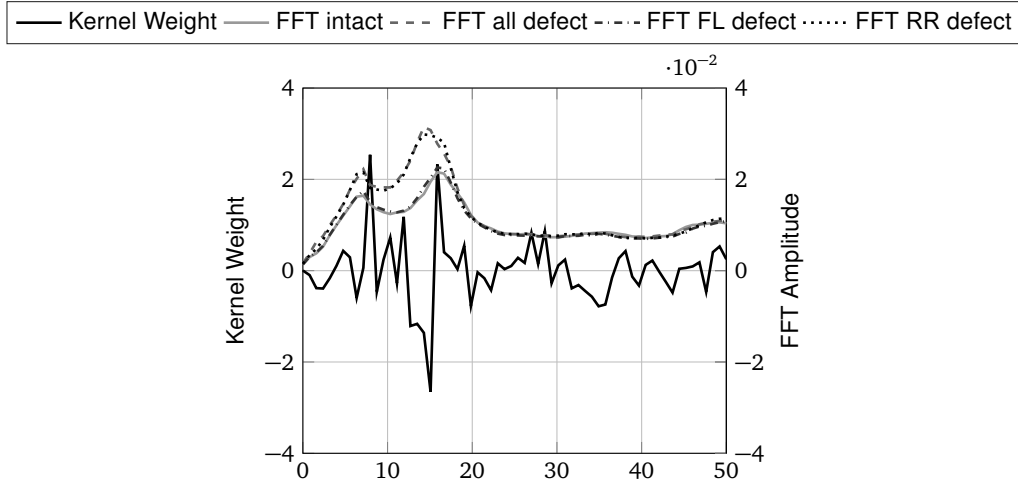


Figure 5.4: Autoencoder weights of one kernel and mean FFT of each health state as input data for wheel speed FL

from the possible occurrence of multiple correlated transformations within the Autoencoder shall be ensured. Therefore, the maximal value across all generated features is taken for each frequency input. The named requirements are considered within the calculation of the importance index for the Autoencoder for the frequency share f_i by

$$\text{importance}_{\text{AE},k}(f_i) = \max_{j \in [1; n_{\text{Feat},\text{AE}}]} \left(\left| w_{i,j,k} * \frac{n_k n_{\text{Feat},\text{AE}} - (\text{rank}_{\text{RFE}}(\text{feature}_{j,k}) - 1)}{n_k n_{\text{Feat},\text{AE}}} \right| \right) \quad (5.2)$$

with the number of sensor signals n_k , the number of Autoencoder features per sensor signal $n_{\text{Feat},\text{AE}}$ and the Autoencoder weight $w_{i,j,k}$ that connects the i -th FFT input data point (the frequency share f_i) with the j -th generated Autoencoder feature of the k -th sensor signal.

Figure 5.5 visualizes the importance score of the input data frequency shares for the wheel speed signal FL and the lateral acceleration exemplary, with the mean FFT of each health state as reference. The importance scores for all sensor signals are presented in Appendix C.2.1 in Figure C.9.

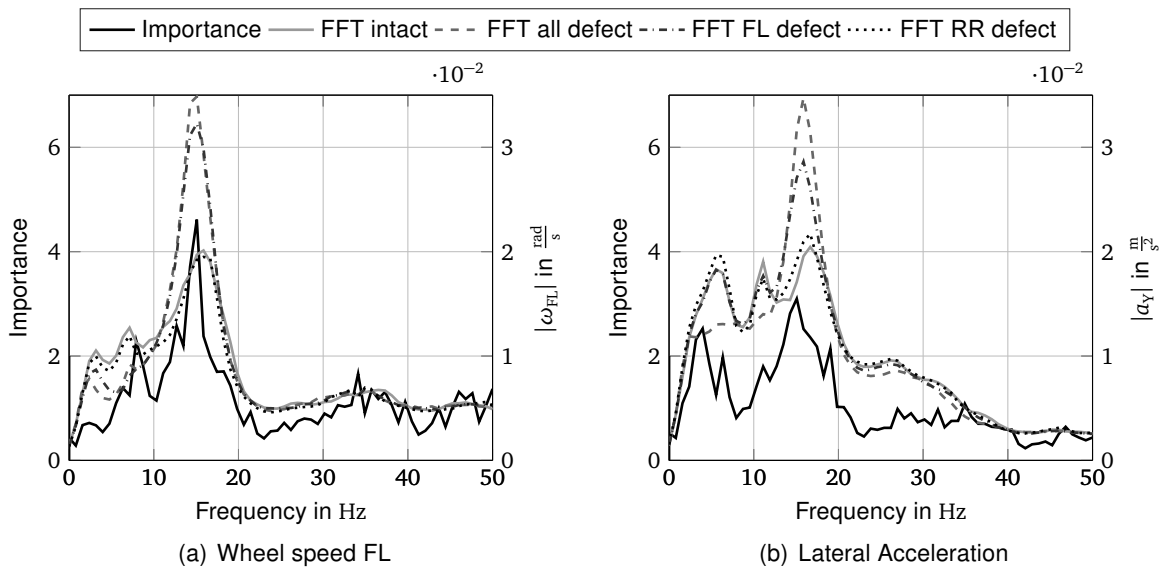


Figure 5.5: Importance index of input data frequency for Autoencoder

The importance of different frequency shares within the Autoencoder feature set is again related to the deviation of the FFT input data for different health states. The frequency range around 15 Hz is again rated as most important for both sensor signals. Overall, the Autoencoder frequency importance index is similar to the Fisher score curves of the FFT data in Figure 5.2. This reveals that the Autoencoder does not incorporate additional information from non-obvious frequency areas of the FFT input data.

5.2.4 Sparsefilter Features for Representation Learning

The analysis of the Sparsefilter feature set from Subsection 4.4.2 is conducted similarly to the analysis of the Autoencoder feature set in Subsection 5.2.3. A first analysis of the Sparsefilter weights was performed by Werk [208, pp. 60-61]. Figure 5.6(a) shows the weights of two kernels of the Sparsefilter for the wheel speed FL exemplary. Due to the input data being time signals, the kernel weights are plotted over the observation time in Figure 5.6(a). The convolution of the time signal Sparsefilter input data with the Sparsefilter kernel results in a frequency analysis of the Sparsefilter input data even though the feature generation process of the Sparsefilter is based on a simple matrix multiplication. Figure 5.6(b) shows the FFT of the Sparsefilter kernels of Figure 5.6(a).

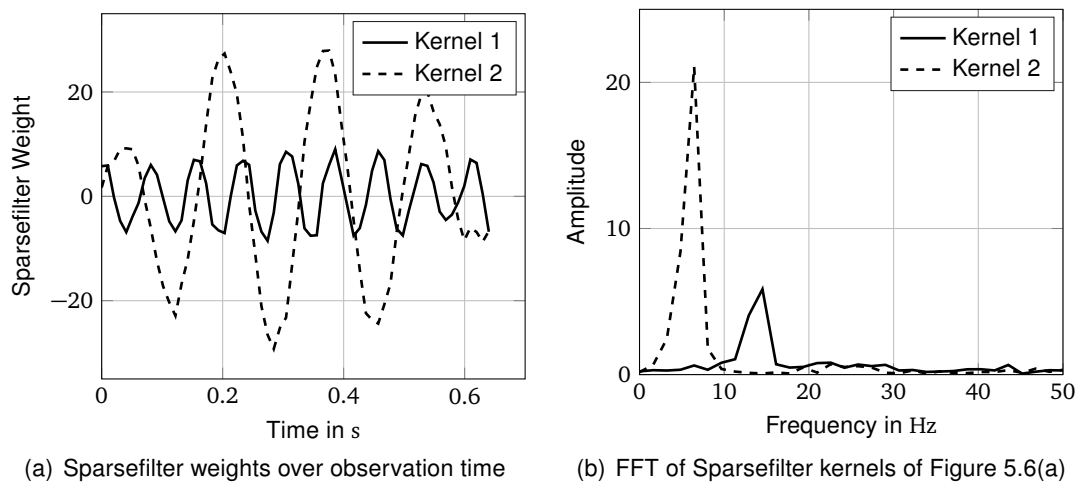


Figure 5.6: Analysis of Sparsefilter weights. Exemplary visualized for two kernels of Sparsefilter for wheel speed FL

The quantification of the importance of the time signal's frequency shares for the Sparsefilter is similar to the quantification for the Autoencoder weights. The FFT of a Sparsefilter kernel is multiplied with the corresponding importance of the RFE feature ranking. However, the Sparsefilter weights may have different amplitudes for different frequencies (Figure 5.6). Hereby, frequency shares that have a low amplitude in the actual sensor signal would be overrated in an importance analysis. Therefore, the FFT transformation of a Sparsefilter kernel is multiplied with the mean of the FFT transformation of all observations of the respective sensor. The importance score of the Sparsefilter feature for the frequency f_i is calculated by

$$\text{importance}_{\text{SF},k}(f_i) = \max_{j \in [1; n_{\text{Feat,SF}}]} \left(\left| \text{FFT}_{w_{j,k}}(f_i) \overline{\text{FFT}_k}(f_i) * \frac{n_k n_{\text{Feat,SF}} - (\text{rank}_{\text{RFE}}(\text{feature}_{j,k}) - 1)}{n_k n_{\text{Feat,SF}}} \right| \right) \quad (5.3)$$

with $\text{FFT}_{w_{j,k}}(f_i)$ being the amplitude at the frequency f_i of the FFT of the Sparsefilter weights $w_{j,k}$ that generate the j -th feature of the k -th sensor signal. The mean of the FFT transformation of the sensor signal is calculated by

$$\overline{\text{FFT}}_k(f_i) = \frac{1}{N} \sum_{n=1}^N \text{FFT}_{x_{n,k}}(f_i) \quad (5.4)$$

with the number of observations N of the complete dataset and the amplitude of the frequency f_i of the fourier-transformation $\text{FFT}_{x_{n,k}}(f_i)$ of the sensor signal $x_{n,k}$ of the n -th observation and the k -th sensor.

The resulting importance scores are visualized in Figure 5.7 for the wheel speed FL and the lateral acceleration with the mean FFT of each health state as reference. Figure C.10 in Appendix C.2.2 shows the importance scores for all sensor signals.

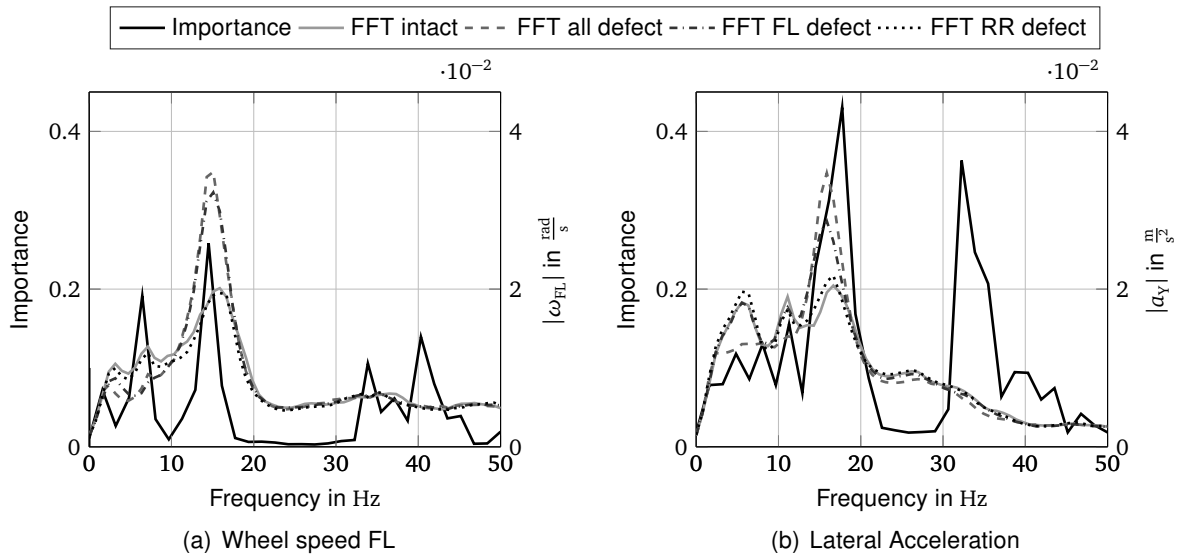


Figure 5.7: Analysis of importance of input data frequency shares for Sparsefilter

The most important frequency shares of the time signal input data for the feature generation using Sparsefilters are located in the region of the eigenfrequencies of the vehicle body and the tire. This is again caused by the large differences of the signal characteristics for different damper health states at these eigenfrequencies. However, there are also Sparsefilter features at frequency ranges with no or just small differences of the FFT signal (> 30 Hz). These frequency locations can be important for the quantification of the wheel speed excitation e.g. due to road excitation.

5.3 Analysis of the Classification Performance

This section analyzes the health monitoring performance of each ML concept. Hereby, variations of conceptual optimization parameters are considered, such as the number of features or the network configuration of neural networks. A high-level comparison of the performance of each approach is performed in Section 5.4.

5.3.1 Supervised Shallow Machine and Representation Learning

The investigation of the classification performance for supervised SML and RL approaches is based on a RFE from Subsection 4.5.1 using individual feature deactivation. The general process of the RFE application is as explained in Subsection 5.2.1. The resulting trained classifiers for each number of selected features are evaluated on the testing data. Figure 5.8 shows the mean classification accuracy of the 5-fold cross validation on the testing data.

The classification accuracy increases with the number of features for all feature sets and there is no distinct peak of the classification accuracy for any feature set. Using manual features results in a maximal classification accuracy of 91.52 %. Using FFT or Autoencoder features results in a slightly lower performance with a maximal accuracy of 90.05 % when using Autoencoder features and 88.80 % for FFT features. Using Sparsefilter features results in the lowest performance with a maximal classification accuracy of 81.45 %. This reveals that using manual features that are selective to the diagnosis of a specific component does not improve the detection of faults significantly when using a SVM as supervised learning approach.

The Autoencoder's input data is selected to be the Fourier-transformed sensor signals. There is no benefit of additional processing of the Fourier-transformed sensor signals using an Autoencoder because of the similar classification performance of using the FFT or Autoencoder feature set. This is identical to findings in Subsection 5.2.3.

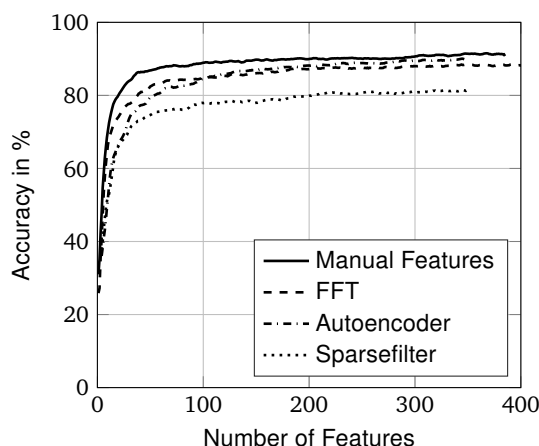


Figure 5.8: Mean test data classification accuracy of a 5-fold cross-validation using a SVM classifier for feature subsets consisting of different numbers of features, selected using a RFE approach. For visualization reasons, standard deviations of the cross-validation are not shown and the curves are smoothed using a moving average filter with a span of five samples. Classification by chance results in $1/4$ classes = 25 % accuracy.

5.3.2 Unsupervised Shallow Machine and Representation Learning

The analysis of the unsupervised learning performance is also conducted using a RFE with the AUC on a validation dataset as ranking criterion. The validation dataset consists of randomly chosen 20 % of the “intact” (inlier) observations of the training dataset and the same amount of randomly chosen defective (outlier) observations of all defective classes.

Figure 5.9 shows the mean AUC of a 5-fold cross-validation on the test dataset. The test dataset consists of 500 randomly chosen “intact” (inlier) observations and 500 randomly chosen defective (outlier) observations.

The novelty detection performance for each feature set has a maximum and is not monotoni-

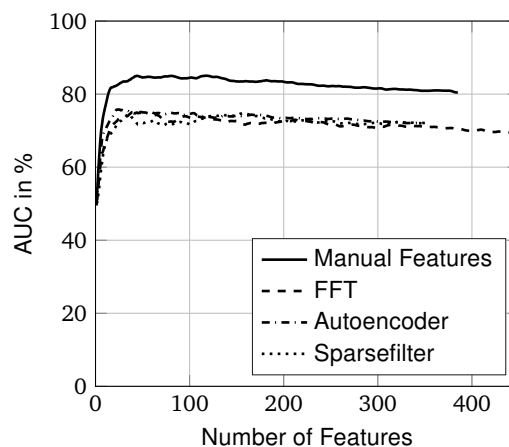


Figure 5.9: Mean test data AUC of a 5-fold cross-validation using a LOF novelty detection classifier for feature subsets consisting of different numbers of features, selected using a RFE approach. For visualization reasons, standard deviations of the cross-validation are not shown and the curves are smoothed using a moving average filter with a span of five samples. Classification by chance results in 50% AUC.

cally increasing with an increasing number of features. This might be due to the classifier being a nearest-neighbor-based approach whose performance is reduced with an increasing dimensionality of the feature space (due to the curse of dimensionality) [218]. The maximal AUC when using manual features is 85.03%. The novelty detection performance for using FFT, Autoencoder or Sparsefilter feature sets is similar to each other. The maximal AUC is 75.09% for FFT features, 75.75% for Autoencoder features and 74.79% for Sparsefilter features.

This reveals that using manual features that are selective to the diagnosis of a specific component improves the detection of faults when using a nearest-neighbor based LOF as unsupervised learning approach.

5.3.3 Supervised Deep Learning

This section summarizes the findings of Zehelein et al. [121] for the supervised Deep Learning (DL) approach using Convolutional Neural Networks (CNNs). The classification performance for different network configurations is presented for the two most powerful data pre-processing methods of [121] using the dataset of this thesis. An investigation of the learned kernels reveals insights regarding the transformations that are performed by a CNN.

A screening of the classification performance using the input data pre-processing methods that are presented in Subsection 4.7.1 showed that the highest classification accuracies are achieved using FFT or STFT as pre-processing of time signals for the network's input data. At a later point in [121], using STFT pre-processed input data revealed a lack of robustness on the tire and mass data. Therefore, STFT pre-processing is not considered in this thesis. The performance using detrended time signal input data is also amongst the best performing pre-processing methods in [121]. Analyzing network architectures that use detrended time signals as input data enables the most tangible analysis of end-to-end data transformations that are performed by a CNN. Figure 5.10 shows the classification accuracy for different network architecture configurations using detrended time signals as input data as well as using the FFT of detrended time signals as input data.

Using detrended time-signals as input data results in lower classification accuracies compared

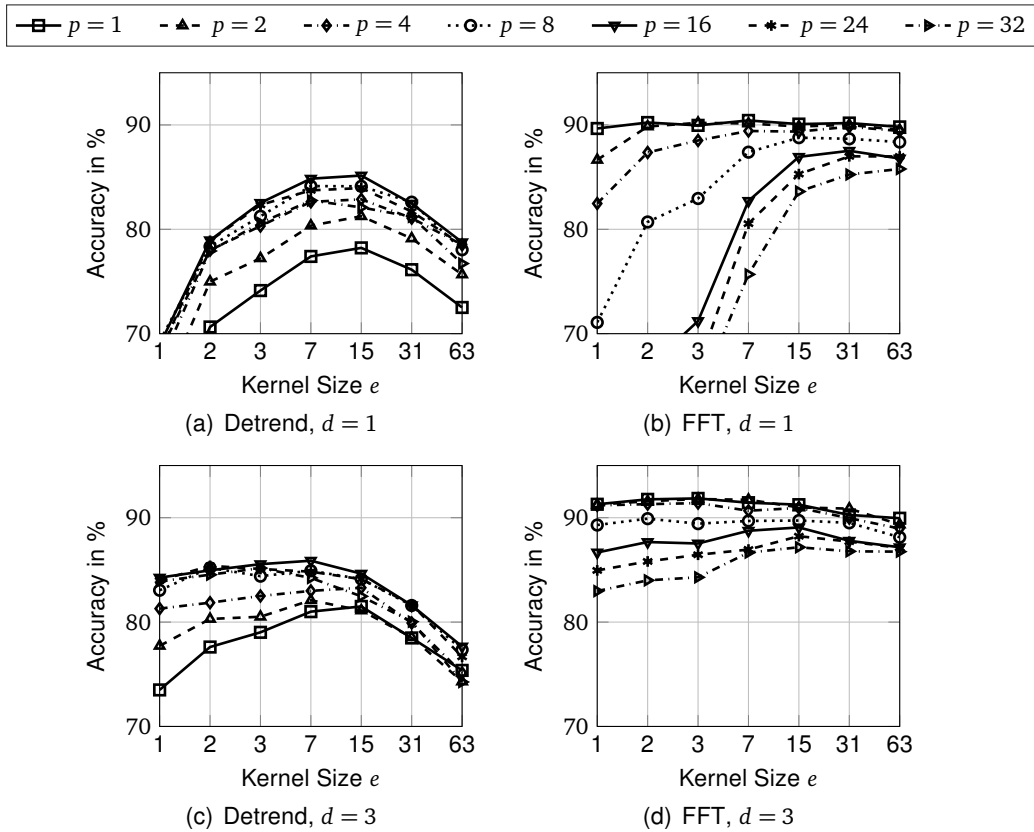


Figure 5.10: Mean test data accuracy of a 5-fold cross-validation for the investigation of the CNN network architecture using detrended time signals or FFT of detrended time signals as input data. The approach and layout are based on [121], classification results are based on the dataset of this thesis. p is the size of the pooling layer (with $p = 1$ effectively resulting in no pooling), e is the spatial extent of a kernel. d is the network depth in terms of the number of convolutional/pooling-layer combinations.

to FFT pre-processed input data. The selection of the kernel size e is especially important for detrended input data. The optimal size of the pooling layer is $p = 16$ data samples. When using FFT input data, a pooling layer size of $p = 1$ (which is effectively no pooling) results in the highest accuracies independently from the size of the convolutional layer's kernel size e for a network depth $d = 1$. Increasing the network depth d results in slightly higher classification accuracies for both input data variants and improves the robustness for tire and mass data [121].

Figure 5.11 presents trained kernels of the first convolutional layer of CNNs using detrended time-signals and FFT input data. As described in Zehelein et al. [121, pp. 10-11], a convolutional kernel of a CNN with time-signal input data performs a frequency analysis on the input data. This can be seen in Figure 5.11(a) and 5.11(c) because the kernel weights are sinusoidal. A kernel analysis of a CNN for bearing fault application shows a similar behavior [286, p. 16]. The kernel that is visualized in Figure 5.11(a) analyzes the input signals for frequencies of around 3.5 Hz because the visualized half period is of a length of 0.14 s. The visualized kernel in Figure 5.11(c) analyzes the input signals for frequencies of around 14 Hz due to the period's length being about 0.07 s.

Using FFT input data leads to the CNN performing a comparison of signal amplitudes at different frequencies. This is indicated by the peaks of the kernel weights in Figure 5.11(b) and 5.11(d). The visualized kernel in Figure 5.11(b) analyzes the input spectrum for amplitudes at frequency differences of 4.5 Hz and the kernel in Figure 5.11(d) analyzes for frequency differences of 7 Hz.

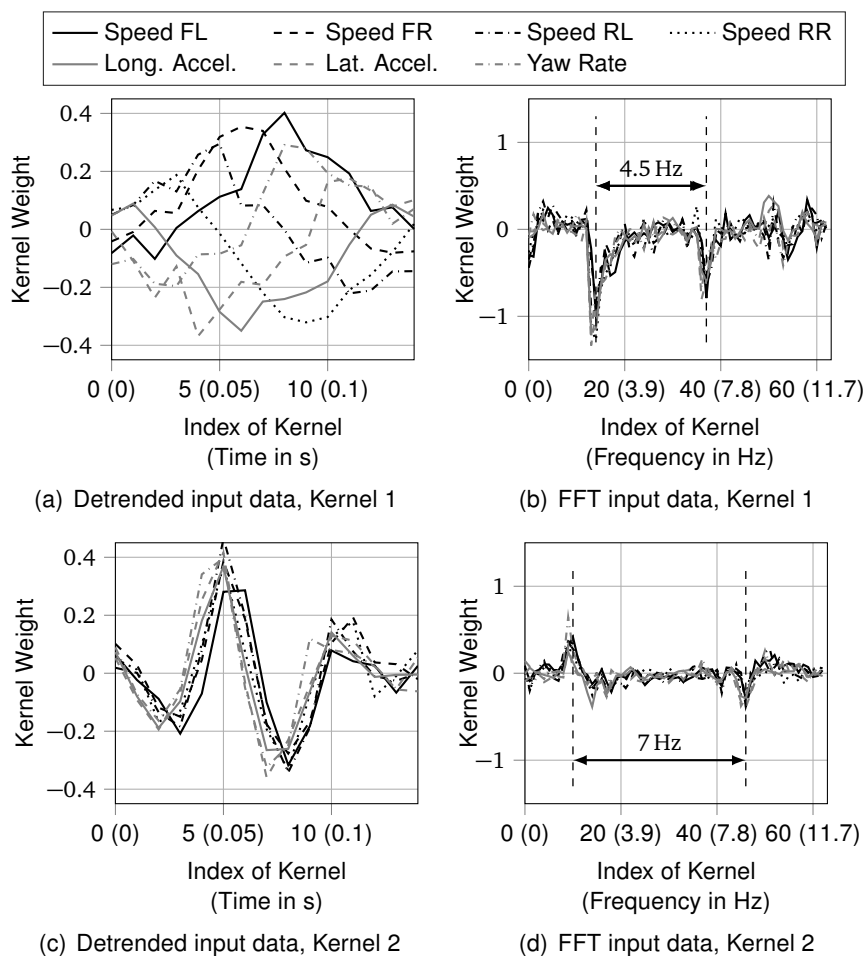


Figure 5.11: Kernel weights of the convolutional layer of different network architectures from Zehelein et al. [121, p. 11]

5.3.4 Unsupervised Deep Learning

The optimization procedure of the Variational Autoencoder (VAE) was conducted by Trumpp [209]. Several parameters are analyzed with a deterministic Stacked Autoencoder (SAE) as basis. These results are then applied to the probabilistic VAE. The investigated parameters are the segmentation of the FFT input data, batch size, scaling methods and activation functions of the neurons. Finally, the best network layer configuration is identified and used in this thesis.

The FFT segmentation was found to have a large impact on the novelty detection result. A segmentation of 64 time signal data samples performed best. The batch size has only a minor impact on the result and a batch size of 64 is selected. Scaling methods have a large impact on the novelty detection performance. A scaling method that transforms the data to a Gaussian or a uniform distribution leads to the best performance. The selected scaling method is the transformation to a Gaussian distribution because this is a more natural distribution than a uniform distribution. Finally the Rectified Linear Unit (ReLU) is the best performing activation function of the neurons.

The optimization of the network's layer configuration is conducted by performing a grid search using the AUC on a validation dataset as optimization criterion. A symmetric network configuration consisting of five hidden layers is selected. Figure 5.12 shows the AUC of the validation data on the y-axis and the number of neurons of each layer at the x-axis. The fitted polynomial curves for the number of neurons of each layer are visualized with the corresponding solid line. The

big cross indicates the network configuration with the highest AUC. It consists of 340 neurons in the first and last hidden layer, 100 neurons in the second and fourth hidden layer and 35 neurons in the third hidden layer. The optimization shows a tendency for many neurons in the first layer. The structure of the VAE is overcomplete with 32 FFT data samples of seven signals resulting in 224 input data points. However, the results show a robust behavior to the network configuration because the AUC for most network configurations are in a similar range of over 85 %. The investigation of the VAE kernel weights did not reveal any meaningful findings.

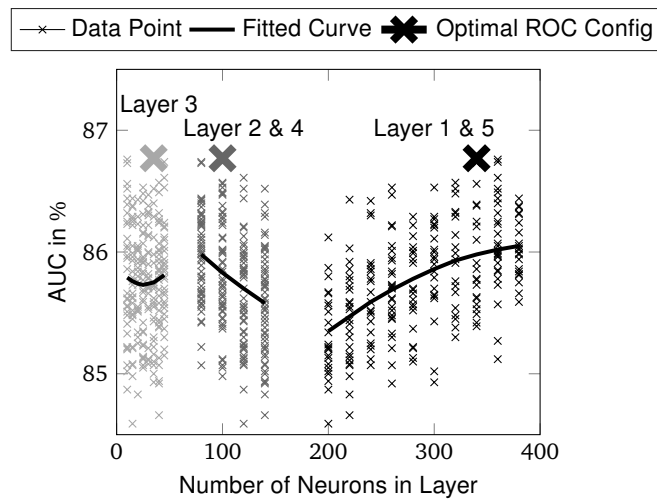


Figure 5.12: AUC on validation data of layer configuration optimization of VAE. The VAE is of a symmetric structure with five hidden layers. Therefore, the number of neurons of layer five is identical to layer one, and layer four is identical to layer two. Blocks of data points with identical gray tones indicate the three different layer configurations of the VAE

5.4 Overall Comparison

This section compares the classification accuracy and the AUC of the investigated approaches on a high level basis. All methods are trained using a 5-fold cross-validation on the training data that consists of 80 % of the complete dataset. The presented performance indicators refer to the performance on the remaining 20 % testing data.

5.4.1 Comparison of Results of Supervised Learning Approaches

The SVM's hyperparameters for SML and RL approaches are optimized using a 5-fold cross-validation. Therefore, the classification performance is higher than the performance in Figure 5.8. All features of each feature set were used for classification because of the results of the RFE analysis in Subsection 5.3.1.

The network architecture of the CNN is selected according to the results in [121]. The input data of the network is the FFT of detrended time signals. The network consists of three convolutional layers ($d = 3$), each followed by a pooling layer. Each convolutional layer consists of 16 kernels. The kernel size is set to $e = 1$ and the size of the pooling layer's kernel is set to $p = 2$. The learning rate and L_2 -regularization hyperparameters of the CNN were optimized using gradient boosted regression trees. The cost function of this optimization is the mean of the classification accuracy on a validation dataset and the difference of the classification accuracy on the training data and the validation data to prevent over-fitting.

Figure 5.13 shows the classification accuracy of the supervised learning approaches on the test dataset as well as on the two datasets for robustness evaluation with additional mass and winter instead of summer tires.

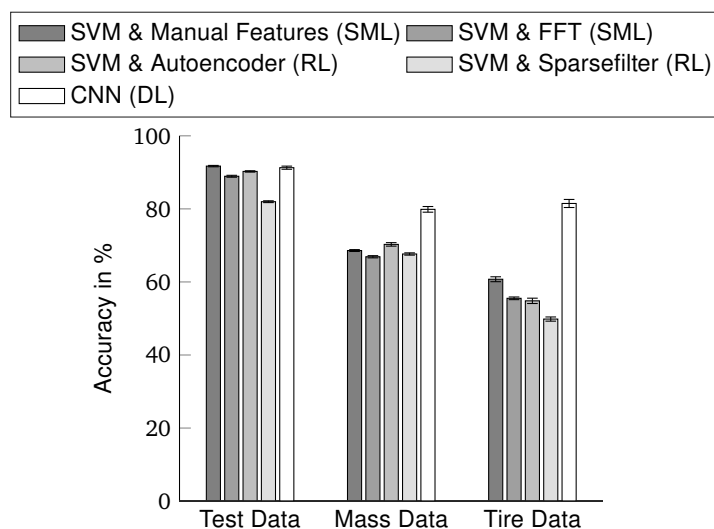


Figure 5.13: Classification accuracy of supervised learning methods that are trained on training data and applied to the test, mass and tire datasets. Whiskers indicate the standard deviation that results from the application of all classifiers of the 5-fold cross-validation to the respective dataset.

The performance on the test data is similar for all approaches except when using a SVM with Sparsefilter features. The highest classification accuracy of 91.71 % on the test data results from the SML concept using manual features in combination with an optimized SVM. The CNN has a slightly lower accuracy of 91.28 %, followed by 90.26 % accuracy when using Autoencoder features in combination with a SVM. All feature-based SML and RL approaches have a low performance on both robustness datasets. The CNN approach remains at 79.87 % and 81.48 % for the mass and tire datasets. It outperforms all other approaches on the tire dataset by about 20 Percentage Points (PPs). This shows that the CNN is able to generate more robust features.

The M -value is calculated using the approach of Subsection 4.8.3 for a comparison of the supervised learning classification performance with the novelty detection performance of unsupervised learning approaches in the next section.

5.4.2 Comparison of Results of Unsupervised Learning Approaches

This section investigates the fault detection performance of the implemented unsupervised learning approaches. The resulting AUC values are visualized in Figure 5.14(a). The selected feature-based unsupervised SML and RL approaches employ the feature subsets that resulted in the highest AUC on the validation dataset for the RFE analysis in Subsection 5.3.2. The hyperparameters of the LOF classifier for the SML and RL approaches are selected in accordance with the results of Zehelein et al. [119]. A Manhattan (or L_1) distance, the number of neighbors $k = 2$ and the power transformer of [287] that scales the data to a Gaussian distribution are selected. The test dataset as well as the mass and tire robustness datasets consists of 250 intact observations and 250 defect observations. The defect observations are randomly selected from all three defect classes. Hereby, the datasets that are used for the evaluation of the performance of the unsupervised learning approaches are balanced.

Using the SML approach of a LOF classifier with manual features results in the highest AUC

value of 84.42 %. The unsupervised DL approach VAE leads to the second highest AUC of 81.32 %. Using FFT, Autoencoder and Sparsefilter features in combination with the LOF classifier results in a fault detection performance of about 75 % for all three approaches.

The fault detection performance of all unsupervised learning approaches is largely reduced for the robustness datasets. An AUC of 50 % is equivalent to a selection by chance. The deviations of the signal characteristics caused by additional mass or changed tires are identified as novelty. From a data analysis perspective, this is correct. However, it is an unintended behavior in the context of damper fault detection. Therefore, it is important that the training data covers the whole spectrum of possible vehicle parameters and driving circumstances.

The novelty detection performance of the unsupervised learning approaches is quantitatively compared to the resulting M -value of the supervised learning approaches. Figure 5.14(b) visualizes the M -value with full length bars and whiskers. Horizontal lines at a lower y-axis level indicate the mean classification accuracy of these methods from Figure 5.13 as reference. The general relations of the resulting M -values across the supervised learning approaches is similar to the corresponding accuracy values. However, the general level of the M -values is higher.

Comparing the M -value of supervised learning approaches and the AUC of unsupervised learning approaches in Figure 5.14(a) and 5.14(b) reveals that applying supervised learning methods results in a fault detection performance on the test data that is about 25 Percentage Points (PPs) higher than the fault detection performance of unsupervised learning approaches. It shall again be noted that the M -value is identical to the AUC for the binary classification case. Especially the robustness of the supervised fault detection performance benefits from the additional information that is incorporated by using labeled training data.

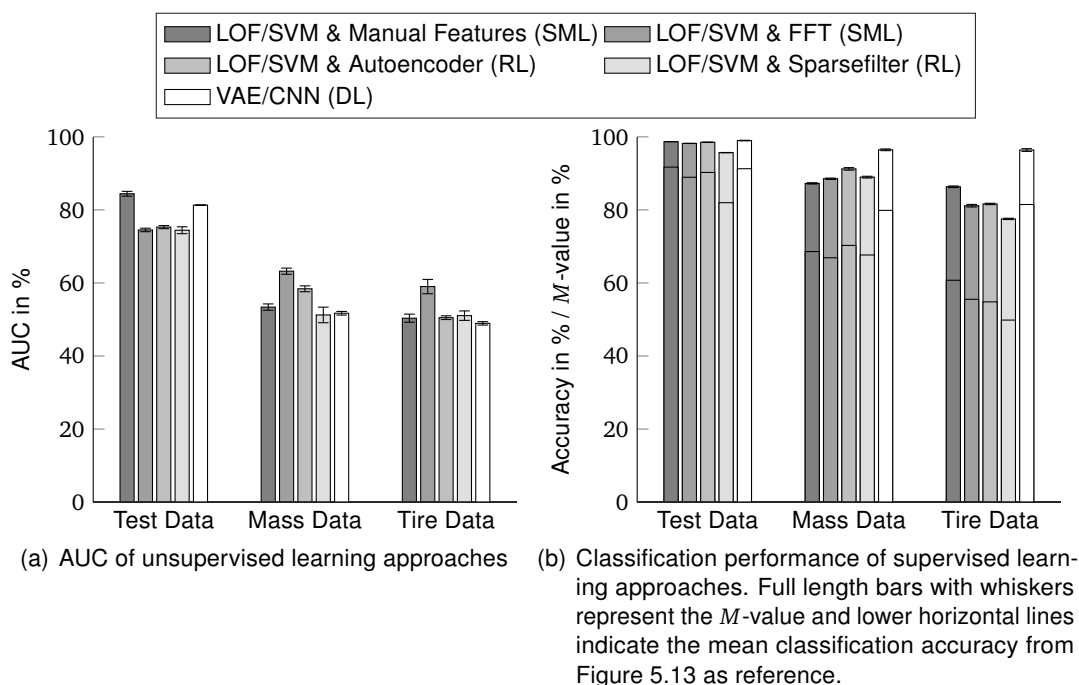


Figure 5.14: Classification performance of unsupervised and supervised learning methods that are trained on training data and applied to the test, mass and tire datasets. Whiskers indicate the standard deviation that results from the application of all classifiers of the 5-fold cross-validation to the respective dataset.

5.4.3 Increasing Robustness of Unsupervised Learning Approaches

Unsupervised learning approaches showed an unrobust behavior regarding mass and tire data in Subsection 5.4.2. Therefore, an analysis of the performance of unsupervised learning algorithms with incorporation of robustness data into the training data is performed. To generate a noticeable effect of the classification performance for optimization based algorithms (e.g. VAE), it is necessary to incorporate an appreciable number of robustness observations into the training data. The size of the mass dataset is smaller than the tire dataset. Therefore, only tire data is added to the training data for the analysis in this section. Hereby, an improvement on the tire data should be noticeable.

The tire dataset consists of 651 intact observations. 250 intact observations are selected as test data and 401 observations are added to the 2538 intact observations of the initial training data. This results in a proportion of $\frac{401}{2538+401} = 13.6\%$ of tire data observations within the training data.

Full length bars in Figure 5.15 represent the unsupervised fault detection performance using the classifiers that are trained with incorporated tire data into the training data. Horizontal lines without whiskers indicate the mean AUC value of the initial classification performance from Figure 5.14(a) for reference.

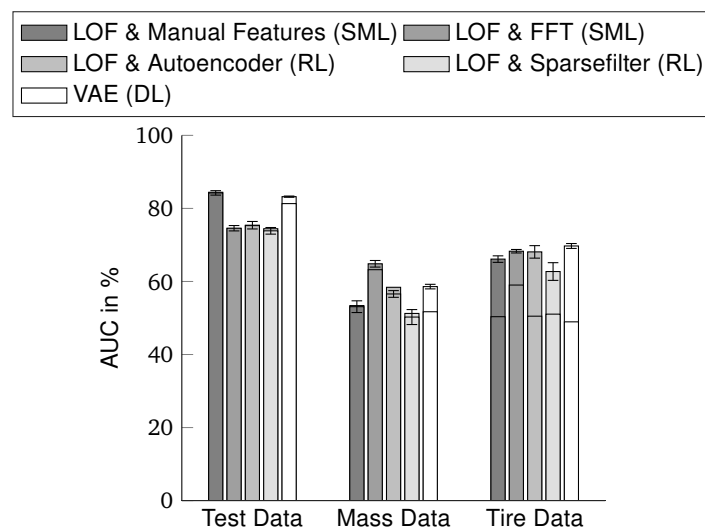


Figure 5.15: AUC of unsupervised learning methods that are trained on training data with incorporated tire data and applied to the test, mass and tire datasets. Whiskers indicate the standard deviation that results from the application of all classifiers of the 5-fold cross-validation to the respective dataset. Horizontal lines without whiskers represent the initial classification performance from Figure 5.14(a).

The classification performance on the normal test data remains at a nearly unchanged level compared to the performance using the initial training data. The performance on the tire data is improved for all approaches. The VAE results in the highest AUC of 69.71 %. No method in Figure 5.15 clearly outperforms the other methods.

The performance on the mass dataset is even slightly reduced for the nearest-neighbor approaches. However, the reduction is in a similar range as the standard deviation of the cross-validation. Nearest-neighbor classifiers rely on the similarity of data characteristics of the training data and the evaluation data. Due to the different characteristics of mass data compared to tire data, the LOF classifier cannot take advantage of the incorporation of tire data for the evaluation of mass data. Therefore, the nearest-neighbor LOF classifier is in general expected to perform unrobustly.

The VAE increases its performance on the mass dataset by 6.9 PPs. Even though it is only a small improvement, it is greater than the standard deviation of the cross-validation and is therefore not caused by random selection of training data. This performance gain reveals that the VAE is able to translate the incorporation of one type of robustness data to another type of robustness data at least slightly. Therefore, the VAE is expected to perform more robust than a nearest-neighbor classifier. It is expected that some extreme variations of the vehicle parameters (e.g. mass, tires etc.) are sufficient for a robust fault detection performance of the VAE.

5.5 Performance Improvements by Post-Processing of the Apriori Classifier

After analyzing the performance of the classification approach, further performance improvements by considering temporal relations of consecutive observations are investigated in this section. Supervised learning approaches are post-processed using HMMs of Subsection 4.9.1 and unsupervised learning approaches are post-processed using LDS of Subsection 4.9.2.

5.5.1 Post-Processing of Supervised Learning using Hidden Markov Models

This section investigates the performance of a HMM for the post-processing of the apriori classification result of supervised learning approaches. The post-processing of the tire dataset of the SML approach using a SVM and manual features shows interesting characteristics and is therefore selected for the visualization of the HMM post-processing performance. In the following paragraphs, an “apriori” estimation represents the estimation of the initial classifier, while a “posteriori” estimation represents the estimation result after the post-processing using the HMM.

Figure 5.16 visualizes estimated class affiliation probabilities and estimated classes for three sequences of consecutive observations of the tire dataset. The first sequence of consecutive observations consists of the observation indices 1280 to 1496, the second sequence consists of observation indices 1497 to 1738 and the last sequence consists of observation indices 1739 to 2049. The top graph shows the estimated class affiliation probability of the predicted class of the apriori classifier as well as of the posteriori HMM for each observation. The mean of the estimated probabilities of the apriori classifier is calculated for each class across each sequence of consecutive observations. The maximal value of the resulting mean probability is shown for reference. The lower graph illustrates the corresponding predicted class of the apriori classifier, of the HMM and the actual true class for each observation. Hereby, misclassifications of the apriori classifier can be identified. Figure 5.16(a) presents the described quantities for a parameterization of the HMM’s emission matrix based on the apriori classifier’s performance on the training dataset. Hereby, the classification characteristic of the apriori classifier on the tire dataset is unknown to the HMM. Figure 5.16(b) is discussed later in this section.

The first visualized sequence of observations (observation index 1280 to 1496) mainly consists of apriori correctly classified observations. The HMM is able to increase the posteriori estimated class affiliation probability in the top graph in Figure 5.16(a) to up to 100% by considering the health state transition probabilities, even though the supplied confusion matrix for the parameterization of the HMM’s emission probability is not based on the tire dataset but the training dataset. This is due to the fact that the true positive rate of the apriori classifier on the

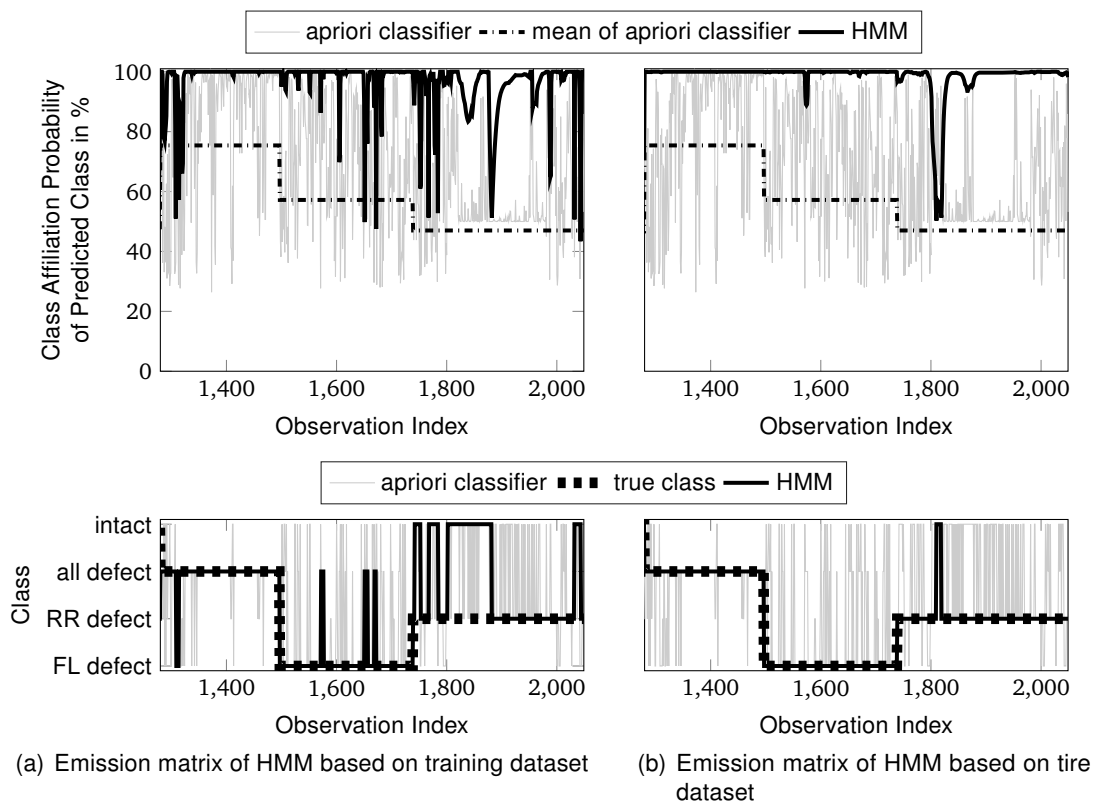


Figure 5.16: Visualization of predicted probabilities using HMM and SVM with manual features on tire data

complete tire dataset for the corresponding true class “all defect” is relatively high with 74.3%. Misclassified observations are evenly distributed across the other three classes. The HMM behaves in this way for all consecutive observation sequences with a classification result of the apriori classifier that is consistent to the corresponding TPR of the supplied confusion matrix for the parameterization of the HMM. The behavior for the second visualized observation sequence (observation index 1497 to 1738) is similar to the first sequence, even though it consists of more misclassified observations by the apriori classifier compared to the first sequence.

The last visualized sequence (observation index 1739 to 2049) consists of many misclassified observations of the apriori classifier. The true positive rate of the apriori classifier on the complete tire dataset for the true class “RR defect” is only 39.2%. 54.6% of these “RR defect”-true class observations are misclassified as “intact” by the apriori classifier. This behavior of the apriori classifier is not known to the HMM because it is not reflected with the parameterization of the HMM’s emission matrix. Hereby, the HMM can misclassify these observations while outputting a high posteriori estimated class affiliation probability (e.g. from observation index 1802 to 1881).

Due to these performance problems, the following paragraphs analyze the performance improvement by a HMM post-processing with a HMM parameterization that incorporates knowledge about the weaknesses of the apriori classifier. A parameterization of the HMM that is based on the apriori classifier’s performance on a different dataset than the training data of the apriori classifier can be beneficial if the re-training of the classifier is not possible or “expensive”. This might be the case if one classifier is trained on a big dataset that consists of different vehicle derivatives. It can also be the case if the classification is computed directly on a vehicle’s ECU and only the apriori classification result is available on a server. The HMM can then be used for derivative-specific tuning of the classification concept.

Figure 5.16(b) shows results for a parameterization of the HMM's emission matrix that is based on the apriori classifier's performance on the tire dataset. Hereby, the classification characteristic of the apriori classifier on the tire dataset is known to the HMM. The post-processed classification performance is improved for all visualized measurements. Observations that were misclassified by the HMM in Figure 5.16(a) are now correctly classified with only a few exceptions (observation indices 1810 to 1818). However, these misclassified observations now have a reduced posteriori estimated class affiliation probability.

Figure 5.17 shows the classification accuracies of the supervised learning approaches using a HMM-based post-processing with full length bars and whiskers. Horizontal lines indicate the mean accuracy of the corresponding apriori classifier without post-processing from Figure 5.13.

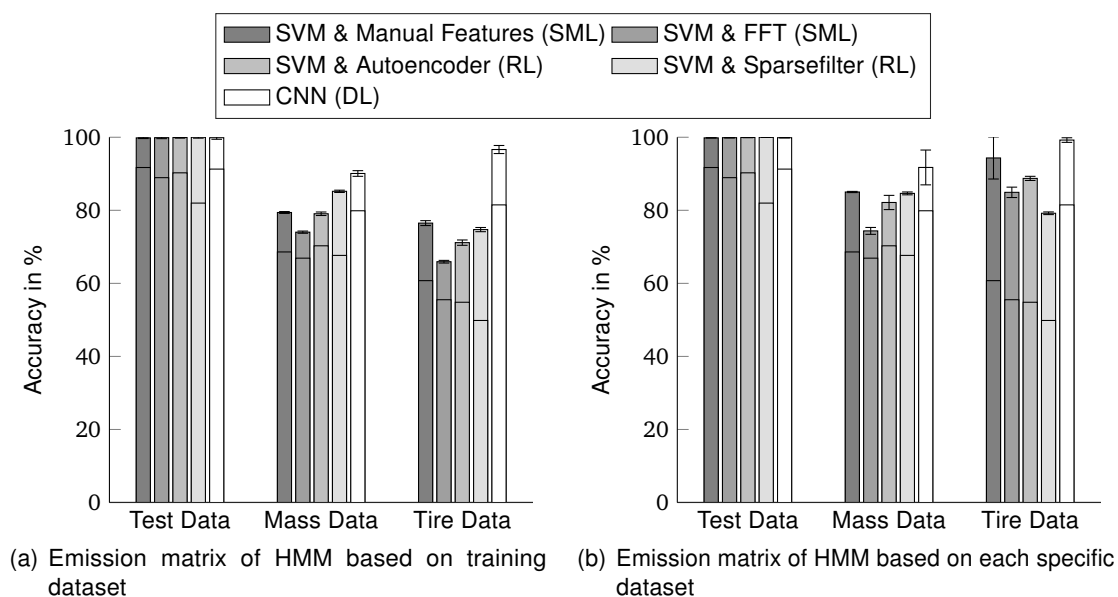


Figure 5.17: Classification accuracy of supervised learning methods that are trained on training data and applied to the test, mass and tire datasets with additional HMM post-processing of the apriori classifier predictions. Whiskers indicate the standard deviation that results from the application of all classifiers of the 5-fold cross-validation to the respective dataset. Horizontal lines without whiskers indicate the mean classification accuracy of the apriori classifier without post-processing from Figure 5.13.

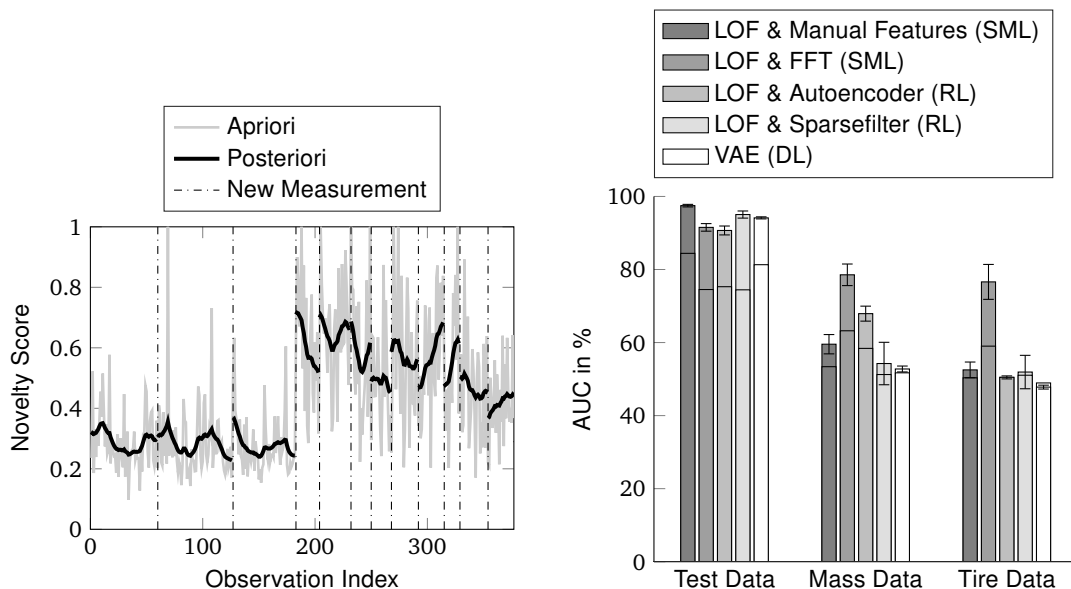
Figure 5.17(a) presents the posteriori classification accuracies for a parameterization of the HMM's emission matrix based on the apriori classifier's performance on the training data. The accuracies on the test data of all methods are above 99.8%. Results on mass and tire data have also increased. The improvement of each classification concept is of different extent and is not derivable to a specific classifier's characteristic.

Figure 5.17(b) shows the posteriori classification accuracies for a parameterization of the HMM's emission matrix based on the apriori classification performance on the corresponding evaluation dataset. The posteriori classification performance on the mass data remains at a similar level. Due to the additional mass in the trunk of the vehicle, the apriori classifier confuses the "intact" and "RR defect" class of the mass dataset (e.g. the true positive rate of the "intact" class is only 27.1% when using a SVM with manual features and 62.8% of the "intact"-true class observations are misclassified as "RR defect"). This weakness of the apriori classifier cannot be compensated by supplying an emission matrix that incorporates this apriori classifier behavior. However, the classification accuracy on the tire data is further increased in Figure 5.17(b) when the HMM is supplied with an emission matrix that incorporates the reduced classification performance of the apriori classifier on the tire dataset compared to Figure 5.17(a).

This section showed that it is possible to improve the classification performance of the overall classification process by using a HMM for the post-processing of the apriori classification result. The parameterization of the HMM based on the performance of the apriori classifier on the training or validation data also improves the performance on the robustness datasets. If the apriori classifier tends to be confused by some special classes, it is beneficial to supply this information to the HMM using the parameterization of the HMM's emission matrix.

5.5.2 Post-Processing of Unsupervised Learning using Linear Dynamical Systems

Figure 5.18(a) shows novelty scores of the LOF algorithm using manual features for consecutive observation sequences of the test dataset. The observation indices 1 to 182 are “intact”, 183 to 249 are “all defect”, 250 to 314 are “FL defect” and 315 to 377 are “RR defect”. The general level of the apriori estimated novelty scores for observations of the “intact” class is lower than for all defect classes. However, the noisy apriori novelty scores lead to the misclassification of some observations. The posteriori estimated novelty scores are generated as described in Subsection 4.9.2. The filtering process is computed for each observation sequence individually. The posteriori estimated novelty scores are less noisy. The classification of each observation based on the comparison of the posteriori estimated novelty score with an arbitrary threshold leads to an improved detection of defective dampers. E.g. a suitable threshold for the visualized classifier would be 0.4 because this threshold separates the visualized intact and defect observations.



(a) Visualization of novelty scores using linear dynamical systems for post-processing of the LOF novelty prediction using manual features on test data. Observations indices 1-182 are “intact”, 183-249 are “all defect”, 250-314 are “FL defect” and 315-377 are “RR defect”.

(b) AUC of unsupervised learning methods that are trained on training data and applied to the test, mass and tire datasets with additional post-processing of the apriori classifier using linear dynamical systems. Whiskers indicate the standard deviation that results from the application of all classifiers of the 5-fold cross-validation to the respective dataset. Horizontal lines without whiskers indicate the AUC of the apriori classifier without post-processing from Figure 5.14(a)

Figure 5.18: Post-Processing of Unsupervised Learning using Linear Dynamical Systems

Figure 5.18(b) shows the novelty detection performance for the three datasets using the LDS post-processing. The performance on the test data is improved for all novelty detection concepts. Using manual features with a LOF classifier reaches 97.5 % AUC. The performance on the mass dataset is only increased by less than 7 PPs when using manual features, Sparsefilter features or when using the VAE. The performance on the tire dataset remains nearly unchanged for all novelty detection concepts except when using FFT features. Obviously, the performance of a classifier that classifies a datasets only by chance will not improve by applying a post-processing except of small improvements by chance. The LOF classifier that uses FFT features outperforms all other classification concepts on the robustness datasets. The FFT features have the highest granularity of information. Hereby, features may have similar values for observations of different health classes. On the one hand, this reduces the separability of these classes and prevents an optimal performance. On the other hand, it incorporates robustness to changed circumstances of the analyzed data (such as additional mass or changed tires). The post-processing reinforces this characteristic for using a LOF classifier with FFT features.

5.6 Analysis of Sensor Signal Importance

An analysis of the importance of the different sensor signals is conducted by applying a RFE. All features that correspond to a sensor signal are deactivated as a block. The number of neurons of the VAE is scaled with the number of input signals. The CNN network architecture remained unchanged for different number of input signals. Figure 5.19 shows the classification performance on the test data for a selection of a reduced number of sensor signals for supervised and unsupervised learning approaches. Table 5.2 presents the corresponding ranking of the sensor signals for supervised learning and Table 5.3 for unsupervised learning approaches. The performance is in general slightly lower than in Figure 5.13 and 5.14(a) because no optimization of the feature set or of the hyperparameters is conducted. The ranking of the sensor signal importance is discussed in the following paragraphs.

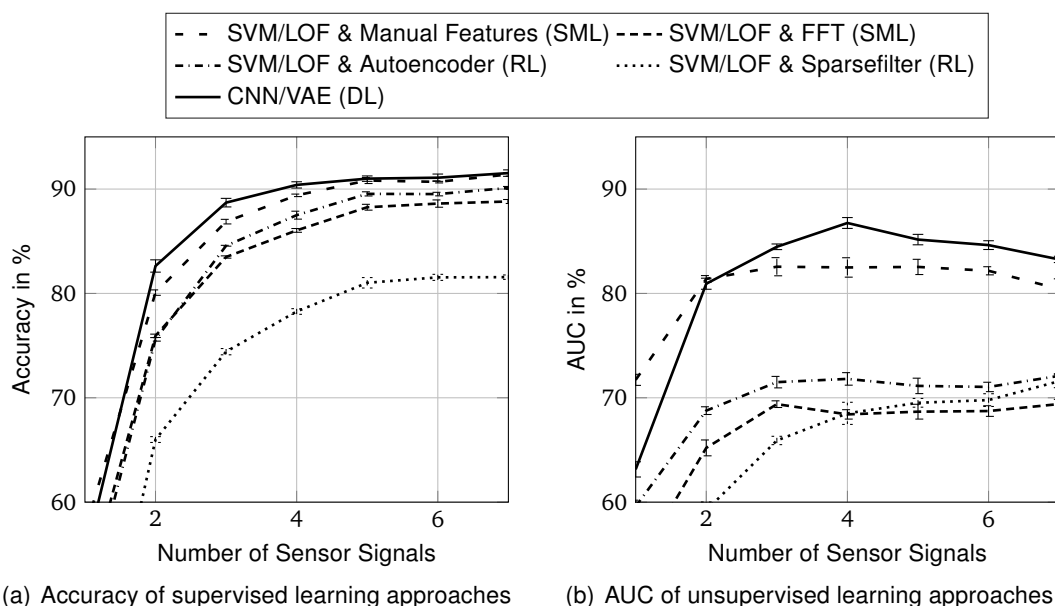


Figure 5.19: Performance of supervised and unsupervised learning methods on the test dataset for feature subsets of a reduced number of sensor signals according to the ranking in Table 5.2 and Table 5.3 using the RFE approach.

Table 5.2: Importance ranking of the sensor signals for supervised learning methods.
 WS = Wheel Speed, Acc X = Longitudinal Acceleration, Acc Y = Lateral Acceleration,
 YR = Yaw Rate

Rank	SVM & Manual Features	SVM & FFT	SVM & Autoencoder	SVM & Sparsefilter	CNN
1.	WS FL	WS FL	WS FL	WS FL	WS FL
2.	WS RR	WS RR	WS RR	WS RR	WS RR
3.	WS FR	WS FR	WS FR	WS FR	WS FR
4.	WS RL	WS RL	WS RL	Acc Y	WS RL
5.	Acc Y	Acc Y	Acc Y	WS RL	Acc Y
6.	Acc X	Acc X	YR	Acc X	Acc X
7.	YR	YR	Acc X	YR	YR

Table 5.3: Importance ranking of the sensor signals for unsupervised learning methods.
 WS = Wheel Speed, Acc X = Longitudinal Acceleration, Acc Y = Lateral Acceleration,
 YR = Yaw Rate

Rank	LOF & Manual Features	LOF & FFT	LOF & Autoencoder	LOF & Sparsefilter	VAE
1.	WS RR	YR	YR	YR	WS FL
2.	WS FL	WS FL	WS FL	WS FL	WS RR
3.	Acc Y	Acc Y	Acc Y	Acc Y	Acc Y
4.	WS FR	Acc X	Acc X	Acc X	WS FR
5.	YR	WS FR	WS FR	WS RL	WS RL
6.	WS RL	WS RL	WS RL	WS FR	Acc X
7.	Acc X	WS RR	WS RR	WS RR	YR

The ranking of the sensor signals for supervised learning approaches is consistent across the tested approaches. The wheel speed signals are most important. The wheel speed signals FL and RR are more important than FR and RL because the dataset consists of the health state classes “intact”, “all defect”, “FL defect” and “RR defect”. The wheel speed signals FR and RL are third and fourth most important sensor signals. Even though, there is no individual damper defect class within the dataset, these sensor values still allows for an easier detection of the health state with all dampers being defect and all dampers being intact. Using only the four wheel speed sensor signals already results in a very high accuracy compared to the accuracy when using all sensor signals. CNNs that use only wheel speed signals already reach over 90 % classification accuracy. This fits to the result of the observability analysis in Chapter 3. However, using vehicle body sensor signals does still increase the classification accuracy slightly. The lateral acceleration is the most important vehicle body sensor signal. Longitudinal acceleration and yaw rate are less important.

The diagnosis performance of unsupervised learning approaches behaves more heterogeneous than supervised learning approaches. For manual features, the wheel speed signals RR and FL are ranked as most important. Selecting these two sensor signals already results in 81.39 % AUC. Manual features have a high focus on the variation of vertical eigenfrequencies of the wheels. This leads to the high importance of these sensor signals for the manual feature set. FFT, Autoencoder and Sparsefilter are neutral feature generation methods without a focus on any specific sensor signals or deviations of eigenfrequencies. These three feature sets result in a very consistent importance ranking of sensor signals. Except for the wheel speed FL, all vehicle body signals are ranked as more important than the wheel speed signals. A closer investigation of the frequency analysis in Figure 5.2 reveals that all defective states lead to a deviation of the vehicle body sensor signal characteristics from the intact state. Wheel speed signals remain

unchanged for damper defects that do not affect the corresponding wheel. Therefore, the shown unsupervised learning concepts are based more on vehicle body signals that deviate slightly for all fault conditions than on wheel speed sensor signals that deviate strongly for only some fault conditions. An interesting fact is that in contrast to the supervised sensor ranking in Table 5.2, the yaw rate signal is ranked as the most important vehicle body sensor signal. However, a good discriminative power of some frequency shares of the yaw rate signal is already presented by the yaw rate's Fisher score in Figure 5.2(g).

The performance of the VAE consists of a distinct peak when using four sensors. This results in the highest AUC of 86.75 %. The sensor signal ranking is similar to the ranking of supervised learning methods. Only the order of lateral acceleration and wheel speed signals that are not directly affected by damper faults (FL and RR) is changed.

5.7 Analysis of Training Data Size

The analysis of the diagnosis performance for different sizes of the training dataset provides an expectation of the performance when applying the diagnosis approaches to larger datasets in real-life. Therefore, the performance of supervised and unsupervised learning approaches on the test data is analyzed for a reduced size of the training data and presented in Figure 5.20. Variations of the performance of SML approaches are caused by a varying performance of the classifier, while the quality of the generated features remains unchanged. RL approaches vary in the classifier's performance as well as the quality of the generated features due to the reduced training data for the training of the feature generation processes. DL approaches are completely dependent on training data due to the end-to-end learning method.

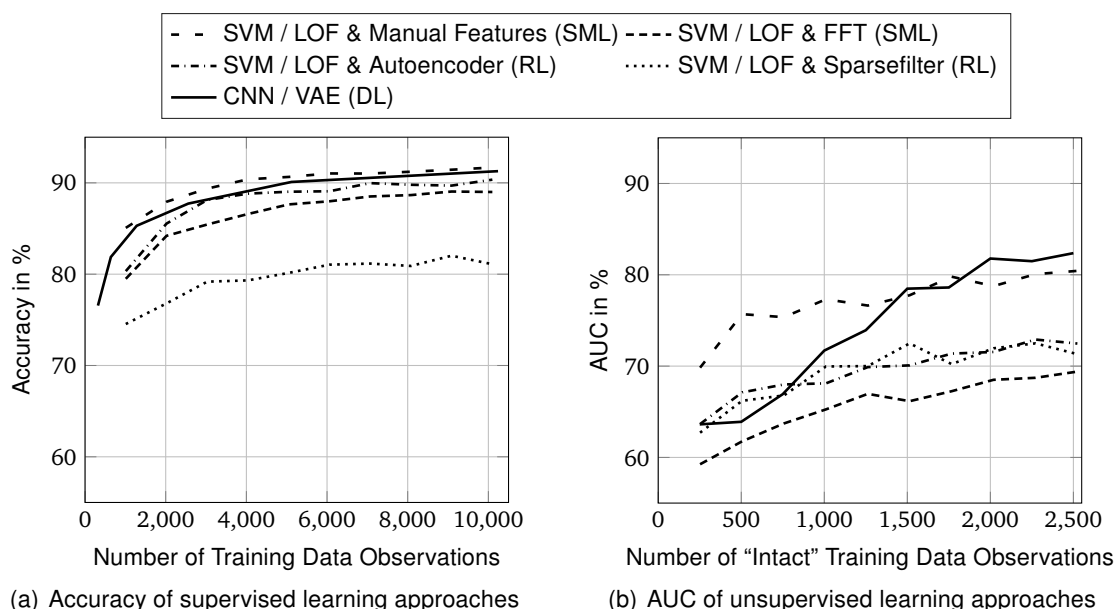


Figure 5.20: Performance of supervised and unsupervised learning methods on the test dataset using a reduced size of the training dataset

Figure 5.20(a) shows that the accuracy of the supervised learning approaches with regard to the size of the training dataset is similar for SML, RL and DL approaches. All approaches flatten their performance increase with an increasing size of the training dataset. This may indicate that the dataset consists of some observations that are hard to classify because of irregular

circumstances (e.g. driving across bumps or short periods of high acceleration). This would require either a larger and more heterogeneous dataset, or a more homogeneous dataset by a more conservative observation generation (using more conservative thresholds for maximal acceleration etc.).

Unsupervised learning approaches use only “intact” observations for training. Therefore the size of the training data is smaller compared to the supervised learning training dataset. Unsupervised SML and RL approaches in Figure 5.20(b) again behave similar. A reduction of the increase of the AUC for larger training datasets can already be observed in Figure 5.20(b). The DL method VAE shows a continuous increase of the AUC with an increasing training dataset. While the gradient of the performance improvement is also slightly decreasing for an increasing size of the training datasets, further improvement is expected for larger training datasets.

5.8 Analysis of Influence of Vehicle Speed and Road Roughness

The theoretical analysis of the observability of a variation of the damper coefficient in Chapter 3 showed that an increased vehicle speed as well as a higher road excitation are beneficial for the diagnosis performance. These theoretical results are investigated in this section. The analysis is performed exemplary with the supervised SML approach using manual features because this required the least computational effort.

The corresponding vehicle speed of an observation is selected as the mean over the observation time and over all wheel speeds. The road roughness is not measured directly within the scope of this thesis. Therefore, the International Roughness Index (IRI) information for each observation is extracted from the mapping information of “here” maps as indicator of the road roughness. The IRI was introduced in [288]. It is based on a simulation of a quarter-vehicle model with specific reference parameters using the corresponding road profile [289, p. 3, 290, pp. 31-43]. The IRI is calculated by

$$\text{IRI} = \frac{1}{L} \int_0^{\frac{L}{v}} |\dot{z}_T(t) - \dot{z}_{Bo}(t)| dt \quad (5.5)$$

with the length L of the analyzed road segment and the reference vehicle speed v of the quarter-vehicle simulation. The vehicle speed within the simulation is typically $80 \frac{\text{km}}{\text{h}}$. $\dot{z}_T(t)$ and $\dot{z}_{Bo}(t)$ are the vertical velocities of the unsprung tire and sprung vehicle body mass of the quarter-vehicle reference model. The IRI’s unit is $\frac{\text{m}}{\text{km}}$ (meter per kilometer) [290, p. 33].

To prevent any biasing effects of the classification performance due to biases within the training data regarding vehicle speed or road roughness, new classifiers are trained using special training datasets for both cases. The analysis of the influence of the vehicle velocity is conducted using a training dataset that consists of 5000 observations that are uniformly distributed from $50 \frac{\text{km}}{\text{h}}$ to $100 \frac{\text{km}}{\text{h}}$ with 500 observations per $5 \frac{\text{km}}{\text{h}}$. The information of the IRI is not available for all observations. Therefore, a training dataset is generated that consists of 3000 observations that are uniformly distributed from an IRI of $0.5 \frac{\text{m}}{\text{km}}$ to $3 \frac{\text{m}}{\text{km}}$ with 300 observations per $0.25 \frac{\text{m}}{\text{km}}$. Realistic IRI values are around $0.25 \frac{\text{m}}{\text{km}}$ to $1.25 \frac{\text{m}}{\text{km}}$ for a German Autobahn and $0.25 \frac{\text{m}}{\text{km}}$ to $3 \frac{\text{m}}{\text{km}}$ for federal or state streets [291, p. 189]. Figure C.11 in the Appendix C.3 shows the distribution of observations for the training and testing dataset.

The influence of the vehicle speed and road roughness is evaluated by investigating the estimated true class affiliation probability for each observation of the testing data in Figure 5.21. Each bar represents the amount of observations of the testing data as shown in Figure C.11. The gray tone indicates the relative amount of observations with an estimated true class affiliation probability within the respective range indicated by the legend for each corresponding speed or IRI range. The classifier’s accuracy and AUC for each speed / road roughness bin is visualized for reference in Appendix C.3 in Figure C.12. Figure 5.22 shows the correlation coefficient between the different true class affiliation probability shares of Figure 5.21 with the vehicle speed and IRI.

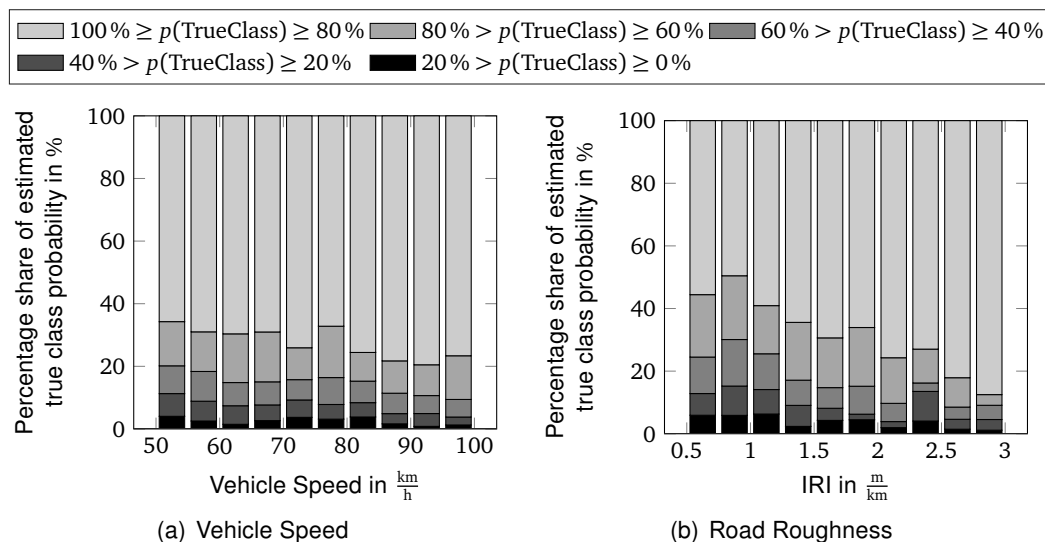


Figure 5.21: Relative shares of the estimated probabilities of the true class for the supervised SML approach using manual features. Each bar is normalized with respect to the amount of observations for each share in the testing data in Figure C.11.

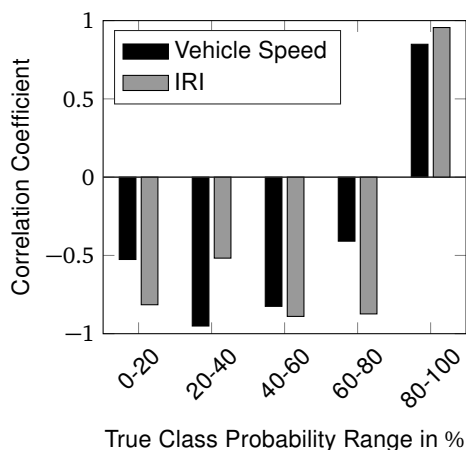


Figure 5.22: Correlation of estimated true class probability with vehicle speed and IRI for each probability share in Figure 5.21

All true class probability shares below 80 % in Figure 5.22 have a negative correlation, while the true class probability shares between 80 % to 100 % are positively correlated with the vehicle speed and the IRI. Therefore, misclassifications (with a low true class probability) are reduced and observations that are already correctly classified, increase their precision. These results show that with an increasing vehicle speed as well as with an increasing road roughness (increasing IRI), the estimated probability for the true class increases. Hereby, global metrics

such as the accuracy or AUC will increase with higher vehicle speeds and higher road excitation. This is also the case in Figure C.12. Additionally, a post-processing of the classification result will be more precise because the apriori estimated probabilities are more reliable.

The results of the theoretical analysis of the observability analysis in Chapter 3 could be confirmed. Higher vehicle speeds as well as an increased road roughness result in an improved classification performance.

5.9 Comparison with Signal-Based Approach

This section compares the performance of the Machine Learning (ML) approaches with the performance of the signal-based damper diagnosis approach of Jautze [17]. An introduction to this approach is given in the following paragraphs based on [17, pp. 71-79].

An index is generated that compares the magnitude of the Power Spectral Density (PSD) at two frequency ranges of the wheel speed signal as indicated in Figure 5.23. The evaluation frequency f_E is selected at the vertical tire eigenfrequency of around 10 Hz to 15 Hz so that the magnitude of the PSD within this range is influenced by a varying damping characteristic. The reference frequency f_R is selected in a frequency range that is independent from the damping coefficient. Jautze [17, p. 76] defines the Damper Damage Value (for German Dämpferschadenskennwert) (DSKW) by averaging across multiple datapoints within the frequency ranges by

$$DSKW = \frac{1}{n} \sum_{i=1}^n \frac{S_{\omega}(f_{E,i})}{S_{\omega}(f_{R,i})} \quad (5.6)$$

with the magnitude of the PSD S_{ω} at an evaluation frequency $f_{E,i}$ and at a reference frequency $f_{R,i}$. The number of investigated frequencies n is selected to result in a small bandwidth of the evaluation and reference frequency range.

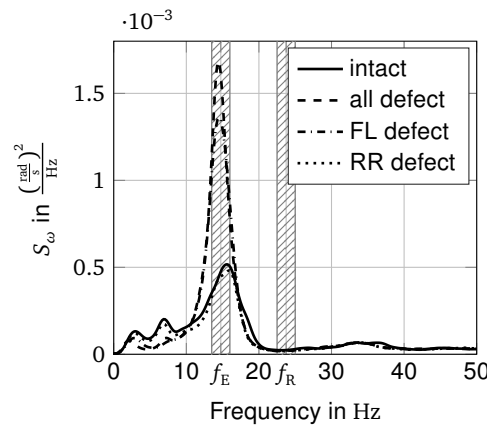


Figure 5.23: PSD of wheel speed Front Left (FL) for the different damper health states with exemplary evaluation and reference frequency range.

The DSKW can be treated as outlier score. The higher the DSKW, the more likely a damper defect is. Therefore, the performance analysis of the signal-based approach within this thesis uses the AUC metric. The four damper health states of this thesis' dataset are converted to an "intact" and "defect" damper health state for each wheel. An AUC value can then be generated for each wheel independently. These wheel-specific AUC values are averaged to get one metric for the signal-based approach of Jautze [17]. Due to the conducted parameter optimization

and speed-correction of the implementation of the signal-based approach within this thesis, the resulting diagnosis performance might be slightly better compared to an actual real-life implementation. See Appendix C.4 for implementation details.

Figure 5.24 compares the performance of the signal-based approach with the classification performance of the supervised and unsupervised approaches from Figure 5.14. The signal-based approach shows a consistent performance on all three datasets with 77.72 % AUC on the testing dataset, 77.21 % AUC on the mass dataset and 74.06 % AUC on the tire dataset. All unsupervised ML approaches in Figure 5.24(a) have at least a similar performance compared to the signal-based approach on the test dataset. Using a LOF with manual features or a VAE perform better than the signal-based approach for the testing dataset. The signal-based approach has a better performance on the mass and tire dataset compared to all unsupervised ML approaches. While the reduced performance of the ML-based novelty detection for unknown data is known from Subsection 5.4.2, the signal-based approach is the better choice if the training data does not cover the real-life driving data to a sufficient extent. If the operating conditions of the diagnosis approach are known, ML approaches can compete with the signal-based approach that requires expert knowledge regarding the symptoms that are caused by a component defect. The performance of ML approaches is even higher if features are supplied that incorporate a sufficient amount of knowledge (as it is the case with statistical or frequency-based features in the manual feature set) or if the supplied training data is efficiently incorporated into the ML approach as it is the case for DL approaches. Figure 5.24(b) shows the AUC values of supervised ML algorithms as shown in Figure 5.14(b) and the AUC value of the signal-based approach. This comparison highlights the beneficial impact of labeled training data again.

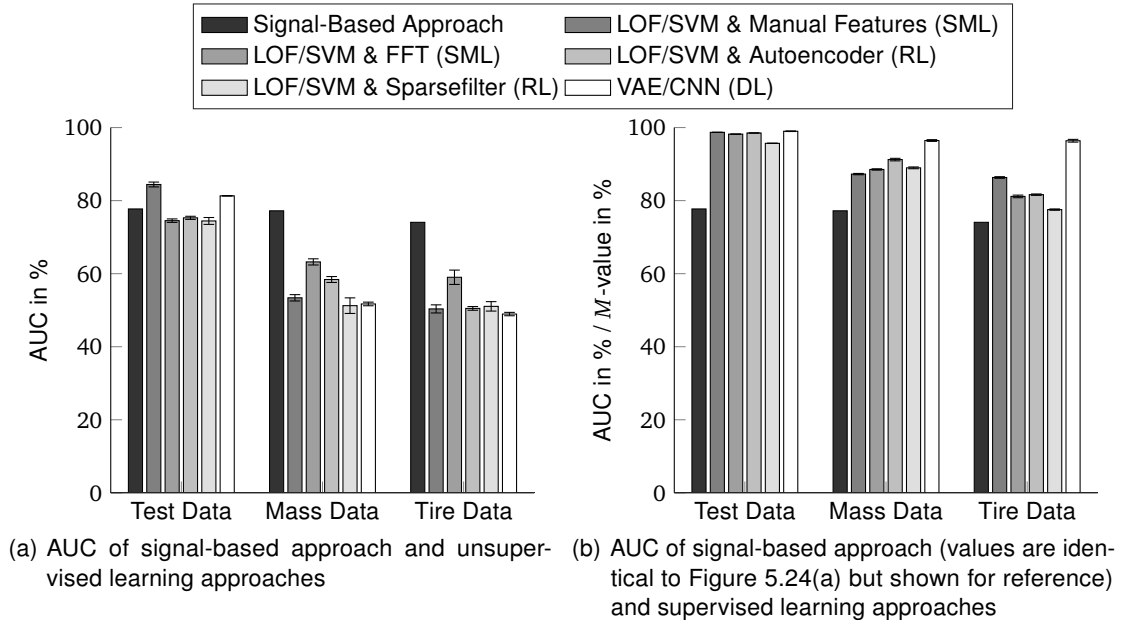


Figure 5.24: Comparison of the damper defect detection performance of the signal-based approach with that of the unsupervised and supervised learning methods that are trained on training data and applied to the test, mass and tire datasets from Figure 5.14.

6 Discussion

This section provides a summary of the results by answering the derived research questions from Section 2.7. Based on these overall results, implications for an actual implementation are discussed. Afterwards, the overall approach is critically assessed and the relevance of this thesis is discussed.

6.1 Overall Assessment of the Results

The overall results show that machine learning methods are suitable for the detection of damper defects using driving data of ESC system measurements. More details are provided with regard to the research objectives from Section 2.7.

I.a. Is it possible to detect defective dampers using only wheel speed measurements with unknown road excitation?

The observability of a quarter-vehicle model with an additional state for the damping coefficient is analyzed under the circumstance of the measurement of the wheel speed and unknown road excitation. Vehicle body sensor signals (yaw rate or accelerations) were not considered to keep the model complexity as simple as possible. The local observability was analyzed using a numeric evaluation of the stochastic observability. Local observability is given for the analyzed system and the defined circumstances. Therefore it is possible to detect defective dampers using only wheel speed measurements with unknown road excitation.

I.b. Which circumstances limit or benefit the detection of defective dampers?

The detection of defective dampers can be improved by an increased observation time of the sensor measurements, higher vehicle speeds or higher road roughness. The theoretical findings for vehicle speed and road roughness are experimentally analyzed and confirmed in Section 5.8. The estimated probability of the observation's true class correlates with the vehicle speed and the International Roughness Index (IRI).

II. Which machine learning concepts are suited for the diagnosis of defective automotive dampers?

Supervised and unsupervised learning methods of Shallow Machine Learning (SML), Representation Learning (RL) and Deep Learning (DL) are identified as suitable machine learning concepts. The most appropriate diagnosis concept depends on the effort that can be spent for data generation and implementation aspects regarding data transmission and computational resources. Supervised learning approaches lead to higher classifications accuracies than unsupervised learning approaches.

The comprehensibility of the algorithm behavior as well as the incorporation of existing model-based knowledge of component behavior is best for SML approaches. DL methods can be transferred to other component faults. RL does not supply any major improvements of the

diagnosis performance compared to SML methods. If no knowledge about the signal-based effects of component faults is available, using FFT data points as features is a reasonable approach. If it is possible to generate labeled data for supervised classification, the choice of a SML or DL approach is based on the required robustness to unknown circumstances of the diagnosis application. SML performs well within the circumstances of its training data. DL does not necessarily result in an improved performance within the circumstances of the training data. However, the robustness to unknown circumstances in the data is increased. If it is not possible to generate labeled data, unsupervised learning methods need to be applied. While the performance of unsupervised SML and DL methods is similar in this thesis, the behavior of the DL approach with respect to the size of the training data suggests a better performance of DL methods for larger training datasets. Therefore, the DL approach is considered as the more suitable approach.

III.a. How accurate are the results?

The performance on homogeneous test data is similar across supervised SML, RL and DL approaches. All approaches result in classification accuracies of around 90% except the Sparsefilter-based RL approach (Figure 5.13). Using hand-crafted manual features for a SML approach leads to the highest AUC of 84.4% across the unsupervised learning approaches on the homogeneous test data (Figure 5.14(a)). The DL method Variational Autoencoder (VAE) is the second best performing algorithm. RL approaches perform worst for unsupervised learning.

To be able to compare the results of supervised and unsupervised learning approaches quantitatively, the accuracy of supervised learning methods is transformed to a multiclass-AUC (or M -value). This metric accounts for the additional information regarding the specific class affiliation of each observation of supervised learning approaches. Hereby, supervised learning approaches result in about 20% to 25% higher AUC values compared to unsupervised learning approaches (Figure 5.14).

Additional improvement of the classification performance can be generated considering the temporal behavior of sequences of consecutive observations. Post-processing the a priori supervised classification using a Hidden Markov Model (HMM) results in accuracies of more than 99.8% on the test dataset for all supervised learning approaches (Figure 5.17(a)). This means that two out of 1000 observations with a length of 5.12 s are misclassified. The post-processing of unsupervised learning approaches is performed by a Linear Dynamical System (LDS). All approaches increase by about 10 to 15 Percentage Points (PPs). The SML approach even reaches 97.5% AUC (Figure 5.18(b)).

III.b. How robust are the results?

The robustness of the applied approaches is evaluated by analyzing the diagnosis performance with additional mass in the vehicle's trunk and with winter instead of summer tires. The performance of supervised SML and RL approaches is reduced by 20 to 40 PPs on these datasets compared to the classification accuracy on the homogeneous test data (Figure 5.13). The DL-based CNN reduces its classification accuracy only slightly by about 10 PPs. Unsupervised learning approaches detect unknown patterns in data. Therefore, they are not robust with regard to additional mass or changed tires (Figure 5.14(a)). The resulting AUC of about 50% is equivalent to randomly guessing. If the investigated circumstances (additional mass or using different tires) is incorporated into the training data, the diagnosis performance of unsupervised learning approaches increases (Figure 5.15). This emphasizes the importance of a heterogeneous training dataset for unsupervised learning approaches. Covering a great variety of vehicle usage circumstances (e.g. the number of passengers, using a roof box etc.) is important for unsupervised learning approaches.

III.c. What is the influence of a varying size of training data on the detection performance?

The behavior of the classification accuracy with regard to the number of training observations is similar for all supervised learning approaches (Figure 5.20(a)). Contradictory, existing literature states that the performance of SML approaches stagnates while the performance of DL approaches increases further with a larger training dataset [28, p. 3]. This may be an indicator that the dataset within this thesis consists of observations that are impossible to classify correctly. A larger and more heterogeneous dataset, or a more homogeneous dataset by a more conservative observation generation (using more conservative thresholds for maximal acceleration etc.) may therefore be required. Unsupervised learning approaches increase their performance with an increasing size of the training dataset. The DL-based VAE has a greater gradient of performance improvement compared to SML and RL methods (Figure 5.20(b)).

III.d. Which sensor signals are most relevant?

All supervised learning approaches rate the wheel speed signals as most important sensor signals (Table 5.2). Slight additional performance improvements result from using lateral acceleration, longitudinal acceleration or yaw rate. The ranking of the sensor signals of the two best performing unsupervised learning approaches, SML using manual features and DL-based VAE, is similar to the supervised learning ranking (Table 5.3).

III.e. How is the performance of machine learning approaches compared to the signal-based diagnosis approach of Jautze [17]?

The signal-based approach of Jautze [17] generates a novelty score and can therefore be directly compared to unsupervised machine learning approaches. The performance of the unsupervised Machine Learning (ML) approaches is in a similar range compared to the signal-based approach. Two ML approaches have a better performance by 4 PPs and 7 PPs AUC than the signal-based approach. The signal-based approach is more robust to unknown operating conditions that is not covered by the training data compared to ML approaches.

IV. Is it possible to derive physical findings from the investigation of the transformations that are performed by machine learning methods?

The investigation of internal transformations of the input data that are performed by RL and DL approaches showed that most methods apply a frequency analysis if the input data is a time signal. If the input data is already a frequency analysis of the time signal, the ML methods perform a comparison of the amplitudes at different frequencies. This behavior and the results of this thesis show that using the FFT data points as features for classification is a simple but reasonable approach. However, the diagnosis performance is improved if knowledge about the system's behavior in case of a component defect is available and more specific features can be generated. The investigation of the feature characteristics in Section 5.2 shows that only a limited amount of frequencies is important for the diagnosis application. The knowledge about the importance of different frequency ranges may be obvious for the diagnosis of some components (e.g. automotive dampers). However, the described feature analysis process can be used as guideline for the development of diagnosis applications for components with an unknown system behavior under faulty conditions.

6.2 Implications for an Actual Implementation

There are two possibilities for an OEM to create value with the damper defect detection: Either showing the information of a defective damper to the driver and sending him to a workshop, or not showing the information to the driver but saving the information within the ECU and displaying the information to the workshop at the vehicle's next inspection. If the information regarding a defective state is shown to the driver, the accuracy of the health monitoring system must be (nearly) 100 %. At this point of the research project, this is only possible with supervised learning approaches. The accuracy of 99.8 % can further be increased if the thresholds for the activation of the system (maximal acceleration, minimal speed of the vehicle or a minimal required road excitation) are further narrowed. Furthermore, the trade-off between the time until a defective state is detected and the amount of false positives can be parameterized with the Hidden Markov Model (HMM). This is similar to implementing a threshold for the required class affiliation that needs to be reached to display the presence of a defective component. An important aspect of the implementation of a supervised health monitoring system is that the failure modes within the training data should match the actual failure modes in the later customer driving data. This requires a careful analysis of the driving data with different failure modes. Furthermore, it needs to be evaluated if different but similar vehicle types (e.g. different engine or different suspension system) can be monitored with a system that is trained on the same training data. In general the generation of labeled training data for supervised methods for various vehicle types can be challenging and costly. However, this thesis showed, that a couple of hundreds or thousands of kilometers for each failure mode are sufficient as training data.

The second possibility is to not display the information of the detection of a defective vehicle state to the driver but only showing it to the workshop at the vehicle's next inspection. Hereby, the health monitoring system can be less accurate because a wrongly detected defective component would not result in sending the customer to the workshop without an actual need. It only results in the car mechanic checking the damper more intensively than usual. Therefore, the monitoring task can be conducted by unsupervised learning approaches and hereby, a large amount of unlabeled data can be used without additional costs for the generation of training data. This is especially interesting because the unsupervised Deep Learning (DL) method Variational Autoencoder (VAE) showed a promising performance gain for an increasing size of the training data. However, it is important that a vast majority of circumstances of the later customer driving data is covered by the training data. More narrow activation circumstances of the health monitoring system as well as further tuning of the post-processing as explained above is also possible. Additionally, unsupervised learning approaches can also be helpful to generate labeled data with low costs: If the unsupervised method raises a component defect, it can be checked during the vehicle's next inspection. The car mechanic can then set a label according to the real vehicle health state. Applying this label to the driving data of a given amount of previous kilometers results in a growing labeled dataset with nearly no additional costs.

6.3 Critical Assessment of the Overall Approach

Section 2.4 showed that many Machine Learning (ML) concepts and methods exist for fault detection and diagnosis. The selection of supervised and unsupervised classification algorithms has low requirements regarding the availability of labeled data and the amount of data compared to regression methods or Remaining Useful Life (RUL) estimation approaches. However,

supervised and unsupervised classification methods do not provide a continuous value of the component's health or its RUL.

The selected classifier for each classification concept is only one representative of each machine learning concept. The employed methods were selected with regard to existing literature and they showed competitive performance in this thesis. However, due to the diversity of ML methods and the associated set of hyper-parameters, it cannot be guaranteed that the selected methods perform best within each machine learning concept.

Especially the area of unsupervised Deep Learning (DL) methods is an evolving field [254, p. 27]. OCNN and deep SVDD are two unsupervised learning approaches that are worth further investigation due to their performance in literature [256, p. 11]. Deep learning could also be used for the monitoring of time-dependent behavior of the machine health state. LSTMs are increasingly applied for this task and also combinations of LSTMs with other classifiers are applied for time-based machine health monitoring [135, 136, 137]. But also the area of Shallow Machine Learning (SML) classifiers is evolving constantly. XGBoost [292] is a tree boosting system that is stated to use fewer resources than existing systems. XGBoost is also applied to unsupervised outlier detection in [293].

Further optimization of the investigated methods or the analysis of additional methods could be conducted to further increase the diagnosis performance. However, this will only lead to a small gain in knowledge on this conceptual level. The consequent next step is the definition of a specific implementation framework because the technical requirements of the diagnosis approach are dependent on this framework. While implementation aspects were discussed for the identification of suited ML concepts in Section 4.1, hard requirements for an actual real-life implementation were not considered because they are dependent on the actual implementation framework. The availability of memory storage and computational power is different for a remote-implementation on a server or an onboard-implementation within the vehicle. Remote- or onboard-implementation decides upon the amount of data that needs to be transmitted via cellular network. This may, in turn, affect the necessary data processing on an ECU.

The selected SML and RL classifiers, SVM and LOF, are memory intensive [18, p. 10, 114, p. 11]. Their requirements for memory space and computational power for the evaluation of the classifier increase with an increasing size of the training data. The selected DL classifiers, CNN and VAE, have higher requirements regarding the computational power for the training process. However, the requirements regarding memory space and computational power for the evaluation of the classifier remains unchanged with an increasing size of the training data. Competitive CNN network architectures are presented by Zehelein et al. [121, p. 14] and are in the area of 70 000 to 270 000 tuneable parameters with 485k to 3.67M Floating Point Operations (FLOPs).

Another aspect that influences the selection of specific methods for an actual implementation is the availability of labeled data. Altering components to simulate a real-life defect is difficult. In the context of this thesis, the realization of a damper oil leakage was conducted by Faist [294] similar to the process in [2]. However, the mechanical altering of the dampers led to a complete failure of the damper rather than the expected reduced damping performance. Real-life data from fleet vehicles might include vehicles with worn components. However, the health state of the components is mostly unknown. Therefore, labeling this data is difficult.

6.4 Relevance of the Research Objective

This thesis investigated the application of existing Machine Learning (ML) methods to a new technical field. Therefore, the scientific and technical contribution as well as the societal relevance of this thesis are discussed in this section.

Scientific Contribution

The functionality of ML methods is often demonstrated on synthetic datasets only. Real-life data is rarely used for the application of ML methods and the data often results from test bench measurements [28, p. 8, 115, p. 18, 116, p. 12]. This thesis uses real driving data for the investigation of the performance of machine learning methods. Even though the damper faults are imitated, the dataset includes characteristics due to an uncontrolled environment such as wind, road excitation or temperature influence. Moreover, the robustness for unknown patterns in the dataset due to changed vehicle parameters is explicitly analyzed in this thesis. The investigation of internal transformations of ML methods is an open field of research [117, p. 19]. The proposed process of the investigation of features can be used for the derivation of insights for the diagnosis of components with unknown behavior in the defective state. It is also possible to aggregate these insights for the development of suited hand-crafted features. Publications such as [141, 129, 134, 242, 249, 250] suggest new algorithms but compare them only briefly to other approaches for a specific problem. Therefore, holistic investigations of the performance of several ML concepts on a specific domain are rarely available. This thesis analyzes six different ML concepts and compares them with a signal-based approach. Finally, a theoretical analysis of the observability of variations of the damping coefficient based on wheel speed measurements with unknown road excitation does not exist in literature. The observability is analyzed in this thesis.

Technical Contribution

The technical contribution of this thesis is especially important for companies that might implement ML based diagnosis methods. Therefore, the most important fact is that the damper diagnosis using ML methods is possible. Different ML methods that are suited for the diagnosis task are provided in this thesis. A broad overview of general requirements for an implementation is provided by the discussion of the advantages and disadvantages of different ML concepts. Explicit technical requirements regarding memory space or calculation power of the analyzed methods would need to be further investigated.

Societal Relevance

Findings in this thesis may also be relevant for society. Reduced maintenance activities of a vehicle reduces costs. An increased availability of fleet vehicles also reduces costs for shared mobility. Therefore, the general costs for mobility may be decreased by an improved vehicle health monitoring. The continuous monitoring of the chassis system's health state results in an improved guarantee of driving safety. Furthermore, continuously monitoring the chassis system's health state by technical inspection agencies (e.g. the German TÜV) would result in an improved guarantee of driving safety not only for single vehicles but for all road traffic. For this, access to data would have to be granted by an appropriate political regulation.

7 Summary and Outlook

The future of automotive is seen to be electric, autonomous, shared and connected. These trends set new challenges and opportunities on the continuous health state monitoring of the chassis system. Therefore, this thesis deals with the analysis of the suitability of Machine Learning (ML) methods for automotive damper diagnosis. To enable a broad applicability of a new diagnosis system to all vehicles, only Electronic Stability Control (ESC) sensors shall be used without the requirement of any vertical dynamics sensors.

ML-based fault diagnosis concepts for mechanical components of the chassis system are a possible solution that fit the presented trends and circumstances. This ensures driving safety and driving comfort continuously, which is especially important for autonomous, shared vehicles. Driving data from connected vehicles can be used for the training of the fault diagnosis concept. Periodic inspections are replaced by a continuous monitoring of the chassis system's health state. Hereby, less service activities are required for the chassis system. In combination with less maintenance requirements of an electric powertrain, the number of service activities for electric vehicles is reduced. Remote on-board diagnostics and predictive maintenance serves as data-driven business model for expanding the aftermarket activities, e.g. by detecting a fault within the vehicle, noticing the driver and sending him to the workshop.

Damper faults are among the most frequent issues of the chassis system. The investigation of the state of the art revealed that diagnosing damper faults is not a new research subject. However, existing methods are mostly model-based or signal-based. They require vertical acceleration sensors and for this reason they are not applied in series production vehicles. This makes one doubt the robustness of the existing diagnosis applications. ML methods show promising diagnosis performance in many other domains and are said to improve their performance with increasing training data. However, they are not yet used for the monitoring of a vehicle's chassis system.

Existing approaches detect damper faults without measuring the road excitation. However, there is no analysis of the observability of a system with varying damping coefficients under the circumstance of only measuring the wheel speed with unknown road excitation. A theoretical analysis of the observability was performed and theoretical insights were generated. An increasing observation time, an increasing vehicle speed and an increasing road excitation improve the observability of the system and are therefore beneficial for defect detection. Knowledge about these facts can be used to improve the diagnosis performance.

Suitable concepts in the context of damper diagnosis were identified. This thesis analyzed the suitability of supervised and unsupervised learning approaches of Shallow Machine Learning (SML), Representation Learning (RL) and Deep Learning (DL) concepts. While supervised learning approaches enable the detection of a specific fault, unsupervised learning approaches only detect a defective state without information about the specific fault. Supervised learning approaches require labeled training data while unsupervised learning approaches require only data of intact driving. SML uses hand-crafted features. Therefore, a feature set was generated

that consists of various hand-crafted features. Using FFT data points as features was a second SML feature set. RL generates features automatically. Autoencoder and Sparsefilter are two methods that were applied for feature generation. Supervised classification of the resulting feature sets was performed using a Support Vector Machine (SVM), while unsupervised classification was performed using the nearest-neighbor-based Local Outlier Factor (LOF) algorithm. The concept of supervised DL was analyzed using a Convolutional Neural Network (CNN) while unsupervised DL used a Variational Autoencoder (VAE).

Methods for considering the temporal behavior of sequences of consecutive observations of the classifier's estimation were identified. Supervised learning approaches were post-processed using a Hidden Markov Model (HMM) and unsupervised learning approaches were processed by a Linear Dynamical System (LDS).

Approximately 18 hours of driving data were gathered using an upper class vehicle for the evaluation of the algorithms. The ESC sensor signals were logged directly from the vehicle's internal FlexRay communication system. Defective dampers were emulated by altering the behavior of the vehicle's semi-active dampers. A dataset that consists of nearly 13 000 observations with four different health states was generated. The robustness of the algorithms was evaluated by additional datasets that incorporate additional mass in the vehicle's trunk and winter tires instead of summer tires.

Supervised SML approaches showed a competitive performance that is comparable to DL approaches with 91 % accuracy. Using RL approaches did not lead to any benefits compared to SML approaches. DL approaches showed a more robust behavior compared to SML methods for unknown circumstances in the dataset. Considering temporal behavior resulted in more than 99.8 % accuracy for all supervised methods. The importance of the different sensor signals was analyzed as well as the impact of the size of the training data. An analysis of the characteristics of the generated feature sets as well as the transformations of a CNN showed that these methods perform a frequency analysis of the input signals or compare amplitudes at different frequencies. The theoretical insights from the observability analysis regarding vehicle speed and road excitation has been confirmed experimentally.

Future tasks should deal with an actual implementation of a machine learning-based fault detection system. This should include using driving data of actual fleet vehicles. Due to the investigation of relevant sensor signals, an implementation of independent fault detection systems for each wheel may be advantageous. Hereby, unsupervised learning systems could be used and a location of the affected wheel is inherently provided.

This conceptual analysis showed that machine learning methods are suitable for the diagnosis of defective automotive dampers. Transferring these methods to other chassis system components enables the continuous monitoring of the chassis system's health state. Hereby, driving comfort and driving safety can be ensured without the need of human monitoring. This enables a safe operation of fleets of autonomous or shared vehicles.

Machine learning-based health state monitoring of vehicles may not only be used by the automotive industry itself. In the long run, if politics grant access to the driving data of vehicles for technical inspection agencies (e.g. the German TÜV), Periodical Technical Inspection (PTI) becomes unnecessary. This reduces costs while increasing driving safety due to the continuous monitoring of the vehicle's health state.

List of Figures

Figure 1.1:	Automotive trends and opportunities with its impact on damper diagnosis	2
Figure 1.2:	Number of Scopus [21] publications per year that deal with fault detection in the field of engineering	3
Figure 1.3:	Structure of the thesis	4
Figure 2.1:	Categorization of quantitative diagnostic methods	6
Figure 2.2:	General schemes of fault detection methods	7
Figure 2.3:	Damper diagnosis publications from the years 2008 to 2019 with their interconnections	9
Figure 2.4:	Categorization of existing approaches for damper diagnosis	11
Figure 2.5:	Chassis system diagnosis methods over publication time	14
Figure 2.6:	Categorization of Machine Learning, Representation Learning and Deep Learning	16
Figure 2.7:	Illustration of machine learning methods	20
Figure 3.1:	Quarter-vehicle model	26
Figure 3.2:	Dependency of tire radius from vertical force	27
Figure 3.3:	Local estimation condition number, local unobservability index and its upper bound of the stochastic system with an unknown road excitation of a street class C and a vehicle speed $v = 100 \frac{\text{km}}{\text{h}}$	34
Figure 3.4:	Local estimation condition index, local unobservability index and maximum upper bound of the local unobservability index for varying vehicle speed and varying known road class for an observation time of $t = 5 \text{ s}$	34
Figure 4.1:	Assessment of suitable machine learning concepts for damper health state monitoring	39
Figure 4.2:	Matrix of investigated machine learning concepts and structure within this thesis	40
Figure 4.3:	Overall machine learning workflow and structure within this thesis	40
Figure 4.4:	Characteristic curve of a single damper [121, p. 5].....	41
Figure 4.5:	Visualization of an Autoencoder	44
Figure 4.6:	Visualization of a Convolutional Neural Network (CNN)	52
Figure 4.7:	Visualization of the network architecture of a Variational Autoencoder (VAE)	54
Figure 4.8:	ROC curve and AUC	58
Figure 5.1:	Fisher score of individual features of the most important manual feature generation methods	67
Figure 5.2:	Fisher score and mean FFT of sensor signals for each damper health state	69
Figure 5.3:	FFT feature importance for classification as mean inverse rank of RFE feature ranking	70
Figure 5.4:	Autoencoder weights of one kernel and mean FFT of each health state as input data for wheel speed FL	71
Figure 5.5:	Importance index of input data frequency for Autoencoder	71

Figure 5.6:	Analysis of Sparsefilter weights	72
Figure 5.7:	Analysis of importance of input data frequency shares for Sparsefilter	73
Figure 5.8:	Mean accuracy on the test data of a 5-fold cross-validation using a SVM classifier for feature subsets consisting of different numbers of features, selected using a RFE approach.....	74
Figure 5.9:	Mean AUC on the test data of a 5-fold cross-validation using a LOF novelty detection classifier for feature subsets consisting of different numbers of features, selected using a RFE approach	75
Figure 5.10:	Mean accuracy on the test data of a 5-fold cross-validation for the investigation of the CNN network architecture using detrended time signals or FFT of detrended time signals as input data	76
Figure 5.11:	Kernel weights of the convolutional layer of different network architectures from Zehelein et al. [121, p. 11]	77
Figure 5.12:	AUC on validation data of layer configuration optimization of VAE	78
Figure 5.13:	Classification accuracy of supervised learning methods that are trained on training data and applied to the test, mass and tire datasets	79
Figure 5.14:	Classification performance of unsupervised and supervised learning methods that are trained on training data and applied to the test, mass and tire datasets	80
Figure 5.15:	AUC of unsupervised learning methods that are trained on training data with incorporated tire data and applied to the test, mass and tire datasets	81
Figure 5.16:	Visualization of predicted probabilities using HMM and SVM with manual features on tire data	83
Figure 5.17:	Classification accuracy of supervised learning methods that are trained on training data and applied to the test, mass and tire datasets with additional HMM post-processing of the apriori classifier predictions.....	84
Figure 5.18:	Post-Processing of Unsupervised Learning using Linear Dynamical Systems	85
Figure 5.19:	Performance of supervised and unsupervised learning methods on the test dataset for feature subsets of a reduced number of sensor signals	86
Figure 5.20:	Performance of supervised and unsupervised learning methods on the test dataset using a reduced size of the training dataset	88
Figure 5.21:	Relative shares of the estimated probabilities of the true class for the supervised SML approach using manual features	90
Figure 5.22:	Correlation of estimated true class probability with vehicle speed and IRI for each probability share in Figure 5.21	90
Figure 5.23:	PSD of wheel speed Front Left (FL) for the different damper health states with exemplary evaluation and reference frequency range.....	91
Figure 5.24:	Comparison of the damper defect detection performance of the signal-based approach with that of the unsupervised and supervised learning methods that are trained on training data and applied to the test, mass and tire datasets	92
Figure A.1:	Estimation condition number, unobservability index and maximum upper bound of the stochastic system with unknown road excitation and unknown road class for a vehicle speed $v = 100 \frac{\text{km}}{\text{h}}$ and a simulated class C road.....	xli

Figure A.2:	Visualization of local estimation condition index, local unobservability index and maximum upper bound of the local unobservability index for varying vehicle speed and varying unknown road class for an observation time of $t = 5\text{ s}$	xli
Figure C.1:	Distribution of vehicle health class for all datasets	xlvi
Figure C.2:	Geographic map of the full dataset (combined training and testing data) ..	xlvi
Figure C.3:	Geographic map of the mass dataset	xlvi
Figure C.4:	Geographic map of the tire dataset	xlvii
Figure C.5:	Distribution of the mean vehicle speed of an observation for different datasets	xlvii
Figure C.6:	Distribution of the mean longitudinal acceleration of an observation for different datasets	xlviii
Figure C.7:	Distribution of the mean lateral acceleration of an observation for different datasets	xlviii
Figure C.8:	Distribution of the International Roughness Index (IRI) of the observations of different datasets. See Section 5.8 for a description of the IRI. Information of the IRI was not available for all observations. Therefore the accumulated amount of observations within each graph is less than the number of observations within the corresponding dataset.	xlx
Figure C.9:	Analysis of importance of input data frequency shares for the feature generation using Autoencoder.....	li
Figure C.10:	Analysis of importance of input data frequency shares for the feature generation using Sparsefilter	lii
Figure C.11:	Distribution of observations for training and testing data for the analysis of the influence of the vehicle speed and IRI on the estimation performance	liii
Figure C.12:	Accuracy and AUC for each testing data bin of Figure C.11	liii
Figure C.13:	Binned median of the DSKW over vehicle speed for the training data for each wheel for an intact and defective health state of the corresponding damper.....	liv
Figure C.14:	ROC curve and AUC values of the wheel-individual approach of Jautze [17] including the optimized evaluation and reference frequencies and speed-correction for the three datasets of this thesis.....	lv

List of Tables

Table 2.1:	Main findings of eleven publications that review ML methods for fault diagnosis	17
Table 2.2:	Strengths and Limitations of Machine Learning methods for fault diagnosis applications	19
Table 2.3:	Fulfillment of derived requirements for different diagnosis approaches.....	23
Table 4.1:	Confusion Matrix	57
Table 5.1:	Ranking of the ten most important manual feature generation methods	66
Table 5.2:	Importance ranking of the sensor signals for supervised learning methods..	87
Table 5.3:	Importance ranking of the sensor signals for unsupervised learning methods	87
Table A.1:	Parameters for numeric investigation of observability in Section 3.5 and Section 3.6	xi
Table B.1:	Summary of manual features for SML classification.....	xliii
Table C.1:	Selected evaluation and reference frequency for the signal-based approach of Jautze [17] for each wheel	liv

Bibliography

- [1] B. Heiing and M. Ersoy, *Chassis Handbook: Fundamentals, Driving Dynamics, Components, Mechatronics, Perspectives*, 1. Aufl., s.l., Vieweg+Teubner (GWV), 2011, ISBN: 978-3-8348-0994-0. Available: <http://gbv.ebib.com/patron/FullRecord.aspx?p=749083>.
- [2] S. Guba et al., „The Impact of Worn Shocks on Vehicle Handling and Stability,“ in *SAE Technical Paper Series*, 2006, DOI: 10.4271/2006-01-0563.
- [3] M. D. Bedk et al., „Effects of damper failure on vehicle stability,“ *Proceedings of the Institution of Mechanical Engineers, Part D: Journal of Automobile Engineering*, vol. 227, no. 7, pp. 1024–1039, 2012, DOI: 10.1177/0954407012465242.
- [4] TV Sd. „Die hufigsten Mngel beim Auto,“ 2020. [Online]. Available: <https://www.tuvsud.com/de-de/publikationen/tuev-report/die-haeufigsten-maengel> [accessed 05/13/2020].
- [5] „. Mercedes-Benz and smart present the future,“ Press Release. Stuttgart, 5.01.2017. Available: https://media.daimler.com/marsMediaSite/instance/ko.xhtml?oid=15178558&resultInfoTypeld=175&rellid=1001&ls=L3NIYXJjaHJlc3VsdC9zZWFFyY2hyZXN1bHQeGh0bWw_c2VhcmNoU3RyaW5nPUNBU0Umc2VhcmNoSWQ9MCZzZWFFyY2hUeXBIPWRldGFpbGVkbnJlc3VsdEluZm9UeXBISWQ9NDA2MjYmYm9yZGVVycz10cnVlJnRodW1iU2NhbGVJbmRleD0wJnJvd0NvdW50c0luZGV4PTUmdmllld1R5cGU9bGlzdCZzb3J0RGVmaW5pdGlvbj1QVUJMSVNIRURfQVQtMg!!#toRelation [accessed 05/13/2020].
- [6] A. Cornet et al. „RACE 2050 – a vision for the European automotive industry,“ 2020. [Online]. Available: <https://www.mckinsey.com/~media/mckinsey/industries/automotive%20and%20assembly/our%20insights/a%20long%20term%20vision%20for%20the%20european%20automotive%20industry/race-2050-a-vision-for-the-european-automotive-industry.ashx> [accessed 05/13/2020].
- [7] F. Kuhnert et al. „Five trends transforming the Automotive Industry,“ 2020. [Online]. Available: <https://www.pwc.com/gx/en/industries/automotive/assets/pwc-five-trends-transforming-the-automotive-industry.pdf> [accessed 05/12/2020].
- [8] B. Propfe et al., „Cost analysis of Plug-in Hybrid Electric Vehicles including Maintenance & Repair Costs and Resale Values,“ *World Electric Vehicle Journal*, vol. 5, no. 4, pp. 886–895, 2012, DOI: 10.3390/wevj5040886.
- [9] K. Heinke et al. „Development in the mobility technology ecosystem—how can 5G help?,“ 2020. [Online]. Available: <https://www.mckinsey.com/~media/McKinsey/Industries/Automotive%20and%20Assembly/Our%20Insights/Development%20in%20the%20mobility%20technology%20ecosystem%20how%20can%205G%20help/Development-in-the-mobility-technology-ecosystem-how-can-5G-help.ashx> [accessed 05/13/2020].

- [10] G. Seiberth and W. Gruendinger. „Data-driven Business Models in Connected Cars, Mobility Services and Beyond,“ 2020. [Online]. Available: https://www.bvdw.org/fileadmin/user_upload/20180509_bvdw_accenture_studie_datadrivenbusinessmodels.pdf [accessed 05/05/2020].
- [11] M. Milojevic and F. Nassah, „Digital Industrial Revolution with Predictive Maintenance,“ *Are European Businesses Ready to Streamline Their Operations and Reach Higher Levels of Efficiency*, 2018. Available: https://www.ge.com/digital/sites/default/files/download_assets/PAC_Predictive_Maintenance_GE_Digital_Executive_Summary_2018_1.pdf [accessed 04/30/2020].
- [12] M. Bertoncello et al. „Monetizing car data: New service business opportunities to create new customer benefits,“ 2020. [Online]. Available: <https://www.mckinsey.com/~media/McKinsey/Industries/Automotive%20and%20Assembly/Our%20Insights/Monetizing%20car%20data/Monetizing-car-data.ashx> [accessed 05/12/2020].
- [13] D. Breitschwerdt et al. „The changing aftermarket game – and how automotive suppliers can benefit from arising opportunities,“ 2020. [Online]. Available: <https://www.mckinsey.com/~media/McKinsey/Industries/Automotive%20and%20Assembly/Our%20Insights/The%20changing%20aftermarket%20game%20and%20how%20automotive%20suppliers%20can%20benefit%20from%20arising%20opportunities/The-changing-aftermarket-game.ashx> [accessed 05/05/2020].
- [14] M. M. Morato et al., „Fault estimation for automotive Electro-Rheological dampers: LPV-based observer approach,“ *Control Engineering Practice*, vol. 85, pp. 11–22, 2019, DOI: 10.1016/j.conengprac.2019.01.005.
- [15] D. H. Alcantara et al., „Fault diagnosis for an automotive suspension using particle filters,“ in *2016 European Control Conference (ECC): June 29–July 1, 2016, Aalborg, Denmark*, Aalborg, Denmark, 2016, pp. 1898–1903, ISBN: 978-1-5090-2591-6. DOI: 10.1109/ECC.2016.7810568.
- [16] D. Hernández-Alcántara et al., „Modeling, diagnosis and estimation of actuator faults in vehicle suspensions,“ *Control Engineering Practice*, vol. 49, pp. 173–186, 2016, DOI: 10.1016/j.conengprac.2015.12.002.
- [17] M. Jautze, *Ein signalmodellbasiertes Verfahren zum Erkennen von Dämpferschäden bei Kraftfahrzeugen*, (Fortschritt-Berichte VDI Reihe 12, Verkehrstechnik/Fahrzeugtechnik). vol. 498, Als Ms. gedr, Düsseldorf, VDI-Verl., 2002, ISBN: 978-3-18-349812-3.
- [18] S. Khan and T. Yairi, „A review on the application of deep learning in system health management,“ *Mechanical Systems and Signal Processing*, vol. 107, pp. 241–265, 2018, DOI: 10.1016/j.ymssp.2017.11.024.
- [19] Y. LeCun et al., „Deep learning,“ *Nature*, vol. 521, no. 7553, pp. 436–444, 2015, DOI: 10.1038/nature14539.
- [20] R. Zhao et al., „Deep learning and its applications to machine health monitoring,“ *Mechanical Systems and Signal Processing*, vol. 115, pp. 213–237, 2019, DOI: 10.1016/j.ymssp.2018.05.050.
- [21] „Scopus,“ 2020. [Online]. Available: <https://www.scopus.com> [accessed 04/28/2020].
- [22] A. R. Mohanty, *Machinery Condition Monitoring*, CRC Press, 2014, ISBN: 9781351228626. DOI: 10.1201/9781351228626.

- [23] E. Lughofer and M. Sayed-Mouchaweh, *Predictive Maintenance in Dynamic Systems: Advanced Methods, Decision Support Tools and Real-World Applications*, Cham, Springer International Publishing, 2019, ISBN: 978-3-030-05645-2. DOI: 10.1007/978-3-030-05645-2.
- [24] R. Isermann and P. Ballé, „Trends in the application of model-based fault detection and diagnosis of technical processes,“ *Control Engineering Practice*, vol. 5, no. 5, pp. 709–719, 1997, DOI: 10.1016/S0967-0661(97)00053-1.
- [25] V. Palade et al., *Computational Intelligence in Fault Diagnosis*, (Advanced Information and Knowledge Processing), London, Springer-Verlag London Limited, 2006, ISBN: 978-1-84628-343-7. DOI: 10.1007/978-1-84628-631-5. Available: <http://site.ebrary.com/lib/alltitles/docDetail.action?docID=10157630>.
- [26] R. Isermann, „Supervision, fault-detection and fault-diagnosis methods — An introduction,“ *Control Engineering Practice*, vol. 5, no. 5, pp. 639–652, 1997, DOI: 10.1016/S0967-0661(97)00046-4.
- [27] A. Varga, *Solving fault diagnosis problems: Linear synthesis techniques*, (Studies in systems, decision and control). vol. volume 84, Cham, Springer, 2017, ISBN: 9783319515595.
- [28] S. R. Saufi et al., „Challenges and Opportunities of Deep Learning Models for Machinery Fault Detection and Diagnosis: A Review,“ *IEEE Access*, vol. 7, pp. 122644–122662, 2019, DOI: 10.1109/ACCESS.2019.2938227.
- [29] V. Venkatasubramanian et al., „A review of process fault detection and diagnosis Part III: Process history based methods,“ *Computers & Chemical Engineering*, vol. 27, no. 3, pp. 327–346, 2003, DOI: 10.1016/S0098-1354(02)00162-X.
- [30] V. Venkatasubramanian et al., „A review of process fault detection and diagnosis Part I: Quantitative model-based methods,“ *Computers & Chemical Engineering*, vol. 27, no. 3, pp. 293–311, 2003, DOI: 10.1016/S0098-1354(02)00160-6.
- [31] Z. Gao et al., „A Survey of Fault Diagnosis and Fault-Tolerant Techniques—Part I: Fault Diagnosis With Model-Based and Signal-Based Approaches,“ *IEEE Transactions on Industrial Electronics*, vol. 62, no. 6, pp. 3757–3767, 2015, DOI: 10.1109/TIE.2015.2417501.
- [32] Z. Gao et al., „A Survey of Fault Diagnosis and Fault-Tolerant Techniques Part II: Fault Diagnosis with Knowledge-Based and Hybrid/Active Approaches,“ *IEEE Transactions on Industrial Electronics*, pp. 3768–3774, 2015, DOI: 10.1109/TIE.2015.2419013.
- [33] J. C. Tudon-Martinez et al., „Parameter-Dependent H_∞ Filter for LPV Semi-Active Suspension Systems,“ *IFAC-PapersOnLine*, vol. 51, no. 26, pp. 19–24, 2018, DOI: 10.1016/j.ifacol.2018.11.174.
- [34] A. E. Vela et al., „H-infinity Observer for Damper Force in a Semi-Active Suspension,“ *IFAC-PapersOnLine*, vol. 51, no. 11, pp. 764–769, 2018, DOI: 10.1016/j.ifacol.2018.08.411.
- [35] T.-P. Pham et al., „Comparative study of three robust observers for automotive damper force estimation,“ *IOP Conference Series: Materials Science and Engineering*, vol. 707, p. 012014, 2019, DOI: 10.1088/1757-899X/707/1/012014.
- [36] T.-P. Pham et al., „Unified H-infinity Observer for a Class of Nonlinear Lipschitz Systems: Application to a Real ER Automotive Suspension,“ *IEEE Control Systems Letters*, vol. 3, no. 4, pp. 817–822, 2019, DOI: 10.1109/LCSYS.2019.2919813.

- [37] T.-P. Pham et al., „Real-time Damper Force Estimation of Vehicle Electrorheological Suspension: A NonLinear Parameter Varying Approach,“ *IFAC-PapersOnLine*, vol. 52, no. 28, pp. 94–99, 2019, DOI: 10.1016/j.ifacol.2019.12.354.
- [38] T.-P. Pham et al., „LPV Force Observer Design and Experimental Validation from a Dynamical Semi-Active ER Damper Model,“ *IFAC-PapersOnLine*, vol. 52, no. 17, pp. 60–65, 2019, DOI: 10.1016/j.ifacol.2019.11.027.
- [39] A. Beckerman et al., „A New Estimation Concept for Automotive Suspensions * *Research supported by the Hyundai Center of Excellence in Vehicle Dynamic Systems & Control,“ *IFAC-PapersOnLine*, vol. 50, no. 1, pp. 15622–15626, 2017, DOI: 10.1016/j.ifacol.2017.08.1898.
- [40] G. Koch et al., „Nonlinear and filter based estimation for vehicle suspension control,“ in *2010 49th IEEE Conference on Decision and Control: (CDC) ; 15 - 17 Dec. 2010*, Atlanta, GA, USA, 2010, pp. 5592–5597, ISBN: 978-1-4244-7745-6. DOI: 10.1109/CDC.2010.5718052.
- [41] G. Malmedahl et al., „Analysis of Automotive Damper Data and Design of a Portable Measurement System,“ in *SAE Technical Paper Series*, 2005, DOI: 10.4271/2005-01-1043.
- [42] L. Ferrari et al., „A simple measuring system for automotive damper wear estimation,“ in *IEEE International Instrumentation and Measurement Technology Conference (I2MTC), 2012: 13 - 16 May 2012, Congress Graz, Graz, Austria ; proceedings*, Graz, Austria, 2012, pp. 539–543, ISBN: 978-1-4577-1772-7. DOI: 10.1109/I2MTC.2012.6229266.
- [43] J. Bußhardt et al., „Ein elektronisches System zur parameteradaptiven Regelung und Diagnose von Kraftfahrzeugstoßdämpfern,“ in *Elektronik im Kraftfahrzeug: Tagung Baden-Baden, 10. und 11. September 1992 = Electronic systems for vehicles (VDI-Berichte)*. vol. 1009 Düsseldorf: VDI-Verl., 1992, pp. 199–216, ISBN: 3180910097.
- [44] J. Bußhardt and R. Isermann, „Verfahren zur Regelung der Dämpfung und/oder zur Diagnose des Fahrwerks eines Kraftfahrzeugs,“ Patent DE4218087A1.
- [45] S. Leonhardt et al., „Parameter Estimation of Shock Absorbers with Artificial Neural Networks,“ in *American Control Conference, 1993*, San Francisco, CA, USA, 1993, pp. 716–720, ISBN: 0-7803-0860-3. DOI: 10.23919/ACC.1993.4792953.
- [46] T. Weispfenning, „Fault Detection and Diagnosis of Components of the Vehicle Vertical Dynamics,“ *Meccanica*, vol. 32, no. 5, pp. 459–472, 1997, DOI: 10.1023/A:1004212001768.
- [47] G. Hardier, „Recurrent RBF networks for suspension system modeling and wear diagnosis of a damper,“ in *1998 IEEE International Joint Conference on Neural Networks Proceedings*, Anchorage, AK, USA, 1998, pp. 2441–2446, DOI: 10.1109/IJCNN.1998.687245.
- [48] M. Börner et al., „Model based fault detection of vehicle suspension and hydraulic brake systems,“ *Mechatronics*, vol. 12, no. 8, pp. 999–1010, 2002, DOI: 10.1016/S0957-4158(02)00008-9.
- [49] S. Azadi and A. Soltani, „Fault Detection for Passive Suspension Systems Using Wavelet Transform,“ in *SAE Technical Paper Series*, 2007, DOI: 10.4271/2007-01-2368.
- [50] S. Azadi and A. Soltani, „Fault detection of vehicle suspension system using wavelet analysis,“ *Vehicle System Dynamics*, vol. 47, no. 4, pp. 403–418, 2009, DOI: 10.1080/00423110802094298.

- [51] P. Metallidis et al., „Parametric Identification and Health Monitoring of Complex Ground Vehicle Models,“ *Journal of Vibration and Control*, vol. 14, no. 7, pp. 1021–1036, 2008, DOI: 10.1177/1077546307085823.
- [52] P. Metallidis et al., „Fault Detection and Optimal Sensor Location in Vehicle Suspensions,“ *Journal of Vibration and Control*, vol. 9, no. 3-4, pp. 337–359, 2003, DOI: 10.1177/107754603030755.
- [53] P. Ventura et al., „An embedded system to assess the automotive shock absorber condition under vehicle operation,“ in *IEEE sensors, 2008: 26 - 29 Oct. 2008, Lecce, Italy ; the Seventh IEEE Conference on Sensors*, Varna, Bulgaria, 2008, pp. 1210–1213, ISBN: 978-1-4244-2580-8. DOI: 10.1109/ICSENS.2008.4716660.
- [54] C. Ferreira et al., „Sensing methodologies to determine automotive damper condition under vehicle normal operation,“ *Sensors and Actuators A: Physical*, vol. 156, no. 1, pp. 237–244, 2009, DOI: 10.1016/j.sna.2009.03.035.
- [55] Y.-m. Liu et al., „Suspension system fault diagnosis method based on fuzzy mathematics,“ in *9th International Conference on Electronic Measurement & Instruments, 2009: ICEMI '09 ; 16 - 19 Aug. 2009, Beijing, China ; proceedings*, Beijing, China, 2009, pp. 210–214, ISBN: 978-1-4244-3863-1. DOI: 10.1109/ICEMI.2009.5274890.
- [56] J. d. J. Lozoya-Santos et al., „A Fault Detection Method for an Automotive Magneto-Rheological Damper,“ *IFAC Proceedings Volumes*, vol. 45, no. 20, pp. 1209–1214, 2012, DOI: 10.3182/20120829-3-MX-2028.00292.
- [57] J. Lozoya-Santos et al., „Fault Detection for an Automotive MR Damper,“ *IFAC Proceedings Volumes*, vol. 45, no. 6, pp. 1023–1028, 2012, DOI: 10.3182/20120523-3-RO-2023.00247.
- [58] D. Hernandez-Alcantara et al., „Fault detection for automotive semi-active dampers,“ in *2013 Conference on Control and Fault-Tolerant Systems (SysTol)*, 2013, pp. 625–630, DOI: 10.1109/SysTol.2013.6693916.
- [59] J. C. Tudon-Martinez et al., „Fault tolerant control with additive compensation for faults in an automotive damper,“ in *10th IEEE International Conference on Networking, Sensing and Control (ICNSC), 2013: 10 - 12 April 2013, Evry Val-d'Essonne University, Evry*, 2013, pp. 810–814, ISBN: 978-1-4673-5200-0. DOI: 10.1109/ICNSC.2013.6548842.
- [60] S. Varrier et al., „Fault Detection in Automotive Semi-Active Suspension: Experimental Results,“ in *SAE Technical Paper Series*, Nice, France, 2013, DOI: 10.4271/2013-01-1234.
- [61] J. C. Tudón-Martínez and R. Morales-Menendez, „Adaptive Vibration Control System for MR Damper Faults,“ *Shock and Vibration*, vol. 2015, pp. 1–17, 2015, DOI: 10.1155/2015/163694.
- [62] M. Hamed, „Characterisation of the Dynamics of an Automotive Suspension System for On-line Condition Monitoring,“ Doctoral Thesis, University of Huddersfield, 2016. Available: <http://eprints.hud.ac.uk/id/eprint/29088/>.
- [63] M. Q. Nguyen et al., „Comparison of observer approaches for actuator fault estimation in semi-active suspension systems,“ in *2016 3rd Conference on Control and Fault-Tolerant Systems (SysTol): Conference proceedings : September 7-9, 2016, Faculty of Mathematics (UPC), Barcelona, Spain*, Barcelona, Spain, 2016, pp. 227–232, ISBN: 978-1-5090-0658-8. DOI: 10.1109/SYSTOL.2016.7739755.

- [64] M. M. Morato et al., „LPV-MPC Fault Tolerant Control of Automotive Suspension Dampers,“ *IFAC-PapersOnLine*, vol. 51, no. 26, pp. 31–36, 2018, DOI: 10.1016/j.ifacol.2018.11.172.
- [65] D. Savaresi et al., „On-line Damping Estimation in Road Vehicle Semi-active Suspension Systems,“ *IFAC-PapersOnLine*, vol. 52, no. 5, pp. 679–684, 2019, DOI: 10.1016/j.ifacol.2019.09.108.
- [66] M. Shahab and M. Moavenian, „A novel fault diagnosis technique based on model and computational intelligence applied to vehicle active suspension systems,“ *International Journal of Numerical Modelling: Electronic Networks, Devices and Fields*, vol. 32, no. 3, e2541, 2019, DOI: 10.1002/jnm.2541.
- [67] O. Sename et al., „The INOVE ANR 2010 Blan 0308 project: Integrated approach for observation and control of vehicle dynamics,“ in *2014 European Control Conference (ECC 2014): Strasbourg, France, 24 - 27 June 2014*, Strasbourg, France, 2014, pp. 2340–2345, ISBN: 978-3-9524269-1-3. DOI: 10.1109/ECC.2014.6862364.
- [68] International Organization for Standardization. „*Mechanical vibration - Road surface profiles - Reporting of measurement data*,“ ISO. Sept. 1, 1995.
- [69] S. Varrier et al., „Applicative Fault Tolerant Control for semi-active suspension system: Preliminary results,“ in *European Control Conference (ECC), 2013: 17 - 19 July 2013, ETH Zurich, Zurich, Switzerland*, Zurich, 2013, pp. 3803–3808, ISBN: 978-3-033-03962-9. DOI: 10.23919/ECC.2013.6669822.
- [70] D. Hernandez-Alcantara et al., „State observers for semi-active suspensions: Experimental results,“ in *IEEE Conference on Control Applications (CCA), 2014: 8 - 10 Oct. 2014, Antibes, France ; part of 2014 IEEE Multi-Conference on Systems and Control*, Juan Les Antibes, France, 2014, pp. 53–58, ISBN: 978-1-4799-7409-2. DOI: 10.1109/CCA.2014.6981328.
- [71] Marble, Robert P., Warren, Mich., US and Moore, „Bestimmung des Gesundheitszustands des Dämpfers mittels indirekter Messungen,“ Patent DE 10 2018 117 680 A1 2019.01.24.
- [72] G. Wang and S. Yin, „Data-driven fault diagnosis for an automobile suspension system by using a clustering based method,“ *Journal of the Franklin Institute*, vol. 351, no. 6, pp. 3231–3244, 2014, DOI: 10.1016/j.jfranklin.2014.03.004.
- [73] K. P. Detroja et al., „A possibilistic clustering approach to novel fault detection and isolation,“ *Journal of Process Control*, vol. 16, no. 10, pp. 1055–1073, 2006, DOI: 10.1016/j.jprocont.2006.07.001.
- [74] S. Yin and Z. Huang, „Performance Monitoring for Vehicle Suspension System via Fuzzy Positivistic C-Means Clustering Based on Accelerometer Measurements,“ *IEEE/ASME Transactions on Mechatronics*, vol. 20, no. 5, pp. 2613–2620, 2015, DOI: 10.1109/TMECH.2014.2358674.
- [75] C. Gangkofer, „Umsetzung von Fahrwerkdefekten mit fahrdynamischen Messungen und Potentialanalyse für ein Fahrwerkdiagnoseverfahren: Implementation of chassis defects with vehicle dynamics tests an potential analysis of a chassis defects diagnostic method,“ Semester’s Thesis, Technical University of Munich, Munich, 2018.
- [76] P. Pisu et al., „Vehicle chassis monitoring system,“ *Control Engineering Practice*, vol. 11, no. 3, pp. 345–354, 2003, DOI: 10.1016/S0967-0661(02)00073-4.

- [77] R. Jegadeeshwaran and V. Sugumaran, „Comparative study of decision tree classifier and best first tree classifier for fault diagnosis of automobile hydraulic brake system using statistical features,” *Measurement*, vol. 46, no. 9, pp. 3247–3260, 2013, DOI: 10.1016/j.measurement.2013.04.068.
- [78] A. Mangai. M., „Vibration based Condition Monitoring of a Brake System using Statistical Features with Logit Boost and Simple Logistic Algorithm,” *International Journal of Performability Engineering*, 2018, DOI: 10.23940/ijpe.18.01.p1.18.
- [79] R. Jegadeeshwaran and V. Sugumaran, „Fault diagnosis of automobile hydraulic brake system using statistical features and support vector machines,” *Mechanical Systems and Signal Processing*, vol. 52-53, pp. 436–446, 2015, DOI: 10.1016/j.ymsp.2014.08.007.
- [80] V. Indira et al., „Determination of minimum sample size for fault diagnosis of automobile hydraulic brake system using power analysis,” *Engineering Science and Technology, an International Journal*, vol. 18, no. 1, pp. 59–69, 2015, DOI: 10.1016/j.jestch.2014.09.007.
- [81] M. L. Schwall et al., „Multi-modal diagnostics for vehicle fault detection,” *American Society of Mechanical Engineers, Dynamic Systems and Control Division (Publication) DSC*, vol. 70, 2002. Available: <https://www.scopus.com/inward/record.uri?eid=2-s2.0-0242467606&partnerID=40&md5=6a12e744c7d2477ec49ce563014db1c9>.
- [82] M. L. Schwall and J. C. Gerdes, „A probabilistic approach to residual processing for vehicle fault detection,” in *Proceedings of 2002 American Control Conference*, Anchorage, AK, USA, 2002, 2552–2557 vol.3, DOI: 10.1109/ACC.2002.1024028.
- [83] M. L. Schwall and J. C. Gerdes. „*A Probabilistic Vehicle Diagnostic System Using Multiple Models*,” 2003.
- [84] M. Börner and R. Isermann, „Supervision, fault detection, and sensor fault tolerance of passenger cars,” *IFAC Proceedings Volumes*, vol. 36, no. 5, pp. 319–326, 2003, DOI: 10.1016/S1474-6670(17)36511-4.
- [85] D. Fischer et al., „Model based Fault Detection for an Active Vehicle Suspension,” *IFAC Proceedings Volumes*, vol. 37, no. 22, pp. 403–408, 2004, DOI: 10.1016/S1474-6670(17)30377-4.
- [86] D. Fischer et al., „Fault detection for lateral and vertical vehicle dynamics,” *Control Engineering Practice*, vol. 15, no. 3, pp. 315–324, 2007, DOI: 10.1016/j.conengprac.2006.05.007.
- [87] I. Unger and R. Isermann, „Sensor fault diagnosis for lateral vehicle dynamics with varying road surface conditions,” *IFAC Proceedings Volumes*, vol. 39, no. 16, pp. 502–507, 2006, DOI: 10.3182/20060912-3-DE-2911.00088.
- [88] J. P. N. González et al., „Fault Diagnosis of a Vehicle with Soft Computing Methods,” in *MICAI 2008: advances in artificial intelligence: 7th Mexican International Conference on Artificial Intelligence, Atizapán de Zaragoza, Mexico, October 27 - 31, 2008 ; proceedings* (Lecture notes in computer science Lecture notes in artificial intelligence). vol. 5317, A. Gelbukh and E. F. Morales, ed. Berlin: Springer, 2008, pp. 492–502, ISBN: 978-3-540-88635-8. DOI: 10.1007/978-3-540-88636-5_47.
- [89] J. P. N. González and P. P. Villanueva, „Vehicle Lateral Dynamics Fault Diagnosis Using an Autoassociative Neural Network and a Fuzzy System,” in *Advances in Computational Intelligence* (Lecture Notes in Computer Science). vol. 7630, D. Hutchison et al., ed. Berlin, Heidelberg: Springer Berlin Heidelberg, 2013, pp. 236–246, ISBN: 978-3-642-37797-6. DOI: 10.1007/978-3-642-37798-3_21.

- [90] J. P. N. González et al., „Vehicle Fault Detection and Diagnosis combining AANN and ANFI,“ *IFAC Proceedings Volumes*, vol. 42, no. 8, pp. 1079–1084, 2009, DOI: 10.3182/20090630-4-ES-2003.00178.
- [91] J. P. N. González, „Vehicle fault detection and diagnosis combining an AANN and multiclass SVM,“ *International Journal on Interactive Design and Manufacturing (IJIDeM)*, vol. 12, no. 1, pp. 273–279, 2018, DOI: 10.1007/s12008-017-0378-z.
- [92] X. Zhang and P. Pisu, „Model-based fault diagnosis for a vehicle chassis system,“ in *2009 American Control Conference*, 2009, pp. 1116–1121, DOI: 10.1109/ACC.2009.5159966.
- [93] L. Haffner et al., „Enhanced Method for Fault Detection and Diagnosis of Vehicle Sensors using Parity Equations,“ in *SAE Technical Paper Series*, St. Louis, MO, USA, 2009, DOI: 10.4271/2009-01-0444.
- [94] J. Kim and H. Lee, „Sensor fault detection and isolation algorithm for a continuous damping control system,“ *Proceedings of the Institution of Mechanical Engineers, Part D: Journal of Automobile Engineering*, vol. 225, no. 10, pp. 1347–1364, 2011, DOI: 10.1177/0954407011404493.
- [95] S. Varrier et al., „A Parity Space-Based Fault Detection On LPV Systems : Approach For Vehicle Lateral Dynamics Control System,“ *IFAC Proceedings Volumes*, vol. 45, no. 20, pp. 1191–1196, 2012, DOI: 10.3182/20120829-3-MX-2028.00053.
- [96] E. Chow and A. Willsky, „Analytical redundancy and the design of robust failure detection systems,“ *IEEE Transactions on Automatic Control*, vol. 29, no. 7, pp. 603–614, 1984, DOI: 10.1109/TAC.1984.1103593.
- [97] S. Varrier et al., „Robust fault detection for Uncertain Unknown Inputs LPV system,“ *Control Engineering Practice*, vol. 22, pp. 125–134, 2014, DOI: 10.1016/j.conengprac.2013.10.002.
- [98] S. Varrier et al., „Robust fault detection for vehicle lateral dynamics,“ in *IEEE 51st Annual Conference on Decision and Control (CDC), 2012: 10 - 13 Dec. 2012, Grand Wailea Waldorf Astoria Resort, Maui, Hawaii*, Maui, HI, USA, 2012, pp. 4366–4371, ISBN: 978-1-4673-2066-5. DOI: 10.1109/CDC.2012.6426809.
- [99] Y. Jeong et al., „Vehicle sensor and actuator fault detection algorithm for automated vehicles,“ in *2015 IEEE Intelligent Vehicles Symposium (IV): June 28, 2015 - July 1, 2015, COEX, Seoul, Korea*, Seoul, South Korea, 2015, pp. 927–932, ISBN: 978-1-4673-7266-4. DOI: 10.1109/IVS.2015.7225803.
- [100] Y. Lin et al., „Model-Based Sensor Fault Detection for Advanced Driver Assistance System,“ 2017, DOI: 10.4271/2017-01-1727.
- [101] W. Na et al., „Sensitivity-Based Fault Detection and Isolation Algorithm for Road Vehicle Chassis Sensors,“ *Sensors (Basel, Switzerland)*, vol. 18, no. 8, 2018, DOI: 10.3390/s18082720.
- [102] K. Jeong and S. Choi, „Model-based Sensor Fault Diagnosis of Vehicle Suspensions with a Support Vector Machine,“ *International Journal of Automotive Technology*, vol. 20, no. 5, pp. 961–970, 2019, DOI: 10.1007/s12239-019-0090-z.
- [103] I. Goodfellow et al., *Deep learning*, (Adaptive computation and machine learning), Cambridge, Massachusetts and London, England, The MIT Press, 2016, ISBN: 9780262035613.
- [104] C. M. Bishop, *Pattern recognition and machine learning*, (Information science and statistics), Corrected at 8th printing 2009, New York, NY, Springer, 2009, ISBN: 978-0387-31073-2.

- [105] M. M. Moya and D. R. Hush, „Network constraints and multi-objective optimization for one-class classification,” *Neural Networks*, vol. 9, no. 3, pp. 463–474, 1996, DOI: 10.1016/0893-6080(95)00120-4.
- [106] Y. Bengio et al., „Representation learning: a review and new perspectives,” *IEEE transactions on pattern analysis and machine intelligence*, vol. 35, no. 8, pp. 1798–1828, 2013, DOI: 10.1109/TPAMI.2013.50.
- [107] G. Zhong et al., „From shallow feature learning to deep learning: Benefits from the width and depth of deep architectures,” *WIREs Data Mining and Knowledge Discovery*, vol. 9, no. 1, 2019, DOI: 10.1002/widm.1255.
- [108] S. Chauhan et al., „A Comparison of Shallow and Deep Learning Methods for Predicting Cognitive Performance of Stroke Patients From MRI Lesion Images,” *Frontiers in neuroinformatics*, vol. 13, p. 53, 2019, DOI: 10.3389/fninf.2019.00053.
- [109] A. Darwish et al., „A survey of swarm and evolutionary computing approaches for deep learning,” *Artificial Intelligence Review*, vol. 53, no. 3, pp. 1767–1812, 2020, DOI: 10.1007/s10462-019-09719-2.
- [110] F. Chollet, *Deep learning with Python*, (Safari Tech Books Online), Shelter Island, NY, Manning, 2018, ISBN: 9781617294433. Available: <http://proquest.safaribooksonline.com/9781617294433>.
- [111] G. Singh and S. Ahmed Saleh Al Kazzaz, „Induction machine drive condition monitoring and diagnostic research—a survey,” *Electric Power Systems Research*, vol. 64, no. 2, pp. 145–158, 2003, DOI: 10.1016/S0378-7796(02)00172-4.
- [112] G. Zhao et al., „Research advances in fault diagnosis and prognostic based on deep learning,” in *Proceedings of 2016 Prognostics and System Health Management Conference (PHM-Chengdu): October 19-21, 2016, Chengdu, Sichuan, China*, Chengdu, China, 2016, pp. 1–6, ISBN: 978-1-5090-2778-1. DOI: 10.1109/PHM.2016.7819786.
- [113] D. Wang et al., „Prognostics and Health Management: A Review of Vibration Based Bearing and Gear Health Indicators,” *IEEE Access*, vol. 6, pp. 665–676, 2018, DOI: 10.1109/ACCESS.2017.2774261.
- [114] R. Liu et al., „Artificial intelligence for fault diagnosis of rotating machinery: A review,” *Mechanical Systems and Signal Processing*, vol. 108, pp. 33–47, 2018, DOI: 10.1016/j.ymsp.2018.02.016.
- [115] Wei et al., „A Review of Early Fault Diagnosis Approaches and Their Applications in Rotating Machinery,” *Entropy*, vol. 21, no. 4, 2019, DOI: 10.3390/e21040409.
- [116] A. Stetco et al., „Machine learning methods for wind turbine condition monitoring: A review,” *Renewable Energy*, vol. 133, pp. 620–635, 2019, DOI: 10.1016/j.renene.2018.10.047.
- [117] S. Zhang et al., „Machine Learning and Deep Learning Algorithms for Bearing Fault Diagnostics – A Comprehensive Review,” *IEEE Access*, vol. 8, pp. 29857–29881, 2020, DOI: 10.1109/ACCESS.2020.2972859. Available: <http://arxiv.org/pdf/1901.08247v3>.
- [118] T. Zehelein et al., „An Evaluation of Autoencoder and Sparse Filter as Automated Feature Extraction Process for Automotive Damper Defect Diagnosis,” in *2019 Fourteenth International Conference on Ecological Vehicles and Renewable Energies (EVER)*, Monte-Carlo, Monaco, 2019, pp. 1–8, ISBN: 978-1-7281-3703-2. DOI: 10.1109/EVER.2019.8813630.

- [119] T. Zehelein et al., „Automotive Damper Defect Detection Using Novelty Detection Methods,“ in *Proceedings of the ASME 2019 Dynamic Systems and Control Conference. Volume 1: Advanced Driver Assistance and Autonomous Technologies; Advances in Control Design Methods; Advances in Robotics; Automotive Systems; Design, Modeling, Analysis, and Control of Assistive and Rehabilitation Devices; Diagnostics and Detection; Dynamics and Control of Human-Robot Systems; Energy Optimization for Intelligent Vehicle Systems; Estimation and Identification; Manufacturing*, Park City, Utah, USA, 2019, ISBN: 978-0-7918-5914-8. DOI: 10.1115/DSCC2019-9188.
- [120] T. Zehelein et al., „Damper diagnosis by artificial intelligence,“ in *9th International Munich Chassis Symposium 2018: Chassis.tech plus* (Proceedings), P. E. Pfeffer, ed. Wiesbaden, Germany: Springer Vieweg, 2019, pp. 461–482, ISBN: 978-3-658-22049-5. DOI: 10.1007/978-3-658-22050-1_31.
- [121] T. Zehelein et al., „Diagnosing Automotive Damper Defects Using Convolutional Neural Networks and Electronic Stability Control Sensor Signals,“ *Journal of Sensor and Actuator Networks*, vol. 9, no. 1, p. 8, 2020, DOI: 10.3390/jsan9010008.
- [122] U. Shafi et al., „Vehicle Remote Health Monitoring and Prognostic Maintenance System,“ *Journal of Advanced Transportation*, vol. 2018, no. 1, pp. 1–10, 2018, DOI: 10.1155/2018/8061514.
- [123] R. Ruiz-Gonzalez et al., „An SVM-based classifier for estimating the state of various rotating components in agro-industrial machinery with a vibration signal acquired from a single point on the machine chassis,“ *Sensors (Basel, Switzerland)*, vol. 14, no. 11, pp. 20713–20735, 2014, DOI: 10.3390/s141120713.
- [124] T. Praveenkumar et al., „Fault Diagnosis of Automobile Gearbox Based on Machine Learning Techniques,“ *Procedia Engineering*, vol. 97, pp. 2092–2098, 2014, DOI: 10.1016/j.proeng.2014.12.452.
- [125] A. Widodo and B.-S. Yang, „Support vector machine in machine condition monitoring and fault diagnosis,“ *Mechanical Systems and Signal Processing*, vol. 21, no. 6, pp. 2560–2574, 2007, DOI: 10.1016/j.ymsp.2006.12.007.
- [126] S. A. Khan and J.-M. Kim, „Automated Bearing Fault Diagnosis Using 2D Analysis of Vibration Acceleration Signals under Variable Speed Conditions,“ *Shock and Vibration*, vol. 2016, pp. 1–11, 2016, DOI: 10.1155/2016/8729572.
- [127] D. Verstraete et al., „Deep Learning Enabled Fault Diagnosis Using Time-Frequency Image Analysis of Rolling Element Bearings,“ *Shock and Vibration*, vol. 2017, pp. 1–17, 2017, DOI: 10.1155/2017/5067651.
- [128] X. Ding and Q. He, „Energy-Fluctuated Multiscale Feature Learning With Deep ConvNet for Intelligent Spindle Bearing Fault Diagnosis,“ *IEEE Transactions on Instrumentation and Measurement*, vol. 66, no. 8, pp. 1926–1935, 2017, DOI: 10.1109/TIM.2017.2674738.
- [129] L. Eren et al., „A Generic Intelligent Bearing Fault Diagnosis System Using Compact Adaptive 1D CNN Classifier,“ *Journal of Signal Processing Systems*, vol. 91, no. 2, pp. 179–189, 2019, DOI: 10.1007/s11265-018-1378-3.
- [130] X. Guo et al., „Hierarchical adaptive deep convolution neural network and its application to bearing fault diagnosis,“ *Measurement*, vol. 93, pp. 490–502, 2016, DOI: 10.1016/j.measurement.2016.07.054.

- [131] C. Lu et al., „Intelligent fault diagnosis of rolling bearing using hierarchical convolutional network based health state classification,“ *Advanced Engineering Informatics*, vol. 32, pp. 139–151, 2017, DOI: 10.1016/j.aei.2017.02.005.
- [132] L. Jing et al., „An Adaptive Multi-Sensor Data Fusion Method Based on Deep Convolutional Neural Networks for Fault Diagnosis of Planetary Gearbox,“ *Sensors (Basel, Switzerland)*, vol. 17, no. 2, 2017, DOI: 10.3390/s17020414.
- [133] O. Janssens et al., „Convolutional Neural Network Based Fault Detection for Rotating Machinery,“ *Journal of Sound and Vibration*, vol. 377, pp. 331–345, 2016, DOI: 10.1016/j.jsv.2016.05.027.
- [134] D.-T. Hoang and H.-J. Kang, „Rolling element bearing fault diagnosis using convolutional neural network and vibration image,“ *Cognitive Systems Research*, vol. 53, pp. 42–50, 2019, DOI: 10.1016/j.cogsys.2018.03.002.
- [135] R. Zhao et al., „Learning to Monitor Machine Health with Convolutional Bi-Directional LSTM Networks,“ *Sensors (Basel, Switzerland)*, vol. 17, no. 2, 2017, DOI: 10.3390/s17020273.
- [136] H. Luo et al., „A dual-tree complex wavelet enhanced convolutional LSTM neural network for structural health monitoring of automotive suspension,“ *Measurement*, vol. 137, pp. 14–27, 2019, DOI: 10.1016/j.measurement.2019.01.038.
- [137] H. Luo et al., „Integration of Multi-Gaussian fitting and LSTM neural networks for health monitoring of an automotive suspension component,“ *Journal of Sound and Vibration*, vol. 428, pp. 87–103, 2018, DOI: 10.1016/j.jsv.2018.05.007.
- [138] Y. Xie and T. Zhang, „Imbalanced Learning for Fault Diagnosis Problem of Rotating Machinery Based on Generative Adversarial Networks,“ in *Proceedings of the 37th Chinese Control Conference: July 25-27, 2018, Wuhan, China = Di san shi qi jie zhong guo kong zhi hui yi lun wen ji ; 2018 nian 7 yue 25-27 ri, zhong guo, wu han*, Wuhan, 2018, pp. 6017–6022, ISBN: 978-988-15639-5-8. DOI: 10.23919/ChiCC.2018.8483334.
- [139] Y. O. Lee et al., „Application of deep neural network and generative adversarial network to industrial maintenance: A case study of induction motor fault detection,“ in *2017 IEEE International Conference on Big Data: Dec 11-14, 2017, Boston, MA, USA : proceedings*, Boston, MA, 2017, pp. 3248–3253, ISBN: 978-1-5386-2715-0. DOI: 10.1109/BigData.2017.8258307.
- [140] F. Wang et al., „A deep feature extraction method for bearing fault diagnosis based on empirical mode decomposition and kernel function,“ *Advances in Mechanical Engineering*, vol. 10, no. 9, 2018, DOI: 10.1177/1687814018798251.
- [141] M. Ma et al., „Deep Coupling Autoencoder for Fault Diagnosis With Multimodal Sensory Data,“ *IEEE Transactions on Industrial Informatics*, vol. 14, no. 3, pp. 1137–1145, 2018, DOI: 10.1109/TII.2018.2793246.
- [142] C. Lu et al., „Fault diagnosis of rotary machinery components using a stacked denoising autoencoder-based health state identification,“ *Signal Processing*, vol. 130, pp. 377–388, 2017, DOI: 10.1016/j.sigpro.2016.07.028.
- [143] F. Jia et al., „Deep neural networks: A promising tool for fault characteristic mining and intelligent diagnosis of rotating machinery with massive data,“ *Mechanical Systems and Signal Processing*, vol. 72-73, pp. 303–315, 2016, DOI: 10.1016/j.ymsp.2015.10.025.
- [144] S. Hitawala, „Comparative Study on Generative Adversarial Networks,“ 2018. Available: <https://arxiv.org/abs/1801.04271>.

- [145] J. R. Quinlan, „Learning decision tree classifiers,“ *ACM Computing Surveys*, vol. 28, no. 1, pp. 71–72, 1996, DOI: 10.1145/234313.234346.
- [146] L. Breiman, „Random Forests,“ *Machine Learning*, vol. 45, no. 1, pp. 5–32, 2001, DOI: 10.1023/A:1010933404324.
- [147] C. Cortes and V. Vapnik, „Support-Vector Networks,“ *Machine Learning*, vol. 20, no. 3, pp. 273–297, 1995, DOI: 10.1023/A:1022627411411.
- [148] E. Fix and J. L. Hodges, „Discriminatory analysis, nonparametric discrimination: consistency properties,“ *Technical Report 4, USAF School of Aviation Medicine, Randolph Field*, 1951.
- [149] T. Cover and P. Hart, „Nearest neighbor pattern classification,“ *IEEE Transactions on Information Theory*, vol. 13, no. 1, pp. 21–27, 1967, DOI: 10.1109/TIT.1967.1053964.
- [150] Y. Le Cun et al., „Handwritten Digit Recognition with a Back-Propagation Network,“ in *Proceedings of the 2nd International Conference on Neural Information Processing Systems*, 1989, pp. 396–404.
- [151] S. Hochreiter and J. Schmidhuber, „Long short-term memory,“ *Neural computation*, vol. 9, no. 8, pp. 1735–1780, 1997, DOI: 10.1162/neco.1997.9.8.1735.
- [152] I. Goodfellow et al., „Generative Adversarial Nets,“ in *Advances in Neural Information Processing Systems 27*, Z. Ghahramani et al., ed. Curran Associates, Inc, 2014, pp. 2672–2680. Available: <http://papers.nips.cc/paper/5423-generative-adversarial-nets.pdf>.
- [153] H. Liu et al., „Unsupervised fault diagnosis of rolling bearings using a deep neural network based on generative adversarial networks,“ *Neurocomputing*, vol. 315, pp. 412–424, 2018, DOI: 10.1016/j.neucom.2018.07.034.
- [154] Y. Bengio, „Learning Deep Architectures for AI,“ *Foundations and Trends® in Machine Learning*, vol. 2, no. 1, pp. 1–127, 2009, DOI: 10.1561/22000000006.
- [155] WePredict. „Predictive Analytics & Predictive modeling for Market Solutions,“ 2020. [Online]. Available: <https://www.wepredict.com/> [accessed 05/05/2020].
- [156] Crunchbase. „We Predict | Crunchbase,“ 2020. [Online]. Available: <https://www.crunchbase.com/organization/we-predict#section-overview> [accessed 05/04/2020].
- [157] WePredict. „Navigating To Success: Predictive analytics and the future of automotive,“ 2020. [Online]. Available: <https://www.wepredict.com/wp-content/uploads/We-Predict-Navigating-To-Success-Whitepaper-March-2019.pdf> [accessed 05/04/2020].
- [158] Carly. „Diagnose and code your car,“ 2020. [Online]. Available: <https://www.mycarly.com/> [accessed 05/05/2020].
- [159] Carly. „CarTech Company, Carly, Launches Universal Onboard Diagnostic Adapter in the U.S.“ [Online]. Available: https://www.mycarly.com/files/EN_Press_Release.pdf.
- [160] COMPREDICT GmbH. „COMPREDICT - Automotive Analytics Suite,“ 2020. [Online]. Available: <https://compredict.de/> [accessed 05/04/2020].
- [161] Crunchbase. „Compredict | Crunchbase,“ 2020. [Online]. Available: <https://www.crunchbase.com/organization/compredict#section-overview> [accessed 05/04/2020].
- [162] R. Kraft. „COMPREDICT’s purely CAN-based Virtual Sensors,“ 2020. [Online]. Available: <https://medium.com/compredict/compredicts-purely-can-based-virtual-sensors-4c9f37a3a6ae> [accessed 05/04/2020].

- [163] O. Esbel. „COMPREDICT Platform Architecture —Part 1: AI Core & ML Framework,“ 2020. [Online]. Available: <https://medium.com/compredict/compredict-platform-architecture-part-1-ai-core-ml-framework-648bc2e1b841> [accessed 05/04/2020].
- [164] J. Prenninger. „Advanced Diagnostics and Predictive Analytics of Vehicle Data,“ Wien, 2013. Available: <https://docplayer.org/1334293-Advanced-diagnostics-and-predictive-analytics-of-vehicle-data-dr-johann-prenninger.html>.
- [165] „. BMW Group launches BMW CarData: new and innovative services for customers, safely and transparently,“ 30.05.2017. Available: www.press.bmwgroup.com/global/article/detail/T0271366EN/bmw-group-launches-bmw-cardata:-new-and-innovative-services-for-customers-safely-and-transparently?language=en [accessed 05/04/2020].
- [166] BMW Group. „CarData in a Nutshell,“ 2020. [Online]. Available: https://www.google.com/url?sa=t&rct=j&q=&esrc=s&source=web&cd=1&cad=rja&uact=8&ved=2ahUKEwiYp5Lc4p3pAhVq_CoKHaOBC54QFjAAegQIAxAB&url=https%3A%2F%2Fbmwcardata.bmwgroup.com%2Fnutshell%2FEN%2FCarData_in_a_nutshell.pdf&usg=AOvVaw3MJ7psfHIDmNwsdm9ZuBej [accessed 05/06/2020].
- [167] High Mobility. „BMW CarData now integrated with Auto API,“ 2020. [Online]. Available: <https://medium.com/high-mobility/integrate-bmw-cardata-in-the-high-mobility-platform-now-335b7d880dd6> [accessed 05/06/2020].
- [168] High Mobility. „Mercedes-Benz car data available via Auto API,“ 2020. [Online]. Available: <https://medium.com/high-mobility/high-mobility-enables-third-party-services-to-mercedes-benz-customers-2d71eb7a005c> [accessed 05/06/2020].
- [169] Crunchbase. „High Mobility | Crunchbase,“ 2020. [Online]. Available: <https://www.crunchbase.com/organization/high-mobility#section-overview> [accessed 05/06/2020].
- [170] High Mobility. „HIGH MOBILITY - Learn: BMW Guide,“ 2020. [Online]. Available: <https://high-mobility.com/learn/tutorials/getting-started/bmw/#pricing> [accessed 05/06/2020].
- [171] High Mobility. „HIGH MOBILITY - Learn: Mercedes-Benz,“ 2020. [Online]. Available: <https://high-mobility.com/learn/tutorials/getting-started/daimler/#data-buckets> [accessed 05/06/2020].
- [172] P. A. Eisenstein. „Tesla Cars Now Can Diagnose Problems, Even Pre-Order Parts,“ 2020. [Online]. Available: <https://www.thedetroitbureau.com/2019/05/tesla-cars-now-can-diagnose-problems-even-pre-order-parts/> [accessed 05/05/2020].
- [173] Tesla. „Service | Tesla,“ 2020. [Online]. Available: <https://www.tesla.com/service> [accessed 05/05/2020].
- [174] A. M. Soliman and M. M. Kaldas, „Semi-active suspension systems from research to mass-market – A review,“ *Journal of Low Frequency Noise, Vibration and Active Control*, p. 146134841987639, 2019, DOI: 10.1177/1461348419876392.
- [175] S. X. Ding et al., „A survey of the application of basic data-driven and model-based methods in process monitoring and fault diagnosis,“ *IFAC Proceedings Volumes*, vol. 44, no. 1, pp. 12380–12388, 2011, DOI: 10.3182/20110828-6-IT-1002.02842.
- [176] M. Wimmer et al., „Method and apparatus for detecting shock absorber damage,“ Patent US20020010533A1, January 24, 2002.
- [177] M. Jautze et al., „Verfahren und Vorrichtung zum Erkennen von Dämpferschäden,“ Patent DE10028749B4, December 12, 2001.

- [178] J. Adamy, *Nichtlineare Systeme und Regelungen*, Berlin, Heidelberg, Springer Berlin Heidelberg, 2014, ISBN: 978-3-642-45012-9. DOI: 10.1007/978-3-642-45013-6.
- [179] R. N. Jazar, „Quarter Car Model,“ in *Vehicle Dynamics*, R. N. Jazar, ed. New York, NY: Springer New York, 2014, pp. 985–1026, ISBN: 978-1-4614-8543-8. DOI: 10.1007/978-1-4614-8544-5_15.
- [180] R. Hermann and A. Krener, „Nonlinear controllability and observability,“ *IEEE Transactions on Automatic Control*, vol. 22, no. 5, pp. 728–740, 1977, DOI: 10.1109/TAC.1977.1101601.
- [181] K. Kassara, „A Set-Valued Approach to Observability,“ *SIAM Journal on Control and Optimization*, vol. 51, no. 6, pp. 4520–4543, 2013, DOI: 10.1137/120897663.
- [182] E. D. Sontag and Y. Wang, „Output-to-state stability and detectability of nonlinear systems,“ *Systems & Control Letters*, vol. 29, no. 5, pp. 279–290, 1997, DOI: 10.1016/S0167-6911(97)90013-X.
- [183] J. P. Hespanha et al., „Nonlinear norm-observability notions and stability of switched systems,“ *IEEE Transactions on Automatic Control*, vol. 50, no. 2, pp. 154–168, 2005, DOI: 10.1109/TAC.2004.841937.
- [184] K. Löhe et al., „Modellierung und Parametrierung stochastischer Fahrbahnunebenheiten mit Hub-, Wank-, Nick- und Verspannanteil: Modeling and Parametrization of Stochastic Road Unevenness with Lift, Roll, Pitch and Torsion Component,“ in *Reifen-Fahrwerk-Fahrbahn 2015: 15. internationale VDI-Tagung ; 4. VDI-Fachkonferenz Innovative Bremstechnik, Hannover, 14. und 15. Oktober 2015* (VDI-Berichte). vol. 2241 Düsseldorf: VDI-Verl., 2015, ISBN: 9783180922416.
- [185] K. Löhe et al., „Ein modulares Konzept zur Fahrbahngüteschätzung und Kalman-Filter-Adaption mittels autoregressiver Filterung: A Modular Concept for Road Quality Estimation and Kalman Filter Adaptation by Autoregressive Filtering,“ in *Autoreg 2015: Auf dem Weg zum automatisierten Fahren ; 7. Fachtagung in Baden-Baden, 09. und 10. Juni 2015* (VDI-Berichte). vol. 2233 Düsseldorf: VDI-Verl., 2015, ISBN: 9783180922331.
- [186] K. Löhe et al., „Fahrbahngüteschätzung mittels autoregressiver Filterung am Zweiachs-Fahrzeug,“ *at - Automatisierungstechnik*, vol. 64, no. 5, pp. 355–364, 2016, DOI: 10.1515/auto-2016-0012.
- [187] P. J. Venhovens, „Optimal control of vehicle suspensions,“ Dissertation, Delft University of Technology, Delft, 1993.
- [188] N. Powel, „Noise-Enabled Observability of Nonlinear Dynamic Systems Using the Empirical Observability Gramian,“ Dissertation, University of Washington, 2016.
- [189] E. Pardoux and A. Rascanu, *Stochastic Differential Equations, Backward SDEs, Partial Differential Equations*. vol. 69, Cham, Springer International Publishing, 2014, ISBN: 978-3-319-05713-2. DOI: 10.1007/978-3-319-05714-9.
- [190] J. M. Davis et al., „Controllability, Observability, Realizability, and Stability of Dynamic Linear Systems,“ *Electron. J. Diff. Eqns.*, 2009. Available: <http://arxiv.org/pdf/0901.3764v2>.
- [191] G. E. Dullerud and F. Paganini, *A Course in Robust Control Theory: A Convex Approach*, (Texts in Applied Mathematics). vol. 36, New York, NY, Springer, 2000, ISBN: 978-1-4757-3290-0. DOI: 10.1007/978-1-4757-3290-0. Available: <http://dx.doi.org/10.1007/978-1-4757-3290-0>.

- [192] A. J. Krener and K. Ide, „Measures of unobservability,“ in *Proceedings of the 48th IEEE Conference on Decision and Control (CDC): Held jointly with 2009 28th Chinese Control Conference [(CCC)] ; Shanghai, China, 15 - 18 December 2009*, Shanghai, China, 2009, pp. 6401–6406, ISBN: 978-1-4244-3871-6. DOI: 10.1109/CDC.2009.5400067.
- [193] N. J. Higham and S. D. Relton, „Higher Order Fréchet Derivatives of Matrix Functions and the Level-2 Condition Number,“ *SIAM Journal on Matrix Analysis and Applications*, vol. 35, no. 3, pp. 1019–1037, 2014, DOI: 10.1137/130945259.
- [194] B. Fornberg, „Generation of finite difference formulas on arbitrarily spaced grids,“ *Mathematics of Computation*, vol. 51, no. 184, p. 699, 1988, DOI: 10.1090/S0025-5718-1988-0935077-0.
- [195] M. Mitschke and H. Wallentowitz, *Dynamik der Kraftfahrzeuge*, Wiesbaden, Springer Fachmedien Wiesbaden, 2014, ISBN: 978-3-658-05067-2. DOI: 10.1007/978-3-658-05068-9.
- [196] T. Zehelein. „*Damper Defect Detection Using Machine Learning*,“ 2020. Available: <https://github.com/TUMFTM/Damper-Defect-Detection-using-Machine-Learning>.
- [197] T. Marwala, *Condition Monitoring Using Computational Intelligence Methods*, London, Springer London, 2012, ISBN: 978-1-4471-2379-8. DOI: 10.1007/978-1-4471-2380-4.
- [198] A. G. Gracia et al., „Theoretical and experimental analysis to determine the influence of the ageing process of the shock-absorber on safety,“ *International Journal of Vehicle Design*, vol. 40, no. 1/2/3, pp. 15–35, 2006, DOI: 10.1504/IJVD.2006.008451.
- [199] B. Juba and H. S. Le, „Precision-Recall versus Accuracy and the Role of Large Data Sets,“ *Proceedings of the AAAI Conference on Artificial Intelligence*, vol. 33, pp. 4039–4048, 2019, DOI: 10.1609/aaai.v33i01.33014039.
- [200] J. C. Dixon, *The shock absorber handbook*, (Wiley-Professional engineering publishing series), 2nd ed., Chichester, England, John Wiley, 2007, ISBN: 978-0-470-51020-9. DOI: 10.1002/9780470516430.
- [201] M. Hamed et al., „A study of the suspension system for the diagnosis of dynamic characteristics,“ in *Proceedings of the 20th International Conference on Automation and Computing (ICAC'14) Future Automation, Computing & Manufacturing*, Cranfield, Bedfordshire, United Kingdom, 2015, pp. 152–157, DOI: 10.1109/IConAC.2014.6935478.
- [202] M. Jautze et al., „The Dynamic Damper Control,“ *ATZextra worldwide*, vol. 13, no. 8, pp. 100–103, 2008, DOI: 10.1365/s40111-008-0110-x.
- [203] A. Merk, „Dämpferdefektdetektion & -diagnose mittels Künstlicher Intelligenz: Damper defect detection and diagnosis by artificial intelligence,“ Master’s Thesis, Technical University of Munich, Munich, 2018.
- [204] A. Bykanov, „Weiterentwicklung eines Machine Learning- Konzepts zur Diagnose defekter Fahrwerksdämpfer: Improvement of a Machine Learning Concept for Diagnosing Damper Defects,“ Semester’s Thesis, Technical University of Munich, Munich, 2018.
- [205] G. Dong and H. Liu, *Feature Engineering for Machine Learning and Data Analytics*, (Chapman and Hall/CRC Data Mining and Knowledge Discovery Ser), Milton, Chapman and Hall/CRC, 2018, ISBN: 9781138744387. Available: <https://ebookcentral.proquest.com/lib/gbv/detail.action?docID=5322971>.
- [206] R. Bos et al., „Autoregressive spectral estimation by application of the burg algorithm to irregularly sampled data,“ *IEEE Transactions on Instrumentation and Measurement*, vol. 51, no. 6, pp. 1289–1294, 2002, DOI: 10.1109/TIM.2002.808031.

- [207] Y. Lei et al., „An Intelligent Fault Diagnosis Method Using Unsupervised Feature Learning Towards Mechanical Big Data,“ *IEEE Transactions on Industrial Electronics*, vol. 63, no. 5, pp. 3137–3147, 2016, DOI: 10.1109/TIE.2016.2519325.
- [208] P. Werk, „Dämpferdefektdiagnose mittels Deep Learning basierend auf unüberwachtem Lernen von Merkmalen: Damper Diagnosis using Deep Learning based on unsupervised Feature Learning,“ Master’s Thesis, Technical University of Munich, Munich, 2018.
- [209] R. F. Trumpp, „Defekterkennung von Fahrzeugdämpfern mittels Deep Learning-basierter Novelty Detection: Deep Learning-Based Novelty Detection of Automotive Chassis Damper Defects,“ Semester’s Thesis, Technical University of Munich, Munich, 2019.
- [210] G. E. Hinton and R. R. Salakhutdinov, „Reducing the dimensionality of data with neural networks,“ *Science (New York, N.Y.)*, vol. 313, no. 5786, pp. 504–507, 2006, DOI: 10.1126/science.1127647.
- [211] P. Baldi and K. Hornik, „Neural networks and principal component analysis: Learning from examples without local minima,“ *Neural Networks*, vol. 2, no. 1, pp. 53–58, 1989, DOI: 10.1016/0893-6080(89)90014-2.
- [212] H. Bourlard and Y. Kamp, „Auto-association by multilayer perceptrons and singular value decomposition,“ *Biological Cybernetics*, vol. 59, no. 4-5, pp. 291–294, 1988, DOI: 10.1007/BF00332918.
- [213] P. Vincent et al., „Extracting and composing robust features with denoising autoencoders,“ in *Proceedings of the 25th international conference on Machine learning - ICML '08*, Helsinki, Finland, 2008, pp. 1096–1103, ISBN: 9781605582054. DOI: 10.1145/1390156.1390294.
- [214] L. Zhang et al., „Sparse Auto-encoder with Smoothed L1 Regularization,“ *Neural Processing Letters*, vol. 47, no. 3, pp. 829–839, 2018, DOI: 10.1007/s11063-017-9668-5.
- [215] A. Y. Ng, „Sparse autoencoder: CS294A Lecture notes,“ 2011. Available: <https://web.stanford.edu/class/cs294a/sparseAutoencoder.pdf> [accessed 04/15/2020].
- [216] J. Ngiam et al., „Sparse Filtering,“ in *NIPS'11: Proceedings of the 24th International Conference on Neural Information Processing Systems*, Granada, Spain, 2011, pp. 1125–1133, ISBN: 9781618395993.
- [217] F. M. Zennaro and K. Chen, „Towards understanding sparse filtering: A theoretical perspective,“ *Neural networks : the official journal of the International Neural Network Society*, vol. 98, pp. 154–177, 2018, DOI: 10.1016/j.neunet.2017.11.010.
- [218] C. C. Aggarwal et al., „On the Surprising Behavior of Distance Metrics in High Dimensional Space,“ in *Database Theory - ICDT 2001: 8th International Conference London, UK, January 4-6, 2001 Proceedings* (Lecture Notes in Computer Science). vol. 1973, J. Bussche and V. Vianu, ed. Berlin and Heidelberg: Springer, 2001, pp. 420–434, ISBN: 978-3-540-41456-8. DOI: 10.1007/3-540-44503-X_27.
- [219] J. Miao and L. Niu, „A Survey on Feature Selection,“ *Procedia Computer Science*, vol. 91, pp. 919–926, 2016, DOI: 10.1016/j.procs.2016.07.111.
- [220] B. Xue et al., „A Survey on Evolutionary Computation Approaches to Feature Selection,“ *IEEE Transactions on Evolutionary Computation*, vol. 20, no. 4, pp. 606–626, 2016, DOI: 10.1109/TEVC.2015.2504420.
- [221] M. Dash and H. LIU, „Feature selection for classification,“ *Intelligent Data Analysis*, vol. 1, no. 1-4, pp. 131–156, 1997, DOI: 10.1016/S1088-467X(97)00008-5.

- [222] I. Guyon et al., „An introduction to variable and feature selection,“ in *Journal of Machine Learning Research*, vol. 3, 2003, pp. 1157–1182.
- [223] I. Guyon et al., „Gene Selection for Cancer Classification using Support Vector Machines,“ *Machine Learning*, vol. 46, no. 1/3, pp. 389–422, 2002, DOI: 10.1023/A:1012487302797.
- [224] Q. Gu et al., „Generalized Fisher Score for Feature Selection,“ 14/02/2012. Available: <https://arxiv.org/abs/1202.3725>.
- [225] R. Caruana and A. Niculescu-Mizil, „An empirical comparison of supervised learning algorithms,“ in *Proceedings of the 23rd international conference on Machine learning*, Pittsburgh, Pennsylvania, 2006, pp. 161–168, ISBN: 1595933832. DOI: 10.1145/1143844.1143865.
- [226] N. Lavesson, *Evaluation and Analysis of Supervised Learning Algorithms and Classifiers*, (Blekinge Institute of Technology Licentiate Dissertation Series), Karlskrona, Blekinge Institute of Technology, 2006, ISBN: 91-7295-083-8.
- [227] C. H. Lampert, „Kernel Methods in Computer Vision,“ *FNT in Computer Graphics and Vision (Foundations and Trends in Computer Graphics and Vision)*, vol. 4, no. 3, pp. 193–285, 2008, DOI: 10.1561/06000000027.
- [228] M. A. Pimentel et al., „A review of novelty detection,“ *Signal Processing*, vol. 99, pp. 215–249, 2014, DOI: 10.1016/j.sigpro.2013.12.026.
- [229] A. Géron, *Hands-on machine learning with Scikit-Learn, Keras, and TensorFlow: Concepts, tools, and techniques to build intelligent systems*, Second edition, 2019, ISBN: 978-1-492-03264-9.
- [230] V. Chandola et al., „Anomaly Detection: A Survey,“ *ACM Computing Surveys*, vol. 41, no. 3, pp. 1–58, 2009, DOI: 10.1145/1541880.1541882.
- [231] M. Markou and S. Singh, „Novelty detection: a review—part 1: statistical approaches,“ *Signal Processing*, vol. 83, no. 12, pp. 2481–2497, 2003, DOI: 10.1016/j.sigpro.2003.07.018.
- [232] S. S. Khan and M. G. Madden, „A Survey of Recent Trends in One Class Classification,“ in *Artificial intelligence and cognitive science: 20th Irish conference, AICS 2009, Dublin, Ireland, August 19 - 21, 2009 ; revised selected papers* (Lecture notes in computer science Lecture notes in artificial intelligence). vol. 6206, L. Coyle and J. Freyne, ed. Berlin: Springer, 2010, pp. 188–197, ISBN: 978-3-642-17079-9. DOI: 10.1007/978-3-642-17080-5_21.
- [233] M. Markou and S. Singh, „Novelty detection: a review - part 2: neural network based approaches,“ *Signal Processing*, vol. 83, no. 12, pp. 2499–2521, 2003, DOI: 10.1016/j.sigpro.2003.07.019.
- [234] R. Domingues et al., „A comparative evaluation of outlier detection algorithms: Experiments and analyses,“ *Pattern Recognition*, vol. 74, pp. 406–421, 2018, DOI: 10.1016/j.patcog.2017.09.037.
- [235] V. J. Hodge and J. Austin, „A Survey of Outlier Detection Methodologies,“ *Artificial Intelligence Review*, vol. 22, no. 2, pp. 85–126, 2004, DOI: 10.1007/s10462-004-4304-y.
- [236] S. Schuck, „Anomaliedetektion mittels Machine Learning in der Dämpferdiagnose: Anomaly Detection using Machine Learning for Damper Diagnosis,“ Master’s Thesis, Technical University of Munich, Munich, 2019.

- [237] M. M. Breunig et al., „LOF: Identifying Density-Based Local Outliers,“ in *Proceedings of the 2000 ACM SIGMOD international conference on Management of data - SIGMOD '00*, Dallas, Texas, United States, 2000, pp. 93–104, ISBN: 1581132174. DOI: 10.1145/342009.335388.
- [238] H. Fawaz et al., „Deep learning for time series classification: a review,“ *Data Mining and Knowledge Discovery*, vol. 33, no. 4, pp. 917–963, 2019, DOI: 10.1007/s10618-019-00619-1.
- [239] L. Zhang et al., „A Review on Deep Learning Applications in Prognostics and Health Management,“ *IEEE Access*, vol. 7, pp. 162415–162438, 2019, DOI: 10.1109/ACCESS.2019.2950985.
- [240] Y. Le Cun et al., „Gradient-based learning applied to document recognition,“ *Proceedings of the IEEE*, vol. 86, no. 11, pp. 2278–2324, 1998, DOI: 10.1109/5.726791.
- [241] G. W. Ding. „DrawConvNet,“ Available: https://github.com/gwding/draw_convnet [accessed 04/17/2020].
- [242] L. Wen et al., „A New Convolutional Neural Network-Based Data-Driven Fault Diagnosis Method,“ *IEEE Transactions on Industrial Electronics*, vol. 65, no. 7, pp. 5990–5998, 2018, DOI: 10.1109/TIE.2017.2774777.
- [243] W. Zhang et al., „Bearings Fault Diagnosis Based on Convolutional Neural Networks with 2-D Representation of Vibration Signals as Input,“ *MATEC Web of Conferences*, vol. 95, no. 8, p. 13001, 2017, DOI: 10.1051/mateconf/20179513001.
- [244] W. Zhang et al., „Fault State Recognition of Rolling Bearing Based Fully Convolutional Network,“ *Computing in Science & Engineering*, p. 1, 2018, DOI: 10.1109/MCSE.2018.110113254.
- [245] Y. Liao et al., „Wavelet transform based convolutional neural network for gearbox fault classification,“ in *Conference proceedings: 2017 Prognostics and System Health Management Conference (PHM-Harbin)*, Harbin, China, 2017, pp. 1–6, ISBN: 978-1-5386-0370-3. DOI: 10.1109/PHM.2017.8079274.
- [246] N. Hatami et al., „Classification of Time-Series Images Using Deep Convolutional Neural Networks,“ 02/10/2017. Available: <http://arxiv.org/pdf/1710.00886v2>.
- [247] Z. Wang and T. Oates, „Imaging Time-Series to Improve Classification and Imputation,“ in *Proceedings of the Twenty-Fourth International Joint Conference on Artificial Intelligence: Buenos Aires, Argentina, 25-31 July 2015*, Q. Yang and M. J. Wooldridge, ed. Palo Alto, California: AAAI Press International Joint Conferences on Artificial Intelligence, 2015, ISBN: 978-1-57735-738-4. Available: <http://arxiv.org/pdf/1506.00327v1>.
- [248] G. Krummenacher et al., „Wheel Defect Detection With Machine Learning,“ *IEEE Transactions on Intelligent Transportation Systems*, vol. 19, no. 4, pp. 1176–1187, 2018, DOI: 10.1109/TITS.2017.2720721.
- [249] W. Zhang et al., „A deep convolutional neural network with new training methods for bearing fault diagnosis under noisy environment and different working load,“ *Mechanical Systems and Signal Processing*, vol. 100, pp. 439–453, 2018, DOI: 10.1016/j.ymssp.2017.06.022.
- [250] M. Xia et al., „Fault Diagnosis for Rotating Machinery Using Multiple Sensors and Convolutional Neural Networks,“ *IEEE/ASME Transactions on Mechatronics*, vol. 23, no. 1, pp. 101–110, 2018, DOI: 10.1109/TMECH.2017.2728371.

- [251] Z. Zilong and Q. Wei, „Intelligent fault diagnosis of rolling bearing using one-dimensional multi-scale deep convolutional neural network based health state classification,“ in *ICNSC 2018: The 15th IEEE International Conference on Networking, Sensing and Control : March 27-29, 2018, Zhuhai, China*, Zhuhai, 2018, pp. 1–6, ISBN: 978-1-5386-5053-0. DOI: 10.1109/ICNSC.2018.8361296.
- [252] T. Hemmert-Pottmann, „Dämpferdefektdiagnose mittels der Deep Learning Architektur Convolutional Neural Networks: Diagnosing Damper Defects using the Deep Learning Architecture Convolutional Neural Networks,“ Master’s Thesis, Technical University of Munich, Munich, 2018.
- [253] T. Zehelein and T. Hemmert-Pottmann. „*Damper Defect Detection Using CNN*,“ 2019. Available: <https://github.com/TUMFTM/Damper-Defect-Detection-Using-CNN>.
- [254] R. Chalapathy and S. Chawla, „Deep Learning for Anomaly Detection: A Survey,“ 2019. Available: <https://arxiv.org/pdf/1901.03407>.
- [255] J. T. A. Andrews et al., „Detecting Anomalous Data Using Auto-Encoders,“ *International Journal of Machine Learning and Computing*, vol. 6, no. 1, pp. 21–26, 2016, DOI: 10.18178/ijmlc.2016.6.1.565.
- [256] R. Chalapathy et al., „Anomaly Detection using One-Class Neural Networks,“ 18/02/2018. Available: <http://arxiv.org/pdf/1802.06360v2>.
- [257] L. Ruff et al., „Deep One-Class Classification,“ in *Proceedings of the 35th International Conference on Machine Learning*, Stockholm, Sweden, 2018, pp. 4393–4402.
- [258] P. Vincent et al., „Stacked Denoising Autoencoders: Learning Useful Representations in a Deep Network with a Local Denoising Criterion,“ *Journal of Machine Learning Research*, vol. 2010, no. 11, pp. 3371–3408, 2010. [Accessed 02/07/2020].
- [259] J. An and S. Cho, „Variational autoencoder based anomaly detection using reconstruction probability,“ *Special Lecture on IE*, vol. 2, no. 1, 2015.
- [260] D. P. Kingma and M. Welling, „Auto-Encoding Variational Bayes,“ Available: <http://arxiv.org/pdf/1312.6114v10>.
- [261] D. P. Kingma and M. Welling, „An Introduction to Variational Autoencoders,“ *Foundations and Trends® in Machine Learning*, vol. 12, no. 4, pp. 307–392, 2019, DOI: 10.1561/22000000056.
- [262] S. Kullback and R. A. Leibler, „On Information and Sufficiency,“ *The Annals of Mathematical Statistics*, vol. 22, no. 1, pp. 79–86, 1951, DOI: 10.1214/aoms/1177729694.
- [263] T. M. Cover and J. A. Thomas, *Elements of information theory*, Hoboken, NJ, Wiley-Interscience, 1991, ISBN: 0-471-20061-1. DOI: 10.1002/0471200611. Available: <http://onlinelibrary.wiley.com/book/10.1002/0471200611> [accessed 04/15/2020].
- [264] C. Doersch, „Tutorial on Variational Autoencoders,“ 19/06/2016. Available: <https://arxiv.org/pdf/1606.05908.pdf>.
- [265] G. McPherson, *Statistics in Scientific Investigation: Its Basis, Application, and Interpretation*, (Springer Texts in Statistics), New York, NY, Springer, 1990, ISBN: 9781475742923. DOI: 10.1007/978-1-4757-4290-9.
- [266] M. Sokolova and G. Lapalme, „A systematic analysis of performance measures for classification tasks,“ *Information Processing & Management*, vol. 45, no. 4, pp. 427–437, 2009, DOI: 10.1016/j.ipm.2009.03.002.

- [267] M. Sokolova et al., „Beyond Accuracy, F-Score and ROC: A Family of Discriminant Measures for Performance Evaluation,“ in *AI 2006: Advances in Artificial Intelligence* (Lecture Notes in Computer Science). vol. 4304, D. Hutchison et al., ed. Berlin, Heidelberg: Springer Berlin Heidelberg, 2006, pp. 1015–1021, ISBN: 978-3-540-49787-5. DOI: 10.1007/11941439_114.
- [268] N. Goix, „How to Evaluate the Quality of Unsupervised Anomaly Detection Algorithms?,“ 05/07/2016. Available: <https://arxiv.org/abs/1607.01152>.
- [269] G. O. Campos et al., „On the evaluation of unsupervised outlier detection: measures, datasets, and an empirical study,“ *Data Mining and Knowledge Discovery*, vol. 30, no. 4, pp. 891–927, 2016, DOI: 10.1007/s10618-015-0444-8.
- [270] D. J. Hand and R. J. Till, „A Simple Generalisation of the Area Under the ROC Curve for Multiple Class Classification Problems,“ *Machine Learning*, vol. 45, no. 2, pp. 171–186, 2001, DOI: 10.1023/A:1010920819831.
- [271] T. Fawcett, „An introduction to ROC analysis,“ *Pattern Recognition Letters*, vol. 27, no. 8, pp. 861–874, 2006, DOI: 10.1016/j.patrec.2005.10.010.
- [272] J. A. Hanley and B. J. McNeil, „The meaning and use of the area under a receiver operating characteristic (ROC) curve,“ *Radiology*, vol. 143, no. 1, pp. 29–36, 1982, DOI: 10.1148/radiology.143.1.7063747.
- [273] J. Huang and C. X. Ling, „Using AUC and accuracy in evaluating learning algorithms,“ *IEEE Transactions on Knowledge and Data Engineering*, vol. 17, no. 3, pp. 299–310, 2005, DOI: 10.1109/TKDE.2005.50.
- [274] M. P. Sampat et al., „Indexes for three-class classification performance assessment—an empirical comparison,“ *IEEE transactions on information technology in biomedicine : a publication of the IEEE Engineering in Medicine and Biology Society*, vol. 13, no. 3, pp. 300–312, 2009, DOI: 10.1109/TITB.2008.2009440.
- [275] N. Japkowicz and M. Shah, *Evaluating Learning Algorithms*, Cambridge, Cambridge University Press, 2011, ISBN: 9780511921803. DOI: 10.1017/CBO9780511921803.
- [276] S. Lenser and M. Veloso, „Non-Parametric Time Series Classification,“ in *2005 IEEE International Conference on Robotics and Automation (ICRA): Barcelona, Spain : 18-22 April, 2005*, Barcelona, Spain, 2005, pp. 3918–3923, ISBN: 0-7803-8914-X. DOI: 10.1109/ROBOT.2005.1570719.
- [277] L. Rabiner and B. Juang, „An introduction to hidden Markov models,“ *IEEE ASSP Magazine*, vol. 3, no. 1, pp. 4–16, 1986, DOI: 10.1109/MASSP.1986.1165342.
- [278] Z. Ghahramani, „An Introduction to Hidden Markov Models and Bayesian Networks,“ *International Journal of Pattern Recognition and Artificial Intelligence*, vol. 15, no. 01, pp. 9–42, 2001, DOI: 10.1142/S0218001401000836.
- [279] B. Esmael et al., „Improving time series classification using Hidden Markov Models,“ in *2012 12th International Conference on Hybrid Intelligent Systems (HIS)*, Pune, India, 2013, pp. 502–507, ISBN: 978-1-4673-5116-4. DOI: 10.1109/HIS.2012.6421385.
- [280] L. R. Rabiner, „A tutorial on hidden Markov models and selected applications in speech recognition,“ *Proceedings of the IEEE*, vol. 77, no. 2, pp. 257–286, 1989, DOI: 10.1109/5.18626.
- [281] R. E. Kalman, „A New Approach to Linear Filtering and Prediction Problems,“ *Transactions of the ASME—Journal of Basic Engineering*, vol. 82, no. Series D, pp. 35–45, 1960.

- [282] H. E. Rauch et al., „Maximum likelihood estimates of linear dynamic systems,“ *AIAA Journal*, vol. 3, no. 8, pp. 1445–1450, 1965, DOI: 10.2514/3.3166.
- [283] S. Aydin et al., „Log energy entropy-based EEG classification with multilayer neural networks in seizure,“ *Annals of biomedical engineering*, vol. 37, no. 12, pp. 2626–2630, 2009, DOI: 10.1007/s10439-009-9795-x.
- [284] Mathworks. „Visualize summary statistics with box plot - Matlab boxplot,“ 2020. [Online]. Available: <https://de.mathworks.com/help/stats/boxplot.html> [accessed 03/20/2020].
- [285] A. Tuononen et al., „Parameterization of in-plane rigid ring tire model from instrumented vehicle measurements,“ in *Proceedings of the 11th International Symposium on Advanced Vehicle Control (AVEC'12)* 2012.
- [286] W. Zhang et al., „A New Deep Learning Model for Fault Diagnosis with Good Anti-Noise and Domain Adaptation Ability on Raw Vibration Signals,“ *Sensors (Basel, Switzerland)*, vol. 17, no. 2, 2017, DOI: 10.3390/s17020425.
- [287] I.-K. Yeo, „A new family of power transformations to improve normality or symmetry,“ *Biometrika*, vol. 87, no. 4, pp. 954–959, 2000, DOI: 10.1093/biomet/87.4.954.
- [288] M. W. Sayers et al., *The international road roughness experiment: Establishing correlation and a calibration standard for measurements*, (World Bank technical paper). vol. no. 45, Washington, DC, World Bank, 1986, ISBN: 0821305891.
- [289] P. Můčka, „International Roughness Index specifications around the world,“ *Road Materials and Pavement Design*, vol. 18, no. 4, pp. 929–965, 2017, DOI: 10.1080/14680629.2016.1197144.
- [290] M. W. Sayers et al., *Guidelines for conducting and calibrating road roughness measurements*, (World Bank technical paper). vol. 46, Washington, D.C., U.S.A, World Bank, 1986, ISBN: 0821305905.
- [291] K. Löhe, *Ein modellgestütztes Konzept zur fahrbahnadaptiven Fahrwerksregelung*, FAU University Press, 2018, ISBN: 978-3-96147-102-7. DOI: 10.25593/978-3-96147-102-7.
- [292] T. Chen and C. Guestrin, „XGBoost: A Scalable Tree Boosting System,“ in *KDD2016: 22nd ACM SIGKDD Conference on Knowledge Discovery and Data Mining, August 13-17, 2016, San Francisco, CA, USA*, San Francisco, California, USA, 2016, pp. 785–794, ISBN: 9781450342322. DOI: 10.1145/2939672.2939785.
- [293] Y. Zhao and M. K. Hryniewicki, „XGBOD: Improving Supervised Outlier Detection with Unsupervised Representation Learning,“ in *2018 International Joint Conference on Neural Networks (IJCNN): 2018 proceedings*, Rio de Janeiro, 2018, pp. 1–8, ISBN: 978-1-5090-6014-6. DOI: 10.1109/IJCNN.2018.8489605.
- [294] M. Faist, „Umsetzung und Analyse realer Dämpferdefekte zur Fahrwerkdiagnose: Implementation and Analysis of Damper Defects for Chassis System Diagnosis,“ Semester’s Thesis, Technical University of Munich, Munich, 2019.
- [295] W. Han and K. E. Atkinson, *Theoretical Numerical Analysis*. vol. 39, New York, NY, Springer New York, 2009, ISBN: 978-1-4419-0457-7. DOI: 10.1007/978-1-4419-0458-4.
- [296] T. H. Cormen et al., *Introduction to algorithms*, 3. ed., Cambridge, Mass., MIT Press, 2009, ISBN: 9780262533058.
- [298] P. Welch, „The use of fast Fourier transform for the estimation of power spectra: A method based on time averaging over short, modified periodograms,“ *IEEE Transactions on Audio and Electroacoustics*, vol. 15, no. 2, pp. 70–73, 1967, DOI: 10.1109/TAU.1967.1161901.

- [299] T. Schreiber and A. Schmitz, „Discrimination power of measures for nonlinearity in a time series,“ *Physical Review E*, vol. 55, no. 5, pp. 5443–5447, 1997, DOI: 10.1103/PhysRevE.55.5443.

List of Prior Publications

During the preparation of this dissertation, publications and research papers were produced in which partial aspects of this work were presented.

Journals; Scopus/Web of Science listed (peer-reviewed)

- [121] T. Zehelein, T. Hemmert-Pottmann and M. Lienkamp, „Diagnosing Automotive Damper Defects Using Convolutional Neural Networks and Electronic Stability Control Sensor Signals,“ *Journal of Sensor and Actuator Networks*, vol. 9, no. 1, p. 8, 2020, DOI: 10.3390/jsan9010008.
- [186] K. Löhe, T. Zehelein and G. Roppenecker, „Fahrbahngüteschätzung mittels autoregressiver Filterung am Zweiachs-Fahrzeug,“ *at - Automatisierungstechnik*, vol. 64, no. 5, pp. 355–364, 2016, DOI: 10.1515/auto-2016-0012.

Conferences, Periodicals, etc.; Scopus/Web of Science listed (peer-reviewed)

- [118] T. Zehelein, P. Werk and M. Lienkamp, „An Evaluation of Autoencoder and Sparse Filter as Automated Feature Extraction Process for Automotive Damper Defect Diagnosis,“ in *2019 Fourteenth International Conference on Ecological Vehicles and Renewable Energies (EVER)*, Monte-Carlo, Monaco, 2019, pp. 1–8, ISBN: 978-1-7281-3703-2. DOI: 10.1109/EVER.2019.8813630.
- [119] T. Zehelein, S. Schuck and M. Lienkamp, „Automotive Damper Defect Detection Using Novelty Detection Methods,“ in *Proceedings of the ASME 2019 Dynamic Systems and Control Conference. Volume 1: Advanced Driver Assistance and Autonomous Technologies; Advances in Control Design Methods; Advances in Robotics; Automotive Systems; Design, Modeling, Analysis, and Control of Assistive and Rehabilitation Devices; Diagnostics and Detection; Dynamics and Control of Human-Robot Systems; Energy Optimization for Intelligent Vehicle Systems; Estimation and Identification; Manufacturing*, Park City, Utah, USA, 2019, ISBN: 978-0-7918-5914-8. DOI: 10.1115/DSCC2019-9188.

Journals, Conferences, Periodicals, Conference Proceedings, etc.; not Scopus/Web of Science listed (not peer-reviewed)

- [120] T. Zehelein, A. Merk and M. Lienkamp, „Damper diagnosis by artificial intelligence,“ in *9th International Munich Chassis Symposium 2018: Chassis.tech plus* (Proceedings), P. E. Pfeffer, ed. Wiesbaden, Germany: Springer Vieweg, 2019, pp. 461–482, ISBN: 978-3-658-22049-5. DOI: 10.1007/978-3-658-22050-1_31.

- [184] K. Löhe, G. Roppenecker and T. Zehelein, „Modellierung und Parametrierung stochastischer Fahrbahnunebenheiten mit Hub-, Wank-, Nick- und Verspannanteil: Modeling and Parametrization of Stochastic Road Unevenness with Lift, Roll, Pitch and Torsion Component,“ in *Reifen-Fahrwerk-Fahrbahn 2015: 15. internationale VDI-Tagung ; 4. VDI-Fachkonferenz Innovative Bremstechnik, Hannover, 14. und 15. Oktober 2015* (VDI-Berichte). vol. 2241 Düsseldorf: VDI-Verl., 2015, ISBN: 9783180922416.
- [185] K. Löhe, G. Roppenecker and T. Zehelein, „Ein modulares Konzept zur Fahrbahngüteschätzung und Kalman-Filter-Adaption mittels autoregressiver Filterung: A Modular Concept for Road Quality Estimation and Kalman Filter Adaptation by Autoregressive Filtering,“ in *Autoreg 2015: Auf dem Weg zum automatisierten Fahren ; 7. Fachtagung in Baden-Baden, 09. und 10. Juni 2015* (VDI-Berichte). vol. 2233 Düsseldorf: VDI-Verl., 2015, ISBN: 9783180922331.

Non-dissertation relevant publications; not Scopus/ Web of Science listed (not peer-reviewed)

M. Schmidt, T. Zehelein and M. Lienkamp, „Chassis design of the aCar – a light commercial vehicle for Sub-Saharan Africa,“ in *9th International Munich Chassis Symposium 2018: Chassis.tech plus* (Proceedings), P. E. Pfeffer, ed. Wiesbaden, Germany: Springer Vieweg, 2019, pp. 89–104, ISBN: 978-3-658-22049-5. DOI: 10.1007/978-3-658-22050-1_10.

Dissertation relevant open source software

- [196] T. Zehelein. „*Damper Defect Detection Using Machine Learning*,“ 2020. Available: <https://github.com/TUMFTM/Damper-Defect-Detection-using-Machine-Learning>.
- [253] T. Zehelein and T. Hemmert-Pottmann. „*Damper Defect Detection Using CNN*,“ 2019. Available: <https://github.com/TUMFTM/Damper-Defect-Detection-Using-CNN>.

Supervised Student's Theses

The following student's theses were developed within the framework of the dissertation under the author's supervision in terms of content, subject matter and scientific research. In the following, the Bachelor, Semester and Master theses relevant and related to this dissertation are listed. Many thanks to the editors for their extensive support within the framework of this research project

- [75] C. Gangkofer, „Umsetzung von Fahrwerkdefekten mit fahrdynamischen Messungen und Potentialanalyse für ein Fahrwerkdiagnoseverfahren: Implementation of chassis defects with vehicle dynamics tests and potential analysis of a chassis defects diagnostic method,“ Semester's Thesis, Technical University of Munich, Munich, 2018.
- [203] A. Merk, „Dämpferdefektdetektion & -diagnose mittels Künstlicher Intelligenz: Damper defect detection and diagnosis by artificial intelligence,“ Master's Thesis, Technical University of Munich, Munich, 2018.
- [204] A. Bykanov, „Weiterentwicklung eines Machine Learning- Konzepts zur Diagnose defekter Fahrwerksdämpfer: Improvement of a Machine Learning Concept for Diagnosing Damper Defects,“ Semester's Thesis, Technical University of Munich, Munich, 2018.
- [208] P. Werk, „Dämpferdefektdiagnose mittels Deep Learning basierend auf unüberwachtem Lernen von Merkmalen: Damper Diagnosis using Deep Learning based on unsupervised Feature Learning,“ Master's Thesis, Technical University of Munich, Munich, 2018.
- [209] R. F. Trumpp, „Defekterkennung von Fahrzeugdämpfern mittels Deep Learning-basierter Novelty Detection: Deep Learning-Based Novelty Detection of Automotive Chassis Damper Defects,“ Semester's Thesis, Technical University of Munich, Munich, 2019.
- [236] S. Schuck, „Anomaliedetektion mittels Machine Learning in der Dämpferdiagnose: Anomaly Detection using Machine Learning for Damper Diagnosis,“ Master's Thesis, Technical University of Munich, Munich, 2019.
- [252] T. Hemmert-Pottmann, „Dämpferdefektdiagnose mittels der Deep Learning Architektur Convolutional Neural Networks: Diagnosing Damper Defects using the Deep Learning Architecture Convolutional Neural Networks,“ Master's Thesis, Technical University of Munich, Munich, 2018.
- [294] M. Faist, „Umsetzung und Analyse realer Dämpferdefekte zur Fahrwerkdiagnose: Implementation and Analysis of Damper Defects for Chassis System Diagnosis,“ Semester's Thesis, Technical University of Munich, Munich, 2019.
- L. Perotti, „Modellbasierte Systemanalyse für eine Fahrwerkdefekterkennung mittels ESP-Sensorik: Model based system analysis for detection of defects in suspension systems by ESC sensors,“ Semester's Thesis, Technical University of Munich, Munich, 2018.

- B. Vorweg, „Umsetzung von Fahrwerksdefekten anhand eines Zweispurmodells und eines Versuchsfahrzeugs und Abschätzung des Diagnosepotentials: Implementation of chassis defects based on a two-track model and a test vehicle and assessment of the diagnostic potential,“ Master’s Thesis, Technical University of Munich, Munich, 2018.
- S. Schaer, „Dämpferdefekterkennung mittels Raddrehzahl-Frequenzanalyse: Detection of damper defects using wheel speed frequency analysis,“ Semester’s Thesis, Technical University of Munich, Munich, 2018.
- F. Müller, „Parametrierung und Validierung eines Zweispurmodells für ein Versuchsfahrzeug: Parametrization and validation of a two-track model for a test vehicle in Matlab Simulink,“ Semester’s Thesis, Technical University of Munich, Munich, 2017.
- F. Schwencke, „Ausgestaltung, konstruktive Umsetzung und Aufbau des aCar Fahrwerks: Design and Implementation of the aCar Chassis Systems,“ Bachelor’s Thesis, Technical University of Munich, Munich, 2017.
- A. Sticht, „Messdatenbasierte Fahrzustandsschätzung mittels Neuronaler Netze: Data driven vehicle dynamics state estimation using Neural Networks,“ Master’s Thesis, Technical University of Munich, Munich, 2017.
- B. Vorweg, „Optimierung von Fahrwerk und Lenkung unter Berücksichtigung von Kinematik, Package und Ergonomie im aCar-mobility-Projekt: Optimization of the chassis and steering system considering kinematics, package and ergonomics in the aCar-mobility project,“ Semester’s Thesis, Technical University of Munich, Munich, 2017.
- L. Arutyunov-Sincuk, „Analyse und Modellierung der Eigenschaftsveränderung von defekten Fahrwerkskomponenten und deren Auswirkung auf die Fahrdynamik: Analysis and modelling of variations of defective chassis component characteristics and their impact on vehicle dynamics,“ Bachelor’s Thesis, Technical University of Munich, Munich, 2017.
- O. Cameron, „Fahrdynamische Optimierung des aCar mittels Mehrkörpersimulation: aCar vehicle dynamics optimization using multi-body simulation,“ Master’s Thesis, Technical University of Munich, Munich, 2017.
- A. Sticht, „Weiterentwicklung einer adaptiven Kalman-Filter-basierten Schwimmwinkel- und Fahrbahnneigungsschätzung: Evolution of an adaptive Kalman-filter-based sideslip angle and bank angle estimation,“ Semester’s Thesis, Technical University of Munich, Munich, 2017.
- M. Böhme, „Potenzialanalyse zur Diagnose des Fahrverhaltens: Potential assessment of vehicle dynamics diagnosis systems,“ Bachelor’s Thesis, Technical University of Munich, Munich, 2016.
- C. Knies, „Potentialanalyse zur Fahrzustandsschätzung mittels Neuronaler Netze: Investigation of driving state estimation using neural networks,“ Master’s Thesis, Technical University of Munich, Munich, 2016.
- M. Weber, „Konstruktive Umsetzung eines Fahrwerks für das aCar - Ein leichtes Nutzfahrzeug für die Subsahara-Region: Design of a suspension system for the aCar - a light commercial vehicle for the Subsahara region,“ Bachelor’s Thesis, Technical University of Munich, Munich, 2016.
- T. Hierlmeier, „Auslegung und Umsetzung eines Lenksystems für das aCar - einem leichten Nutzfahrzeug: Design of a steering system for the aCar - a lightweight commercial vehicle,“ Semester’s Thesis, Technical University of Munich, Munich, 2016.

K. Medrisch, „Schwimmwinkel- und Fahrbahnneigungsschätzung auf Basis von ESP-Sensorik: Estimation of vehicle sideslip angle and road bank angle with ESC sensors,“ Master’s Thesis, Technical University of Munich, Munich, 2016.

F. Otter, „Konzeptstudie zur Schätzung des Reifenluftdrucks: Concept study of vehicle tire pressure estimation,“ Semester’s Thesis, Technical University of Munich, Munich, 2015.

E. Olcay, „Evaluation verschiedener Regelkonzepte eines Torque Vectoring Systems: Evaluation of different control concepts for a torque vectoring system,“ Semester’s Thesis, Technical University of Munich, Munich, 2015.

A. Metz, „Aufbau eines Setup-Tools zur fahrdynamischen Auslegung eines Formula Student Rennwagens: Development of a setup tool for vehicle dynamics analysis of a formula student race car,“ Semester’s Thesis, Technical University of Munich, Munich, 2015.

Appendix

A	Observability Analysis	xxxvii
A.1	Derivation of System Equations	xxxvii
A.2	Analysis of Observability with Known Road Excitation	xxxviii
A.3	Calculation of Fréchet derivative	xxxix
A.4	Parameters for Numeric Investigation of Stochastic Observability	xl
A.5	Analysis of Observability with Unknown Road Excitation and Unknown Road Class	xl
B	Manual Feature Set	xliii
C	Results	xliv
C.1	Description of the Dataset	xliv
C.2	Investigation of Feature Characteristics	l
C.2.1	Autoencoder Features	li
C.2.2	Sparsefilter Features	lii
C.3	Analysis of Influence of Vehicle Speed and Road Roughness	liii
C.4	Comparison with Signal-Based Approach	liii

A Observability Analysis

A.1 Derivation of System Equations

The following derivation of the equations of the quarter vehicle is based on [17, pp. 28-29]. The vertical displacement coordinates are chosen so that their zero positions are at the system's static equilibrium. The equilibrium of forces for the mass of the sprung vehicle body and the unsprung tire and axle gives

$$m_{Bo} \ddot{z}_{Bo} = -c_{z,Bo} (z_{Bo} - z_T) - d_{z,Bo} (\dot{z}_{Bo} - \dot{z}_T) \quad (A.1)$$

$$m_T \ddot{z}_T = c_{z,Bo} (z_{Bo} - z_T) + d_{z,Bo} (\dot{z}_{Bo} - \dot{z}_T) + \Delta F_{z,C}. \quad (A.2)$$

When neglecting the small vertical damping of the tire [1, p. 56], the vertical force in the tire contact patch is based on the tire deflection by [17, p. 28]

$$\Delta F_{z,C} = -c_{z,T} (z_T - z_R) \quad (A.3)$$

with the vertical tire stiffness $c_{z,T}$ and the displacement of the unsprung mass of the tire and axle z_T and the road excitation z_R . The states of the quarter-vehicle model are selected as¹

$$\mathbf{x} = \begin{bmatrix} x_1 \\ x_2 \\ x_3 \\ x_4 \end{bmatrix} = \begin{bmatrix} z_T \\ \dot{z}_T \\ z_{Bo} \\ \dot{z}_{Bo} \end{bmatrix} \quad (A.4)$$

with the vertical displacement of the unsprung mass of the tire and axle z_T and its velocity \dot{z}_T as well as the vertical displacement of the sprung mass of the vehicle body z_{Bo} and its velocity \dot{z}_{Bo} . The road excitation is selected as input of the system $u = z_R$ and the deviation of the vertical tire force in the contact patch is selected as output of the system $y = \Delta F_{z,C}$. The system equations of the quarter-vehicle model in matrix notation are then given by

$$\dot{\mathbf{x}} = \begin{bmatrix} 0 & 1 & 0 & 0 \\ -\frac{c_{z,Bo} + c_{z,T}}{m_T} & -\frac{d_{z,Bo}}{m_T} & \frac{c_{z,Bo}}{m_T} & \frac{d_{z,Bo}}{m_T} \\ 0 & 0 & 0 & 1 \\ \frac{c_{z,Bo}}{m_{Bo}} & \frac{d_{z,Bo}}{m_{Bo}} & -\frac{c_{z,Bo}}{m_{Bo}} & -\frac{d_{z,Bo}}{m_{Bo}} \end{bmatrix} \mathbf{x} + \begin{bmatrix} 0 \\ \frac{c_{z,T}}{m_T} \\ 0 \\ 0 \end{bmatrix} u \quad (A.5)$$

$$y = [-c_{z,T} \ 0 \ 0 \ 0] \mathbf{x} + c_{z,T} u. \quad (A.6)$$

¹For readability, the time-dependence of states $x(t)$, output $y(t)$ and input $u(t)$ is not shown

A.2 Analysis of Observability with Known Road Excitation

The calculations of the observability analysis were performed using the Matlab Symbolic Math Toolbox because of the complexity of the resulting equations. The resulting intermediate equations are given in this section.

The Lie-derivatives of Section 3.3 according to Equations (3.13) and (3.14) are as follows:

$$g = \frac{v}{2 r_{w,dyn,0} \pi} - \frac{c_{z,T} v (u - x_1)}{2 c_{r,dyn,F,C} r_{w,dyn,0}^2 \pi} \quad (A.7)$$

$$h_1 = - \frac{c_{z,T} v (\dot{u} - x_2)}{2 c_{r,dyn,F,C} r_{w,dyn,0}^2 \pi} \quad (A.8)$$

$$h_2 = - \frac{c_{z,T} v (\ddot{u} m_T - c_{z,T} u + c_{Bo} x_1 - c_{z,Bo} x_3 + c_{z,T} x_1 + d_{z,Bo,0} x_2 - d_{z,Bo,0} x_4 + x_2 x_5 - x_4 x_5)}{2 c_{r,dyn,F,C} m_T r_{w,dyn,0}^2 \pi} \quad (A.9)$$

$$h_3 = - \frac{c_{z,T} v}{2 c_{r,dyn,F,C} m_T^2 m_{Bo} r_{w,dyn,0}^2 \pi} * \left(d_{z,Bo,0}^2 m_T x_4 - d_{z,Bo,0}^2 m_T x_2 - d_{z,Bo,0}^2 m_{Bo} x_2 + d_{z,Bo,0}^2 m_{Bo} x_4 - m_T x_2 x_5^2 + m_T x_4 x_5^2 - m_{Bo} x_2 x_5^2 + m_{Bo} x_4 x_5^2 + u^{(3)} m_T^2 m_{Bo} - c_{z,T} \dot{u} m_T m_{Bo} + c_{z,T} d_{z,Bo,0} m_{Bo} u - c_{z,Bo} d_{z,Bo,0} m_T x_1 + c_{z,Bo} d_{z,Bo,0} m_T x_3 - c_{z,Bo} d_{z,Bo,0} m_{Bo} x_1 + c_{z,Bo} d_{z,Bo,0} m_{Bo} x_3 - c_{z,T} d_{z,Bo,0} m_{Bo} x_1 + c_{z,Bo} m_T m_{Bo} x_2 - c_{z,Bo} m_T m_{Bo} x_4 + c_{z,T} m_T m_{Bo} x_2 + c_{z,T} m_{Bo} u x_5 - c_{z,Bo} m_T x_1 x_5 + c_{z,Bo} m_T x_3 x_5 - c_{z,Bo} m_{Bo} x_1 x_5 + c_{z,Bo} m_{Bo} x_3 x_5 - c_{z,T} m_{Bo} x_1 x_5 - 2 d_{z,Bo,0} m_T x_2 x_5 + 2 d_{z,Bo,0} m_T x_4 x_5 - 2 d_{z,Bo,0} m_{Bo} x_2 x_5 + 2 d_{z,Bo,0} m_{Bo} x_4 x_5 \right) \quad (A.10)$$

$$h_4 = \frac{c_{z,T}^2 \ddot{u} v}{2 c_{r,dyn,F,C} m_T r_{w,dyn,0}^2 \pi} - \frac{c_{z,T} u^{(4)} v}{2 c_{r,dyn,F,C} r_{w,dyn,0}^2 \pi} - \frac{c_{z,T}^2 \dot{u} v (d_{z,Bo,0} + x_5)}{2 c_{r,dyn,F,C} m_T^2 r_{w,dyn,0}^2 \pi} - \frac{c_{z,T} v (c_{z,Bo} x_1 - c_{z,Bo} x_3 + d_{z,Bo,0} x_2 - d_{z,Bo,0} x_4 + x_2 x_5 - x_4 x_5)}{2 c_{r,dyn,F,C} m_T^2 m_{Bo}^2 r_{w,dyn,0}^2 \pi} * \left(d_{z,Bo,0}^2 (m_T + m_{Bo}) + x_5^2 (m_T + m_{Bo}) - c_{z,Bo} m_T m_{Bo} + 2 d_{z,Bo,0} (m_T + m_{Bo}) x_5 \right) + \frac{c_{z,T} v (c_{z,T} u - c_{z,Bo} x_1 + c_{z,Bo} x_3 - c_{z,T} x_1 - d_{z,Bo,0} x_2 + d_{z,Bo,0} x_4 - x_2 x_5 + x_4 x_5)}{2 c_{r,dyn,F,C} m_T^3 m_{Bo} r_{w,dyn,0}^2 \pi} * \left(d_{z,Bo,0}^2 (m_T + m_{Bo}) + x_5^2 (m_T + m_{Bo}) - m_T m_{Bo} (c_{z,Bo} + c_{z,T}) + 2 d_{z,Bo,0} (m_T + m_{Bo}) x_5 \right) + \frac{c_{z,T} v x_2 (d_{z,Bo,0} + x_5) (c_{z,Bo} m_T + c_{z,Bo} m_{Bo} + c_{z,T} m_{Bo})}{2 c_{r,dyn,F,C} m_T^2 m_{Bo} r_{w,dyn,0}^2 \pi} - \frac{c_{z,Bo} c_{z,T} v x_4 (m_T + m_{Bo}) (d_{z,Bo,0} + x_5)}{2 c_{r,dyn,F,C} m_T^2 m_{Bo} r_{w,dyn,0}^2 \pi} \quad (A.11)$$

The Jacobian matrix

$$Q(x, u, \dot{u}, \ddot{u}, \dots, u^{(n-1)}) = \frac{\partial q(x, u, \dot{u}, \ddot{u}, \dots, u^{(n-1)})}{\partial x} \quad (A.12)$$

is not displayed here because of its size.

The full determinant $\det \mathbf{Q}(\mathbf{x}, \mathbf{u}, \dot{\mathbf{u}}, \ddot{\mathbf{u}}, \dots, \mathbf{u}^{(n-1)})$ (not evaluated at an operating point \mathbf{x}_0) is

$$\begin{aligned} \det \mathbf{Q}(\mathbf{x}, \mathbf{u}, \dot{\mathbf{u}}, \ddot{\mathbf{u}}, \dots, \mathbf{u}^{(n-1)}) &= -\frac{c_{z,\text{Bo}}^2 c_{z,\text{T}}^5 \nu^5}{32 c_{r,\text{dyn},\text{FC}}^5 m_{\text{T}}^5 m_{\text{Bo}}^2 r_{w,\text{dyn},0}^{10} \pi^5} * \\ &* \left(d_{z,\text{Bo},0}^2 m_{\text{T}}^2 x_2 - d_{z,\text{Bo},0}^2 m_{\text{T}}^2 x_4 + d_{z,\text{Bo},0}^2 m_{\text{Bo}}^2 x_2 - d_{z,\text{Bo},0}^2 m_{\text{Bo}}^2 x_4 + m_{\text{T}}^2 x_2 x_5^2 \right. \\ &- m_{\text{T}}^2 x_4 x_5^2 + m_{\text{Bo}}^2 x_2 x_5^2 - m_{\text{Bo}}^2 x_4 x_5^2 + c_{z,\text{T}} \dot{u} m_{\text{T}} m_{\text{Bo}}^2 - c_{z,\text{T}} d_{z,\text{Bo},0} m_{\text{Bo}}^2 u \\ &+ c_{z,\text{Bo}} d_{z,\text{Bo},0} m_{\text{T}}^2 x_1 - c_{z,\text{Bo}} d_{z,\text{Bo},0} m_{\text{T}}^2 x_3 + c_{z,\text{Bo}} d_{z,\text{Bo},0} m_{\text{Bo}}^2 x_1 - c_{z,\text{Bo}} d_{z,\text{Bo},0} m_{\text{Bo}}^2 x_3 \\ &+ c_{z,\text{T}} d_{z,\text{Bo},0} m_{\text{Bo}}^2 x_1 - c_{z,\text{Bo}} m_{\text{T}} m_{\text{Bo}}^2 x_2 - c_{z,\text{Bo}} m_{\text{T}}^2 m_{\text{Bo}}^2 x_2 + c_{z,\text{Bo}} m_{\text{T}} m_{\text{Bo}}^2 x_4 \\ &+ c_{z,\text{Bo}} m_{\text{T}}^2 m_{\text{Bo}}^2 x_4 - c_{z,\text{T}} m_{\text{T}} m_{\text{Bo}}^2 x_2 + 2 d_{z,\text{Bo},0}^2 m_{\text{T}} m_{\text{Bo}}^2 x_2 - 2 d_{z,\text{Bo},0}^2 m_{\text{T}} m_{\text{Bo}}^2 x_4 \\ &- c_{z,\text{T}} m_{\text{Bo}}^2 u x_5 + c_{z,\text{Bo}} m_{\text{T}}^2 x_1 x_5 - c_{z,\text{Bo}} m_{\text{T}}^2 x_3 x_5 + c_{z,\text{Bo}} m_{\text{Bo}}^2 x_1 x_5 - c_{z,\text{Bo}} m_{\text{Bo}}^2 x_3 x_5 \\ &+ c_{z,\text{T}} m_{\text{Bo}}^2 x_1 x_5 + 2 d_{z,\text{Bo},0} m_{\text{T}}^2 x_2 x_5 - 2 d_{z,\text{Bo},0} m_{\text{T}}^2 x_4 x_5 + 2 d_{z,\text{Bo},0} m_{\text{Bo}}^2 x_2 x_5 \\ &- 2 d_{z,\text{Bo},0} m_{\text{Bo}}^2 x_4 x_5 + 2 m_{\text{T}} m_{\text{Bo}}^2 x_2 x_5^2 - 2 m_{\text{T}} m_{\text{Bo}}^2 x_4 x_5^2 - c_{z,\text{T}} d_{z,\text{Bo},0} m_{\text{T}} m_{\text{Bo}}^2 u \\ &+ 2 c_{z,\text{Bo}} d_{z,\text{Bo},0} m_{\text{T}} m_{\text{Bo}}^2 x_1 - 2 c_{z,\text{Bo}} d_{z,\text{Bo},0} m_{\text{T}} m_{\text{Bo}}^2 x_3 + c_{z,\text{T}} d_{z,\text{Bo},0} m_{\text{T}} m_{\text{Bo}}^2 x_1 \\ &- c_{z,\text{T}} m_{\text{T}} m_{\text{Bo}}^2 u x_5 + 2 c_{z,\text{Bo}} m_{\text{T}} m_{\text{Bo}}^2 x_1 x_5 - 2 c_{z,\text{Bo}} m_{\text{T}} m_{\text{Bo}}^2 x_3 x_5 + c_{z,\text{T}} m_{\text{T}} m_{\text{Bo}}^2 x_1 x_5 \\ &\left. + 4 d_{z,\text{Bo},0} m_{\text{T}} m_{\text{Bo}}^2 x_2 x_5 - 4 d_{z,\text{Bo},0} m_{\text{T}} m_{\text{Bo}}^2 x_4 x_5 \right) \end{aligned} \quad (\text{A.13})$$

A.3 Calculation of Fréchet derivative

The Fréchet derivative $L_y(\mathbf{x}_0, \mathbf{e}_i)$ of a function y at \mathbf{x}_0 that is linear in the direction \mathbf{e}_i is defined in [193, p. 1, 295, p. 226] as

$$y(\mathbf{x}_0 + \mathbf{e}_i) - y(\mathbf{x}_0) - L_y(\mathbf{x}_0, \mathbf{e}_i) = o(\|\mathbf{e}_i\|) \quad (\text{A.14})$$

with a rest term $o(\|\mathbf{e}_i\|)$ that is linear in \mathbf{e}_i [296, pp. 50-51]. A Fréchet derivative is also a Gâteaux derivative [295, p. 227] and it is therefore possible to calculate the Gâteaux derivative that is defined in [295, pp. 226-227, 193, p. 4] as

$$L_y(\mathbf{x}_0, \mathbf{e}_i) = \lim_{\nu \rightarrow 0} \frac{y(\mathbf{x}_0 + \nu \mathbf{e}_i) - y(\mathbf{x}_0)}{\nu}. \quad (\text{A.15})$$

Higher orders of Fréchet derivatives are defined recursively [295, p. 228, 193, p. 3]. The k -th Fréchet derivative can also be described as a mixed partial derivative [193, p. 3]

$$L_y^{(k)}(\mathbf{x}_0, \mathbf{e}_1, \dots, \mathbf{e}_k) = \frac{\partial}{\partial \nu_1} \dots \frac{\partial}{\partial \nu_k} \Big|_{(\nu_1, \dots, \nu_k)=0} y(\mathbf{x}_0 + \nu_1 \mathbf{e}_1 + \dots + \nu_k \mathbf{e}_k). \quad (\text{A.16})$$

A.4 Parameters for Numeric Investigation of Stochastic Observability

Table A.1: Parameters for numeric investigation of observability in Section 3.5 and Section 3.6

Symbol	Value	Description	Source
$c_{z,Bo}$	$2.8 \times 10^4 \frac{N}{m}$	stiffness of vehicle body spring	[17, p. 124]
$c_{z,T}$	$3.9 \times 10^5 \frac{N}{m}$	stiffness of tire spring in z -direction	[17, p. 124]
$d_{z,Bo,0}$	$2.1 \times 10^3 \frac{Ns}{m}$	stationary value of vehicle body damping coefficient	[17, p. 124]
m_T	55.1 kg	unsprung mass	[17, p. 124]
m_{Bo}	458.4 kg	sprung mass of vehicle	[17, p. 124]
$r_{dyn,0}$	0.318 m	stationary value of dynamic tire radius	[17, p. 124]
$c_{r,dyn,F,C}$	-1.6×10^6 m	stiffness coefficient between tire load and dynamic tire radius	[17, p. 124]
v	$100 \frac{km}{h}$	vehicle speed	-
$a_{z,R}$	$1 \times 10^{-9} \frac{1}{m}$	road category parameter, selected slightly different from 0 to comply with requirement in Section 3.4	[186, p. 358]
$b_{z,R}$	3.5×10^{-3}	road category parameter for category C	[186, p. 358]

A.5 Analysis of Observability with Unknown Road Excitation and Unknown Road Class

The full result to Equations (3.44) in Section 3.6 is

$$\begin{aligned}
\det Q(\mathbf{x}, \mathbf{u}, \dot{\mathbf{u}}, \ddot{\mathbf{u}}, \dots, \mathbf{u}^{(n-1)}) \Big|_{\mathbf{x}_0} &= \frac{a_{z,R}^2 b_{z,R,0}^2 c_{z,Bo}^2 c_{z,T}^8 d_{z,Bo,0} v^{11}}{128 c_{r,dyn,F,C}^7 m_T^8 m_{Bo}^4 r_{dyn,0}^{14} \pi^7} * \\
&* (c_{z,Bo} m_T + c_{z,Bo} m_{Bo} - a_{z,R} d_{z,Bo,0} m_T v - a_{z,R} d_{z,Bo,0} m_{Bo} v + a_{z,R}^2 m_T m_{Bo} v^2) * \\
&* (u^{(5)} \dot{u} m_T^3 m_{Bo}^3 - c_{z,Bo} u^{(2)2} m_T^3 m_{Bo}^2 - u^{(4)} u^{(2)} m_T^3 m_{Bo}^3 - c_{z,Bo} u^{(2)2} m_T^2 m_{Bo}^3 \\
&- d_{z,Bo,0}^3 u^{(3)} m_T^3 u - d_{z,Bo,0}^3 u^{(3)} m_{Bo}^3 u + c_{z,Bo} u^{(3)} \dot{u} m_T^2 m_{Bo}^3 + c_{z,Bo} u^{(3)} \dot{u} m_T^3 m_{Bo}^2 \\
&- d_{z,Bo,0} u^{(3)} u^{(2)} m_T^2 m_{Bo}^3 - d_{z,Bo,0} u^{(3)} u^{(2)} m_T^3 m_{Bo}^2 + d_{z,Bo,0}^2 u^{(3)} \dot{u} m_T m_{Bo}^3 \\
&+ d_{z,Bo,0}^2 u^{(3)} \dot{u} m_T^3 m_{Bo} + 2 d_{z,Bo,0} u^{(4)} \dot{u} m_T^2 m_{Bo}^3 + 2 d_{z,Bo,0} u^{(4)} \dot{u} m_T^3 m_{Bo}^2 \\
&- c_{z,Bo} d_{z,Bo,0}^2 u^{(2)} m_T^3 u - c_{z,Bo} d_{z,Bo,0}^2 u^{(2)} m_{Bo}^3 u + c_{z,Bo} u^{(4)} m_T^2 m_{Bo}^3 u \\
&+ c_{z,Bo} u^{(4)} m_T^3 m_{Bo}^2 u + c_{z,Bo}^2 u^{(2)} m_T m_{Bo}^3 u + c_{z,Bo}^2 u^{(2)} m_T^3 m_{Bo} u \\
&+ c_{z,T} u^{(4)} m_T^2 m_{Bo}^3 u - 3 d_{z,Bo,0}^3 u^{(3)} m_T m_{Bo}^2 u - 3 d_{z,Bo,0}^3 u^{(3)} m_T^2 m_{Bo} u \\
&- 2 d_{z,Bo,0}^2 u^{(4)} m_T m_{Bo}^3 u - 2 d_{z,Bo,0}^2 u^{(4)} m_T^3 m_{Bo} u - d_{z,Bo,0} u^{(5)} m_T^2 m_{Bo}^3 u \\
&- d_{z,Bo,0} u^{(5)} m_T^3 m_{Bo}^2 u + 2 d_{z,Bo,0}^2 u^{(3)} \dot{u} m_T^2 m_{Bo}^2 + 2 c_{z,Bo}^2 u^{(2)} m_T^2 m_{Bo}^2 u \\
&- 4 d_{z,Bo,0}^2 u^{(4)} m_T^2 m_{Bo}^2 u + c_{z,Bo} d_{z,Bo,0} u^{(2)} \dot{u} m_T m_{Bo}^3 + c_{z,Bo} d_{z,Bo,0} u^{(2)} \dot{u} m_T^3 m_{Bo} \\
&+ c_{z,Bo} c_{z,T} u^{(2)} m_T m_{Bo}^3 u + c_{z,T} d_{z,Bo,0} u^{(3)} m_T m_{Bo}^3 u + 2 c_{z,Bo} d_{z,Bo,0} u^{(2)} \dot{u} m_T^2 m_{Bo}^2 \\
&+ c_{z,Bo} c_{z,T} u^{(2)} m_T^2 m_{Bo}^2 u - 3 c_{z,Bo} d_{z,Bo,0}^2 u^{(2)} m_T m_{Bo}^2 u \\
&- 3 c_{z,Bo} d_{z,Bo,0}^2 u^{(2)} m_T^2 m_{Bo} u + c_{z,T} d_{z,Bo,0} u^{(3)} m_T^2 m_{Bo}^2 u)
\end{aligned} \tag{A.17}$$

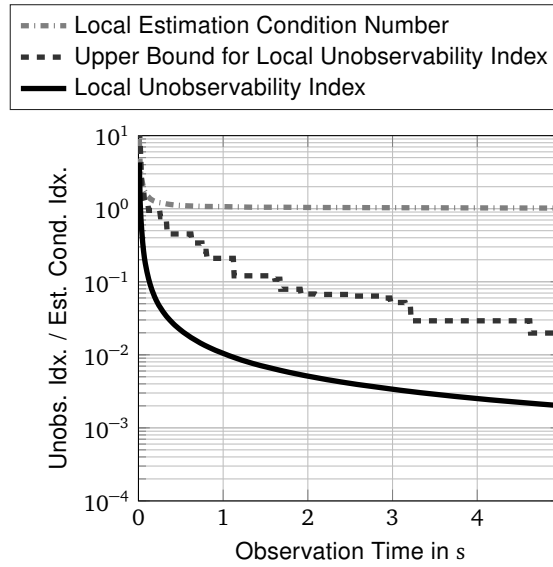
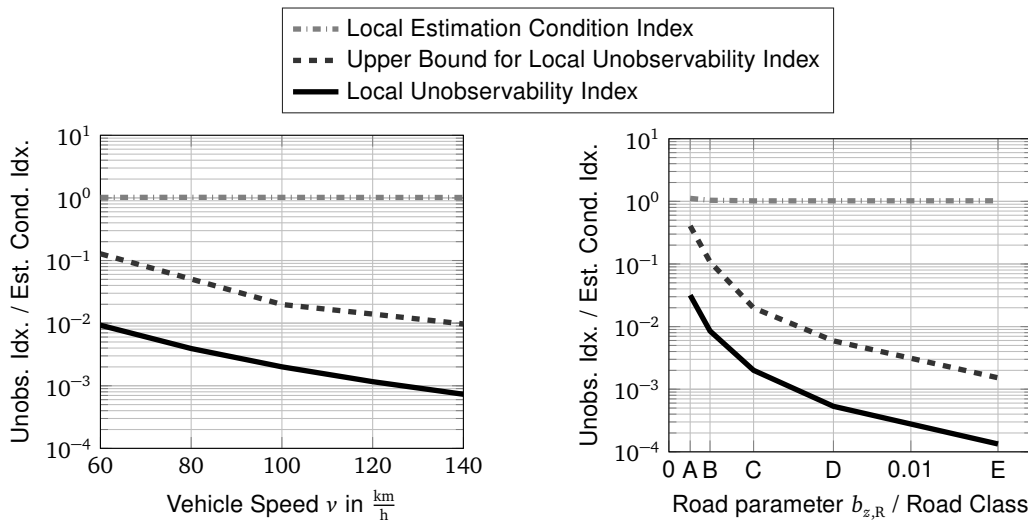


Figure A.1: Estimation condition number, unobservability index and maximum upper bound of the stochastic system with unknown road excitation and unknown road class for a vehicle speed $v = 100 \frac{\text{km}}{\text{h}}$ and a simulated class C road



(a) Varying vehicle speed v and fixed unknown road class of category C with $b_{z,R} = 0.0035$

(b) Varying unknown road class $b_{z,R}$ and fixed vehicle speed $v = 100 \frac{\text{km}}{\text{h}}$

Figure A.2: Visualization of local estimation condition index, local unobservability index and maximum upper bound of the local unobservability index for varying vehicle speed and varying unknown road class for an observation time of $t = 5$ s

B Manual Feature Set

Table B.1: Summary of manual features for SML classification. Feature generation methods that result in a “in total” amount of features are based on the assumption of 7 sensor signals.

Description of Feature Generation Method	Number of features
Maximal value of the time signal	1 (per sensor signal)
Minimal value of the time signal	1 (per sensor signal)
Range of maximal to minimal value of the time signal data points of each sensor signal	1 (per sensor signal)
Euclidean vector norm of the time signal data points of each sensor signal	1 (per sensor signal)
Mean of the absolute deviation from the mean value	1 (per sensor signal)
Sum of absolute differences of consecutive data samples of each sensor signal	1 (per sensor signal)
3rd-order autocovariance (sum of product of three lagged data points of each sensor similar to [299, Eq. 5])	1 (per sensor signal)
Square root of cumulative sum of time series differences $\sqrt{\sum_{n=3}^N (x_n - x_{n-2})}$	1 (per sensor signal)
Accumulated square of signal amplitude (proportional to signal energy)	1 (per sensor signal)
Interquartile range of the time signal data points of each sensor signal	1 (per sensor signal)
Standard deviation of the time signal data points of each sensor signal	1 (per sensor signal)
Skewness of the time signal data points of each sensor signal	1 (per sensor signal)
Kurtosis of the time signal data points of each sensor signal	1 (per sensor signal)
Crest factor of the time signal data points of each sensor signal	1 (per sensor signal)
Parameters of an auto-regressive signal model of 10th order that is fitted on the time signal data points of each sensor signal for each observation [120, p. 11]	10 (per sensor signal)
Correlation coefficient of two different sensor signals	21 (in total)
Singular value decomposition of a matrix that contains the time signal data points of each sensor signal as columns for each observation	7 (in total)
Normalized singular values relative to the highest calculated singular value for each observation	7 (in total)
Auto-correlation coefficient for 1 to 8 lags of sample points [120, pp. 11-12]	8 (per sensor signal)
Sample entropy as measure of the complexity of a time signal	1 (per sensor signal)
Log-energy entropy of a signal $E(s) = \sum_{n=1}^N \log(s_n^2)$ with the convention $\log(0) = 0$ for a signal s with its data points s_n [283, p. 2]	1 (per sensor signal)
Shannon entropy of each sensor time signal	1 (per sensor signal)
Approximate entropy of each sensor time signal	1 (per sensor signal)
Estimated mean frequency of the time signal of each sensor	1 (per sensor signal)
Signal energy calculated as sum of the square of the FFT of each sensor signal	1 (per sensor signal)
Frequency band energy of a sensor signal in the frequency ranges 1 Hz to 5 Hz, 5 Hz to 10 Hz, 10 Hz to 15 Hz, 15 Hz to 20 Hz, 20 Hz to 25 Hz	5 (per sensor signal)
Frequency band energy in frequency range around vertical tire eigenfrequency	1 (per sensor signal)
Amplitude and frequency location of signal spectrum at peak of vertical tire eigenfrequency	2 (per sensor signal)
Amplitude and frequency location of signal spectrum at peak of vertical vehicle body eigenfrequency	2 (per sensor signal)
Ratio of signal amplitudes at vertical tire and vehicle body eigenfrequency	1 (per sensor signal)

C Results

C.1 Description of the Dataset

The following graphs show the distribution of different properties of each observation (e.g. mean vehicle speed of an observation) for the different datasets.

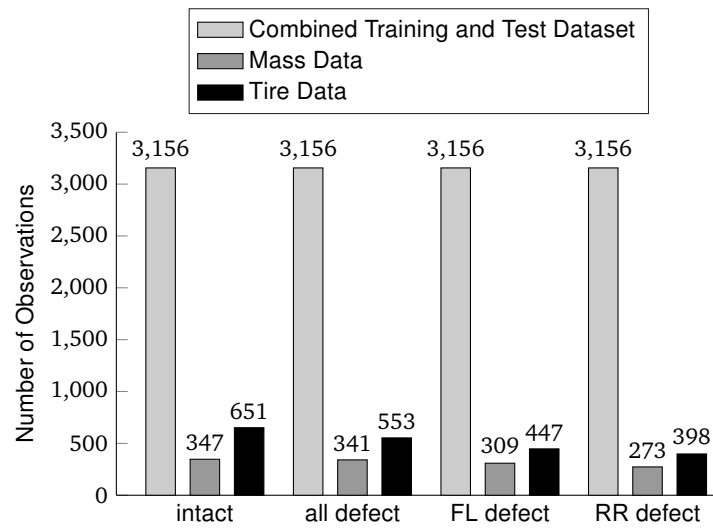


Figure C.1: Distribution of vehicle health class for all datasets

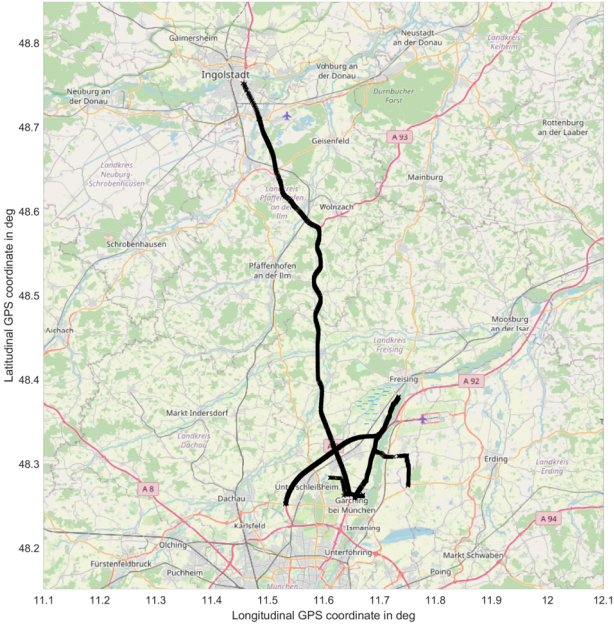


Figure C.2: Geographic map of the full dataset (combined training and testing data). The black lines consists of many crosses. Each cross represents the location of an observation.



Figure C.3: Geographic map of the mass dataset. The black lines consists of many crosses. Each cross represents the location of an observation.

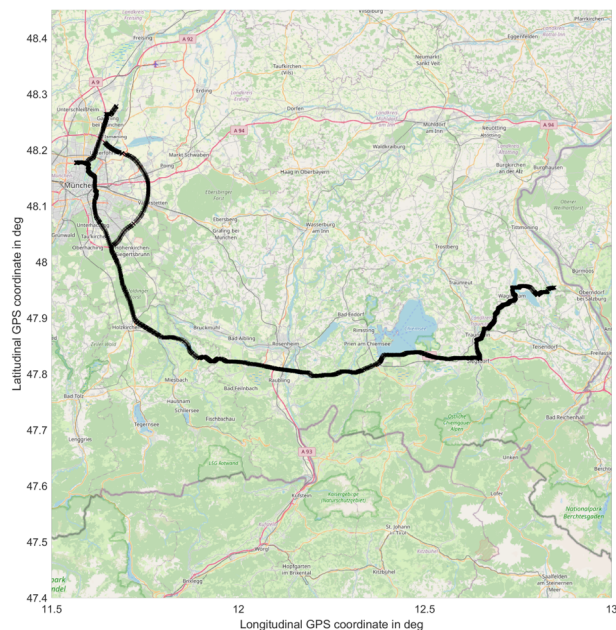
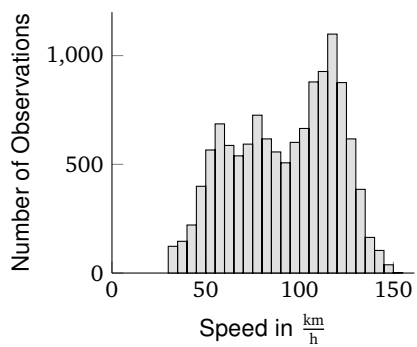
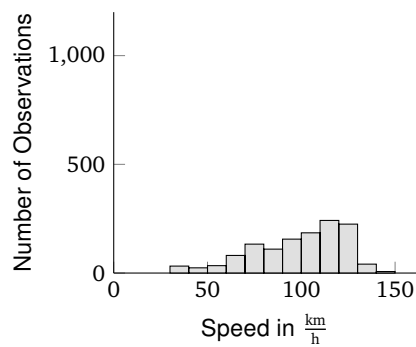


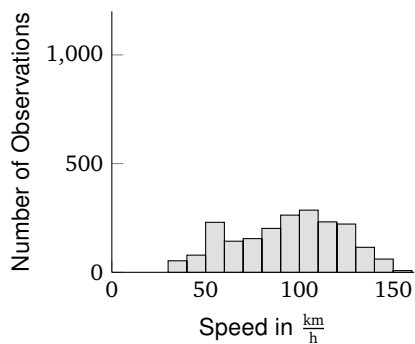
Figure C.4: Geographic map of the tire dataset. The black lines consists of many crosses. Each cross represents the location of an observation.



(a) Full dataset (combined training and testing data)



(b) Mass dataset



(c) Tire dataset

Figure C.5: Distribution of the mean vehicle speed of an observation for different datasets

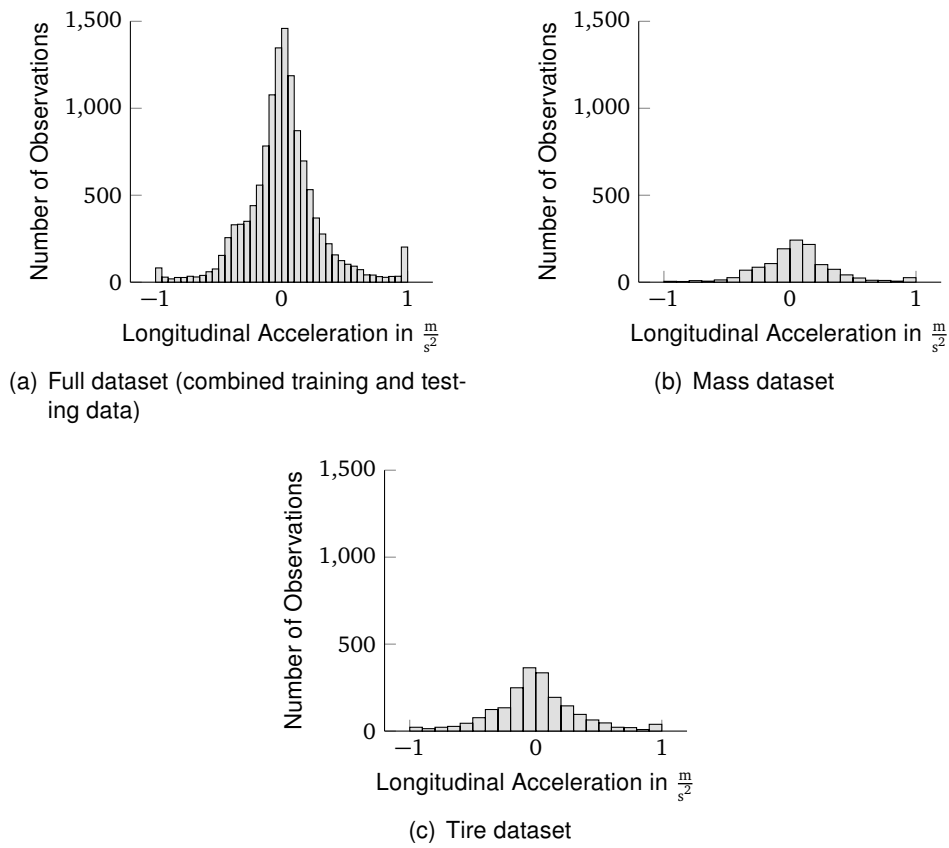


Figure C.6: Distribution of the mean longitudinal acceleration of an observation for different datasets

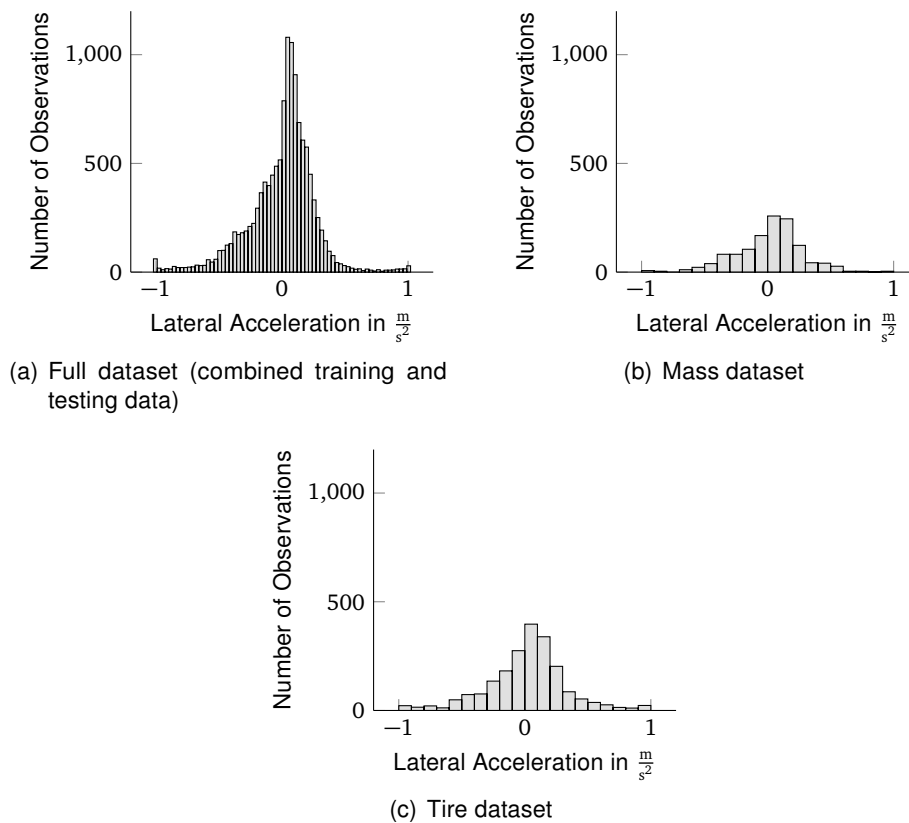


Figure C.7: Distribution of the mean lateral acceleration of an observation for different datasets

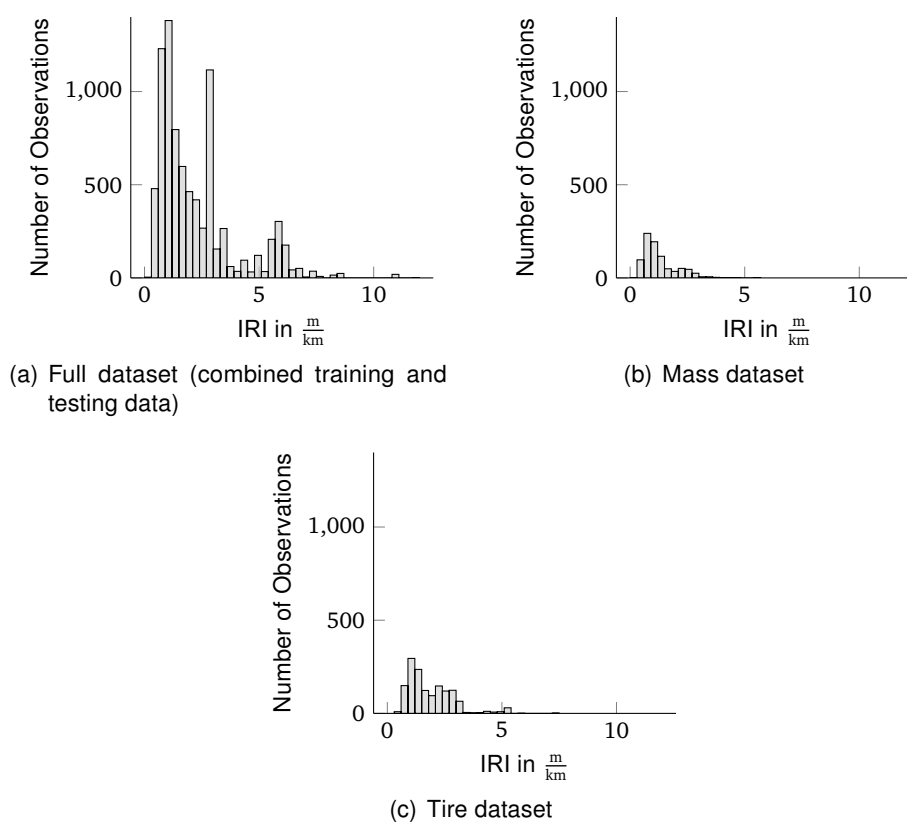


Figure C.8: Distribution of the International Roughness Index (IRI) of the observations of different datasets. See Section 5.8 for a description of the IRI. Information of the IRI was not available for all observations. Therefore the accumulated amount of observations within each graph is less than the number of observations within the corresponding dataset.

C.2 Investigation of Feature Characteristics

C.2.1 Autoencoder Features

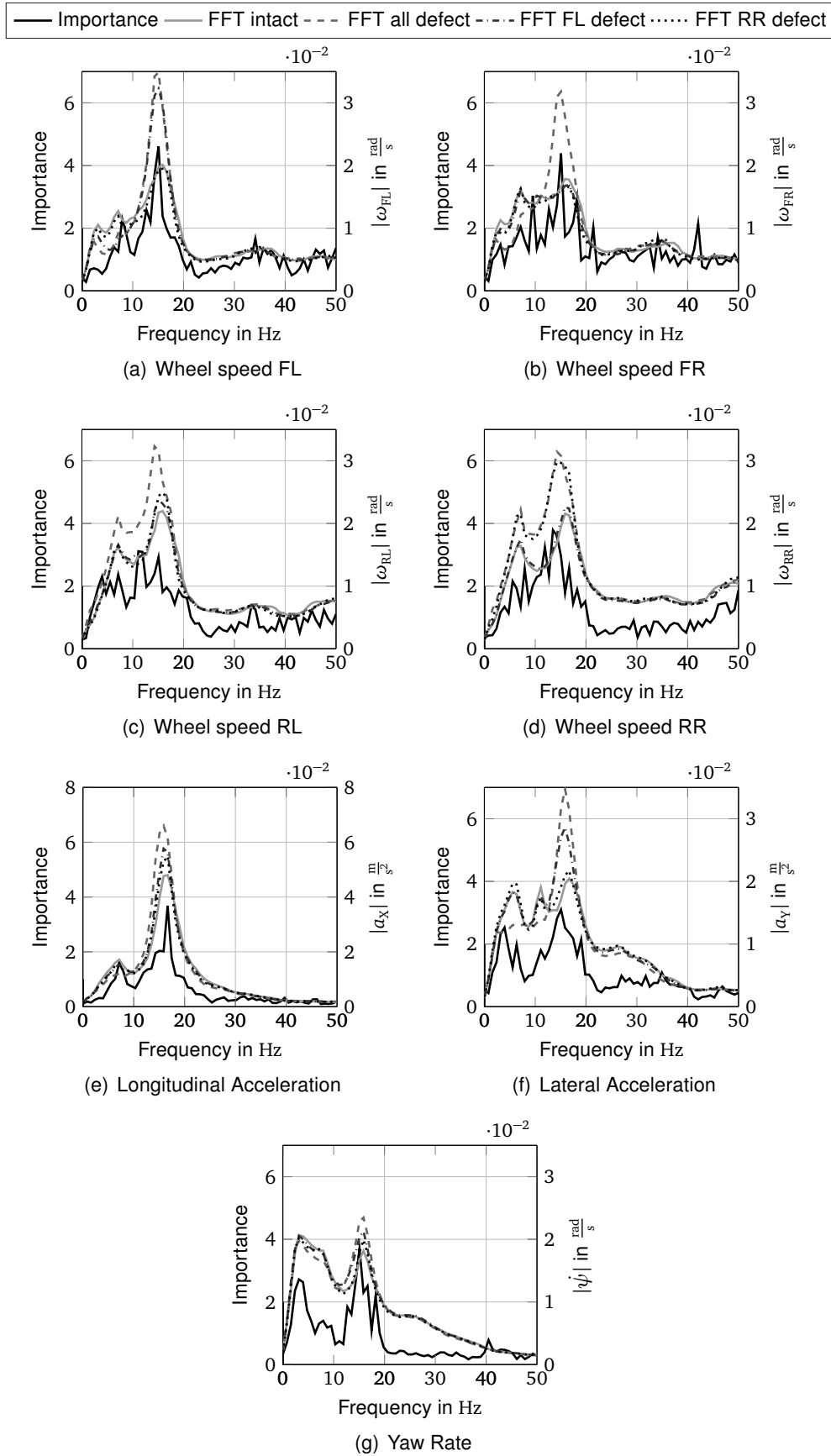


Figure C.9: Analysis of importance of input data frequency shares for the feature generation using Autoencoder

C.2.2 Sparsefilter Features

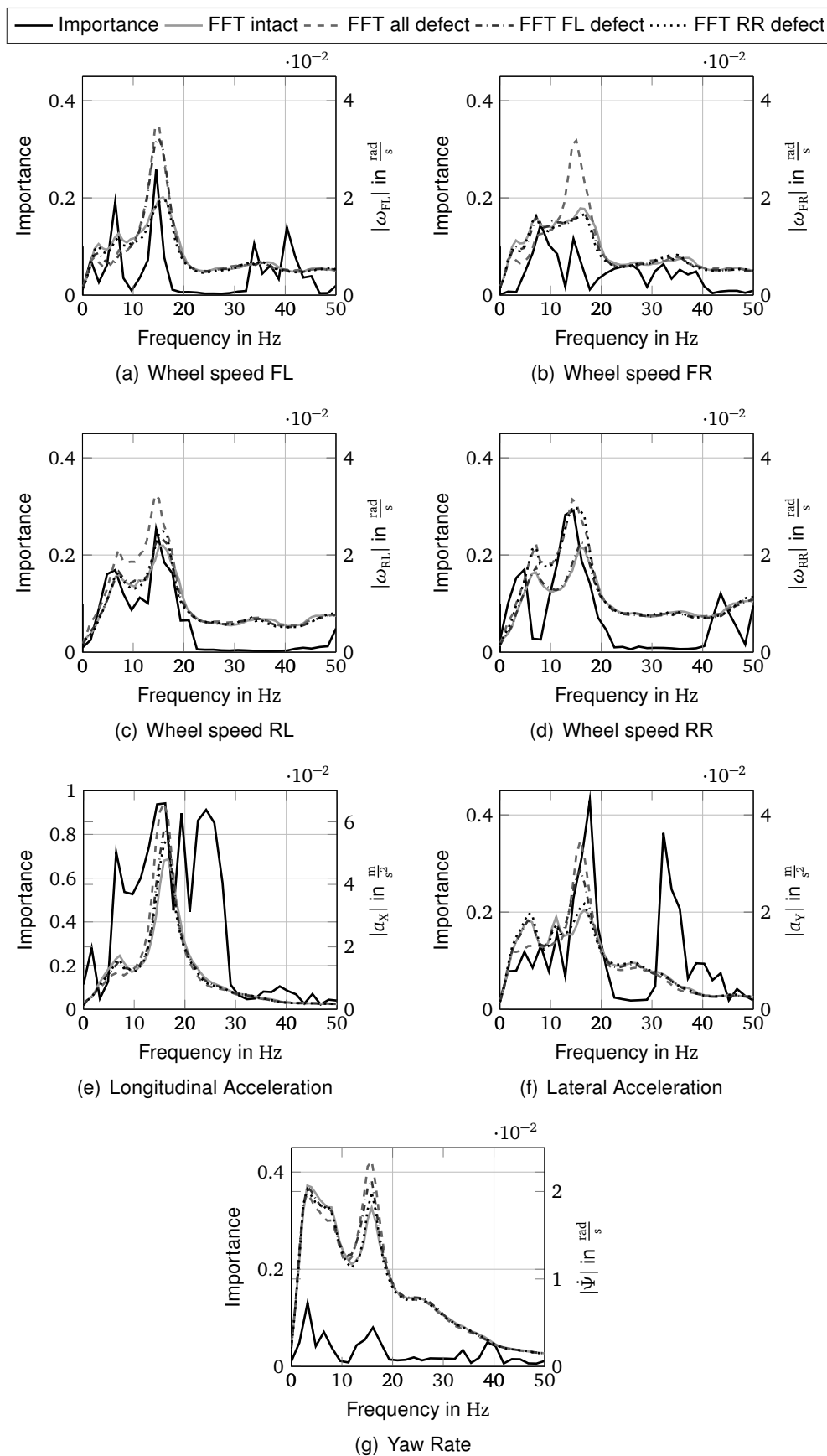


Figure C.10: Analysis of importance of input data frequency shares for the feature generation using Sparsefilter

C.3 Analysis of Influence of Vehicle Speed and Road Roughness

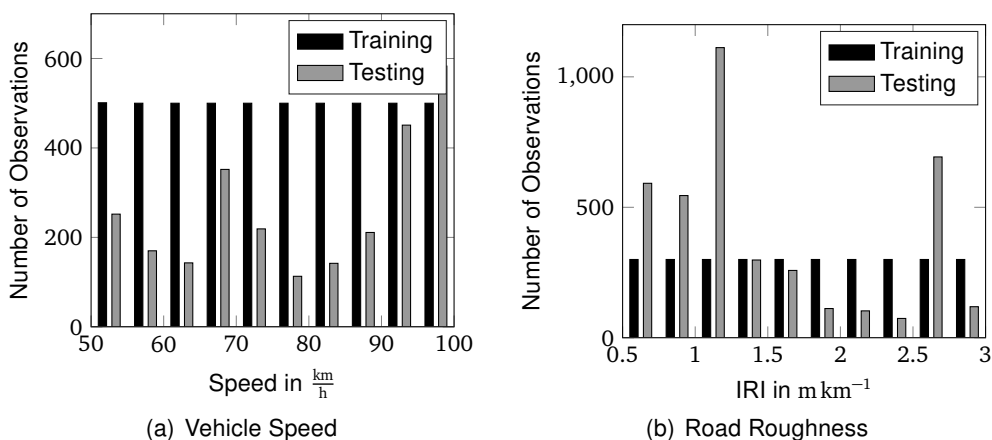


Figure C.11: Distribution of observations for training and testing data for the analysis of the influence of the vehicle speed and IRI on the estimation performance

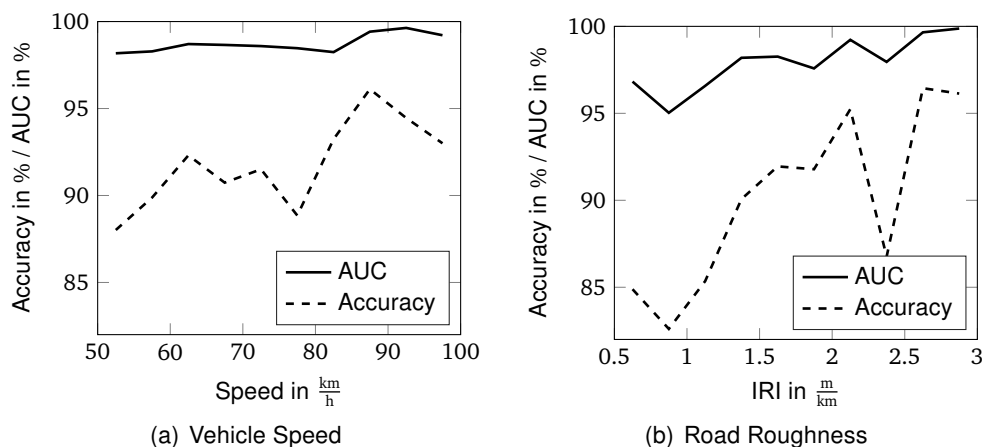


Figure C.12: Accuracy and AUC for each testing data bin of Figure C.11

C.4 Comparison with Signal-Based Approach

Within this thesis, the Power Spectral Density (PSD) magnitude of the wheel speed signals is estimated using the Matlab implementation of the PSD estimation method of Welch [298]. Because the generated PSD is sufficiently smooth, an averaging across a frequency range is not performed but the PSD is directly estimated for one specific evaluation and reference frequency. The two frequencies are selected using an optimization approach within this thesis. A genetic algorithm is used to maximize the resulting Area Under Curve (AUC) value on the training dataset. Because the Damper Damage Value (for German Dämpferschadenskennwert) (DSKW) calculation is performed independently for each wheel, the evaluation and reference frequencies are also optimized for each wheel independently resulting in the frequencies presented in Table C.1.

The DSKW is dependent on the vehicle speed as well as on the road corrugation [17, pp. 110-

Table C.1: Selected evaluation and reference frequency for the signal-based approach of Jautze [17] for each wheel. The selected values result from an optimization of the AUC of the training data using a genetic algorithm.

Wheel	Evaluation Frequency	Reference Frequency
Front Left (FL)	14.35 Hz	20.32 Hz
Front Right (FR)	14.84 Hz	22.02 Hz
Rear Left (RL)	12.09 Hz	22.65 Hz
Rear Right (RR)	13.24 Hz	20.36 Hz

111]. An extend DSKW calculation includes a second reference frequency and resolves the dependency on the road corrugation [17, p. 78]. However, this algorithm resulted in reduced AUC values compared to the DSKW calculation in Equations (5.6) and is therefore not used in this thesis.

The dependency of the algorithm on the vehicle speed is resolved using a speed correction factor for the DSKW based on known behavior of the DSKW with regard to the vehicle speed [17, pp. 116-117]. Within this thesis, this speed correction factor is selected as a characteristic curve of the DSKW over the vehicle speed. Figure C.13 shows this characteristic curve of the generated DSKW values for the training data for each wheel for an intact and defective health state of the corresponding damper. The curves show the median of the DSKW values within small bins of $8 \frac{\text{km}}{\text{h}}$. The curve of the “intact” damper is selected as characteristic curve for the speed correction factor for each wheel individually. Due to the overall optimization approach of the evaluation and reference frequencies as well as the speed correction, the resulting diagnosis performance might be slightly better compared to an actual real-life implementation.

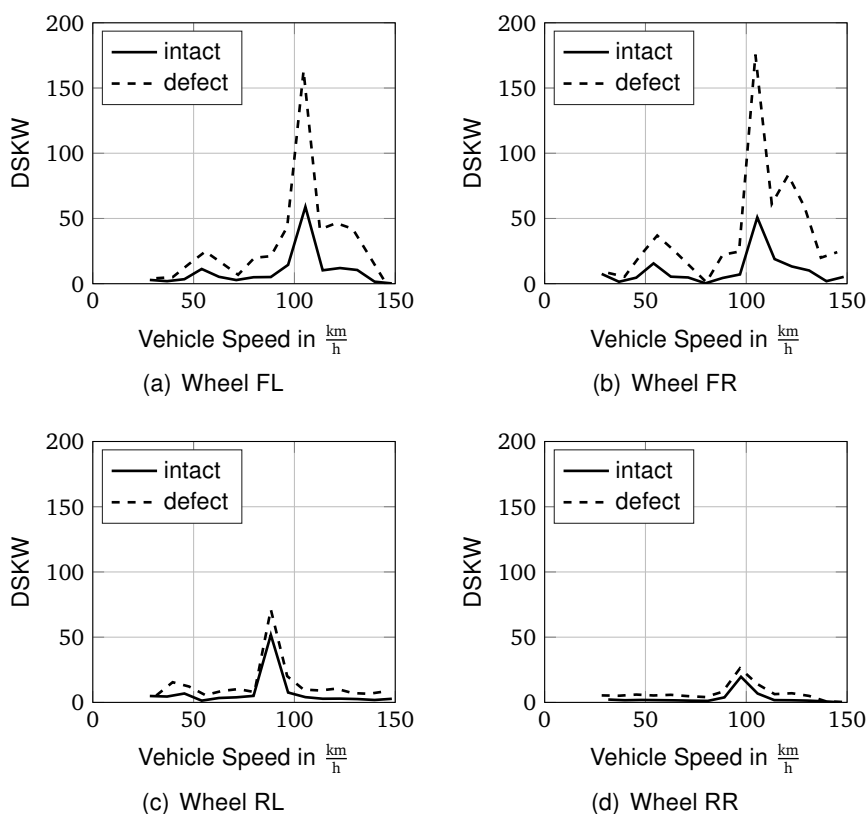


Figure C.13: Binned median of the DSKW over vehicle speed for the training data for each wheel for an intact and defective health state of the corresponding damper.

Figure C.14 shows the ROC curve with the corresponding AUC values of the wheel-individual approach of Jautze [17] including the optimized evaluation and reference frequency and speed-correction for the three datasets of this thesis. The final performance indicator of the signal-based approach that is used for a comparison with the Machine Learning (ML) approaches is the mean AUC value of all wheels.

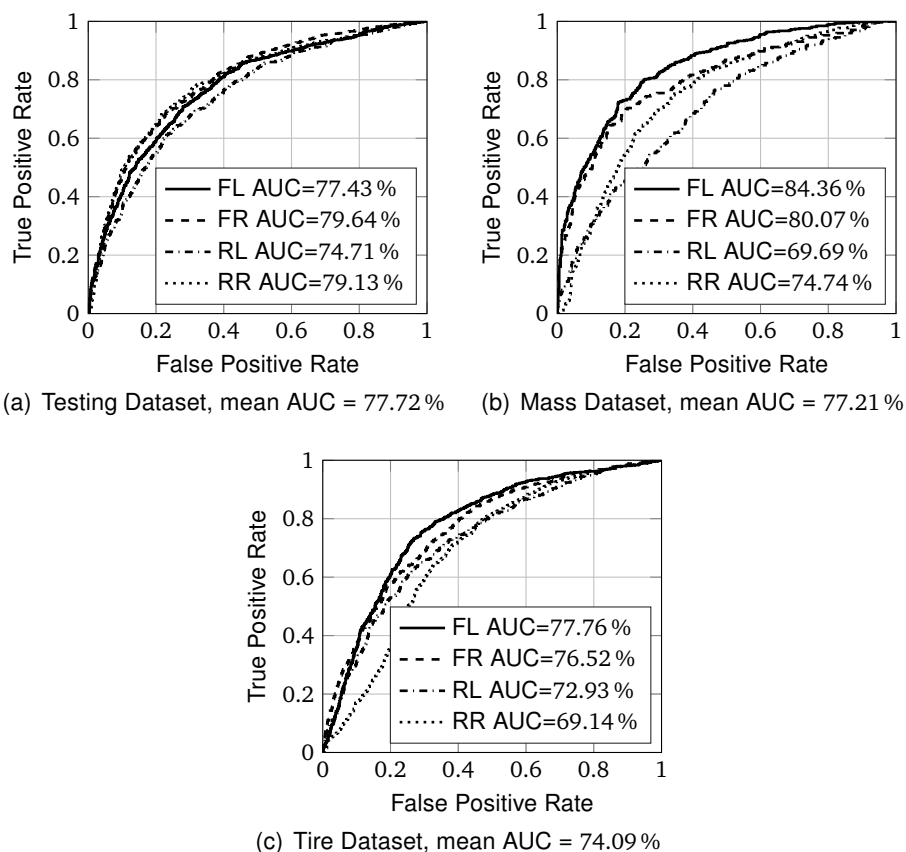


Figure C.14: ROC curve and AUC values of the wheel-individual approach of Jautze [17] including the optimized evaluation and reference frequencies and speed-correction for the three datasets of this thesis.